Dynamic Behaviour of Long-Span Timber Ribbed-Deck Floors

by Bella Maria Basaglia

Thesis submitted in fulfilment of the requirements for the degree of

Doctor of Philosophy

under the supervision of Dr Rijun Shrestha, Prof Jianchun Li and Prof Keith Crews

University of Technology Sydney
Faculty of Engineering and Information Technology

August 2019

Certificate of Original Authorship Template

Graduate research students are required to make a declaration of original authorship when they submit the thesis for examination and in the final bound copies. Please note, the Research Training Program (RTP) statement is for all students. The Certificate of Original Authorship must be placed within the thesis, immediately after the thesis title page.

Required wording for the certificate of original authorship

CERTIFICATE OF ORIGINAL AUTHORSHIP

I, *Bella Maria Basaglia* declare that this thesis, is submitted in fulfilment of the requirements for the award of *Doctor of Philosophy*, in the *Faculty of Engineering and IT* at the University of Technology Sydney.

This thesis is wholly my own work unless otherwise referenced or acknowledged. In addition, I certify that all information sources and literature used are indicated in the thesis.

This document has not been submitted for qualifications at any other academic institution.

This research is supported by the Australian Government Research Training Program.

Signature: Production Note:
Signature removed prior to publication.

Date: 27/09/20

"And once the storm is over, you won't remember how you made it through, how you managed to survive. You won't even be sure, whether the storm is really over. But one thing is certain. When you come out of the storm, you won't be the same person who walked in. That's what this storm's all about."

- Haruki Murakami

To my mother, Papa, jiji-san and baba-san

Acknowledgements

I wish to express my sincere gratitude to Professor Yutaka Yokoyama who welcomed me into his laboratory group at Tokyo Institute of Technology for five months in 2017. Professor Yokoyama's technical guidance expanded and enriched my research in ways I could not have imagined. This experience was truly one of my fondest memories of my PhD and I could not have found a better group to have had that experience with in Japan.

I am grateful for the friendship of my university comrades, particularly Kirsten Lewis, Le Hong Thuy Nguyen, John Phung, Van Vu Nguyen and Federico Volpin. Although we may have been researching different areas, I found great comfort in their support during the highs and lows of research.

This journey would not have been possible without the understanding and encouragement from my personal friendships. In particular, I would like to thank my close friends Bec Reel, Amanda Hanna and Emily Choi who always listened to my stresses with intent and care. I also appreciate the advice from Ian Fraser who has been somewhat like a father figure and always supported me in my life decisions. I would also like to express my appreciation for my partner, Noah Homayed, who gave me a shoulder to cry on when things weren't going as planned and lifted me back up with his constant words of encouragement.

Lastly, I would like to express my deepest love and appreciation for my family: my mother, Papa, my grandmother (baba-san) and grandfather (jiji-san). My mother's endless care and emotional support for me is something I could never repay. I just hope that I can make her proud and to answer her question 'Yes, I have finally finished!'. To my Papa, baba-san and jiji-san, who sadly were not able to see me complete: I know you were there in spirit and appreciate your presence throughout this journey. This thesis is dedicated to you.

Bella Basaglia
August, 2019

List of Publications

Conference Papers

1. <u>Basaglia, B.,</u> Lewis, K., Shrestha, R., Crews, K., (2015), 'A comparative life cycle assessment approach of two innovative long span timber floors with its reinforced concrete equivalent in an Australian context' , *International Conference on Performance-based and Life-cycle Structural Engineering,* 9 – 11 December 2015, Brisbane, Australia (presented)

2. Lewis, K., <u>Basaglia, B.,</u> Shrestha, R., Crews, K., (2015), 'Innovation in the design of cross laminated timber for long span floors', *International Conference on Performance-based and Life-cycle Structural Engineering,* 9 – 11 December 2015, Brisbane, Australia

3. Hough, R., <u>Basaglia, B.,</u> Passerini, S., (2016), 'Design and construction of a novel stacked glulam wall structure', *World Conference on Timber Engineering,* 22 – 25 August 2016, Vienna, Austria

4. Lewis, K., <u>Basaglia, B.,</u> Shrestha, R., Crews, K.,(2016), 'The use of cross laminated timber for Long span flooring in commercial buildings', *World Conference on Timber Engineering,* 22 – 25 August 2016, Vienna, Austria

5. <u>Basaglia, B.,</u> Shrestha, R., Crews, K., Yokoyama, Y., (2018), 'Vibration Response of a Long-Span LVL Floor: Comparison Between Japanese and Australian Assessment Measures', *World Conference on Timber Engineering,* 20 – 23 August 2018, Seoul, Republic of Korea (presented)

Journal Articles

1. <u>Basaglia, B.,</u> Li, J., Shrestha, R., Crews, K., Forthcoming. 'Response prediction to walking-induced vibrations of a long-span timber floor', ASCE Journal of Structural Engineering. 10.1061/(ASCE)ST.1943-541X.0002888

List of Notations

[ ]	Matrix
{ } or **x**	Curly brackets or bold parameters indicate vectors
[M]	Mass matrix
[K]	Stiffness matrix
[C]	Damping matrix
α_i; α_i^s	DLF of the i-th harmonic and subharmonic, respectively.
$\bar{\alpha}_i(\bar{f}_j)$; $\bar{\alpha}_i^s(\bar{f}_j^s)$	Normalised dynamic load factor for i-th harmonic and subharmonic, respectively – in Živanović et al. (2007b) load model (Chapter 5)
δ	Joist mid-span deflection due to point load P applied at centre of joist
δ_c, δ_{mid}	Floor mid-span deflection due to point load P applied in the centre of the floor
$\theta(\bar{f}_j)$; $\theta(\bar{f}_j^s)$	Normalised phase angle for harmonic and subharmonic, respectively – in Živanović et al. (2007b) load model (Chapter 5)
$\mu_{e,n}$; $\mu_{r,n}$	Mass-normalised mode shape amplitudes of mode n at excitation and response nodes, respectively.
ξ	Damping ratio
ρ, ρ_m, DENS	Density (kg/m³)
ρ_r	Resonant build-up factor
σ	Standard deviation
τ	Integration time constant for running root-mean-square average (s)
ϕ_i	Phase angle of the i-th harmonic
$\varphi_{FE,i}$; $\varphi_{FE,j}$	Numerically obtained mode shape vector for mode i and j, respectively.
$\varphi_{exp,i}$; $\varphi_{exp,j}$	Experimentally obtained mode shape vector for mode i and j, respectively.
$\{\psi_n\}$	Eigenvector of mode n
ω	Circular natural frequency (rad/s)

ω_i	Circular frequency of the i-th harmonic load component
ω_n	Eigenvalue or circular frequency of mode n
ω_D	Damped circular frequency (rad/s)
A_0	Mean value of weight normalised force (Chapter 5)
A_i	Dynamic load factor for the i-th harmonic – single footfall trace (Chapter 5)
a_{MTVV}	MTVV from weighted acceleration response (m/s^2)
$a_{w,p}$	Frequency-weighted peak acceleration (m/s^2)
$a_{w,rms}$	Frequency-weighted RMS acceleration (m/s^2)
$a_w(t)$	Frequency-weighted acceleration at time t (m/s^2)
$a_{w,rms}(t_0)$	Rolling frequency-weighted RMS acceleration (m/s^2) at instantaneous time of observation t_0
b	Floor width
c	Damping constant
c_{cr}	Critical damping
d	Diameter of screw
DLF_i	Dynamic load factor of the i-th harmonic
$D_x; D_y$	Flexural rigidity in the joist and cross-joist direction, respectively (Nm) – in Hu and Chui equation (2004)
D_{xy}	Shear rigidity of the multi-layered floor deck and torsion rigidity of the joist (Nm) – in Hu and Chui equation (2004)
$\bar{E}$	Mean modulus of elasticity
$\bar{E}_J$	Mean modulus of elasticity of the joist
$eVDV; eVDV_E$	Estimated VDV as per BS 6472-1 (1984); as per Ellis (2001)
$(EI)_l; (EI)_b$	Equivalent flexural rigidity of the floor structure about an axis perpendicular and parallel to the beam direction, respectively.
EX; EY; EZ	ANSYS notation for modulus of elasticity in element x-, y- and z-axes, respectively.
f	Cyclic frequency (Hz)
$f'b$	Bending strength (N/mm^2)
$f'c$	Compression parallel to grain (N/mm^2)

f_i^{FE}	Numerically obtained natural frequency for mode i (Hz)
f_i^{exp}	Experimentally obtained natural frequency for mode i (Hz)
$\bar{f_j}$	Frequency ratio between the current frequency line and pace frequency – in Živanović et al. (2007b) load model (Chapter 5)
f_{joist}; f_{girder}	Natural frequency of the joist and girder, respectively (Hz).
f_n; f_i	Cyclic frequency or natural frequency of mode n or i (Hz)
f_p	Pace frequency or walking frequency (Hz)
f_s	Sampling frequency (Hz)
$f's$	Shear in beams (N/mm^2)
$f't$	Tension parallel to grain (N/mm^2)
$F(\omega)$	Fourier transform of the excitation (input) signal
$F(t)$	Time varying force
F(x)	Objective function (Chapter 4)
G	Modulus of rigidity
g	Gravity (9.81 m/s^2)
g(x)	Constraint vector (Chapter 4)
GXY; GXZ; GYZ	ANSYS notation for shear modulus in x-y, x-z and y-z planes, respectively.
$H(\omega)$	Frequency response function for the input and output signals
$H_1(\omega)$; $H_2(\omega)$	FRF estimators
I	Moment of inertia
I_{eff}	Effective impulse (Ns)
I_j	Moment of inertia of the joist member
k	Stiffness (N/m)
K_{ser}	Slip modulus
KTx; KTy; KTz	Support stiffness for spring elements in the x-, y- and z-directions, respectively.
L, l	Length, floor span
m	Mass (kg)
m_a	Mass per unit area (kg/m^2)
m_l	Mass per unit length (kg/m)

M_n	Modal mass of mode n (kg)
m_s	Mass per unit area of floor sheathing (kg/m^2)
MAC_{ij}	Modal assurance criterion between mode i and j
$MAC_{ERROR,ij}$	$1 - MAC_{ij}$
$NF_{ERROR,i}$	Natural frequency error for mode i
n	Mode number
n_{40}	Number of eigenmodes with eigenfrequencies lower than 40 Hz for unit impulse calculation in Eurocode 5
n_j	Number of joists
P	1 kN point load (kN)
PRXY; PRXZ; PRYZ	ANYS notation for Poisson's ratio in x-y, x-z and y-z planes, respectively.
P_j	Parameter j for sensitivity study (Chapter 4)
Q	Walker weight (N)
R_i	Response i for sensitivity study (Chapter 4)
s	Spacing
S_{ij}	Sensitivity coefficient for each target response R_i to a certain change in parameter P_j
$S_{n,ij}$	Normalised sensitivity coefficient for each target response R_i to a certain change in parameter P_j
t	Time (s)
T	Duration of response measurement or exposure period (s)
T_f	Duration of a single footfall (s)
t_{RMS}	Period of 1/f_p from which RMS response is calculated (Chapter 5)
$u_{vel,max}$	Maximum unit impulse velocity response (m/Ns^2)
v_{MTVV}	MTVV from integrated velocity response (m/s)
v_{rms}	Root-mean-square velocity response (m/s)
w	Maximum instantaneous vertical deflection caused by a vertical concentrated static force F applied at any point on the floor
$w_{f,i}$	Weighting factor for the NF_{ERROR} of mode i (Chapter 4)

$w_{\varphi,i}$	Weighting factor for the *MAC*_{*ERROR*} for mode i (Chapter 4)
w_l	Load per unit length
W_m; W_b; W_k	Frequency-weighting curves provided in ISO 2631-2 (2003), BS 6471-1 (2008a), and ISO 2631-1(1997), respectively.
$X(\omega)$	Fourier transform of the response (output) signal
x_{min}; x_{max}	Lower and upper constraints for design variable x (Chapter 4)
x_u	Updated parameter from model updating (Chapter 4)
$y(t)$	Time varying displacement (m)
$\dot{y}(t)$	Time varying velocity (m/s)
$\ddot{y}(t)$	Time varying acceleration (m/s^2)

List of Acronyms

ASD	Auto-spectral density
CE	Complex exponential
CLT	Cross-laminated timber
CoV	Coefficient of variance
DAQ	Data acquisition
DFT	Discrete Fourier transform
DLF	Dynamic load factor
DMF	Dynamic magnification factor
DOF	Degree-of-freedom
EMA	Experimental modal analysis
ESPA	Equivalent sinusoidal peak acceleration
EWP	Engineered wood product
FE	Finite element
FFT	Fast Fourier transform
FRF	Frequency response function
FS	Footstep
FT	Fourier transform
IRF	Impulse response function
LSCE	Least-squares complex exponential
LSFD	Least-squares frequency domain
LVL	Laminated veneer lumber
MAC	Modal assurance criterion
MDOF	Multi-degree-of-freedom
MoE	Modulus of elasticity
MPC	Modal phase collinearity
MPD	Modal phase deviation
MTVV	Maximum transient vibration value
OSB	Oriented strand board
OS-RMS$_{90}$	One-step RMS for the 90th percentile (HIVOSS guide)
PR	Pin-roller
RF	Response factor

RMS	Root-mean-square
SDOF	Single-degree-of-freedom
SFT	Single footfall trace
SIMO	Single-input, multiple-output
SISO	Single-input, single-output
SRSS	Square-root sum of squares
VDV	Vibration dose value

Table of Contents

List of Figures

List of Tables

Abstract

The development of engineered wood products and the environmental benefits of timber over conventional building materials has led to an increased interest in the use of timber for the construction of multi-storey buildings. Timber has a high strength-to-weight ratio making it structurally efficient for long-span floor applications (a common practice in commercial buildings). However, the low mass of such floors makes them more susceptible to walking-induced vibrations compared to heavier floors such as those made from concrete. In fact, when designing long-span timber floors, dynamic performance criteria tends to govern the design rather than strength. Unfortunately, there is a lack of specific vibration design guidance for long-span timber floors with much of the current criteria based on tests of short-span timber joist floors in residential applications. In addition, there is uncertainty as to how accurately other vibration design guides, mainly used for concrete and steel-concrete composite floors, predicts and assesses floor performance of long-span timber floors.

This thesis addresses this gap by investigating the dynamic behaviour of a long-span timber floor through both experimental and numerical methods. Impact hammer and walking tests with two subjects were performed on a 9 m span ribbed-deck floor which consists of a laminated veneer lumber (LVL) panel glued and screwed to three LVL web members, forming one cassette. The influence of various boundary conditions and cassette-to-cassette connections on the modal properties and floor response were explored. A numerical model of a single cassette, calibrated to measured results through model updating, was used to investigate three human walking load models including the deterministic modelling approach adopted in current vibration design guides. In addition, a numerical model representing the cassette-to-cassette connection was developed and updated using measured results of double cassette tests. These details were adopted in a multi-cassette floor model, based on the dimensions of a typical commercial building floor grid, to investigate the influence of common design parameters on modal properties and floor response.

One of the main findings from walking tests was that the floor exhibited neither a completely transient nor a completely resonant response, despite being classified as a 'high-frequency' floor. This assumption of floor behaviour resulted in inaccuracies in response prediction using current vibration design guides and it is proposed that a step-by-step load model which considers the stochastic nature of walking is more appropriate. This load model also provides the response time-history which allows an assessment of the duration of certain vibration amplitudes (through a cumulative distribution function) during the walking event to be considered in design.

Modal clustering was consistently observed, particularly for the first two or three modes, in the single and double cassette experiments as well as the multi-cassette numerical model. Furthermore, the multi-cassette model revealed that higher modes with low modal masses largely contributed to the floor response. This finding highlights that criterion which only considers the fundamental mode may not be adequate. In regards to design considerations which may benefit the floor response, damping was found to play a key role. This may be in the form of incorporating an elastomer (such as Sylomer®) at the support locations where experimental tests revealed that the damping ratio could increase from 1% to approximately 5% and 7% for the first and second modes, respectively. The findings from all investigations were used to provide guidance and commentary for a vibration design procedure, based on a finite element approach, suitable for long-span timber ribbed-deck floors which was presented in the form of a flow chart.

Chapter 1

Introduction

1.1 Background

1.1.1 Timber as a structural material

Timber, one of the oldest building materials in the world, was the most widely used materials until the beginning of the twentieth century (Harte 2009). Prior to the 1900's, timber was directly cut from fell logs (often referred to as 'sawn timber') and thus was limited in shape (due to the size of the tree) and strength (due to the presence of strength-reducing characteristics). In the early 19th century, industrialisation had a large influence on the building industry where new methods of processing and building including steel and concrete were introduced (Kolb 2008). The ease and cost-effectiveness of transport, together with the demand for larger structures, meant that these modern materials became those preferred for building.

However, the scarcity of resources in the late 1920s and early 1930s as well as the two World Wars led to an increased consumption of raw materials including timber (Kolb 2008). It is important to note here that the word 'timber' is used to refer to the 'wood' (term given to the substance that makes up the tree) at any stage after the tree has fell

which includes both the processed and raw material. In the United States and Canada, 'timber' is generally referred to as 'lumber' so these words can be used interchangeably.

During the same time, the nature of timber as a structural material was also evolving. The advancement of technology and research into the efficient use of timber led to the development of a wide range of engineered wood products (EWPs) such as plywood (first patented in 1865 (Smith & Frangi 2015)), glued-laminated timber (glulam) (first patented in 1906 (Smith & Frangi 2015)), laminated veneer lumber (LVL) and cross-laminated timber (CLT). These products are manufactured from timber strands, veneers or boards bonded together using heat and pressure where, with the exception of CLT, each bonded element is arranged with the grain running parallel to the principal axis of the element being formed. The significant advantage of EWPs over traditional sawn timber were their superior reliability in strength and stiffness properties and higher dimensional stability. In addition, as EWPs, timber elements could now span further and have greater cross-sectional depth, launching timber as a strong candidate for long-span structures.

To the benefit of timber, the 'green building' movement was also gaining momentum in the early 1990's and people were becoming increasingly aware of the importance of sustainable building design and energy efficiency for the environment and human health. In 2010, the construction industry accounted for 18% of global greenhouse gas emissions (IPCC 2014), of which a large contribution was the production of concrete and steel. Timber has a significantly lower environmental footprint than concrete and steel, a result of trees being able to absorb carbon dioxide into their wood as part of the photosynthesis process. The stored carbon remains within the timber when used in buildings and only releases at the end of the buildings life-cycle when the timber is either burned or decomposes; although, the rate of decomposition is slow (Ximenes, Robinson & Wright 2006). Indeed, the sustainability of timber depends on sound forestry practices and to encourage awareness of the source of the timber products used, all major green building rating tools including Leadership in Energy and Environmental Design (LEED) in the US, the Building Research Establishment Environmental Assessment Method (BREEAM) in the UK and Green Building Council Australia (GBCA) Green Star provide credits for the use of certified timber.

Changes in building codes internationally raising the allowable height of timber buildings, combined with government initiatives, also increased interest in building with timber. For example, in the province of British Columbia (BC) in Canada, code changes in 2009 resulted in increasing the maximum height of timber buildings from four- to six-storeys (BC Housing 2017). At the same time, the Wood First Act was enacted where government-funded building projects were required to be constructed from timber where possible. Since then, more than 100 five- and six-storey timber framed buildings have been completed in BC with many more either designed or under construction. The success of this initiative saw the adoption of a similar change in the National Building Code of Canada in 2015 (BC Housing 2017). Similarly, in Australia, the National Construction Code was amended in 2016 to allow the use of lightweight or massive timber construction (also referred to as mass timber construction) for apartments, hotels and office buildings up to an effective height of 25 m (approx. 8 storeys). This change brings Australia in line with other European countries including Finland and Slovenia and has resulted in a number of mid-rise timber buildings including International House in Sydney, a seven-storey commercial building completed in 2017 (shown in Figure 1-1(a)) and 25 King in Brisbane, a nine-storey commercial building completed in 2018 (shown in Figure 1-1(b)). At the time of writing, 25 King was titled the world's largest and tallest engineered timber office building. These examples show a significant shift in interest from the traditional building materials to using timber, which has been particularly rapid over the last decade.
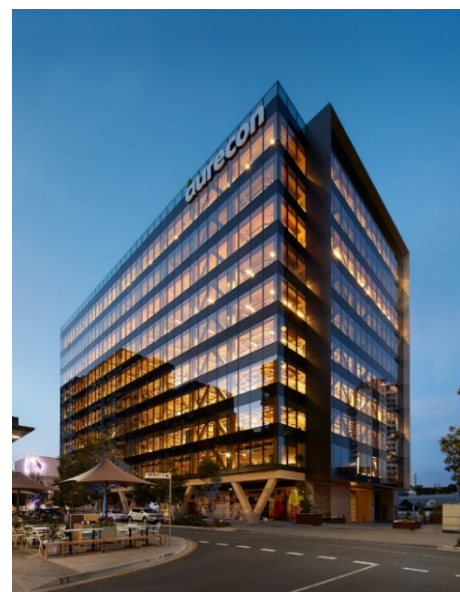
| (a) | (b) |

Figure 1-1 Commercial timber buildings in Australia (a) International House (Guthrie 2018)*; (b) 25 King, Brisbane* (Bates Smart 2018)

1.1.2 Long-span timber floors

A long-span timber floor can be defined as a floor spanning in the range of 6.5 – 10 m between primary beams. Although CLT (a solid panel element made from several layers of timber boards) is one of the more common EWPs used for mass timber building floors, the cost begins to outweigh structural efficiency for spans over 6.5 m. Therefore, for longer span floors, secondary beams are introduced. The beams (often referred to as 'ribs') are connected to the panel element via glue and screws and consequently, the section can be assumed to act as a full composite under serviceability limit state design (Zabihi 2014). The composite behaviour increases the cross-sectional stiffness allowing the floor to efficiently span longer lengths of 6.5 m or greater (KLH Massivholz GmbH 2014). These longer spanning floor systems (often referred to as 'ribbed-deck' or 'cassette type' floors) are subsequently the focus of research presented in this thesis. A diagram of a ribbed-deck floor system is shown in Figure 1-2(a).

(a) Ribbed-deck floor

(b) Traditional joist floor

***Figure 1-2** Schematic diagram of a (a) ribbed-deck floor system and (b) traditional joist floor*
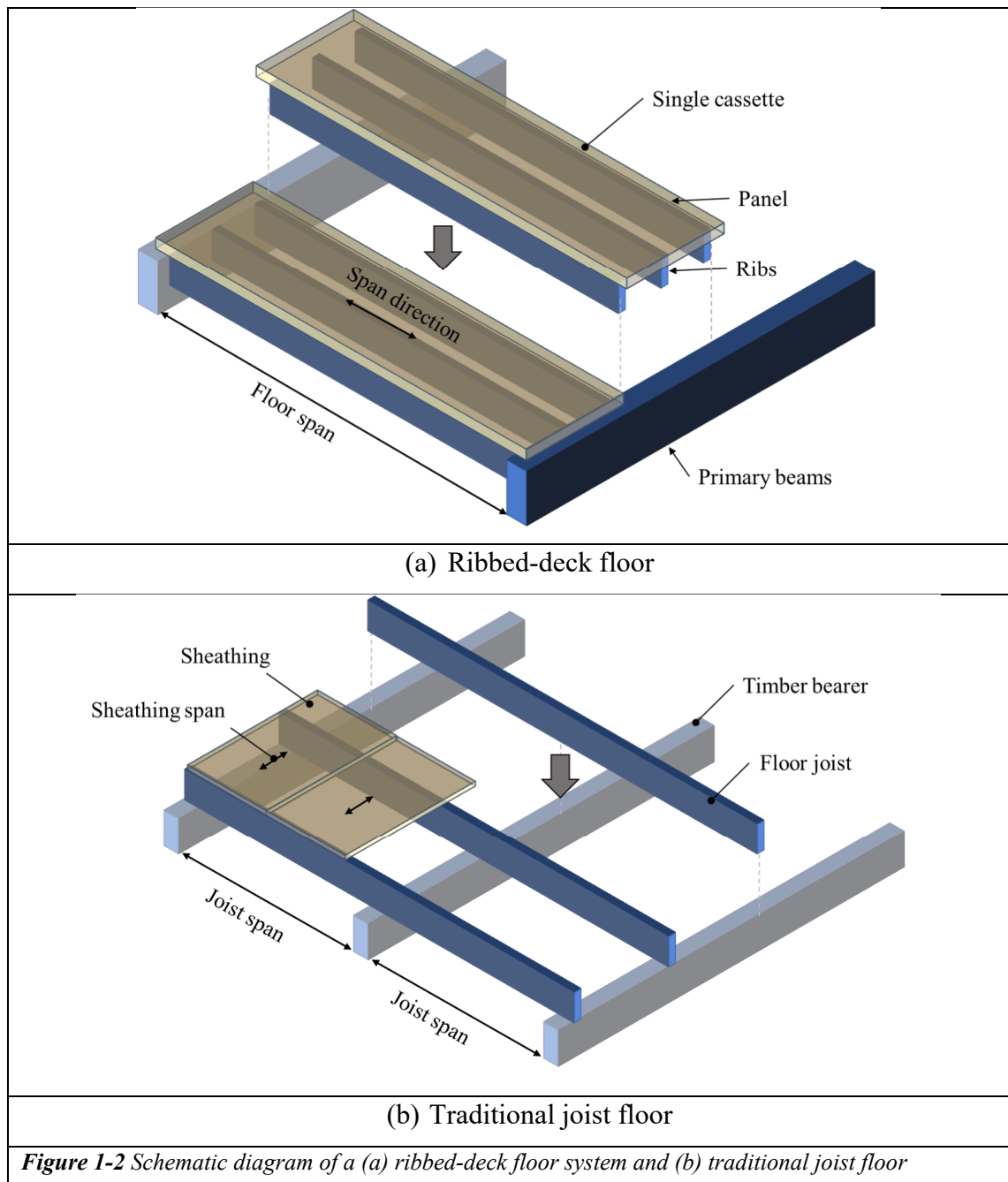
Ribbed-deck floors behave similarly to traditional linear joist floors (as shown in Figure 1-2(b)) in that they act mainly in one direction. However, one of the main differences is that the sheathing (often made from plywood or oriented strand board) is generally not considered to provide additional stiffness to the system. An overview of the differences between a traditional joist floor, a ribbed-deck floor and a CLT floor is shown in Table 1-1.

Table 1-1 *Overview of differences between traditional joist floor and ribbed-deck floor system*

	Traditional joist floor	Ribbed-deck floor	CLT
Material	Sawn timber typical	Engineered wood product	Engineered wood product
Use	Residential	Residential and commercial	Residential and commercial
Structural system	Linear	Linear	Two-way
Span	< 6 m	> 6.5 m	< 6.5 m
Span type	Single span or continuous over bearers	Single span	Two-way spanning
Panel-to-joist connection	No composite action or semi-rigid	Composite action	-
Prefabrication	No	Yes	Yes
Boundary condition	Joists span over timber bearers	Flange and web members span between primary beams	Panel spans between primary beams or walls
Structural floor depth	Bearer depth + joist depth + sheathing thickness	Web depth + flange depth	Panel depth

There are several proprietary ribbed-deck floor systems including the KLH® rib element (Figure 1-3(a)), CLT rib panel by Stora Enso (Figure 1-3(b)), the Lignatur® element (Figure 1-3(c)) and the Kerto-Ripa™ floor element by Metsä Wood (Figure 1-3(d)). The former two systems consist of a CLT panel with glulam ribs while the latter two are made from different forms of laminated timber. All proprietary systems are currently manufactured in Europe where CLT and glulam are readily available.
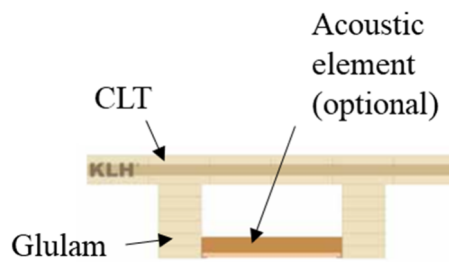
(a) KLH® rib element (KLH 2014)   (b) CLT rib panel (Stora Enso 2018)
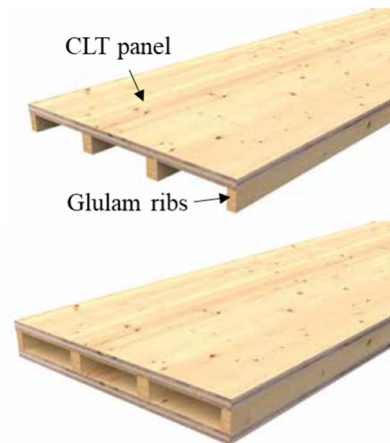
(c) Lignatur® element (Lignatur 2019)   (d) Kerto-Ripa™ floor (Metsä Wood 2015)
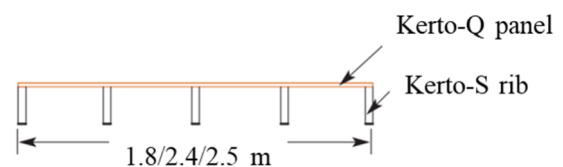
Figure 1-3 *Proprietary ribbed-deck floor systems. Note Kerto-Q and Kerto-S in (d) are LVL products manufactured by Metsä Wood.*

1.2 Research problem

With the evolution of work environments to allow for flexible layouts and open-plan spaces, longer lengths of uninterrupted floor are now a common requirement for new commercial buildings. Consequently, the high strength-to-weight ratio of engineered timber, which provides a high degree of structural efficiency in terms of its load-carrying capacity on supporting its self-weight (Ramage et al. 2017), puts timber among the best candidate of materials for long-span floor structures. Ironically however, this combination of lightweight and long-span ability also means that timber floor systems can be prone to 'annoying' floor vibrations (i.e. vibrations which can cause a sense of discomfort to the occupant and/or interfere with their activity). In fact, when designing long-span timber floors, the dynamic performance induced by human activities is generally the governing design parameter rather than strength (Dolan et al. 1999; Glisovic & Stevanovic 2010; Hassan & Girhammar 2013; Hu & Chui 2004; Mohr 1999; Ohlsson 1988a).

In structural engineering, user discomfort resulting from floor vibrations falls under serviceability design which involves the consideration of occupant comfort during the service life of the building. If the dynamic performance of the floor is not adequately designed for, it can have a detrimental effect on the building occupancy and, depending on the extent of the problem, can be extremely complex and costly for the building owner to rectify. Apart from the rectification cost, other financial losses can include rental revenue loss, legal expenses, and consulting fees (Hanagan 2005). Thus, it is imperative to ensure that engineers are able to accurately predict and design for floor vibrations in the design stage of the project.

Unfortunately, there is not yet a conclusive design procedure for long-span timber floors. Recent studies show that existing procedures and criterion that have been developed from experiments on timber floors in residential dwellings, are unreliable, inconsistent with subjective opinions or unnecessarily penalise modern timber floor systems (Ebadi, Doudak & Smith 2018; Hamm, Richter & Winter 2010; Ussher et al. 2017a; Weckendorf, Ussher & Smith 2016). For timber floors in commercial building applications, designers may turn to more established criterion based on steel-composite or reinforced concrete floors such as those published by the Concrete Centre (Willford & Young 2006), Steel Construction Institute (Smith, Hicks & Devine 2009) and American Institute of Steel Construction (Murray et al. 2016). However, in many cases, the prediction of floor performance is excessively higher than the recommended limits, leading designers down a path of design changes which are uneconomical and reduce the competitiveness of long-span timber floors (Chang, Goldsmith & Harris 2018). Moreover, as long-span timber floors are still an emerging structural system in the commercial building market, there are limited examples to test how these floors actually respond to walking vibrations in comparison to the predictions. Consequently, the development of appropriate design methods and criterion has been highlighted as a crucial issue for the viability of timber floors in non-residential buildings (Abeysekera et al. 2018; Ebadi, Doudak & Smith 2018; Homb & Kolstad 2018; Negreira et al. 2015; Weckendorf et al. 2015).

An adequately designed floor for vibration depends on the accuracy of the predicted response to walking-induced loads, which is in turn contingent on the accuracy of the

modal properties, and the appropriateness of the criterion. With this in mind, this thesis addresses the following unanswered research questions:

- What is the dynamic behaviour of a long-span ribbed-deck timber floor system and how does it respond to human walking loads?
- How can we adequately model long-span timber floors in a finite element program to accurately predict modal properties?
- Do response predictions using established guidelines accurately represent the response of a long-span timber floor? If not, why?
- Are there any design considerations which can improve the performance of a long-span timber floors?
- Can we develop a simple design method for the vibration design of long-span ribbed deck floors?

1.3 Research objectives

The main aim of this thesis is to provide guidance and commentary for a vibration design procedure suitable for long-span timber floors. Although the research involves experimental and numerical investigations of a 9 m spanning LVL ribbed-deck floor, the research findings are intended to be applicable for other ribbed-deck floor systems such as those in Figure 1-3. The specific objectives of this research work are:

1. To conduct laboratory investigations to obtain the modal properties and floor response to walking excitation on a long-span timber floor system with varying boundary conditions and cassette-to-cassette connections.
    - To investigate different numerical quantities which can be used to quantify floor response based on current standards and literature.
    - To investigate the influence of various boundary conditions on the modal properties and floor response on a single cassette floor.
    - To investigate the influence of various cassette-to-cassette connections on the modal properties and floor response on a double cassette floor.
2. To develop a procedure for finite element modelling of a ribbed-deck floors which has been validated based on the measured modal properties.
    - To conduct a sensitivity analysis to determine the critical input parameters for model updating.

> · To investigate the numerical representation of certain boundary conditions and cassette-to-cassette connections.

3. To investigate the influence of different walking load models to predict floor response and propose an appropriate model for ribbed-deck floors.

> · To investigate different walking load models based on a literature search which may be appropriate to predict floor response on timber floor systems.
>
> · To compare the predicted response using the different load models to the measured response of the floor.

4. To perform a parametric study on a floor model, which represents the dimensions of a typical floor grid in a commercial building, to investigate the effect of common design considerations on the modal properties and floor performance.

1.4 Research scope

As noted in Section 1.1.1, many proprietary ribbed-deck floors are manufactured using glulam web members and a CLT panel. In Australia and New Zealand, however, LVL is the most readily available EWP with a large number of fabricators including Carter Holt Harvey and Nelson Pine Industries. The LVL in Australia and New Zealand is generally made from Radiata Pine. As such, the ribbed-deck element, which is of focus in this research, consists of an LVL panel glued and screwed to LVL web elements. Although LVL was the EWP used for the floor system, the research methodology and findings can be extended to ribbed-deck systems made from other EWPs.

The floor was fabricated at the University of Technology Sydney using products from Carter Holt Harvey and Nelson Pine. The fabrication process and cross-section details of this floor are discussed in Chapter 3. It should be noted that the purpose of the research was not to propose a floor system for commercialisation, but rather fabricate a similar product to the other proprietary systems which has the potential to be used in mid-rise commercial buildings in Australia.

The research is also limited to the following areas:

- Two specimens of equal dimensions were fabricated with each specimen having a different experimental purpose. One specimen was used to investigate influence

10

of boundary conditions while the second specimen was connected to the first using various connections so that cassette-to-cassette connections could be investigated.

- Floor testing was performed in a laboratory environment. No tests were undertaken in-situ.

- Four different simply-supported boundary conditions were investigated.

- Cassette-to-cassette connections considered a web-to-web screws as well as two flange-to-flange connections (splice and diagonal screws). Screw spacing of 300 mm and 150 mm centre-to-centre were considered.

- Only walking-induced excitation was considered as the source of vibration as this is the most common form of excitation experienced in buildings.

- The dynamic behaviour of the supporting primary beams were not considered.

- For majority of tests, the floor was tested under self-weight only. Additional loading along support edges was considered for one test set-up to represent the effect of partitions or other super-imposed dead loads commonly found in commercial buildings. Effect of the presence of humans on the floor was not considered.

1.5 Structure of thesis

The thesis is divided into nine chapters as shown by the thesis outline flowchart in Figure 1-4. The current chapter has detailed the background and context of the research problem and has defined the research objectives and scope. Chapter 2 provides a comprehensive literature review of the essential areas of floor vibration design including current research on human walking load models, the key issues surrounding timber floor as a transmission path and the complexities of human sensitivity to vibration. This chapter also details the evolution of criterion for residential timber floors as well as the vibration design guides commonly used for other floor constructions.

In Chapter 3, the tested ribbed-deck floor is introduced and the dynamic testing methods to obtain the modal properties and floor response are explained. The schedule of all performed tests in this research is also presented.

Chapters 4 – 7 discuss the dynamic properties and numerical modelling of ribbed-deck floors in increasing complexity. The thesis was purposefully structured in this format to

logically build upon the findings from previous chapters. Chapter 4 discusses the numerical modelling procedure in parallel with the measured modal properties of a single cassette under three of the four simple boundary conditions where appropriate. A sensitivity study is conducted to first define the most influential parameters to the frequencies of the first five modes and the model updating procedure is detailed. Chapter 5 uses the updated model to investigate the differences of various proposed human walking load models on response prediction. The chapter also proposes the most appropriate load models based on a comparison between predicted and measured results.

In Chapter 6, the thesis moves into the test results of the last simple boundary condition (elastomer) and double cassette tests involving various cassette-to-cassette connections. The double cassette tests are then used to define the modelling approach for the cassette-to-cassette connections. The proposed load models from Chapter 5 are also applied to the double cassette model and compared to measured results.

Based on the updated single cassette model from Chapter 4 and cassette-to-cassette connection modelling of Chapter 6, Chapter 7 presents a multi-cassette model based on the dimensions of a typical commercial building floor. The influence of various commonly considered design parameters on the modal properties and floor response (using the proposed walking load model from Chapter 5) is then investigated.

In Chapter 8, a flow chart for a vibration design procedure for long-span ribbed-deck floor is proposed based on the findings from Chapter 4 – 7. Commentary and discussion is provided for each key area with reference to previous chapters.

The final chapter concludes this thesis with a summary of the conclusions and recommendations for further research.
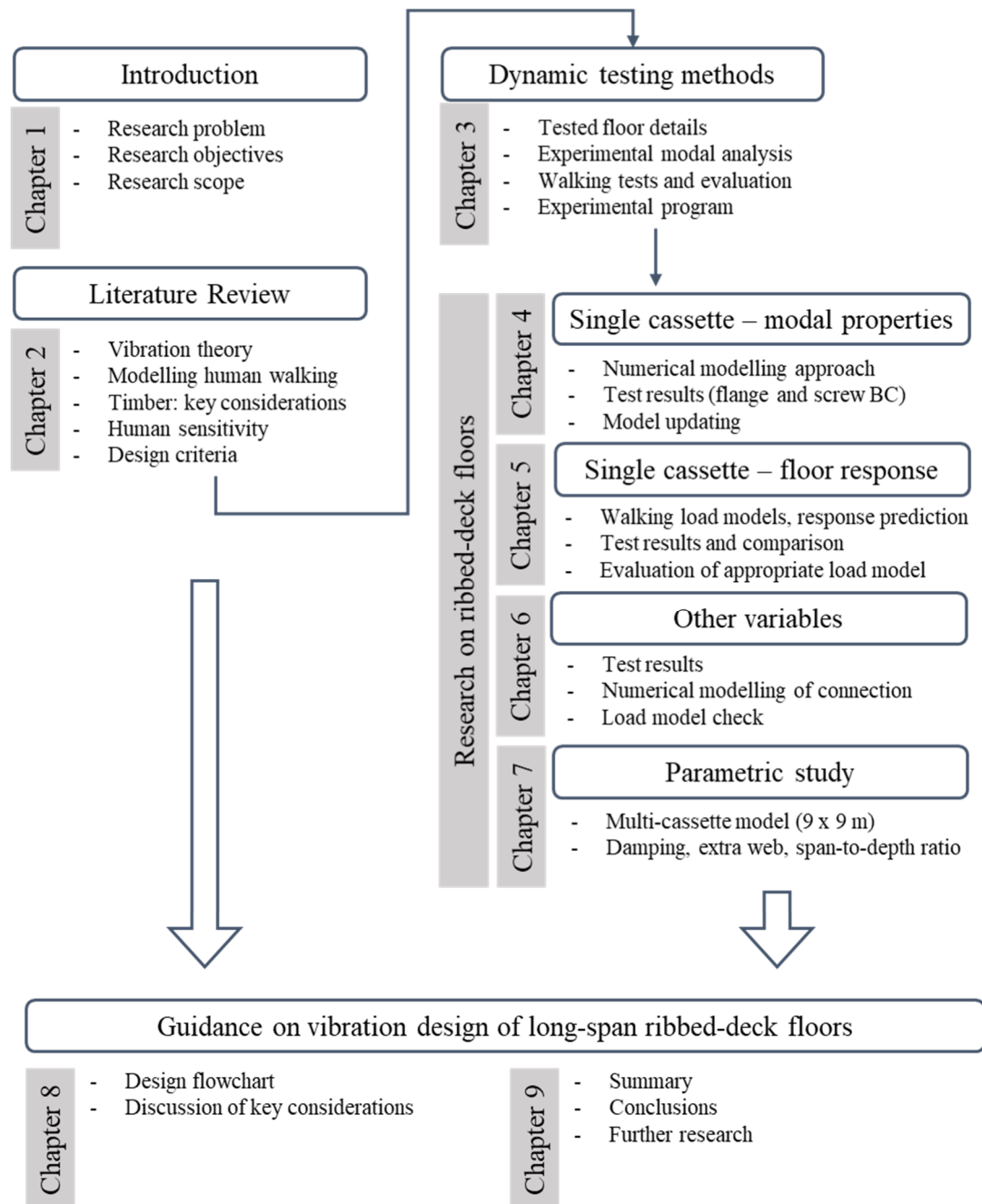
Figure 1-4 *Outline of thesis*

Chapter 2

Literature Review

2.1 Introduction

Following a section on the fundamentals of vibration theory, this chapter first details the three key elements which require thoughtful consideration for the accurate prediction and assessment of floor response. As shown in Figure 2-1 these elements are: the vibration source, timber floors as a transmission path and human perception of vibration. Following this, an overview of significant works regarding the development of vibration serviceability design criteria in both timber and non-timber floors are discussed. Finally, the research needs that are addressed in this thesis are identified.
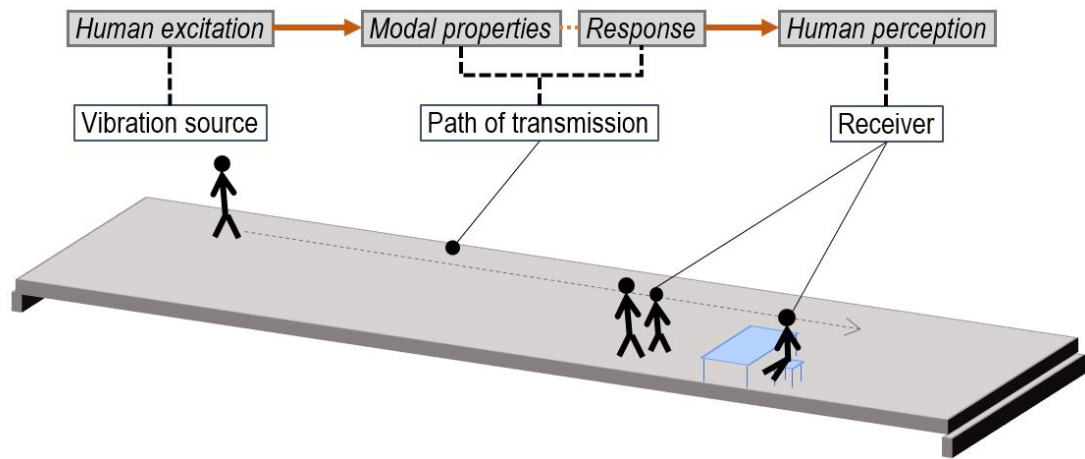
Figure 2-1 *An overview of floor vibration*

2.2 Fundamentals of vibration theory and experimental modal analysis

This section provides a brief overview of the fundamentals of vibration theory and experimental modal analysis with a specific focus on floor systems. This theory is crucial in understanding the essential characteristics of a dynamic problem and subsequently how modal properties of the floor can be extracted through experimental modal analysis. For more detailed explanation of vibration theory, the reader is referred to structural dynamics textbooks including those by Clough and Penzien (1993) and Humar (2012).

2.2.1 Forced vibration of a damped single degree-of-freedom system

When an external force, $F(t)$, such as human walking, excites a floor system, the dynamic equilibrium equation of a damped single-degree-of-freedom (SDOF) takes the form:

$$m\ddot{y}(t) + c\dot{y}(t) + ky(t) = F(t) \qquad (2.1)$$

where m = mass (kg); c = damping constant; k = stiffness (N/m); $y(t)$ = displacement (m); $\dot{y}(t)$ = velocity (m/s) and $\ddot{y}(t)$ = acceleration (m/s^2). The total solution, $y(t)$, is a combination of what the system wants to do under free-vibration (homogenous solution) and what the system is forced to do under the external force (particular solution) which can be expressed as follows:

$$y(t) = y_h(t) + y_p(t) \qquad (2.2)$$

where $y_h(t)$ and $y_p(t)$ are the homogenous and particular solutions, respectively.

To obtain the homogenous solution, the dynamic equilibrium equation where $F(t) = 0$ must first be solved. A solution for $y_h(t)$ can be first assumed as:

$$y_h(t) = Xe^{st} \tag{2.3}$$

where X and s are constants. Considering the SDOF system is underdamped (as is the case for floor systems) and substituting Equation 2.3 and its differentiated forms into the dynamic equilibrium equation (since $Xe^{st} \neq 0$), the solution for s becomes:

$$s = -\xi\omega \pm i\omega_D \tag{2.4}$$

where ξ = damping ratio, ω = circular natural frequency = $\sqrt{k/m}$ and ω_D = damped circular frequency = $\omega\sqrt{1 - \xi^2}$. Since the damping ratio in many structural systems including floors is generally less than 10%, $\sqrt{1 - \xi^2}$ is minimal and the damped frequency is usually approximated as the undamped natural frequency; this same approximation has been taken in this research.

Substituting Equation 2.4 into 2.3 and using Euler's formula, $e^{\pm ix} = \cos x \pm i \sin x$, the general solution can be expressed as follows:

$$y_h(t) = e^{-\xi\omega t}(X_A[\cos\omega_D t + i\sin\omega_D t] + X_B[\cos\omega_D t - i\sin\omega_D t])$$

$$y_h(t) = e^{-\xi\omega t}(A\cos\omega_D t + B\sin\omega_D t) \tag{2.5}$$

where: $\qquad A = (X_A + X_B); B = i(X_A - X_B)$

By introducing the amplitude constant, $X = \sqrt{A^2 + B^2}$, and phase angle, $\tan\varphi = B/A$, Equation 2.5 can be expressed as:

$$y_h(t) = Xe^{-\xi\omega t} \cdot \sin(\omega_D t + \varphi) \tag{2.6}$$

Physically, the first part of Equation 2.6 characterises the rate of decay of the displacement response while the second part defines the frequency of the oscillation. This solution is also often referred to as the 'transient response' of the system.

For the particular solution, Equation 2.1 must be solved where the external force $F(t)$, assumed here as a simple harmonic load for the purpose of simplicity, can be expressed as:

$$F(t) = F_0 \sin\omega_0 t \tag{2.7}$$

where F_0 and ω_0 is the amplitude and circular frequency of the loading, respectively. One option to solve the differential equation is to assume that the particular solution is of the form:

$$y_p(t) = X_C \sin \omega_0 t + X_D \cos \omega_0 t \qquad (2.8)$$

Substituting Equation 2.8 and its derivatives into Equation 2.1 and noting that $\xi = c/2m\omega$, X_C and X_D can be derived using simultaneous equations:

$$X_C = \frac{F_0}{k} \frac{1 - (\omega/\omega_0)^2}{\left(1 - (\omega/\omega_0)^2\right)^2 + (2\xi\,\omega/\omega_0)^2}$$

$$X_D = \frac{F_0}{k} \frac{2\xi\,\omega/\omega_0}{\left(1 - (\omega/\omega_0)^2\right)^2 + (2\xi\,\omega/\omega_0)^2} \qquad (2.9)$$

Similar to Equation 2.6, by introducing constant $X_0 = \sqrt{X_C^2 + X_D^2}$ and $\tan\varphi_0 = X_D/X_C$, Equation 2.8 can then be expressed as:

$$y_p(t) = X_0 \sin(\omega_0 t + \varphi_0) \qquad (2.10)$$

The sum of the homogenous and particular solutions results in the total solution:

$$y(t) = X e^{-\xi\omega t} \cdot \sin(\omega_D t + \varphi) + X_0 \sin(\omega_0 t + \varphi_0) \qquad (2.11)$$

Once the transient solution decays to zero, only the steady-state response will remain. An important parameter contained in the steady-state response is the dynamic magnification factor (DMF) which is the dynamic-to-static ratio of peak displacement. The factor is dependent on the damping ratio and frequency ratio (ratio between forcing frequency and circular frequency of the system). The DMF is at its maximum when the forcing frequency is equivalent to the circular frequency where, at this point, the system is in resonance. The DMF can be calculated as follows for small damping ratios:

$$DMF\ (\omega_0 = \omega) = \frac{1}{2\xi} \qquad (2.12)$$

For example, for a system with a damping ratio of 2%, the DMF would reach 25 at resonance i.e. the displacement under dynamic loading is 25 times the displacement under a static load.

For a more general periodic function, the external load can be expressed as a superposition of h harmonic contributions:

$$F(t) = \sum_{i=0}^{\infty} A_i e^{i\omega_i t} \tag{2.13}$$

where A_i is the Fourier amplitude of the i-th harmonic load component and ω_i is the circular frequency of the i-th component. The Fourier series concept is explored further in Section 2.2.4.1.

2.2.2 Forced vibration of a damped multi degree-of-freedom system

The dynamic properties of a SDOF system is only explained through its natural frequency (approx. equivalent to the damped natural frequency for structures with damping ratio less than 10%), damping factor and response in one direction. This means that an SDOF system only has one 'mode' of vibration in its direction of displacement. In reality, however, structures have multiple degrees-of-freedoms (MDOF) with the mass, stiffness and damping properties (also referred to as the 'spatial model' of a structure) expressed in matrix form and the responses defined in vector form, as shown in Equation 2.14. The dynamic equilibrium equation to an N degree-of-freedom system then becomes an eigenvalue problem which yields N different eigenvalues ω_n and eigenvectors $\{\psi_n\}$ for each mode n; the eigenvalues refer to the natural frequencies of each unique mode while the eigenvectors, each associated to a specific natural frequency and damping factor, describe the mode shape of the system (Ewins 2000). These modal properties are often referred to as the 'modal model' of the structure. As an MDOF system can be represented as the linear superposition of a number of SDOF systems (Ewins 2000), a detailed solution for Equation 2.14 is not provided here. Although, one method to convert the spatial model to the modal model is through modal analysis which will be detailed further in the following section.

$$[M]\{\ddot{y}(t)\} + [C]\{\dot{y}(t)\} + [K]\{y(t)\} = \{F(t)\} \tag{2.14}$$

2.2.3 Experimental Modal Analysis

Experimental Modal Analysis (EMA), also referred to as 'modal parameter extraction' or 'modal parameter identification', is a procedure of obtaining the modal properties (i.e. the modal model) through curve fitting of an analytical transfer function. This modal model, which consists of natural frequencies, modal damping ratios and mode shape

vectors, can then be used to extract the mass, damping and stiffness matrix to determine the spatial model of the system. Consequently, EMA is useful in a range of areas including design, diagnosis and control of systems in regards to vibration (de Silva 2000). As defined in de Silva (2000), the general steps of EMA as undertaken in this research are as follows and will be described in greater detail in the subsequent sections:

1. Obtain a set of test data which consists of force excitation (input) and motion response (output) of the test object.

2. Compute the frequency response functions (FRFs) of the pairs of test data using Fourier analysis. This process can generally be undertaken using computing software such as MATLAB.

3. Curve fit analytical transfer functions to the computed transfer functions. This process is generally undertaken in commercial experimental modal analysis software such as LMS Test.Lab (LMS International 2012).

4. Compute mode shape vectors.

2.2.3.1 Measurement procedure and equipment

The basic measurement system consists of three main items: an excitation mechanism, transducers which measure the force input and response (output) of the system and a means of data recording and analysis. The source of excitation is typically either from a portable shaker or instrumented impact hammer with each having their advantages and disadvantages. The selection of which source to use depends on availability of equipment, the type of structure and requirements of results (Friswell & Mottershead 1995).

Hammer excitation involves impacting the structure to generate an impulsive excitation followed by the structure undergoing a free decay of vibration. The hammer head contains a force transducer with a piezoelectric crystal which generates an electric charge due to deformation (Sinha 2015a). The hammer tip can be changed depending on the required frequency band of excitation; a soft hammer tip is used for a low frequency band of excitation while a harder tip is used if a larger frequency band is required.

Unlike the instrumented hammer, a shaker allows for a precise frequency range to be excited where a known signal can be generated (sinusoidal, random multisine, or sweep-sine). However, the shaker must be fixed to the structure which, particularly for lighter

structures, may subsequently change the dynamic properties through the addition of mass, or local stiffening though the connection point.

Figure 2-2 illustrates the measurement procedure for input and output signals for impact hammer excitation with accelerometers as response transducers; such a set-up is also referred to as a SISO (single-input, single-output) or SIMO (single-input, multiple-output) test.
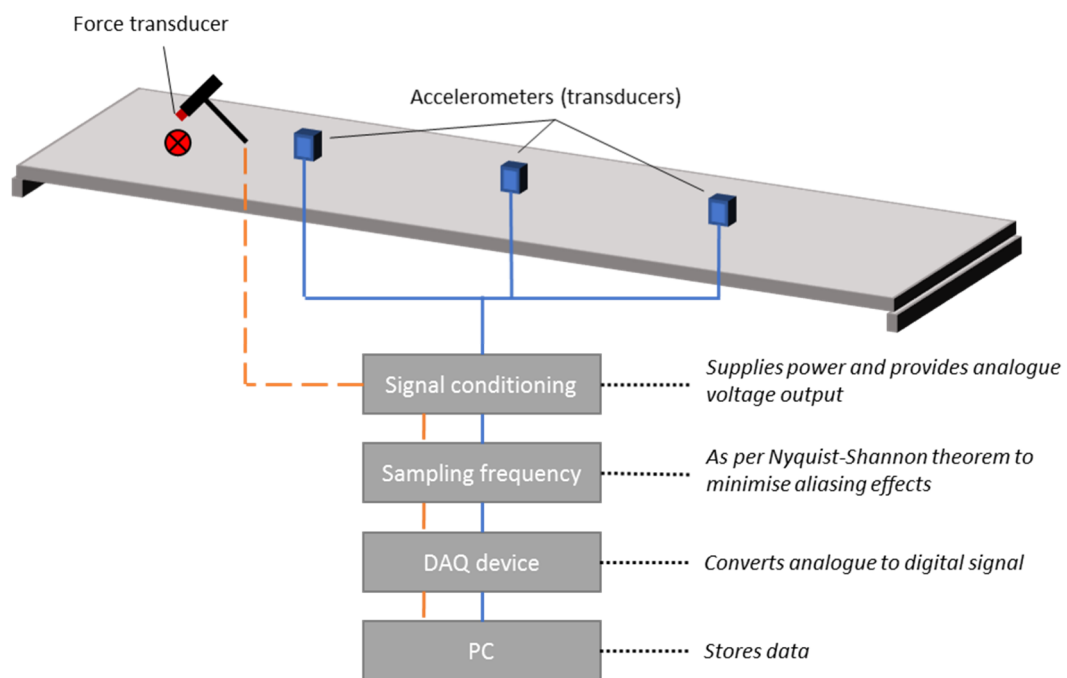
Figure 2-2 *Measurement procedure for modal analysis using hammer excitation (diagram adapted from Friswell and Mottershead* (1995) *and Sinha* (2015b))

Piezoelectric accelerometers are the most popular and commonly used acceleration transducers in practice and consist of a piezoelectric crystal (acting as a spring) attached to a mass, as shown in Figure 2-3. The acceleration response of the floor system causes an inertial force in the piezoelectric crystal and generates an electric charge which is proportionate to the acceleration. Piezoelectric accelerometers typically have a resonant frequency ≥ 50 kHz and are therefore appropriate for the low frequencies experienced in floor systems. Through signal conditioning and correct calibration of the sensitivity of each accelerometer (typically 100 mV/g), the electric charge can then be converted to an analogue voltage signal.
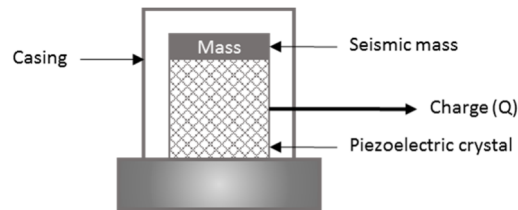
Figure 2-3 *Piezoelectric accelerometer components*

One important consideration in signal processing is the selection of an appropriate sampling frequency (f_s) which defines a rate at which the computer stores data (Sinha 2015b). If the sampling rate is too slow, a phenomenon referred to as 'aliasing' can occur. This phenomenon is illustrated in Figure 2-4 where two sinusoidal signals with frequencies $f_1 = 0.2$ Hz and $f_2 = 0.8$ Hz are shown. With a sampling rate of 1 Hz, the data samples of both signals will be identical which means the higher frequency signal cannot be distinguished from the lower frequency signal. One solution to minimise aliasing is by following the Nyquist sampling theorem which states that the sampling frequency must be at least twice the maximum frequency of interest i.e. if the maximum frequency of interest is 1 Hz (as per the illustration in Figure 2-4), a sampling frequency of at least 2 Hz or 2 samples per second should be selected. In conjunction with an appropriate sampling frequency, an anti-aliasing filter is then used to prevent all frequencies above the cut off frequency, which is equal to the Nyquist frequency (half the sampling frequency), from appearing in the analogue signal. The signal then passes through the data acquisition (DAQ) device, transferring the analogue (continuous) signal into a digital (discrete) format through a binary representation and is collected on the PC. The accuracy of the digital signal depends on the number of binary digits (bits) of the device; nowadays, at least 16-bit devices are normally used (Friswell & Mottershead 1995).
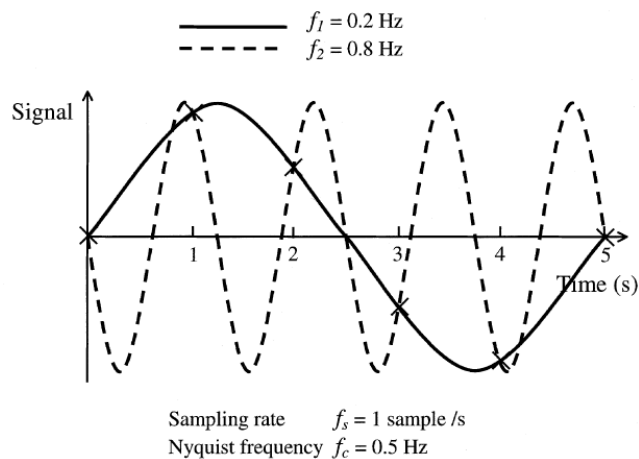
Figure 2-4 *Illustration of aliasing phenomenon (Clarence W. de Silva 2000)*

2.2.4 Computing the frequency response functions

2.2.4.1 Fourier analysis

For complex waveforms (i.e. signals made up of more than one sine wave as shown in Figure 2-5), visualising the characteristics of the signal is difficult and thus the preferred approach is to transform the time domain data to the frequency domain through a Fourier Transform (FT). The FT theory states that any periodic signal with time period T can be represented by a superimposition of an infinite series of sinusoids of different frequencies, amplitudes and phases referred to as the 'Fourier series'. In reality, many signals are non-periodic (for example, a floor system response from occupant walking) and in this case, the series is represented by a Fourier integral of complex form with time period T approaching infinite (Ewins 2000):

$$x(t) = \int_{-\infty}^{\infty} X(\omega)e^{i\omega t} d\omega \tag{2.15}$$

where: $$X(\omega) = \frac{1}{2\pi} \int_{-\infty}^{\infty} x(t)e^{-i\omega t} dt \tag{2.16}$$

Equation 2.15 and 2.16 are commonly known as the Fourier transform pair where $x(t)$ is called the inverse Fourier transform of $X(\omega)$. As described in Section 2.2.3.1, both input and output signals are measured at discrete time intervals defined by the sampling frequency ($\Delta t = dt = 1/f_s$). Consequently, numerical evaluation of the Fourier integral pair involves a finite number of the sampled values N with an artificial time period equivalent to $T = Ndt$ and maximum frequency considered up to the Nyquist frequency ($f_s/2$). Therefore, the Fourier transform pair defined in Equation 2.15 and 2.16 can be expressed as a finite sum (Maia et al. 1997):

$$x(k) = \sum_{j=0}^{N-1} X(j)e^{i2\pi jk/N} \tag{2.17}$$

where: $$X(j) = \frac{1}{N} \sum_{k=0}^{N-1} x(k)e^{-i2\pi jk/N} \tag{2.18}$$

for j = 0, 1, 2,…, N-1; k = 0, 1, 2,…, N-1. Equations 2.17 and 2.18 are referred to as the discrete Fourier transform (DFT) which is nowadays efficiently evaluated using the Fast Fourier Transform (FFT) algorithm developed by Cooley and Tukey (1965).
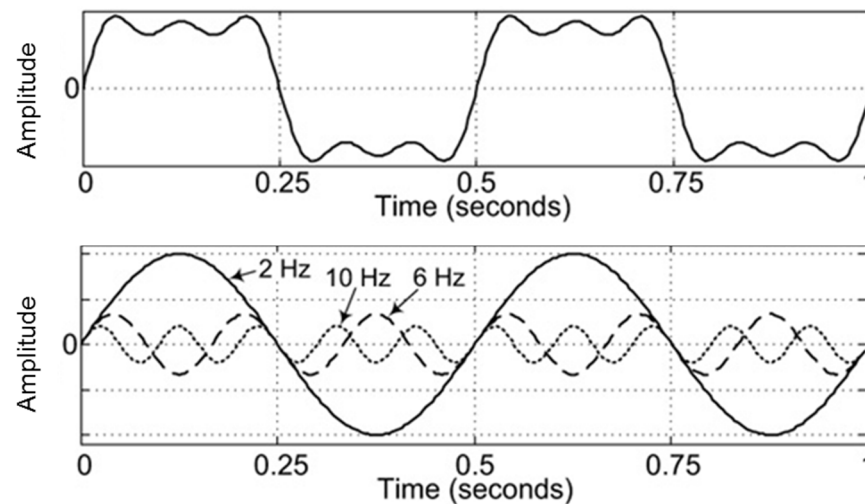
Figure 2-5 *A square sine (top) and its sine wave components (bottom)* (Lyons & Fugal 2014)

The DFT assumption that a non-periodic signal repeats periodically based on an artificial period creates a challenge for signal processing, causing a phenomenon called 'leakage' to occur. In relation to periodic signals, this issue also occurs when the selected time period does not match the true period of the signal. This is illustrated in Figure 2-6 where leakage causes energy to spill into the adjacent frequencies resulting in a reduced amplitude representation of the true signal. Ways to reduce the effect of leakage include applying a window function to the signal; a commonly used window for continuous signals is the Hanning window, while for transient signals, an exponential window may be used (Friswell & Mottershead 1995).
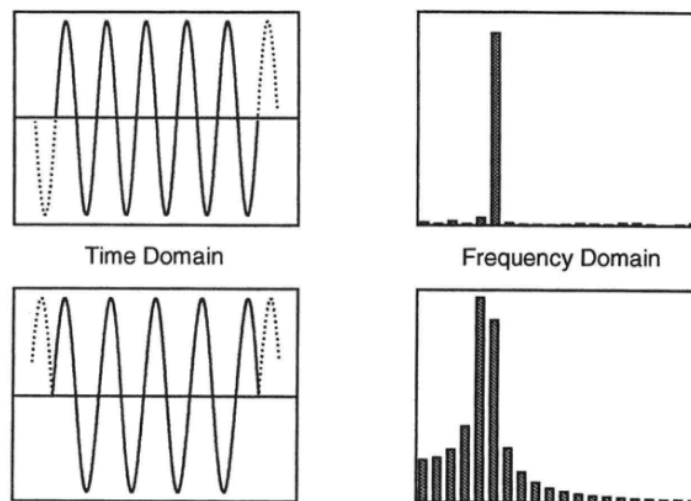
Figure 2-6 *Effect of sample length and leakage Fourier transform of a periodic signal* (Friswell & Mottershead 1995)

2.2.4.2 The frequency response function

The primary objective of performing modal testing is to obtain the frequency response function (FRF) from which the modal properties of the system can be estimated. Recalling the Fourier transform pair (Equation 2.15 and 2.16), we can mathematically express the fundamental relationship between the measured input and output of a system as:

$$X(\omega) = H(\omega)F(\omega) \tag{2.19}$$

where $H(\omega)$ = FRF for the input and output signals; $X(\omega)$ and $F(\omega)$ are the Fourier transforms of the response (output) and excitation (input) signals, respectively. Estimates of the FRF (referred to as 'FRF estimators') are then calculated using either $H_1(\omega)$ or $H_2(\omega)$ estimators which are found via auto-spectral and cross-spectral densities defined by auto-correlation and cross-correlation functions. The former estimator is used if the output is expected to contain more noise than the input while the latter is used when there is more noise expected on the input signal. By dividing the $H_1(\omega)$ estimator by the $H_2(\omega)$ estimator, the coherence function can be obtained which illustrates the quality of the measured data as a function of frequency. A value of coherence is always between 0 and 1 where a higher coherence value indicates accurate data while low values indicate poor quality data. The reader is referred to Friswell and Mottershead (1995) for detailed formulas for the $H_1(\omega)$ or $H_2(\omega)$ estimators. Figure 2-7 reveals an example of the force input and output signal and the subsequent FRF amplitude and coherence plots.
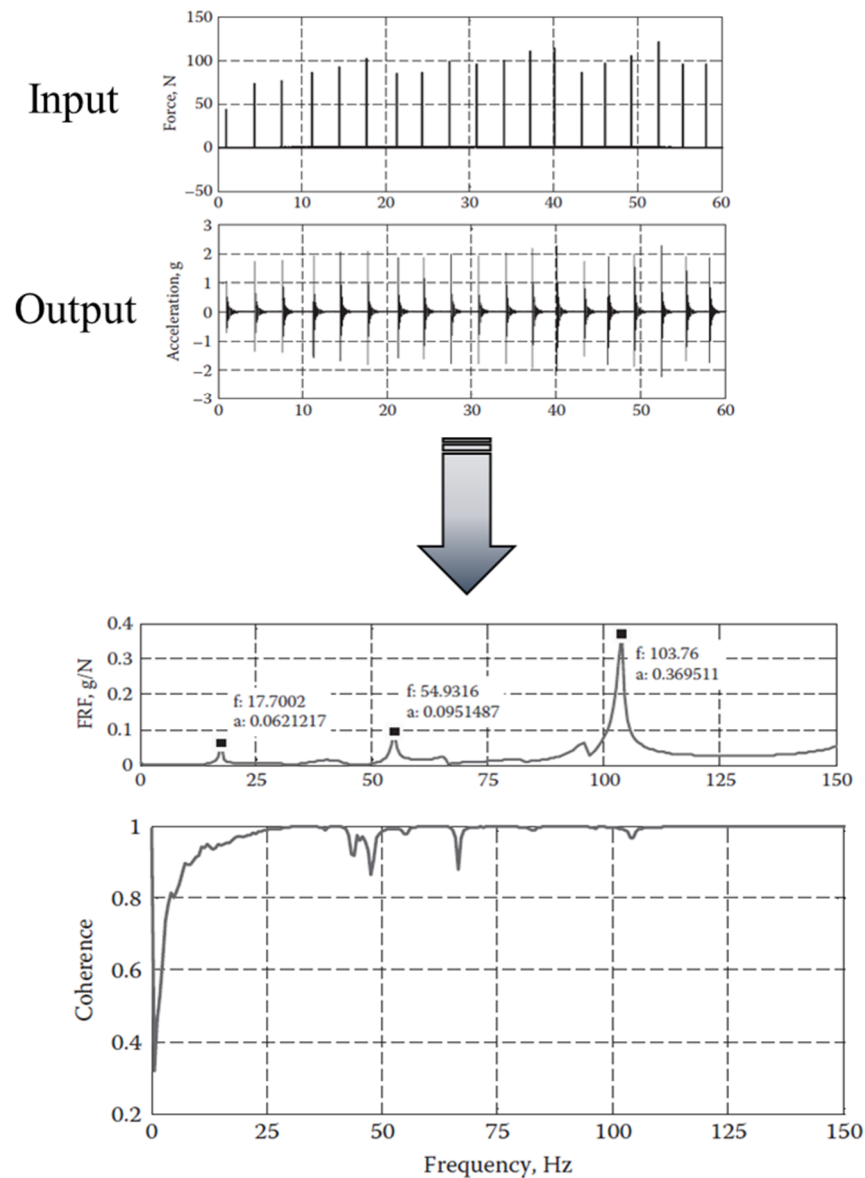
Figure 2-7 *Example of typical measured data from an instrumented hammer test and subsequent FRF amplitude and coherence, adapted from* (Sinha 2015b)

2.2.5 Curve fitting methods

Modal parameters of a system can be identified by curve fitting an analytical or synthesised FRF to the computed FRF from test data. Parameter identification methods are first distinguished by the domain in which the data are treated numerically: time domain or frequency domain. In general, time domain models tend to provide the best results when a large frequency range or large number of modes exist in the data, while frequency domain methods provide better results when frequency range is limited and there is a small number of modes (Maia et al. 1997). Depending on whether a single mode is to be extracted at a time, or several, a single-degree-of-freedom (SDOF) or multi-

degree-of-freedom (MDOF) procedure is chosen, respectively (Ewins 2000). This section provides fundamentals of the least-squares complex exponential (LSCE) time domain method and the least-squares frequency domain (LSFD) frequency domain method, which are two often coupled methods that are widely used in practice including in the EMA software LMS Test.Lab (LMS International 2012). A comprehensive review of these and other modal parameter identification methods can be found in Maia and Silva (1997).

2.2.5.1 Least-squares complex exponential method

The LSCE is a SIMO, indirect, MDOF approach based on the SISO complex exponential (CE) method. SIMO modal analysis methods (also referred to as global methods) allow multiple FRFs to be obtained from a number of points on the structure due to excitation at one location. This provides more information of the modal model compared to SISO methods. The CE (and LSCE) method works with data derived from the inverse Fourier transform of the FRF (i.e. from frequency to time domain), also called the impulse response function (IRF), and is based on the principle that any IRF for a viscously damped system can be expressed as a series of complex exponential components (Ewins 2000). As the FRFs are typically measured with a constant sampling frequency, the IRFs obtained will also be sampled at equally spaced time intervals.

The LSCE method simultaneously processes several IRFs (depending on the number of output points) and provides a consistent set of global parameters (natural frequencies, damping ratios and residues) using a technique called 'Prony's method' named after the 18th century French mathematician Prony (1795). The only unknown is the number of modes that need to be considered; this is determined through an iterative process of repeating the analysis for a decreasing number of assumed modes. For each analysis, the error between the regenerated FRF (from the modal properties identified) and the original measured data is calculated and subsequently plotted on a 'stabilisation diagram', as shown in Figure 2-8. When there is an overestimation of the number of modes, 'computational' modes will appear in addition to the 'physical' or genuine modes. Distinguishing a computational mode from a genuine mode can involve checking that a mode has recurring stability with near identical frequency and damping ratios. Further, computational modes typically have unusually high damping ratios (Ewins 2000).

Symbols

S - Stable frequency, damping and vector within tolerance
V - Stable vector within tolerance
D - Stabe frequency and damping within tolerance
F - Stable frequency within tolerance
O - Pole is not stable
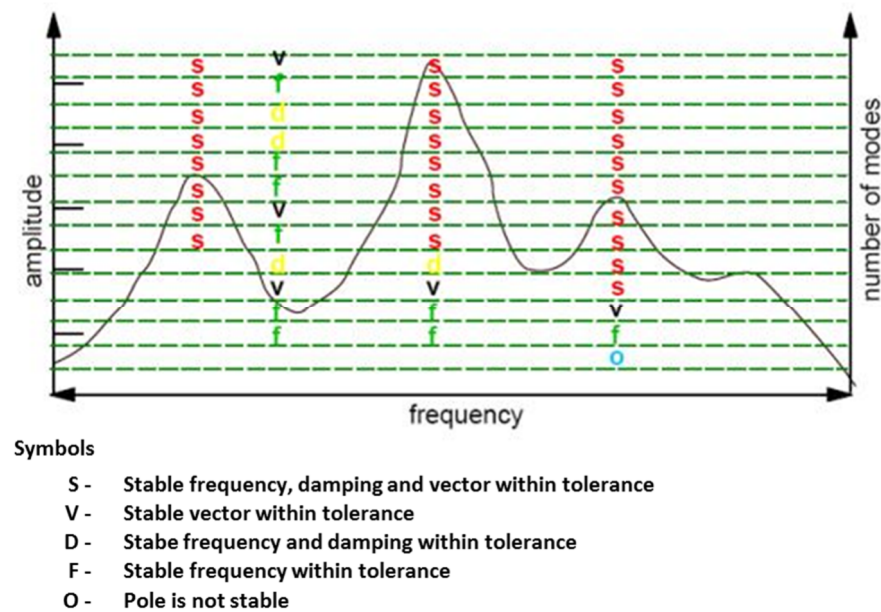
Figure 2-8 *Example of a stabilisation diagram* (LMS International 2012)

2.2.5.2 Least-squares frequency domain method

The least-squares frequency domain (LSFD) is an indirect, MDOF, SIMO method which uses the frequency and damping ratio estimates from the LSCE method to estimate the mode shape coefficients. Firstly, the frequency band of interest is defined by specifying the start and end frequencies. Residual effects of modes outside the defined frequency band are then taken into account by including the mass-like behaviours for the modes lower than the lower frequency boundary and the stiffness-like behaviours for the modes higher than the upper frequency boundary (Ewins 2000).

2.3 Humans as vibration source for floors

Humans are the most usual and important internal source of dynamic excitation for floors in office buildings or apartments (Ellingwood & Tallin 1984; Smith, Hicks & Devine 2009). Other vibration sources include machinery with rotating or oscillating parts and external sources such as road and rail traffic and construction works. However, when problems from these sources are expected, the common approach is to isolate the machine (in the case of vibrating machinery) or building as a whole (Wyatt 1989). As such, these sources have not been concerned with in this research.

2.3.1 Gait cycle

Gait analysis is a branch of biomechanics which investigates the study of human locomotion from mechanical perspectives. Civil and structural engineers rarely come across gait analysis. However, to understand the nature of human induced vibration of structures, especially in terms of footfall, it is essential to be familiar with basic terminology. In literature, gait normally describes the manner or style of human locomotion where a gait cycle is the period of time between any two nominally identical events in the walking process (Racic, Pavic & Brownjohn 2009). In other words, the gait cycle starts from the moment the right heel comes into contact with the floor and finishes when the right heel once again touches the floor, as shown in Figure 2-9.
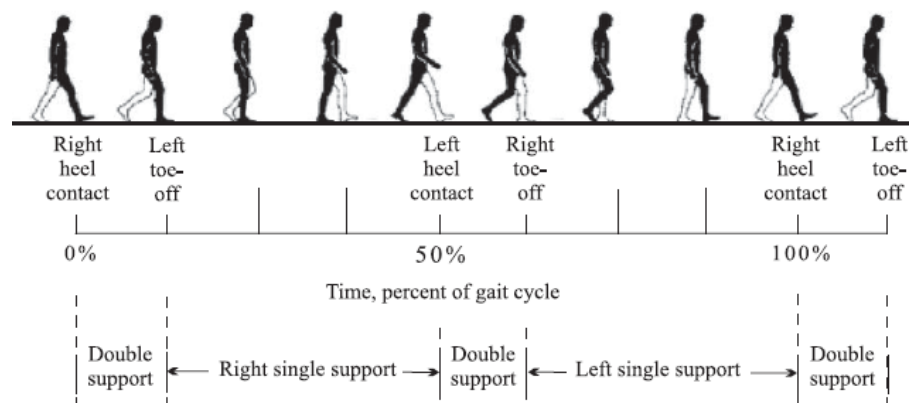
Figure 2-9 *The gait cycle* (adapted from Inman, Ralston & Todd 1981; Racic, Pavic & Brownjohn 2009)

Gait contains large inter- and intra-subject variabilities which influence the shape of the ground reaction force. The former refers to the differences between different individuals such as body mass and spatial and temporal parameters of gait, while the latter refers to the differences between two consecutive footsteps performed by the same person. Typical spatial parameters include the step length, stride length, step width (or stride width) and step duration (Racic, Pavic & Brownjohn 2009); some of these concepts have been illustrated in Figure 2-10. The temporal parameters involve the pace frequency (or step frequency) which is expressed in Hz (i.e. steps per second), and the walking speed expressed in metres per second.
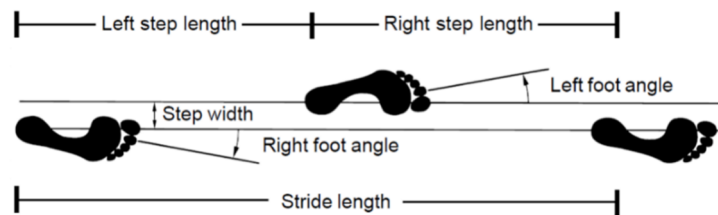
***Figure 2-10** Spatial parameters of human walking (Vaughan, Davis & O'Connor 1999)*

2.3.2 Ground reaction force

When a person walks across a floor, the loading is primarily in the vertical direction (Fujino et al. 1993). An example of the vertical ground reaction force of one footstep normalised by the walker weight is shown in Figure 2-11. The footfall trace starts with a short spike, typically lasting for 10 – 20 ms (Racic, Pavic & Brownjohn 2009), when the heel strikes the ground (referred to as the heel strike transient in Figure 2-11). The weight is then accepted by the heel creating the first peak (F1) to which the foot then rolls across the surface (F2) and transfers the weight to the front part of the foot with the push-off phase causing the second peak (F3) (Racic, Pavic & Brownjohn 2009). The heel strike transient has been shown to contain frequency components in the 10 to 75 Hz range while the rest of the trace contains frequency components up to 10 Hz (Kerr 1998; Simon et al. 1981).
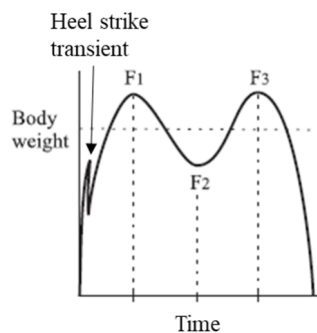
***Figure 2-11** Vertical ground reaction force of one footstep normalised by walker weight (adapted from Racic, Pavic and Brownjohn (2009))*

An early study on ground loading from footsteps found that the subject weight and pace frequency were the most important parameters in defining the shape of the forcing function (Galbraith & Barton 1970). Footwear (with or without) and type of floor surface (sand or hand surface) were shown to have little effect. The importance of the pace frequency to the ground reaction force was also shown by Wheeler (1982) who compiled the works of other researchers to present the forcing functions for six modes of human

movement including slow walk, normal walk, brisk walk, fast walk, slow jog and running; these forces have been reprinted in Figure 2-12. Further, it was revealed that spatial gait parameters such as stride length and step duration (or contact time) have a strong dependence on the pace frequency. For example, longer stride lengths occurred as pace frequency increased up until 3 Hz, after which the stride length plateaued as the subject breaks into a jog or run (Wheeler 1982).
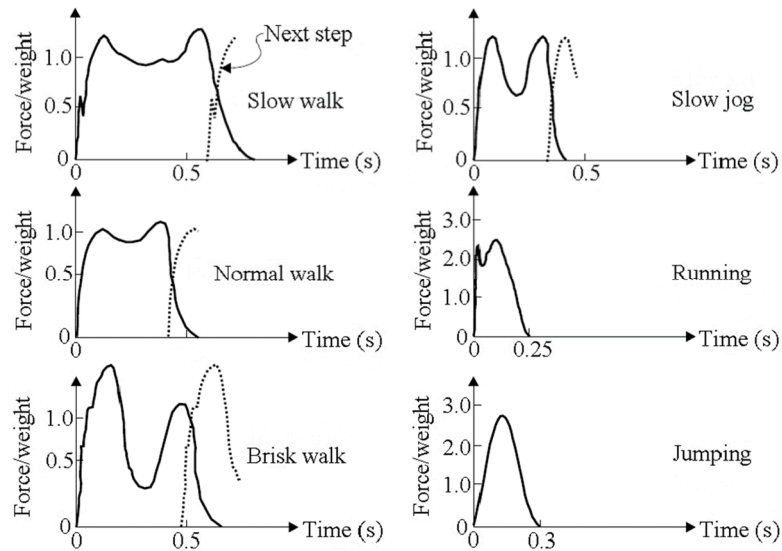
Figure 2-12 Force patterns for different types of human activities as investigated by Wheeler (1982) *(image from Glisovic & Stefanovic* (2010) *adapted from Wheeler* (1982))

2.3.3 Modelling of human walking

Adequate modelling of human walking is instrumental in achieving a sufficiently accurate response prediction for design purposes. As shown in Figure 2-13, human walking models can be expressed in the time- or frequency-domain. The time-domain force model can be further separated into a deterministic or probabilistic model.
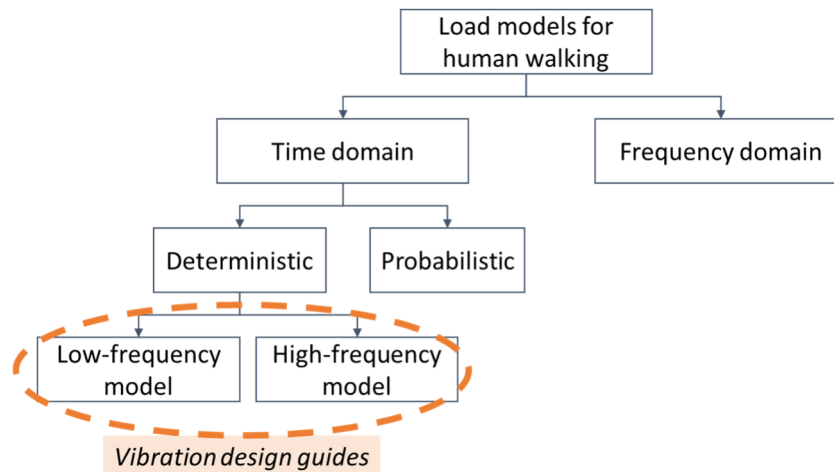
Figure 2-13 *Mathematical modelling of human walking*

2.3.3.1 Deterministic time-domain force models

Figure 2-14 shows an example of a continuously measured walking force signal. The intra-subject variability is clearly visible and is characterised by the slightly different peak amplitudes formed during the double support phase (as shown in Figure 2-9). As a result, the action of continuous human walking is, in reality, a near-periodic action. To simplify the design process, deterministic force models disregard these variabilities by making a number of assumptions including:

- The ground reaction force of the left and right footsteps is identical.
- The pace frequency that a person adopts is constant for that walking activity.
- There is no interaction between the walker and the structure.

These assumptions mean that the action of continuous walking can be regarded as a perfectly periodic process represented by a Fourier series of *n* harmonics and is uniform for any individual with the same mass. This is the common approach assumed in the three main vibration design guides published by the Concrete Centre (referred to as CCIP-016) (Willford & Young 2006), Steel Construction Institute (referred to as SCI P354) (Smith, Hicks & Devine 2009) and the American Institute of Steel Construction (referred to as AISC DG11) (Murray et al. 2016).
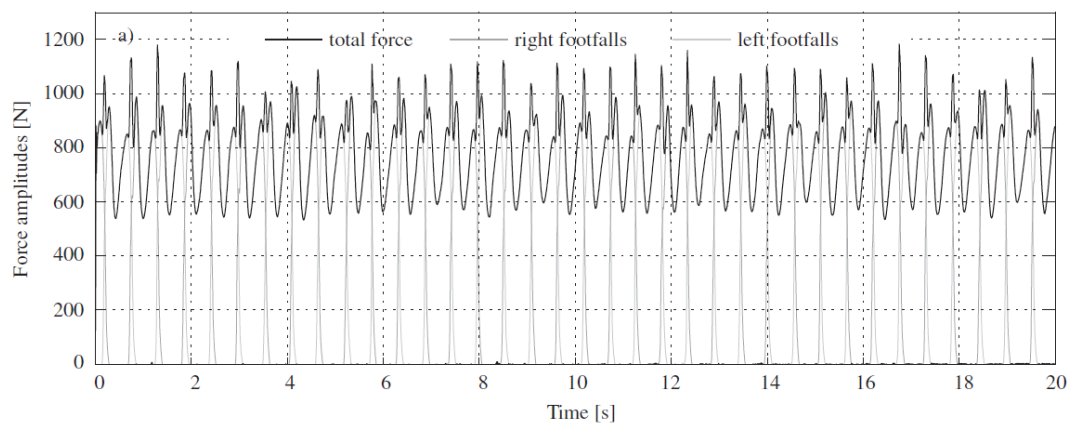
Figure 2-14 *An example of continuously measured walking force signal as measured by Racic and Brownjohn (2011)*

Continuous force models are synthesised by adding identical single footfall traces in sequence with an overlapping period equal to the double support phase (the small period between two footsteps in which the two feet are in contact with the ground at the same time); an example of this process is shown in Figure 2-15. The Fourier series load is expressed as follows (Bachmann, Pretlove & Rainer 1995):

$$F(t) = Q\left[1 + \sum_{i=1}^{n} \alpha_i \sin(2\pi i f_p t - \phi_i)\right] \tag{2.20}$$

where Q = walker weight (N); α_i = Fourier coefficient of the i-th harmonic generally known as the Dynamic Load Factor (DLF); f_p = pace frequency (Hz); ϕ_i= phase angle of the i-th harmonic. Note this equation is in similar form to Equation 2.131313 and essentially becomes the external forcing function in the dynamic equilibrium equation.

The total number of contributing harmonics n can approach infinity, however, generally only the first four harmonics are considered with studies showing that this is where most of the energy is contained (Jacobs & Skorecki 1972; Rainer, Pernica & Allen 1988). A harmonic can be defined as an integer magnitude of the pace frequency where, for example, the second harmonic of a pace frequency of 2 Hz would be 4 Hz while the third harmonic would be 6 Hz, and so on. Equation 2.20 is the walking load function applied to floors classified as low-frequency which are supposed to be more susceptible to resonance with one of the harmonics of human walking; an example of a typical resonant response of a low-frequency floor is shown in Figure 2-16. Floors are classified as low-

frequency if their fundamental frequency is less than approximately four times the maximum human walking pace (i.e. < 10 Hz).
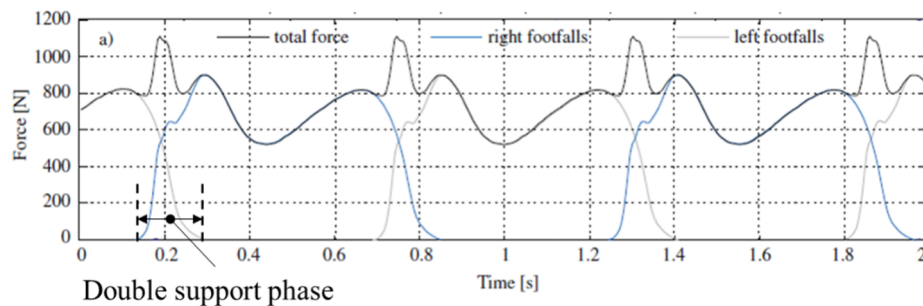
Figure 2-15 *Example of duplication of a single footfall trace to create a synthetic continuous time history. Double support phase has been annotated. Adapted from Racic and Brownjohn* (2011).
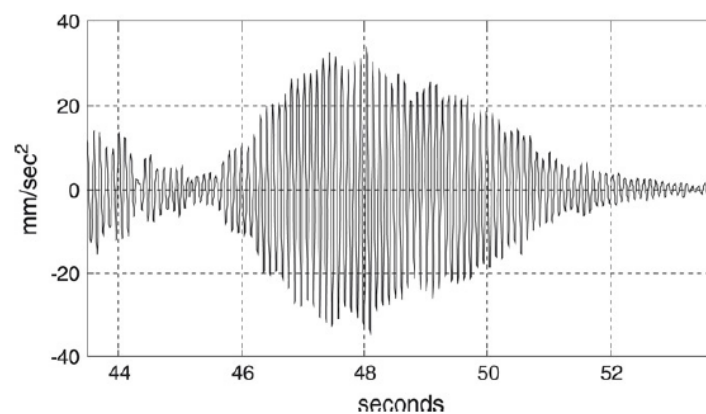
Figure 2-16 *Typical floor response of a low-frequency floor from walking* (Brownjohn & Middleton 2008)

For high-frequency floors, the floor response is generally characterised by an initial peak, associated with each heel impact, followed by a decay to practically zero before the next footstep occurs, as shown in Figure 2-17. Willford et al. (2006) proposed that this action is similar to a SDOF system subject to a series of impulses. If the modal mass of the SDOF system is 1.0, then the initial velocity is numerically equal to the applied impulse. Using continuous walking forces synthesised from 880 single footfall traces measured by Kerr (1998), the velocity response of a SDOF system with various natural frequencies and damping ratios were calculated. The peak velocities were then extracted which numerically are the values of the effective impulse for that footfall record as the floor frequencies varied; hence this modelling approach is often referred to as the 'effective impulse' approach. Willford et al. (2006) proposed a 'design' effective impulse (in Ns) which has a 25% chance of exceedance:

$$I_{eff} = A \frac{f_p^{1.43}}{f_n^{1.3}} \tag{2.21}$$

where A = coefficient equal to 54 and f_n is the natural frequency of mode n. The approach has been validated with on-site measurements of steel-concrete composite and reinforced concrete floors (Willford, Young & Field 2006) and is incorporated in floor vibration design guides such as CCIP-016 (Willford & Young 2006) and the Concrete Society in Appendix G (Pavic & Willford 2005).
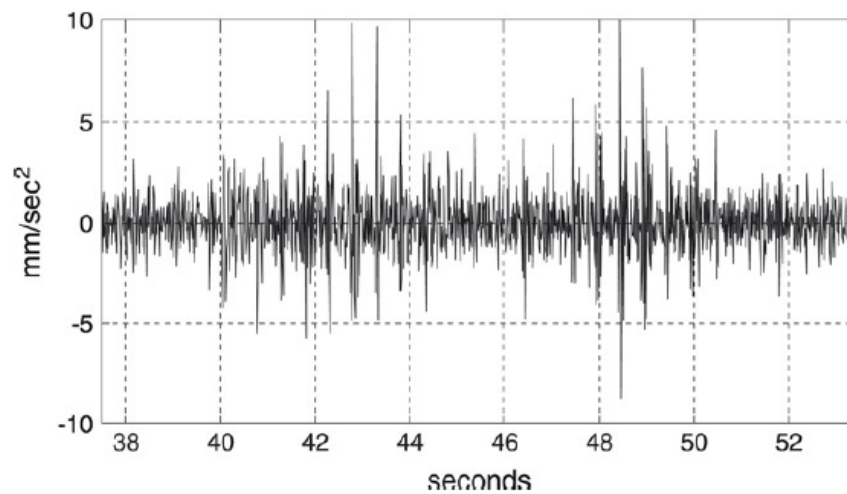
Figure 2-17 *Typical floor response of a high-frequency floor from walking* (Brownjohn & Middleton 2008)

The appropriateness of separating floors by their anticipated response has been debated by a number of researchers (Brownjohn & Middleton 2008; Ellis 2000; Živanovic & Pavic 2009) with studies showing that a degree of resonant amplification can still be caused by harmonics above the fourth multiple (Brownjohn & Middleton 2008; Ellis 2000). Furthermore, Brownjohn et al. (2016) noted that, in the UK, there have been cases observed in practice of floors classified as 'low-frequency' having high-frequency modes with low modal masses which can be excited by footstep impulses. Although the type of floor construction of these floors is not stated, floors with frequencies less than 8 Hz are likely to be long-span with low damping. In addition, Živanović et al. (2009) also noted that there is a grey area for the reliability of response prediction for floors which sit on the borderline of the cut-off frequency. To avoid some of these inconsistencies a recent study has suggested that a 14 Hz cut-off frequency is more appropriate (Mohammed, Pavic & Racic 2018), while another study has proposed a Fourier series equation including five harmonics to represent the continuous walking load (Živanović, Pavic &

Reynolds 2007b). Frequency domain methods (as will be discussed in Section 2.3.3.3) such as the response spectrum approach by Brownjohn et al. (2016) have also been suggested which can be used for any floor types with a fundamental frequency between 1 – 20 Hz.

2.3.3.2 Probabilistic time-domain force models

Probabilistic time-domain force models consider the inherent inter- and intra-subject variabilities through statistical distributions of key gait parameters including step frequency and step length, as well as DLFs and phase angles. The advantage of this model over a deterministic modelling approach is that predicted response can be expressed through a range of possible responses and the probability that the response will not exceed a certain level of vibration can be obtained. The probabilistic approach to human walking models allows the engineer to make a more informed decision on the response of the floor which can be particularly beneficial for floors governed by vibration serviceability design.

Studies have shown that the pace frequency of humans under natural walking generally follows a normal distribution with a mean of 2 Hz and small standard deviations. Matsumoto et al. (1978) were the first to report the statistics of step frequencies through measurement of pace frequencies of 505 people walking naturally along roads in Japan. It was found that walking pace frequencies ranged from 1.5 – 2.5 Hz and followed a normal distribution with a mean of 1.99 Hz and standard deviation (σ) of 0.173 Hz. Bachmann and Ammann (1987) noted that investigations by Schulze (1980) also found a mean of 2 Hz ($\sigma = 0.13$ Hz). Similar findings have been reported by Pachi and Ji (2005) who measured the number of steps and time taken to cross two shopping floors and footbridges. Results showed an average walking pace of 1.8 Hz ($\sigma = 0.11$ Hz) and 2.0 Hz ($\sigma = 0.13$ Hz) for footbridges and shopping floors, respectively. The study also found that men and women had different mean step lengths of 0.75 m and 0.67 m, respectively. In contrast, a study undertaken in an office building in Delft found that the distribution appeared to be lognormal rather than a normal distribution, although the mean pace frequency of 2.0 Hz ($\sigma = 0.17$ Hz) was still similar to other studies (Sedlacek et al. 2006).

Deterministic models generally assume an average weight of 76 kg for pedestrians (Smith, Hicks & Devine 2009; Willford & Young 2006). Although not stated, this value appears to be from a study undertaken by Portier et al. (2007) who reported an average weight of 75.61 kg (σ = 18.02 kg) following a lognormal distribution from a sample of 13,462 adults in the U.S. aged between 18 – 65. However, as reported in Chen et al. (2019), Xiao-guang et al.(2005) collated body weight statistics on a sample of 202,749 Chinese participants in urban areas which showed that young adults (18 – 44 years) presented a normal distribution with mean of 62.4 kg (σ = 12.0 kg). Middle-age adults (45 – 59 years) also presented with a normal distribution with mean of 64.5 kg (σ = 10.9 kg). This highlights the differences between average weights in countries and the potential for probabilistic models to be customised to the individual country's statistics.

Other parameters where probability distributions can be considered are the DLF and the phase angles. Kerr (1998) measured of over 1000 individual footfall traces from 40 subjects and found that the DLF for the first harmonic was dependent on the walking frequency with a mean as follows:

$$\mu_{DLF1} = -0.2649f_p^3 + 1.3206f_p^2 - 1.7597f_p + 0.7613 \tag{2.22}$$

The distribution about the mean can be obtained by a normally distributed factor *MF* with mean of 1 and standard distribution of 0.16 (Živanović, Pavic & Reynolds 2007b). For the DLFs of the second (DLF_2), third (DLF_3) and fourth (DLF_4) harmonics, there was no relationship to the pace frequency and large amounts of scatter were reported. The mean values reported by Kerr (1998) were 0.07, 0.05 and 0.05 for the DLF_2, DLF_3 and DLF_4, respectively. Using Kerr's (1998) data and assuming a normal distribution for each walking frequency, Živanović et al. (2007b) obtained the standard distribution for the second, third and fourth harmonics as 0.03, 0.02 and 0.02. Based on 95 force time histories measured by Brownjohn et al. (2004), Živanović et al. (2007b) also determined the mean and standard distribution of the fifth harmonic as 0.03 and 0.015, respectively. In Živanović et al. (2007b) study, phase angles were found to be uniformly distributed in the interval of [-π,+ π] for any force time history analysed. Nevertheless, variability in phase angles have been reported to have little difference to structural response (Wang & Chen 2017).

Probabilistic force models for human walking have been proposed by Živanović et al. (2007b) and Chen et al. (2019) which will be discussed further in Chapter 5 when walking load models are investigated.

2.3.3.3 Frequency-domain force models

Frequency-domain force models formulate the action of human walking in terms of its frequency contents. On the basis of Ohlsson's (1982) initial study of the auto-spectral density (ASD) of the walking force, Eriksson (1994) investigated the frequency-domain modelling of continuous walking for floors with fundamental frequency below 6 Hz. His research found that although the main peaks of the ASD occurred at the harmonics of the walking pace, there was some 'leakage' of energy into adjacent frequencies, as shown by the arrows in Figure 2-18. These results indicated that human walking forces are not perfectly periodic and should be described as a random process (Eriksson 1994). Studies by Brownjohn et al. (2004) revealed that this leakage was more pronounced for higher harmonics and generally resulted in a reduced response compared with the response prediction using a perfectly periodic model (Equation 2.26). Brownjohn et al. (2016) has since proposed a response spectrum method for predicting walking-induced floor vibration which was validated with 14 floors of varying construction and occupancies.

The time-domain load model proposed by Živanović et al. (2007b) is first constructed in the frequency domain using 40 amplitudes for each harmonic including five harmonics and five subharmonics; the walking force is therefore formulated for a frequency range of $0.25f_p$ to $5.25f_p$. This is in contrast to the deterministic low-frequency time-domain model (Equation 2.20) which only calculates the force at the first four integer multiples of the pace frequency. More recently, Chen et al. (2019) proposed a frequency domain load model considering the first four harmonics and subharmonics which was validated through field measurements on an as-built long-span floor.
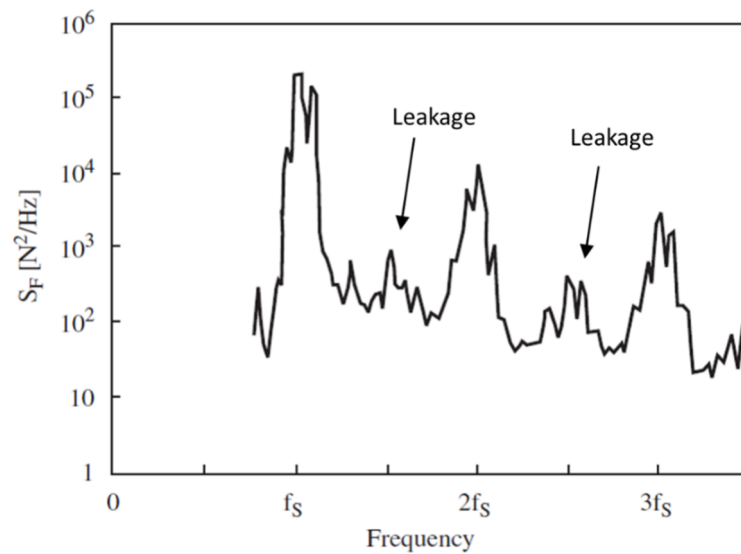
Figure 2-18 *Autospectral density of the walking force (annotated with points of leakage) (after Eriksson (1994))*

2.4 Timber floors as a transmission path

As shown in the dynamic equilibrium equation (Equation 2.124), the response of the transmission path due to walking-induced excitation is dependent on the mass, stiffness and damping which are physical properties of the floor. Solving the eigenvalue problem then leads to the modal properties of the floor where behaviour is described in terms of the mode shapes, eigenfrequencies, modal damping and modal mass. A reliable estimate of the floor response is contingent on accurate estimation of these modal properties. Simple equations based on theoretical solutions for simply-supported beams or plates can be useful for quick estimates of frequencies and modal mass. However, for the design of mid-rise commercial buildings which warrants a more thorough analysis, finite element (FE) software is generally used to develop a model of the floor.

For timber floors, there are several unique physical characteristics which will influence the modal properties that should be considered in the FE model. These include: support conditions, orthotropic behaviour, damping and floor connections. Although properties such as mass and span also play a role, these have not been discussed as they are aspects which are inherent to the material or design requirement and generally cannot be modified.

2.4.1 Support conditions

Ribbed-deck floors in commercial buildings are usually incorporated into a post-and-beam timber frame system and span between primary beams. Vertical gravity forces are transferred via a corbel, pocket or steel hanger connection, as shown in Figure 2-19(a), (b) and (c) respectively. At the same time, horizontal shear forces can be transferred by directly screwing the top flange to the primary beam. Since the majority of the vertical forces are transferred in shear through the web member, shear deformation of the web element should be considered, particularly since the shear modulus of timber is low (i.e. 0.66 GPa for LVL13 grade compared to 80 GPa for structural steel). Skaggs and Bender (1995) found that for relatively longer spans where span-to-depth ratio is greater than 20, the simple deflection equations due to bending slightly over-predicted deflections. Conversely, if the span-to-depth ratios were less than 20, the predicted deflection was significantly under-predicted.
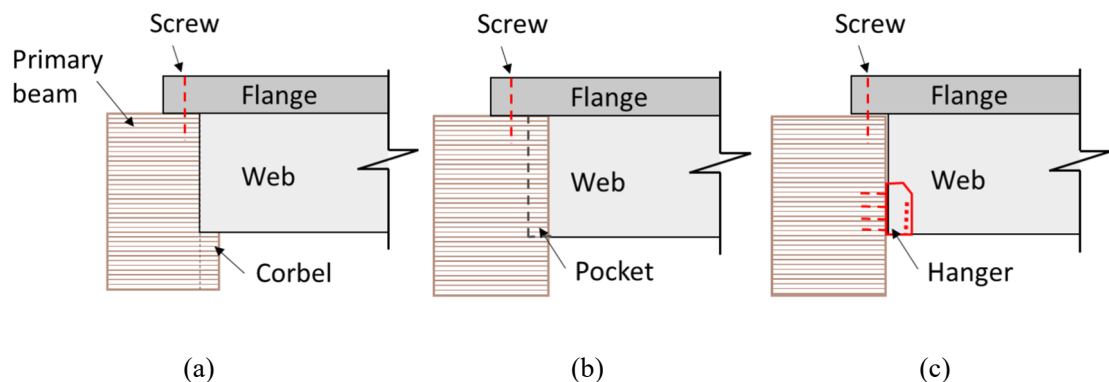
Figure 2-19 *Example of floor cassette to frame connection (adapted from* (Moroder, Pampanin & Buchanan 2016) *(a) cassette webs supported by corbel; (b) cassette webs supported by pocket; (c) cassette webs supported by steel joist hanger*

To the author's knowledge at time of writing, there are no studies on the dynamic behaviour of long-span cassette floors with the support conditions shown in Figure 2-19. However, some investigations have included the influence of more simple support conditions on short-span joist floors. One study undertaken by Weckendorf (2009) investigated the influence of support conditions (among other variables) on three full-scale timber I-joist floors. Two of the floors used the 'TJI' joist which has 38 mm thick LVL flanges and a 9.5 mm thick OSB web, while the other two floors used the 'JJI' joist which has 45 mm thick C24 grade flanges and 9 mm thick OSB web. The two floors fabricated with the TJI joist were 4.4 m wide while having differing spans of 3.7 m (TJI

Floor 1) and 5.1 m (TJI Floor 2). The floor fabricated with the JJI joist spanned 3.5 m with a width of 2.44 m. In these tests, the joists spanned onto the supporting beams (representing wall panels) rather than sitting flush as shown in Figure 2-19; this is typical for residential construction. The two support conditions investigated included: I-joists bearing onto support with no fixings and I-joists fixed to the support with screws. For all three floors, results showed that the screwed support condition had higher frequencies for all five modes (< 40 Hz), although the difference was less than 5%. Damping ratios were fairly consistent between the different boundary conditions with the damping ratio remaining at approximately 2.5 – 3.0 % for the fundamental mode and 1.0 to 1.5 % for the higher modes, despite the varying boundary condition. A numerical model based on the JJI floor with screwed boundary conditions was also created and correlated to experimental results. Weckendorf (2009) highlighted that consideration of spring stiffness at the supports in the three translational directions and, particularly the vertical direction, was important for an accurate model.

In another study, Jarnerö et al. (2015) investigated the difference in modal properties between three types of simply-supported boundary conditions on a single cross-laminated timber (CLT) panel and glulam joist floor element. The floor element, tested under laboratory conditions, consisted of three glulam joists spanning 5.5 m glued and screwed to a 1500 × 73 mm thick CLT top panel. Two of the boundary conditions tested included the CLT panel 'floating' (i.e. bearing) or screwed to the supports; the joist members were not supported. Dynamic excitation was performed with a shaker and modal properties extracted using LMS Test.Lab software. Results showed that the first torsion mode appeared before the first longitudinal bending mode for both cases. There was an almost negligible increase in the frequency of the first bending mode from 20.2 Hz to 21.0 Hz for the floating to screwed support condition, respectively. Damping ratios increased on average from 1.4% to 1.8% for the screwed setup when compared to the floating case.

An alternate support condition often found in timber frame buildings in Europe involve the addition of an acoustic interlayer at boundaries between floor and supporting beam/wall, as shown as the 'Sylodyn interlayer' in Figure 2-20(b). Sylodyn® has strong spring and small damping properties while Sylomer®, another commonly used interlayer, has a combination of spring and damping properties; both are manufactured by Getzner.

These closed cell polyurethane interlayers are generally used to reduce the flanking transmission of sound from footsteps, however are also suitable as a vibration isolation element in the rail industry or elastic machine bearing (Getzner GmbH 2016).

The CLT panel bearing onto a Sylodyn interlayer with no fastening, as shown in Figure 2-20(a), was the third simply-supported boundary condition investigated by Jarnerö et al. (2015). Comparing the results from the Sylodyn support condition to the two other afore-mentioned simply-supported boundary conditions, it was found that the order of mode shapes changed where the first longitudinal bending and torsion modes switched positions. The frequency of the first bending mode decreased by approximately 2 Hz and 3 Hz from the floating and screwed cases, respectively, and the frequencies of the higher modes also decreased. The average damping ratio across all modes increased to approximately 2.5%.

The floor element with the Sylodyn support condition was also tested in-situ, as shown in Figure 2-20(b), at different stages of construction; the floor was situated on the second storey of an eight-storey residential building. It was found that the in-situ conditions have a significant beneficial effect on the damping ratio which increased to 6% when the last storey was added.

(a)   (b)
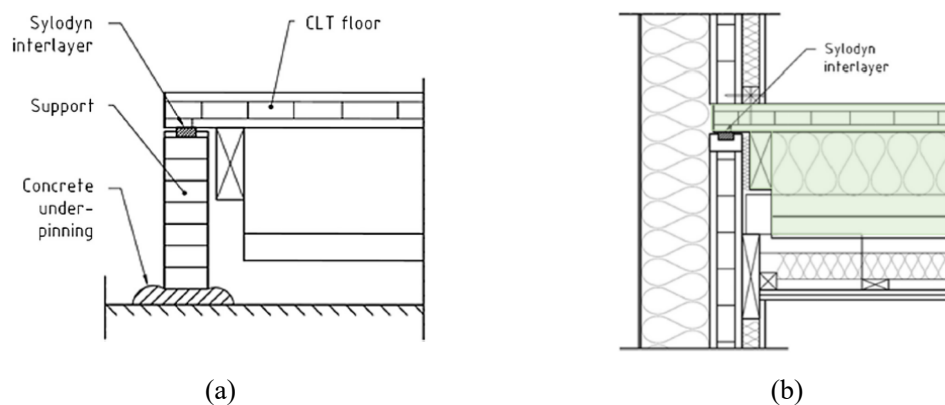
Figure 2-20 *Support condition with Sylodyn interlayer tested by Jarnerö et al. (2015) (a) tested in the laboratory; (b) tested in-situ.*

2.4.2 Orthotropic behaviour

Ribbed-deck floors have a higher cross-sectional stiffness along-joist than across-joist which makes the system highly orthotropic. Due to this characteristic, modes are more closely spaced which may interact and amplify the floor response (Chui 1986; Filiatrault,

Folz & Foschi 1990; Khokhar 2004). Further, subjective testing undertaken on 15 subjects has shown that 'annoyance' increases when there are two closely spaced frequencies (Ljunggren 2006; Ljunggren, Wang & Ågren 2007) and therefore consideration of these higher modes during design has been recommended (Brownjohn & Middleton 2008; Ljunggren 2006). Although there is no clear definition of spacing required between modes to avoid interaction, a minimum separation of 3 Hz was suggested by Ljunggren (2006) while 5 Hz has been suggested by Ohlsson (1982).

Between-joist bracing, also known as 'blocking', is typically used as a construction technique in prefabricated timber cassettes to keep the joists in place and at the correct spacing before the flange is connected. Blocking can also act as joist stiffeners improving the transverse stiffness of the floor. Khokhar (2012) undertook laboratory tests on a 4.2 m span LVL joist floor supported on all four sides. The influence of various joist bracing methods were investigated including solid blocking (Figure 2-21(a)), cross-bridging (Figure 2-21(b)) and cross-bridging and strapping. Results showed that the addition of blocking had little difference on the fundamental mode, a finding also supported by Bernard (2008). However, compared to the base case (no joist bracing), the spacing between the first two modes increased from 5 Hz to approximately 10 Hz, 8.5 Hz and 10.9 Hz for the blocking, cross-bridging and cross-bridging with strapping cases, respectively.

(a) solid timber blocking   (b)) cross-bridging
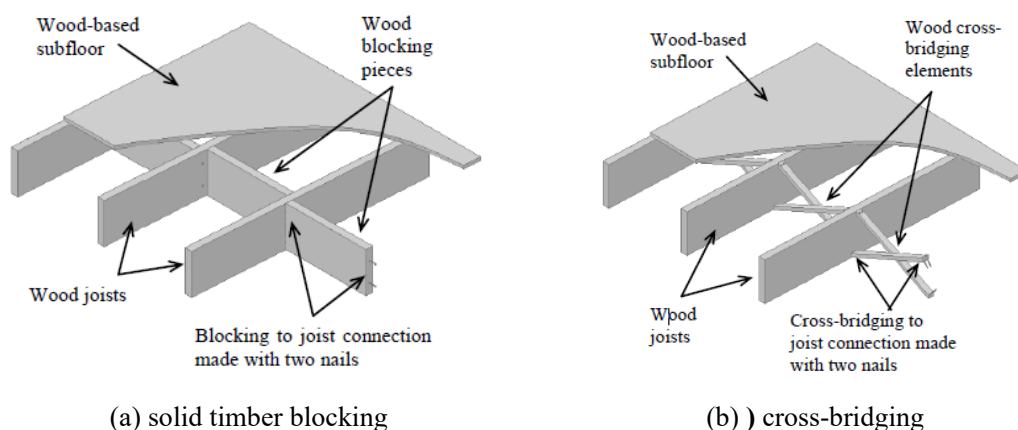
Figure 2-21 *Types of joist bracing tested by Khokhar (2012)*

Olsson et al. (2008) investigated the vibration performance of three different timber floors of dimensions 2.4 m × 8.0 m with varying degrees of transverse stiffness. Floor 'A' and 'B' had a longitudinal stiffness of 18900 and 18300 kN/m^2, respectively, while Floor 'C'

had a longitudinal stiffness of 4550 kN/m^2. The percentage of the transverse to the longitudinal stiffness was approximately 21%, 7% and 0.1% for Floor 'A', 'B' and 'C', respectively. Each floor was simply-supported on two opposite sides. Results showed that for Floor C, the number of modes under 40 Hz increased from 2, for Floor A and B, to 12. A numerical simulation of Floor A was then developed and the effects on natural frequencies and deflection when reducing the transverse stiffness by a factor of 10, 20 and 100 were obtained. It was found that for the tested floor dimensions where the span was approximately four times the width, changes in transverse stiffness had small influence on the dynamic properties. However, the influence was expected to increase for floors with wider floor dimensions in relation to span.

2.4.3 Damping

Damping, typically quantified as a damping ratio, plays an important role in the structural response to dynamic excitation. Higher damping enables structural systems to dissipate energy faster resulting in reduced amplitudes and shorter vibration duration times, a factor which has shown to be strongly influence annoyance. Damping is made up of two main categories: material and structural damping. Material damping involves the internal friction within the material which is created through energy dissipation associated with microstructure defects such as grain boundaries and impurities (Labonnote 2012). Structural damping is a form of mechanical energy dissipation by friction of movement between components such as at support connections or between the floor and furniture or partitions. Unfortunately, however, damping is often difficult to estimate in practice, particularly since structural damping is heavily reliant on workmanship and type of floor occupancy. Consequently, a conservative approach is usually taken with recommended damping ratios neglecting the contribution of structural damping.

From laboratory investigations on eight timber joist floors, Ohlsson (1982) found damping ratios ranged from 0.5% to 1.3% and rarely surpasses 1.5% for the first five first order principal modes. Tested timber floors were constructed from solid timber joists screwed or screwed and glued to a 22 mm thick OSB sheathing. Little difference was found between the floors with sheathing glued and screwed to joists compared to the floors which were simply screwed.

In contrast to Ohlsson (1982) studies, laboratory tests conducted by Weckendorf et al. (2008) on 24 composite timber flooring systems found clear differences in damping ratios between the first and higher modes. Results showed damping ratios for the first mode were usually between 2.0 – 3.5% with a mean of 2.5% while those for the second and third mode were mainly in the range of 0.8 – 1.5% with a mean of 1.1% and 1.2%, respectively. In his thesis, Weckendorf (2009) also found that the damping ratios increase if the floor is supported on all four sides instead of two.

Labonnote et al. (2015) undertook tests on the material and structural damping of two glulam joist floors with top and bottom sheathing. Each floor had different joist-to-sheathing connections: one floor used screw connectors while the other used nails. It was found that the sheathing, particularly the bottom sheathing, had the largest contribution to material damping as they are subject to larger deformation. Further, it was found that the use of material damping as the lower boundary of total damping is less accurate as the mode number increases. For example, for the third mode, the structural damping represents around 62% of the total damping while for the first mode, structural damping represents only 48%. Similarly to Ohlsson (1982), there was very little difference found between the different joist-to-sheathing connection types; the reason likely due to the small amplitude of vibrations under testing.

Tests undertaken on in-situ timber floors have shown that damping ratios increase substantially when incorporated into the main structure (Jarnerö, Brandt & Olsson 2015; Ohlsson 1982) or when non-structural elements are added onto the floor (Ebadi, Doudak & Smith 2019; Ohlsson 1982; Reynolds et al. 2015). Further, the presence of humans on timber floors have been shown to act as a simple spring-mass-damper, raising the damping capability of floors (Foschi et al. 1996; Fujino, Suzuki & Noguchi 2008). Despite these aforementioned studies, recommended damping ratios for timber floors remain at 1% in Eurocode 5 (2004) or 2% in the UK National Annex to Eurocode 5 (British Standards Institution 2008b) and ISO 10137 (2007) . The Eurocode 5 (2004) value originates from Ohlsson's (1982) research. A summary of various damping ratios reported in standards and literature for timber floors are shown in Table 2-1; the test environment (either laboratory or in-situ) has been noted where known.

Table 2-1 *Various damping ratios recommended in standards and reported in literature*

Reference	Test condition	Floor description	Damping ratio
Ohlsson (1982)	Laboratory (8 of)	Solid timber joists connected to a OSB sheathing and with/without ceiling board on bottom	0.75% (recommended)
	In-situ (2 of) – empty house	As above with ceiling board	3.4 – 4.1% (mode 1); 4.6% average (higher modes)
	In-situ (2 of) – furnished house		2.6% (mode 1); 3.5% average (higher modes)
Eurocode 5 (2004)	See Ohlsson (1982) 'Laboratory'	Timber floors	1%
ISO 10137 (2007)	Unknown	Wood joist floors – preliminary design value	2%
		Wood joist floors – typical range	1.5 – 4.0%
		Wood joist floors – extreme range	1.0 – 5.5%
UK NA to Eurocode 5 (British Standards Institution 2008b)	Unknown	Timber floors	2%
HIVOSS (Feldmann 2008)	Unknown	Timber floor with no furniture or finishes	6%

Stated in Hamm et al.(2010) but taken from (Holzbau 2003) and (Blaß et al. 2005)	Unknown	Timber floors without any floor finish	1%
		Plain glued laminated timber floors with floating screed	2%
		Girder floors and nail laminated timber floors with floating screed	3%
Jarnerö et al. (2015)	In-situ – bare floor	CLT panel and glulam joist floor (5.1 m span) on 3rd floor of 8-storey building; Sylodyn interlayer at support	5.7% (mode 1); 4.5% average (higher modes)
	In-situ – complete building except for roof		6.5 % (mode 1); 5.8% average (higher modes)
Abeysekera et al. (2018)	Unknown	Joisted floors	2.0%
		Timber-concrete and mass timber floors	2.5%
		Joisted floors with a floating layer	3.0%
		Timber-concrete composite and mass timber floors with a floating layer	3.5%
		All floors with a floating layer and supported on 4 sides	4.0%
		All floors with a floating layer and supported on 4 sides by timber walls via flexible bearings	6.0%
Ebadi et al. (2019)	In-situ – bare floor	Long-span (8.0 – 10.7 m) glulam beam and deck floor	2.7% (mode 1); 2.2% average (higher modes)

2.4.4 Connections between adjacent cassettes

Ribbed-deck floors are prefabricated off site and arrive to the building site as individual floor cassettes. Typically, a combination of glue and screws are used to connect the panel and web elements; the bond formed through the glue, which is assisted through the clamping action of the screws, allows the cross-section to act as a fully-composite section under both serviceability and ultimate limit state design (Crews & Shrestha 2016; Zabihi 2014). Consequently, for vibration design, a rigid connection at the interface of the flange and web is typically assumed for the purpose of numerical modelling.

Connections between adjacent cassettes are made via adjacent web members and flange elements. Web-to-web to connections allow shear transfer to form diaphragm action (Moroder, Pampanin & Buchanan 2016) and are also imperative to ensure that the two joists do not separate during fire exposure (Gerber, Crews & Shrestha 2012). The connections between flange elements may be added to provide additional shear transfer to the floor. Examples of web-to-web and flange-to-flange connections are shown in Figure 2-22.
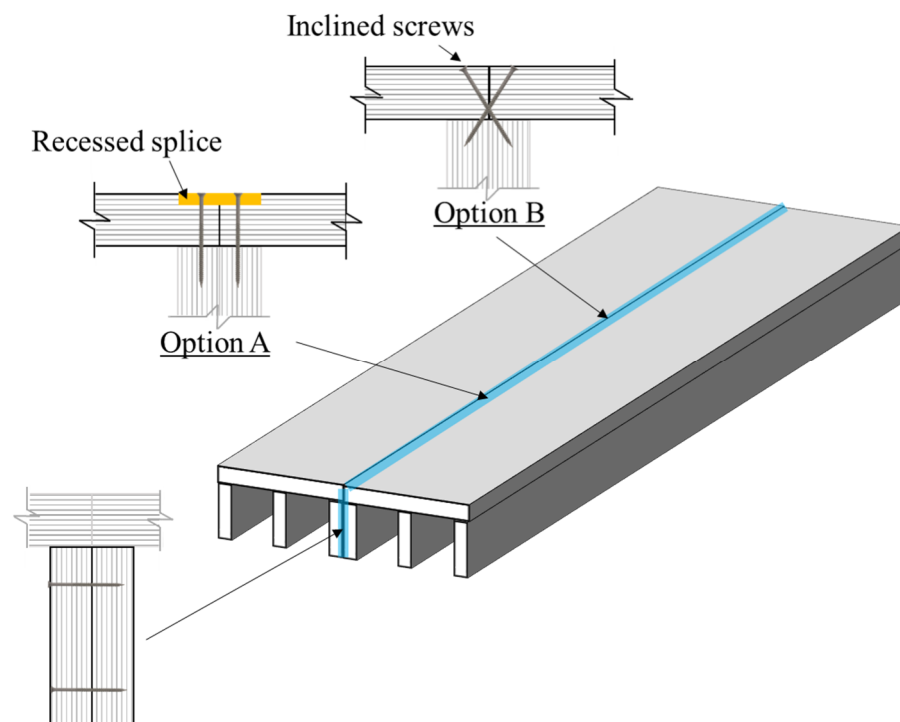
***Figure 2-22** Typical connections between adjacent cassettes*

Numerical modelling of connections between adjacent timber elements have been investigated mainly in relation to half-lap joints connecting adjacent CLT floor panels (Figure 2-23) (Hassanieh et al. 2019; Ussher et al. 2017b; Weckendorf, Ussher & Smith 2016). A study undertaken by Ussher et al. (2017a) found that ignoring the semi-rigid behaviour of these different connections joints in timber floors can lead to large inaccuracies in mode shape and frequency predictions. Three modelling approaches were analysed: completely disconnected plate, continuity of only shear forces via translational springs and full continuity. Between these approaches, there was very little difference on the fundamental mode or modes where the order was 1 in the plan width direction (i.e. longitudinal bending modes). However, the presence of a construction joint with no or only shear continuity strongly influenced the number, mode order and frequencies of other types of modes. Other researchers have taken a similar modelling approach to Ussher et al. (2017a) with the screws modelled as zero-mass spring elements in the translational x-, y- and z-directions with assigned stiffness values based on load-slip tests. Although a recent study has shown that CLT half-lap joints have some rotational stiffness (Macpherson et al. 2018), moment continuity across joints are rarely considered in a design scenario.

In Hassanieh et al. (2019), diagonal screws (similar to Option B in Figure 2-22) were used to connect adjacent CLT flange elements of a steel beam and CLT composite floor system. Screws were also modelled as spring elements with serviceability stiffness taken as 85% of the static stiffness values based on connection tests conducted by Loss et al. (2016).
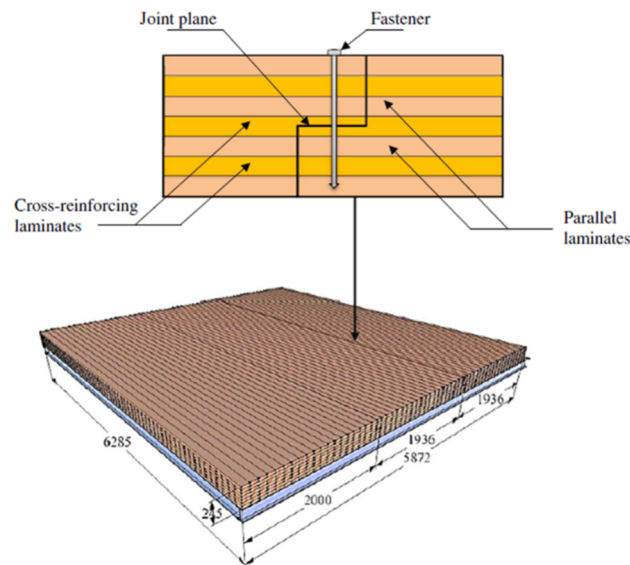
Figure 2-23 *Half-lap connection between adjacent CLT panels*

2.5 Human sensitivity to vibrations

Human perception of vibrations is dependent on vibration characteristics such as frequency, amplitude and duration. However, perceived vibrations may not necessarily be annoying. Psychological factors including knowing the source of vibration, whether or not the vibration is expected and visual cues such as shaking monitors or rattling windows all influence the human response. These variables make human response to vibrations extremely complex. This section first introduces how vibrations are measured to quantify vibration exposure. The following sections thereafter discuss the early works on human sensitivity, the standardisation of human perception and studies on annoyance of building vibrations.

2.5.1 Measurable quantities

2.5.1.1 Averaging methods

As seen in Equation 2.124, the response to an external dynamic load can be expressed in terms of deflection, velocity or acceleration. Typically, acceleration is used to measure human exposure to vibrations, which is mainly due to the ease of accessibility to accelerometers (Griffin 1990). Time-domain data is then frequency-weighted to take into consideration of the human sensitivity to certain frequency ranges. Separate weighting curves are used for each vibration direction with the two most commonly used curves for

z-axis (parallel to spine) vibrations, as provided in BS 6472-1 (2008a) and ISO 2631-1 (1997), shown in Figure 2-24. The weighting curve used in Japan, as provided in JIS C1510 (1995), is also shown to highlight the differences in human perception between different countries. ISO 2631-2 (2003) recommends a W_m weighting curve if the vibration direction is unknown (also shown in Figure 2-24). Despite the different weighting curves, it is generally agreed that humans are most sensitive to z-axis vibrations at frequencies in the range of 4 to 8 Hz while amplitudes at other frequencies can be attenuated.

After the frequency-weighting is applied, the response is evaluated by an averaging method such as root-mean-square (RMS) which can be calculated as follows (ISO 1997):

$$a_{w,rms} = \sqrt{\frac{1}{T} \int_0^T [a_w(t)]^2 \, dt} \qquad (2.23)$$

where $a_w(t)$ = weighted acceleration at time t (m/s^2); T = duration of the measurement (s). The RMS rather than peak acceleration became the preferred measurement quantity not due to reasons of accuracy but rather due to the convenience of measurement and analysis and the harmonisation with other areas of engineering (Griffin 1990). For continuous, 'well-behaved', statistically stationary motions where the amplitudes do not vary significantly between certain time periods, the RMS acceleration works well. However, as walking vibrations are often transient, intermittent and non-stationary, it is difficult to estimate the duration T over which to average the response and from when to start the measurement. Ellis (2001) stated this was a 'major weakness' of the RMS acceleration as calculated by Equation 2.23.
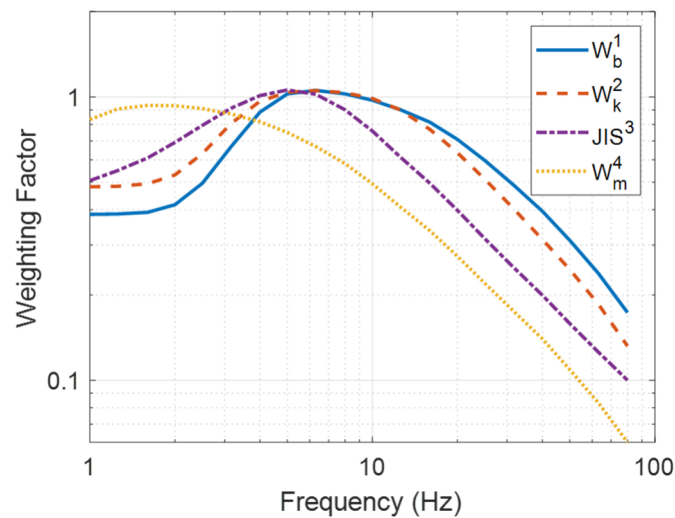
Notes: [1](British Standards Institution 2008a); [2](International Standards Organisation 1997); [3](Japanese Standards Association 1995); [4](International Standards Organisation 2003)

Figure 2-24 *Frequency-weighting filters provided in BS 6471-1* (2008a)*, ISO 2631-1(1997) and JIS C1510* (1995) *for z-axis vibration. Frequency weighting W_m is recommended if the vibration direction is unknown as stated in ISO 2631-2*(2003)

Therefore, for walking vibrations, an alternative measure using a running root-mean-square method is generally recommended:

$$a_{w,rms}(t_0) = \sqrt{\frac{1}{\tau} \int_{t_0-\tau}^{t_0} [a_w(t)]^2 \, dt} \qquad (2.24)$$

where $a_{w,rms}(t_0)$ = rolling frequency-weighted RMS acceleration (m/s^2) at instantaneous time of observation t_0; τ = integration time interval for running averaging which is recommended as 1 second (s). The vibration magnitude is then defined as the maximum transient vibration value (MTVV) which is the highest magnitude of $a_{w,rms}(t_0)$ read during the measurement period.

2.5.1.2 Dose methods

Ellis (2001) and Griffin (1990) have suggested that for transient vibrations, a cumulative measure such as the Vibration Dose Value (VDV) is more appropriate. The VDV, as shown in Equation 2.25, places importance on higher magnitudes of the vibration and how many times they occur during a certain exposure period. This fourth power relation between acceleration and exposure time is supported by numerous studies (Griffin &

Whitham 1980a, 1980b; Howarth & Griffin 1988) and consistent with observations by Siskind et al. (1989).

The VDV is the only quantity adopted in the current British standard BS 6472-1 (2008a) for evaluation of human exposure to all types of vibration (continuous, intermittent, occasional and impulsive) in buildings. It is also published in ISO 2631-1 (1997), however is not required to be calculated if the running RMS method is used. Similarly to the RMS acceleration, the acceleration is frequency weighted before the VDV is calculated.

$$VDV = \left[\int_0^T a_w^4(t)\, dt \right]^{\frac{1}{4}} \text{m/s}^{1.75} \tag{2.25}$$

To calculate the VDV, the total duration of the vibration exposure period, *T*, must be considered. In BS 6472-1 (2008a), this duration is recommended as a 16-hour day and an 8-hour night for residential buildings. Alternatively, a VDV estimation can be calculated from one walking event by assuming the event occurs for *P* number of times during the exposure period. Therefore, Equation 2.25 can also be expressed as follows:

$$VDV_{Total} = \sqrt[4]{P} \left[\int_0^{T_{single}} a_w^4(t)\, dt \right]^{\frac{1}{4}} \text{m/s}^{1.75} \tag{2.26}$$

Ellis (2001) proposed walking occurrences for three scenarios: extremely busy, reasonably busy and quiet. An extremely busy environment was one where occupants were continuously crossing the floor. For example, if an occupant took 6 seconds to cross the floor, the number of potential crossings within an 8 h workday would be $(8\times60\times60)/6 = 4800$. A reasonably busy environment (considered as a more normal situation) was suggested to have one person crossing every minute while a quiet scenario may have one person walking across the floor four times an hour.

In the 1984 edition of in BS 6472-1 (1984), an estimated VDV (eVDV) was proposed which estimates VDV based on the weighted RMS acceleration, as shown in Equation 2.27; this equation is also included in the current BS 6472-1 (2008a). Concerned about the weaknesses of $a_{w,rms}$ for intermittent footfall vibrations, Ellis (2001) proposed a different eVDV based on the weighted peak acceleration ($a_{w,p}$) as shown in Equation

2.28 where t is the total time during the exposure period which the vibration will occur (in seconds). Note the eVDV proposed by Ellis (2001) has a subscript 'E' to distinguish the equations.

$$eVDV = 1.4 \times a_{w,rms} \times T^{0.25} \tag{2.27}$$

$$eVDV_E = 0.48 \times a_{w,p} \times T^{0.25} \tag{2.28}$$

2.5.2 Early works on vibration perception thresholds

Early experiments in the field of human sensitivity to vibration involved subjecting the test subject to steady-state vibrations with varying frequencies, amplitudes and durations (exposure periods). One of the most widely referenced studies on human sensitivity to steady-state vibrations was undertaken by Reiher and Meister (1931). Ten subjects were exposed to vertical and horizontal vibrations with frequencies of 5 to 100 Hz and amplitudes of 0.01 mm to 10 mm through a motor driven platform for approx. 5 minutes. The subjects were then asked to rate the vibration on a six class scale: 'barely perceptible', 'just perceptible', 'clearly perceptible', 'annoying', 'unpleasant' and 'intolerable'. Reiher and Meister (1931) found that the threshold of perception was dependent on vibration velocity from 5 to 60 Hz where the perception threshold for standing subjects was around ± 0.3 mm/s (Griffin 1990). For frequencies less than 10 Hz, research undertaken by Postlethwaite (1944) found that human sensitivity was related to acceleration with a perception threshold of approximately 0.003 m/s^2 (3.1 × 10^{-4} g). A higher tolerance of approximately 0.03 m/s^2 was found for a frequency of 10 Hz with perception related to vibration velocity (King 1957).

In 1966, Lenzen (1966) suggested that perception thresholds based on steady-state vibrations were not appropriate for occupants on building floors since the main source of vibration came from human walking which is intermittent in nature. Subjective test results on steel-concrete composite floors revealed that damping (i.e. the vibration duration) was the main factor influencing vibration perception in buildings. He proposed that the Reiher and Meister (1931) curves would be applicable to floors with a damping ratio less than 5% if the amplitudes were increased by a factor of 10; these were subsequently called the 'modified Reiher-Meister' curves. This meant that humans were more tolerant to vibrations of short duration.

53

Wiss and Parmalee's (1974) study on human perception to transient vibrations resulted in similar findings to Lenzen (1966) where transient vibrations are particularly less perceptible as the damping increases. Effect of steady-state vibrations were also investigated, however, only for a 5 second exposure. The vibrations were found to be less perceptible than was indicated when compared to the 5 minute exposure time of Reiher and Meister (1931) study.

2.5.3 Standardisation of human perception

The first international standard for human response to whole-body vibration, ISO 2631 (1974), was drafted for the evaluation of vibrations transmitted to the body in 'vehicles, in vibrating buildings and in the vicinity of working machinery' (Oborne 1983). Three limits were given in reference to three criteria (listed in order from highest to lowest limits):

- exposure limits (concerned with the preservation of health or safety),
- fatigue-decreased proficiency boundary (concerned with the preservation of working efficiency), and
- reduced comfort boundary (concerned with the preservation of comfort).

The guides stated that the fatigue-decreased proficiency boundary was based on data 'mainly from studies on aircraft pilots and drivers' of vehicles. The exposure limit was 'set at approximately half the level considered to be the threshold of pain (or limit of voluntary tolerance) for healthy human subjects' and finally the reduced comfort boundary 'is derived from various studies conducted for the transport industries' (International Standards Organisation 1974; Oborne 1983). The standard also suggested that vibration acceptability in buildings may lie near the threshold of z-axis (parallel to spine) perception which is claimed to be about 0.01 m/s^2 for a frequency range of 4 – 8 Hz (Griffin 1990). As shown in Figure 2-25, the 24 h reduced comfort boundary (i.e. for a vibration with duration of 24 h) is around three times the perception threshold suggested in the standard. Although, to the author's knowledge, no explicit reference to the experiments is made to which this threshold is based on, it seems to be very similar to the threshold found by Miwa (1967).

The standard was met with much criticism, mainly due to questioned credibility of the experiments from which the recommended comfort boundaries were established. The standard also appeared to make assumptions on boundaries due to the lack of information at the time (Allen 1975). A critical assessment of the code can be found in Allen (1975) and Oborne (1983) and a summary of problems in Griffin (1990). Consequently, after much review and amendments, ISO 2631-2 (1989) (similar to BS 6472 (1984)) was published presenting 'baseline curves' for both RMS acceleration and velocity for the perception of continuous vibration. As stated in the American standard, ANSI S3.29:1983 (American National Standard Institute 1983), which also uses the same curves, the curves are approximately half the mean threshold of perception claimed in ISO 2631 (1974) and correspond to the perception threshold of the most sensitive humans (Al-hunaidi 1996). As a result, the base curve, as shown in Figure 2-25, shows a minimum threshold of 0.005 m/s^2 for a frequency range of 4 to 8 Hz. For frequencies greater than 8 Hz, the threshold is related to a constant RMS velocity limit of 1×10^{-4} m/s.
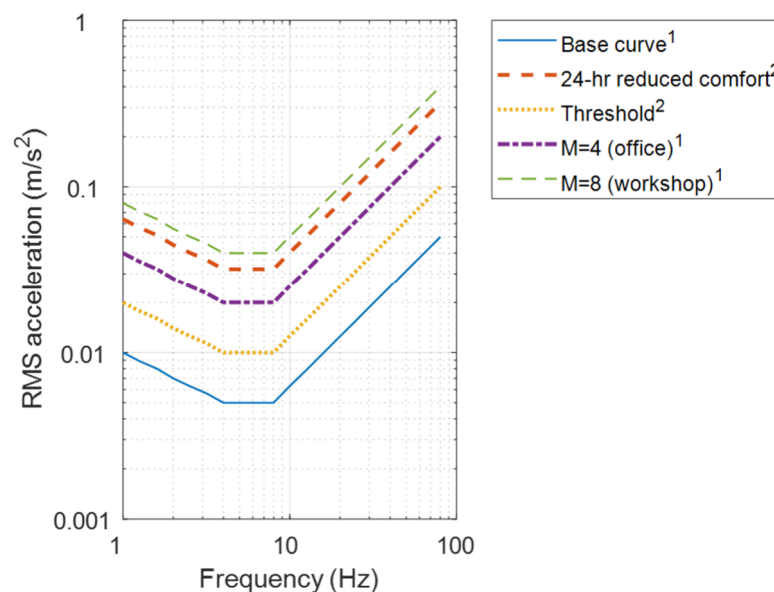
Note: [1] (International Standards Organisation 1989); [2] (International Standards Organisation 1974)

Figure 2-25 *Z-axis perception curves for continuous vibration including recommended limits*

Tables of multipliers on top of the base curve were also provided to assess vibrations in different buildings, different times of day and for different types of motions. These have been reprinted in Table 2-2. It should be highlighted that 'intermittent vibrations and repeated impulsive shocks' are assessed the same as 'continuous' vibrations, despite studies (Lenzen 1966; Parmelee & Wiss 1974) showing the sensitivity to these vibrations

are different. The multiplied base curves recommended for offices and workshops are also shown in Figure 2-25. It is suggested that these base curves 'represent magnitudes of approximately equal human response with respect to human annoyance and/or complaints about interference with activities' (International Standards Organisation 1989). If RMS accelerations fall below the curves as recommended for the occupancy, the probability of adverse human reaction is low or 'adverse comment is very rare' as stated in ISO 2631-2 (1989). Interestingly, these base curves have since been withdrawn from the current ISO 2631-2 (2003) as well as the BS 6472-1 (2008a) citing that 'the range of applications is too widespread' for an International Standard. However, ISO 10137 (2007) does include these as an 'informative' annex section citing that although withdrawn, 'portions of it are still relevant as criteria for building vibrations'.

Table 2-2 Multiplying factors given in ISO 2631-2 (1974) to define vibration magnitudes below which the probability of adverse comment is 'low'

Place	Time	Continuous or intermittent vibration and repeated impulsive shocks	Impulsive vibration excitation with several occurrences per day
Critical working areas	Day	1.0	1.0
	Night	1.0	1.0
Residential	Day	2.0 – 4.0	60.0 – 90.0
	Night	1.4	1.4 – 20.0
Office	Day	4	128.0
	Night	4	128.0
Workshop	Day	8	128.0
	Night	8	128.0

2.5.4 Annoyance

The feeling of annoyance in relation to floor vibrations is related to the experience of the perceiver, the expectation of the vibration occurring and whether the source can be identified (Griffin 1990). Consequently, annoyance is also related to the senses of hearing and seeing objects or furniture move as a result of the vibration. For example, based on extensive laboratory and field tests of floors constructed with different materials (including timber), Toratti and Talja (2006a) proposed a five-class classification of floors

which relates the body perception to the vibration of objects including clinking of glassware and leaf movements from a plant. For a base class floor (Class C), which indicates that the vibrations are perceptible, leaf movements would be perceptible but clinking of glassware is barely perceptible.

A correlation between annoyance in buildings and the frequency of the event occurring has also been established. Howarth and Griffin (1988) undertook experiments on the annoyance level of 24 male and 24 female subjects between the ages of 18 and 60 years to the repetition of a z-axis vibration measurement recorded in a house during the passage of a nearby train. The duration of the stimulus was 12.5 seconds with an overall RMS acceleration of 0.059 m/s^2. The vibration was repeated to represent 4, 8, 16 and 32 trains at equal intervals within a one hour period. Results showed that annoyance increased with the number of trains passing per hour.

The relationship between annoyance and vibrations with multiple frequency components was carried out by Ljunggeren (2006). Fifteen subjects were asked to sit on a chair secured to a motion simulator and were exposed to sinusoidal signals with varying magnitudes and frequencies. The annoyance was then assessed using an 11-point scale ranging from 'not at all annoying' to 'extremely annoying' with subjects instructed to think of themselves within a home or office environment. The base frequency was set at 8 Hz with a magnitude of 0.035 m/s^2 RMS acceleration which was the upper acceptance limit for homes and office environments according to an older version of the AISC design guideline (Murray, Allen & Ungar 1997). The second frequency component was added at a frequency of either 10, 12.5, 17, 20 or 25 Hz. Amplitudes also varied from 20% to 100 % in intervals of 20% of the upper acceptance limit. Results showed that annoyance was higher if the second frequency component had a frequency close to the first; as noted in Section 2.4.2, this is crucial for closely spaced modes and is evidence that criteria focussing purely on the fundamental mode may not be appropriate. Based on regression analysis, an equation was proposed to define annoyance for a vibration containing multiple frequency components in relation to the fundamental frequency and frequency-weighted RMS acceleration ($a_{w,rms}$) of the floor response:

$$Annoyance = -3.17 + 0.43 \cdot a_{w,rms} + 0.24 \cdot f_1 \qquad (2.29)$$

where $a_{w,rms}$ is in mm/s^2 and f_1 is in Hz. If the annoyance as calculated by Equation 2.29 is less than or equal to 4, the floor is deemed acceptable. It is important to highlight that the above equation is based on a W_m frequency weighting curve proposed in ISO 2631-2 (2003) (see Figure 2-24) and therefore may inappropriately attenuate frequencies in the range of 4 to 8 Hz which humans are most sensitive to.

2.6 Vibration serviceability design procedures and criteria

In Australia, UK and North America, acceptability of floor vibration is most commonly determined through a pass-fail approach. For example, the criterion generally takes the form of '*the floor is deemed acceptable if the response is less than limit Y*' where the recommended limit is typically related to the magnitude or frequency of the floor response. This 'blanket' approach may unnecessarily penalise long-span timber floors where floor vibration governs the design.

Some studies have recommended that a more probabilistic approach to floor vibration design is taken (Pridham 2013, 2014; Živanovic & Pavic 2009). This can take the form of using a probabilistic human walking force model (as discussed in Section 2.3.3.2) which can be used to calculate the cumulative distribution of potential responses generated by a pedestrian population. For example, the criterion may be '*the floor is deemed acceptable if the probability of the response exceeding the limit Y is less than 70% for a population of 100 people*'. Another way that the probabilistic approach can be considered is by considering the duration that the vibration exceeds the recommended limit rather than assessing performance based on the maximum amplitude (as is the case for pass-fail criteria). In this instance, the criterion may be '*the floor is deemed acceptable if the response is less than limit Y for 80% of the duration of the event*'. For a walking event lasting 10 seconds, the aforementioned statement means that the recommended limit was only surpassed for 2 seconds. Lastly, a probabilistic approach can also be taken with respect to human perception levels and the likelihood that the occupant will perceive the vibration. For example, the criterion may be '*the floor is deemed acceptable if the response is less than 50% likelihood of perception*'.

The latter approach has already been followed for the last 15 years in Japan through their guideline AIJES-V001 (2004) (superseded). In contrast to multiplying factors (as

proposed in ISO 2631-2 (1974)) for various occupancies, different curves are provided which define the percentage likelihood of perception by occupants. These curves, established from the base curve for human perception of continuous vibration (see Section 2.5.3), correspond to 10, 30, 50, 70 and 90% likelihood of perception. Research was undertaken to correlate these perception curves to a 7-level annoyance scale (Yokoyama 2018); 50% likelihood of perception was correlated to an annoyance level between 'not unpleasant (not annoyed)' (level 7) and 'slightly unpleasant (slightly annoyed)' (level 5). In the newest update of AIJES-V001 (2018), the duration T of the vibration amplitude is considered in relation to human perception, where for vibration durations less than 10 s, the amplitude is attenuated by a factor equal to $(T/10)^{0.25}$.

Despite these advancements in research and approaches to vibration design taken in other countries, the pass-fail criterion still dominates, as will be revealed in the following sections. This final part of the literature review explores the most significant works in relation to proposed criterion for timber floors as well as those for floors constructed from other materials.

2.6.1 Procedures and criteria for timber floors

2.6.1.1 Residential floors

The cost of residential dwellings often does not justify a detailed engineering analysis and, as a result, proposed criterion is generally simple and easily calculated by hand (Kalkert, Dolan & Woeste 1993). Consequently, many criteria, as will be discussed in the following sections, are based on theoretical solutions for simply-supported beams or plates. The criteria discussed in this section has been separated into the different limiting parameters and highlights the evolution of design criteria for residential timber floors.

(1) Limiting static deflection

Early timber floor serviceability design was established on limiting deflection under a uniformly distributed load to a value equal to span/360 which, as stated in Percival (1979), seems to have originated from Kidder (1885). The basis of Kidder's (1885) deflection criteria for timber beams remains unclear (Hansen 1960; Polensek 1973), although it is stated to having evolved from opinions of his architect and engineer friends (Percival 1979). The objective of the criterion was to prevent plaster cracks in ceilings, although

regulatory bodies and engineers recognised that it also helped minimise the occurrence of problematic floor vibration (Hu, Chui & Onysko 2001).

However, changes in floor construction methods meant that traditional timber joist floors were becoming lighter and more flexible (Chui 1986; Onysko 1988) resulting in a growing number of complaints from occupants in residential dwellings. Examples of these construction changes included building larger houses, changes in lumber sizes, the introduction of plywood and OSB sheathing, and new engineering wood products and fastening methods (Onysko et al. 2000). Consequently, floor vibration serviceability of wood joist floors became an increasing concern.

Based on a mathematical model, Foschi and Gupta (1987) proposed a reliability-based design criterion after finding the span/360 limit did not adequately address vibration serviceability. The criterion was as follows:

$$\delta = \frac{Pl^3}{48\bar{E}I} < 1 \text{ mm} \tag{2.30}$$

where δ = joist deflection due to point load applied at centre of joist; P = 1 kN; l = span; $\bar{E}$ = mean modulus of elasticity of the floor joists; I = moment of inertia of the joist. It was proposed that achieving this limit would lead to a 2% probability that the vibration would be distinctly perceptible under certain types of footfalls. If the deflection was limited to 0.8 mm, the probability decreased to 0.1%. The limitation of this criterion was that any contribution from composite action between the joist and sheathing was ignored.

After a large number of complaints were received about the liveliness of residential timber floors (Onysko 1970, 1988), Onysko (1988) performed an extensive investigation to understand the correlation between measured floor performance and occupant acceptability. Static and dynamic tests and consumer reviews of over 100 floors in a residential context were conducted as well as a number of tests in a laboratory setting (Onysko 1988). This work resulted in the following criteria which was subsequently adopted for Part 9 construction (mainly residential construction) in the 1990 edition of the National Building Code of Canada (Onysko et al. 2000):

$$\delta_c \leq 2 \text{ mm for spans} < \text{approx. 3.0 m} \tag{2.31}$$

$$\delta_c \leq 8/l^{1.3} \text{ mm for spans} > \text{approx. } 3.0 \text{ m}$$

where δ_c = floor deflection for a point load applied in the centre of the floor considering two-way action. The application of the load at the centre of the floor is in contrast to Foschi and Gupta (1987) where only the stiffness of a single joist was considered in the deflection calculation.

(2) Limiting static deflection and peak velocity

Ohlsson (1982, 1988a, 1988b, 1991) was one of the first researchers to propose criteria which included a dynamic based parameter. He distinguished between floors which are more susceptible to be excited by the lower-frequency components of the footstep force and those excited by the higher-frequency components in the heel strike transient. The former category was defined by more heavyweight, long-span floors with fundamental frequencies less than 8 Hz, while the latter generally occurs for lightweight floors with spans less than 6 – 8 m or heavy floors with short spans. At the same time, Ohlsson (1991) believed that human sensitivity to vibrations greater than 8 Hz was proportional to vibration velocity. Based on findings from numerous measurements on timber residential floors, Ohlsson (1988a) proposed two criterion for floors with a fundamental frequency greater than 8 Hz. The first was a static deflection limit:

$$\delta_c \leq 1.5 \text{ mm/kN} \tag{2.32}$$

The second criterion involved the maximum unit impulse velocity response $u_{vel,max}$, which included modes up to 40 Hz and is shown in Equation 2.33. Modes with eigenfrequencies greater than 40 Hz were not included as results from field tests on timber floors showed that the impulsive forces induced by footfall was confined to the frequency range below 40 Hz (Ohlsson 1982).

$$u_{vel,max} = \frac{4(0.4+0.6n_{40})}{(m+200)} \leq 100^{(f_1\xi-1)} \text{ m/(Ns}^2) \tag{2.33}$$

where:
$$n_{40} = \left\{ \left(\left(\frac{40}{f_1}\right)^2 - 1 \right) \left(\frac{b}{l}\right)^4 \frac{(EI)_l}{(EI)_b} \right\}^{0.25} \tag{2.34}$$

and b = floor width; ξ = damping ratio; n_{40} = number of eigenmodes with eigenfrequencies lower than 40 Hz; $(EI)_l$ and $(EI)_b$ are the equivalent flexural rigidity of the floor structure about an axis perpendicular and parallel to the beam direction, respectively, where $(EI)_b < (EI)_l$. The fundamental frequency criterion can be checked

using the following equation (Ohlsson 1991) which is based on the theoretical equation for a simply-supported beam:

$$f_1 = \frac{\pi}{2L^2} \sqrt{\frac{(EI)_l}{m_l}} \text{ Hz} \tag{2.35}$$

where m_l = mass per unit length (kg/m). Ohlsson's (1982, 1988a) research was the basis of the current criteria presented in Eurocode 5 (2004) for vibration design of residential floors. Porteous and Kermani (2007) note that $(EI)_l$ should only be based on the flexural rigidity of the beams/joists unless the decking is glued to the joists in accordance with Clause 9.1.2 in Eurocode 5 (2004). In the latter case, composite action between the decking and joists can be assumed. The limits to the two criterion can be adjusted depending on the performance demand and are as follows:

$$\frac{w}{F} \leq a \text{ mm/kN} \tag{2.36}$$

$$u_{vel,max} \leq b^{(f_1 \zeta - 1)} \text{ m/(Ns}^2) \tag{2.37}$$

where w = maximum instantaneous vertical deflection caused by a vertical concentrated static force F applied at any point on the floor. Parameters a and b are constants whose recommended range and relationship can be seen in Figure 2-26.
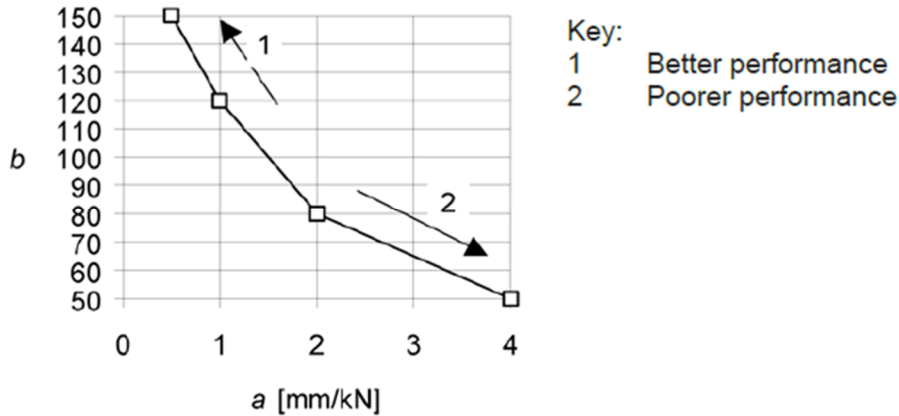
Figure 2-26 Recommended range of and relationship between parameters a and b, as published in Eurocode 5 (European Committee for Standardisation 2004)

Research undertaken on timber floors in New Zealand found that some floors satisfied Ohlsson's (1991) criteria but were unacceptable in practice (Beattie 1998). A 'modified' criterion for the maximum unit impulse velocity was proposed which was suggested to be suitable for timber floors in New Zealand (King 1999):

$$u_{vel,max} < 2 \cdot 100^{f_1 \xi} \text{ m/(Ns}^2) \tag{2.38}$$

Bainbridge and Mettem (1998) undertook a number of impact and static deflection tests with the aim of investigating the accuracy of Eurocode 5 (2004) frequency equation (Equation 2.35) in predicting the fundamental frequency of both residential and non-residential timber floors. The four tested timber floor configurations include two 4.8 m × 4.8 m, one 4.8 m span × 7.2 m and another with 7.2 m span × 4.8 m; the latter two floors were LVL joist floors. Results showed that the measured frequencies were consistently higher than predicted values by approximately 50% and consequently, a modified frequency equation was proposed:

$$f_1 = \frac{3\pi}{4L^2} \sqrt{\frac{(EI)_l}{m_l}} \text{ Hz} \tag{2.39}$$

where $(EI)_l = 1.2\bar{E}_j I_j \times 1000/s$; $\bar{E}_j$= mean modulus of elasticity of the joists (N/m^2); I_j= moment of inertia of the joist (m^4) and s = joist spacing (mm). The 1.2 factor in $(EI)_l$ was derived from test data and signifies the deck contribution to the floor stiffness.

(3) Limiting fundamental frequency and root-mean-square acceleration

On the basis that acceleration is a more reliable measure of human response to vibration than deflection, Smith and Chui (1988) proposed that a frequency and RMS acceleration limit should also be satisfied. Similar to Ohlsson (1988a), the sheathing is not considered to provide any contribution to the floor stiffness. The first criterion requires the fundamental frequency, calculated using Equation 2.40, to be greater than 8 Hz frequency to avoid the vibrations in the 4 – 8 Hz frequency band to which humans are most sensitive to.

$$f_1 = \frac{\pi}{2L^2} \sqrt{\frac{(EI)_l(n_j-1)}{m_s b + m_l(n_j-1)}} \text{ Hz} \tag{2.40}$$

where n_j = number of joists; m_s= mass per unit area of floor sheathing; m_l= mass per unit length of joists.

After satisfying the frequency limit, the RMS acceleration criterion was as follows:

$$a_{w,rms} = \frac{P_0}{m\omega_n} K = \frac{2000}{m\pi f_1^2} K > 0.45 \text{ m/s}^2 \tag{2.41}$$

where K is a function of damping ratio, angular natural frequency and t_1 which is the duration of the heel-drop impact. A modified frequency equation is proposed for use in

Equation 2.41 which considers the influence of human presence on the mass of the floor by adding the term $4W/L$ to the denominator of the square-root of Equation 2.40 where W = mass of observer (kg).

Figure 2-27 shows the typical and simplified force-time function of a heel-drop impact as assumed for Smith and Chui's (1988) RMS acceleration calculation. The impact is characterised by P_0 and duration of heel-drop t_1 which is typically in the range of 0.05 – 0.07 s (Smith & Chui 1988). The final equation for $a_{w,rms}$ is derived from the assumption that $P_0 = 500$ N (corresponding to approximately 70% of the weight of a 70kg person) and converting the angular natural frequency to circular frequency. The frequency weighting of 8/f_1, as per ISO 2631 (1978), for frequencies greater than 8 Hz has also been considered in the equation. Smith and Chui (1988) provide various values for K depending on f_1 and t_1 assuming a damping ratio of 3%, based on the fact that the presence of human bodies on a residential floor contributes to the damping of the system (Smith & Chui 1988). The 0.45 m/s^2 limit was a result of heel drop response measurements by Chui (1986) on both laboratory and in-situ floors in domestic structures.

Figure 2-27 Shape of forcing function of a heel-drop impact (Smith & Chui 1988)

Using a finite-element approach, Al-Foqaha'a et al. (1999) calculated the RMS acceleration and fundamental frequency for floors with varying span length, joist stiffness and mass density. It was found that the relationship between $a_{w,rms}$ and f_1 followed a power series relationship with mass-density dependent parameters where for the same fundamental frequency, higher mass-density floors had a lower $a_{w,rms}$ response. The proposed curves, as shown in Figure 2-28, were only validated with measurements from five floors with mass densities ranging from 450 – 512 Ns^2/m^4. The same limits as reported by Smith and Chui (1988) were recommended i.e. $a_{w,rms} < 0.45$ m/s^2 and $f_1 > 8$ Hz.
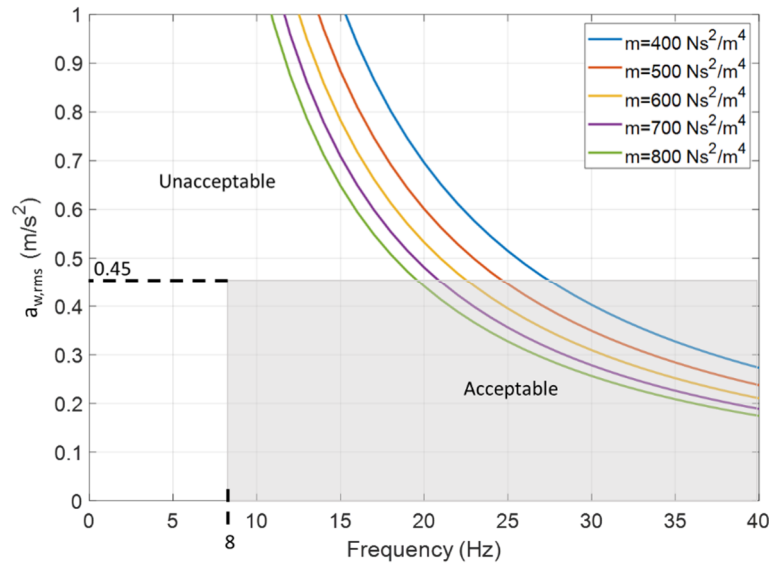
***Figure 2-28** Proposed $a_{w,rms}$ curves, adapted from Al-Foqaha'a et al. (1999)*

(4) Limiting fundamental frequency

Johnson (1994) and Dolan et al. (1999) introduced a unique criterion which only limited the fundamental frequency:

$$f_1 > 15 \ Hz \ \text{(unoccupied floors)} \tag{2.42}$$

$$f_1 > 14 \ Hz \ \text{(occupied floors)} \tag{2.43}$$

For a typical wood-joist floor with joists and decking, the proposed frequency equation is similar to Equation 2.35 and disregards composite action between the two components i.e. *E* and *I* are for the joist alone. For a structural system which includes joist and girders, the fundamental frequency of both the joist (f_{joist}) and girder (f_{girder}) are calculated separated and the final fundamental frequency of the system estimated using the Dunkerly equation:

$$f = \sqrt{\frac{f_{joist} \times f_{girder}^2}{f_{joist} + f_{girder}^2}} \tag{2.44}$$

Unlike Ohlsson's (1988a) recommendations, damping was not included as part of the criterion based on the fact that it cannot be accurately estimated or controlled by the designer. The criterion was validated by undertaking 126 and 54 in-situ tests of residential wood floor systems for unoccupied and occupied situations, respectively. Floor systems included lumber, I-joist and parallel chord truss joist systems. Hu (2000), using field test results of around 100 floors, later confirmed that this criterion works reasonably well for lightweight floors, however is too conservative for heavy floors such as those with a concrete topping and ceiling (Hu 2002).

65

(5) Limiting fundamental frequency and static deflection

Toratti and Talja (2006b) was the first to propose a five-class classification of floors in residential and office buildings with suggested vibration criteria being more or less stringent depending on the floor class. The categories ranged from Class A for premium floors where 'vibration is usually imperceptible' to Class E which has no restrictions to vibration perception. An extensive test program spanning 10 years resulted in measurements from a wide range of floors including steel- and wood-framed floors with floor boards or concrete topping, hollow-core concrete slabs, laminated veneer lumber (LVL) floors and floating and raised floors were correlated to subjective ratings. These parameters were then correlated to subjective ratings with observations made from body sensing as well as from visual or aural impressions of vibration objects and resulted in the annoyance scale discussed in Section 2.5.4. From these correlations, it was found that weighted RMS acceleration provided the best fit for both low- and high-frequency floors (defined as floors with a fundamental frequency greater than 10 Hz). Further, for high-frequency floors, peak velocity and static deflection also separated floors deemed 'acceptable' and 'unacceptable' fairly accurately. Consequently, simplified design procedures were proposed for high-frequency floors which considered fundamental frequency and global point load deflection. Other dynamic criterion involving acceleration, velocity and displacements were deemed too difficult to estimate and serve to classify floors based on experimental measurements. The fundamental frequency can either be calculated using the equation for a simply-supported uniform beam, as shown in Equation 2.35, or for a floor simply-supported on all four edges:

$$f_1 = \frac{\pi}{2l^2}\sqrt{\frac{(EI)_l}{m_a}}\sqrt{1 + \left[2\left(\frac{l}{b}\right)^2 + \left(\frac{l}{b}\right)^4\right]\frac{(EI)_l}{(EI)_b}} \text{ Hz} \qquad (2.45)$$

where m_a = mass per unit area and should include an additional service of 30 kg/m². The global deflection due to a 1 kN point load at the centre of the floor can be calculated by using the theoretical equation for the deflection of an orthotropic plate with all edges simply-supported or by neglecting the edge condition parallel to the joist as expressed below:

$$\delta_c = \frac{1}{42\left[\frac{(EI)_l}{(EI)_b}\right]^{0.25}} \cdot \frac{Pl^2}{(EI)_l} \qquad (2.46)$$

For normal class floors (Class C) where 'vibration is often perceptible and some people may find it annoying', δ_c is recommended to be less than 0.5 mm while for higher class floors (Class B), the limit is reduced to 0.25 mm.

(6) Limiting combination of parameters

Hu and Chui (2004) undertook extensive field testing of 130 timber floors in Canada, with the aim of developing an improved design method to control vibrations for wood-based floor constructions. First, static and dynamic parameters were evaluated for each floor and included static deflection under 1kN, natural frequency, peak velocity and acceleration and RMS acceleration. The footstep impact force was simulated by dropping a soft ball onto the floor. Occupants' subjective responses were then correlated to the measured parameters which found that perception correlated well with most of the parameters. This led to the formulation of several forms of limiting criterion (Hu 2002):

- Fundamental frequency with static deflection,
- Fundamental frequency with peak velocity,
- Fundamental frequency with peak acceleration, and
- Fundamental frequency with RMS acceleration.

Based on the fact that 1kN static deflection and fundamental frequency can be easily calculated by the designer and measured, the combination involving these two parameters was selected as the most appropriate for timber floors. Through regression analysis, the following formula was proposed:

$$\frac{f_1}{\delta_c^{0.44}} > 18.7 \tag{2.47}$$

The proposed equations to predict the fundamental frequency (Equation 2.48) and static deflection were based on ribbed-plate theory assuming semi-rigid behaviour between joist and sheathing, torsional rigidity of joists, and orthotropic properties of sheathing (Hu & Chui 2004).

$$f_1 = \frac{\pi}{2\sqrt{\rho}}\sqrt{D_x\left(\frac{1}{l}\right)^4 + 4D_{xy}\left(\frac{1}{lb}\right)^2 + D_y\left(\frac{1}{b}\right)^4} \text{ Hz} \tag{2.48}$$

where $\rho = m_j/s + \rho_s t_s + \rho_c t_c$ in kg/m²; ρ_s and ρ_c is the density of the sub-floor and topping, respectively (kg/m³); t_s and t_c are the thickness of the sub-floor and topping, respectively (m); D_x and D_y is the system flexural rigidity in the joist and cross-joist direction (Nm), respectively, and D_{xy} is the shear rigidity of the multi-layered floor deck

and torsion rigidity of joist (Nm). The method was validated through data obtained for 106 timber floors with varying constructions and spans ranging from 3 – 13m. Depths of floor joists ranged from 140 to 450mm. The subjective rating of these floors were compared to the proposed acceptance criteria, as shown in Figure 2-29, which found that the method was fairly effective in differentiating between unacceptable and acceptable floors.
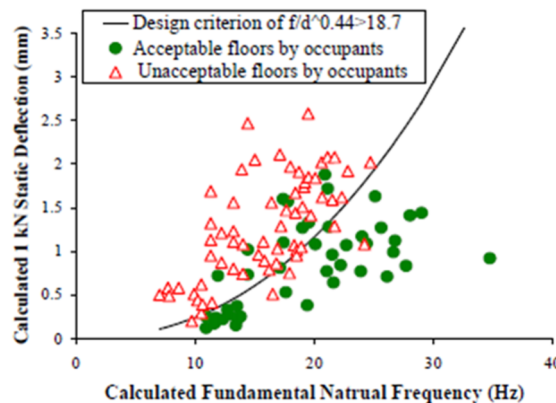
Figure 2-29 *Comparison between the proposed criterion and subjective rating of 106 field floors* (Hu & Chui 2004)

2.6.1.2 Office floors

Due to the popularity of open-plan work spaces, architects are demanding longer lengths of unsupported floor. Longer spans reduce the fundamental frequency making the floor more prone to excitation from one of the harmonics of walking. There are a number of reasons why the vibration criteria discussed in Section 2.6.1.1 may not be appropriate for long-span timber floors in commercial buildings:

- Criterion was founded on measurements on short-span floors within a residential context (Al-foqaha, Cofer & Fridley 1999; Dolan et al. 1999; Ohlsson 1988a; Onysko 1988; Smith & Chui 1988) which typically span between walls. In many cases, timber commercial buildings use a post-and-beam method of construction which means floors will span between primary beams.

- Combined frequency and deflection criterion may be too severe leading to increased dimensions for timber floor joists (Hamm, Richter & Winter 2010).

- The floor is assumed to undergo a transient response with some criterion using a unit impulse approach to represent the heel strike transient and predict floor response (Ohlsson 1988a; Smith & Chui 1988). The longer spans in commercial building floors coupled with closely spaced modes and low modal masses may in

fact give rise to resonant responses. Further, response measurements from which criterion were developed have been based on dynamic tests involving a heel drop impact (Dolan et al. 1999; Smith & Chui 1988) or an impact from an object to simulate the heel strike transient (Hu & Chui 2004).

- The decking in residential timber floors is generally thin and assumed to provide little if any additional stiffness to the floor system. On the other hand, timber floor structures for commercial buildings typically have a thicker decking (referred to as the *flange)* which is generally glued and screwed to joists (referred to as *webs*). The section can thus be assumed to act compositely under serviceable loads (Zabihi 2014).

- Criterion typically only consider the contribution of the fundamental mode (Al-foqaha, Cofer & Fridley 1999; Dolan et al. 1999; Onysko 1988; Smith & Chui 1988) even though timber floors are prone to modal clustering due to the orthotropic behaviour of the system (Chui 1986; Filiatrault, Folz & Foschi 1990).

- Criterion which suggest that the fundamental frequency should be calculated based on theoretical equations of a simply-supported beam or plate do not consider the potential flexibility of the support itself. This is particularly important since ribbed-deck floors span between primary beams which can contribute to the floor vibration problem.

- Design of commercial buildings are complex and require more engineering analysis than the design of residential dwellings. Consequently, finite element analysis software is likely to be used to obtain the modal properties of all relevant modes of the floor rather than theoretical equations.

Research on suitable vibration criteria for timber floors in commercial buildings are limited, in part due to the lack of practical examples from which measurements can be taken. There are, to the authors knowledge, only three criterion which are proposed to be applicable to long-span timber floors: Hamm et al. (2010), Chang et al. (2018) and Abeysekera et al. (2018).

(1) Hamm et al. (2010) method

The motivation for Hamm et al. (2010) vibration criteria was based on two reasons:

- Timber floors were still found to have vibration problems despite satisfying Eurocode 5 (2004) criteria.

- Frequency/deflection limits were too severe which led to larger timber beam cross-sections.

A total of 131 in-situ floor measurements were taken on a variety of timber floor constructions including those with screed, massive wood (i.e. floors made from engineered wood products including cross-laminated timber and laminated veneer lumber) and floors with and without any floor finishes. Measured values included the natural frequency of the floor after a jump or heel drop, acceleration due to walking, velocity due to a heel drop and damping of the floor after a heel drop. The floors were also subjectively evaluated through a rating scale from 1 (no vibration problem) to 4 (heavy vibration problem). In terms of natural frequency, there was found to be no correlation with the subjective evaluation, indicating that frequency alone cannot be an indicator for vibration behaviour. These results culminated into a set of rules for design and construction in the form of a flow chart shown in Figure 2-30.

Similar to the approach taken by Toratti and Talja (2006b), criteria are separated depending on the demand of the floor: floors without demands, floors with lower demands and floors with higher demands. The higher demand floor criteria are recommended for floors in office buildings which result in vibrations that 'are not perceptible or only perceptible when concentrating on them'; floor vibrations under this demand are also expected not to be 'annoying'. The frequency, stiffness and additional acceleration criterion for higher demand floors are as follows:

$$f_{limit} = 8 \text{ Hz}$$

$$w_{limit} = 0.5 \text{ mm}$$

$$a_{limit} = 0.45 \text{ m/s}^2$$

Note the static deflection is calculated under a 2 kN point load rather than the typical 1 kN point load; this is a result of better correlation between Equation 2.49 and subjective evaluation.

$$w(2kN) = \frac{2l^3}{48(EI)_l b_{w(2kN)}} \tag{2.49}$$

where: $$b_{w(2kN)} = \min(b_{ef}, b)$$

$$b_{ef} = \frac{l}{1.1} \cdot \left(\frac{(EI)_b}{(EI)_l}\right)^{0.25}$$

Hamm et al. (2010) is the first to provide an equation to calculate the acceleration response of the floor when the fundamental frequency is less than the 8 Hz limit (and $\geq$ 4.5 Hz):

$$a = \frac{F_{dyn}}{M^* \cdot 2\xi} = \frac{0.4 \cdot F(t)}{m \cdot 0.5l \cdot 0.5b \cdot 2\xi} \qquad (2.50)$$

where M^*=modal mass of the floor; F_{dyn}= total dynamic force; $F(t)$= harmonic parts of the force on the floor which depends on the natural frequency (provided in Hamm et al. (2010)). The 0.4 factor for F_{dyn} is used to take into account that the force acts for a limited duration and is not always in the centre of the floor.
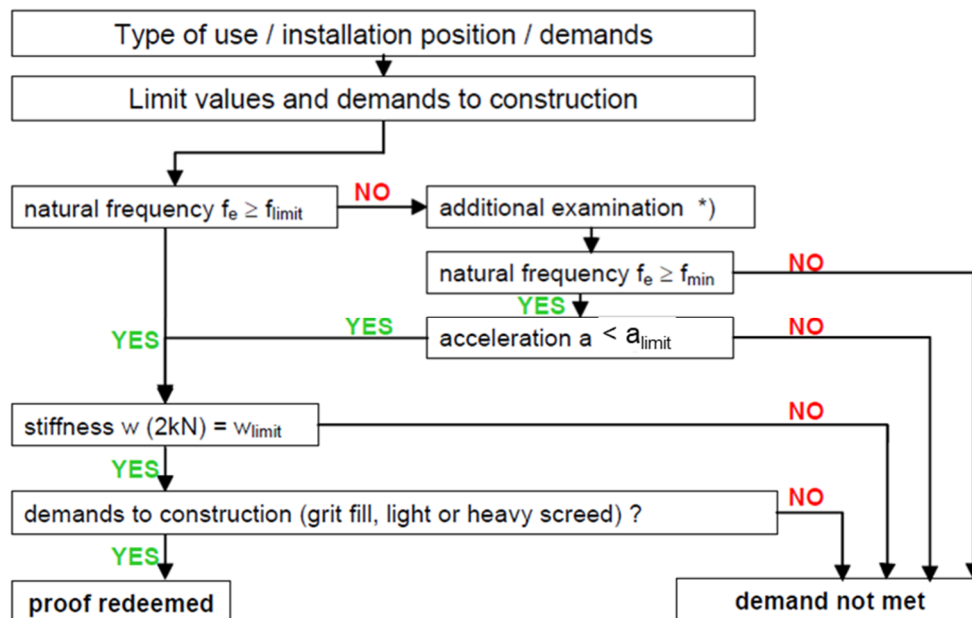
Figure 2-30 Proposed vibration design flow chart, adapted from Hamm et al. (2010)

(2) Chang et al. (2018) method

Due to the absence of a vibration design method for long-span timber floors, Chang et al. (2018) proposed a new design method that harmonises with current design practices for concrete and steel framed floors. The testing program involved a total of 16 floors including four CLT floors with spans ranging from 7.2 m to 9.0 m, eight timber joist floors with spans of 3.6 m to 5.8 m and four 'Profi Deck' floors with spans of 6.2 m to 14.0 m. The uses of the floors were mainly residential, although three floors were used in an office building and the four Profi Deck floors were used in schools. Modal properties were obtained using a heel-drop test while the acceleration response at the centre of the floor was obtained using a 76 kg walker with varying pace frequencies. Using an FE

model correlated to the measured modal properties of each floor, the acceleration response, and subsequent response factor (RF), was predicted using the effective impulse method for high-frequency floors provided in SCI P354 (Smith, Hicks & Devine 2009) and CCIP-016 (Willford & Young 2006). The RF is a measure generally used in vibration design guides for floors constructed from other materials and has been detailed in Section 2.6.2.

After finding high correlation between the measured RF and predicted Vibration Dose Value (VDV) ($R^2 = 0.9457$) as well as between the predicted peak acceleration and the measured RF ($R^2 = 0.8926$), Chang et al. (2018) proposed that the VDV should be used to determine satisfactory floor performance. The design guide requires the user to first calculate the weighted peak acceleration under a footfall impulse which is then used to estimate the VDV for the event as follows:

$$VDV_{event} \cong 0.27 \cdot a_{w,peak} = 0.27 \cdot 2\pi K f_n \sqrt{1 - \xi^2} \frac{I_{eff}}{M_n} W_b \qquad (2.51)$$

where K = empirical factor to modify the acceleration based on the results of Chang et al. (2018) floor measurements; I_{eff} = design footfall impulse force (Ns) as per CCIP-016 equation (Equation 2.21); W_b = frequency-weighting factor. The total VDV for the complete exposure period is estimated as:

$$VDV_{total} = 1.31 n^{0.25} \cdot VDV_{event} \qquad (2.52)$$

where *n* is the estimated number of events. The VDV limits specified in BS 6472 (2008a) and shown in Table 2-3 are recommended to be followed. It is important to highlight that this design method assumes the floor will undergo a transient response and, similarly to other criterion for residential floors, assumes that the fundamental mode contributes the majority of the floor response.

Chang et al. (2018) also noted the results of subjective testing performed on these floors showed that a RF limit of 12 or even 18 may be more appropriate. This is in contrast to the RF limit of 8 which is proposed in vibration design guides SCI P354 and CCIP-016 (as will be detailed in Section 2.6.2.1).

Table 2-3 *VDV limits for 16 hour day for residential and commercial buildings* (British Standards Institution 2008a)

	VDV (m/s$^{1.75}$)	
	Residential	Commercial
Low probability of adverse comment[1]	0.2 – 0.4	0.4 – 0.8
Adverse comment possible	0.4 – 0.8	0.8 – 1.6
Adverse comment probable[2]	0.8 – 1.6	1.6 – 3.2

[1] Below these ranges adverse comment is not expected.

[2] Above these ranges adverse comment is very likely.

(3) Abeysekera et al. (2018) method

Abeysekera et al. (2018) proposed a new vibration design method for timber floors with performance-based frequency, stiffness and RF criteria. The method is only applicable to floors which span between rigid (wall) supports and thus is not appropriate for long-span timber floors spanning between primary beams. It follows a similar approach to CCIP-016 and SCI P354 in that the fundamental frequency is used to determine whether the floor will undergo a resonant (f_1<8 Hz) or transient response (f_1>8 Hz). A stiffness and RF criterion is proposed for both floor categories with three different limits depending on the required performance level of the floor. For offices, the RF limit is 8, 12 and 16 for a quality, base and economy choice, respectively; these values are similar to the limits recommended by Chang et al. (2018). Unlike most other vibration design methods for timber floors, the method for transient response floors considers the contribution of higher modes through a factor K_{imp} which is calculated as follows:

$$K_{imp} = \max \left\{ \begin{array}{c} 0.48 \left(\frac{b}{l}\right) \left(\frac{(EI)_b}{(EI)_l}\right)^{0.25} \\ 1 \end{array} \right\}$$ (2.53)

However, for design of resonant response floors, only the contribution of the first resonant mode is considered. Stiffness criterion are also provided, although as they are based on tests of traditional timber joist floors, they are deemed to be 'less applicable'.

Using existing test data from Toratti and Talja (2006b) and Hamm et al. (2010), the transient response design method provided a good prediction of the vibration

performance. The resonant response method was checked with only one example (due to the limited test data for resonant timber floors), although the predicted acceleration provided a close match to the measured.

2.6.2 Procedures and criteria for other floors

The most widely used floor vibration design guides for concrete and steel-concrete composite floors include those published by:

- Concrete Centre (CCIP-016) (Willford & Young 2006) in the UK
- Steel Construction Institute SCI P354 (Smith, Hicks & Devine 2009) in the UK
- American Institute of Steel Construction (AISC DG11) (Murray et al. 2016) in North America
- Human Induced Vibrations of Steel Structures (HIVOSS) in Germany

The CCIP-016 is applicable to floor structures of any form of construction and thus should be suitable for long-span timber floors. SCI P354 and AISC DG 11 have similar principles to response prediction to CCIP-016, however have been recommended for use only with steel-framed structures. There have been limited studies on the applicability of these widely adopted vibration design guides to long-span timber floors.

Most guides provide two options to estimate modal properties and predict floor response: simplified and finite element (FE) analysis methods. Estimating modal properties based on a simplified approach is performed through theoretical equations for the modal properties (frequencies and modal mass) of beams and plates with ideal support conditions. However, as floors in modern commercial buildings may involve openings and/or irregular shaped floor plates, it is generally assumed that a designer will have an FE model of the floor structure from which an accurate prediction of mode shapes and frequencies can be obtained.

2.6.2.1 CCIP-016 and SCI P354

The design approach in CCIP-016 and SCI P354 first involves characterising the floor as a low- or high-frequency floor with the assumption being that higher frequency floors will not sustain resonance with walking forces. CCIP-016 bases the cut-off frequency on 4.2 times the maximum expected walking pace in the specific environment; a maximum walking frequency of 2.5 Hz is proposed for circulation zones in any building, while for

areas within office bays and residential rooms the maximum proposed walking pace is 2.0 Hz. SCI P354 is the only guide which provides a frequency cut-off depending on the floor occupancy with a cut-off of 10 Hz suggested for 'open plan offices'.

The guides follow a deterministic approach to human walking load modelling (as discussed in Section 2.3.3.1) with the load model applied at the expected excitation location (corridors or pathways). If the excitation location is unknown, the analysis can be performed for the worst case node i.e. at antinodes of each mode. For low-frequency floors, the Fourier series continuous walking load function (Equation 2.20) including four harmonics is used. For each considered walking frequency, the four harmonics are calculated and the harmonic amplitude is quantified by multiplying the weight of the walker (generally assumed to be 756 N for a 76 kg person) by the dynamic load factor (DLF) specific for each harmonic. The DLF suggested in CCIP-016 follows data from Kerr (1998) who measured 880 single footfall time histories from 40 individuals, as well as data from Rainer et al. (1988), Ohlsson (1982), Galbraith et al. (1970) and Harper (1962). From this data, there is a clear trend of the first harmonic force increasing with pace frequency. However, for the second, third and fourth harmonic forces, there is significant scatter (Willford, Young & Field 2006). Consequently, statistical regression was performed on the footfall load measurements to obtain a mean and 'design' DLF value (25% chance of exceedance) for each of the four harmonics. SCI P354 propose slightly different DLF values as the guide uses measurements from Rainer et al. (1988), Alves et al. (1999), Kerr (1998) and Ellis (2000).

The total floor response from each harmonic is then calculated by summing the acceleration response of each relevant mode and dividing the response by the base curve for human perception (Figure 2-25) to obtain the response factor (RF). The total RF generated by the specific walking pace is then calculated using the square-root of sum of the squares (SRSS) method and compared to the recommended limit. The critical walking frequencies which will induce the largest floor response would align with the first four integer divisions of the relevant low-frequency modes. CCIP-016 considers all modes up to 15 Hz while SCI P354 considers modes up to 12 Hz.

For high-frequency floors, both guides have adopted the effective impulse method developed by Arup (Willford, Young & Field 2006) which assumes the response of high-frequency floors is governed by the initial peak amplitude from the impulsive heel-strike component of the footstep. In CCIP-016, the effective impulse equation is as per Equation 2.21 while the effective impulse in SCI P354 has coefficient *A* equal to 60Q/700 which incorporates factors provided in EN 1990 Annex C (British Standards Institution 2002). This results in a 19% larger effective impulse for a 76 kg person than the design I_{eff} listed in CCIP-016. Since faster walking speeds induce greater responses, typically only the response from the fastest anticipated walking pace needs to be checked. The total velocity (for CCIP-016) or acceleration response (for SCI P354) is then calculated by summing the responses for each mode up to 2 $\times f_1$ Hz and the RF is assessed. If the RF limit is not satisfied, SCI P354 recommends that a VDV is calculated based on Ellis (2001) equation shown in Equation 2.28.

The recommended limits are similar in concept to the multiplying factors noted in Table 2-2 and do not vary depending on the type of floor response (i.e. resonant or transient). CCIP-016 recommends a more stringent limit (RF < 4) for premium quality open-plan offices and open-plan offices with busy corridor zones near mid-span.

2.6.2.2 AISC DG11

Section 7 of AISC DG11 (2016), which is a new addition to the first edition of the design guide (Murray, Allen & Ungar 1997), describes the finite element analysis methods recommended for low- and high-frequency floors. The approach is slightly different from CCIP-016 and SCI P354 in that the frequency response function (FRF) is used to determine the most responsive modes. The FRF plot at response location *j* is obtained by applying a sinusoidal load with unit amplitude at the expected excitation location *i.* Frequencies of the applied load range from 1 Hz below the fundamental frequency up to approximately 20 Hz and should include the eigenfrequencies. For low-frequency floors, defined as those with a fundamental frequency less than 9 Hz, the peak sinusoidal acceleration due to walking is calculated:

$$a_p = FRF_{max}\alpha Q\rho_r \qquad (2.54)$$

where FRF_{max} = maximum FRF magnitude at frequencies below 9 Hz; Q = body weight (assumed as 746 N); α = dynamic coefficient; ρ_r = resonant build-up factor. Instead of calculating the response due to each harmonic, AISC DG11 (2016) approximates the Willford et al. (2007) second to fourth dynamic load factors and provides an equation for the α:

$$\alpha = 0.09e^{-0.075fn} \tag{2.55}$$

where f_n = dominant frequency (Hz). The peak acceleration is calculated for each responsive mode under 9 Hz and expressed in %g to compare with recommended criterion.

For high-frequency floors, AISC DG 11 also uses the effective impulse approach as detailed in the previous section. However, unlike CCIP-016 and SCI P354, the pace frequency from which I_{eff} is calculated is based on the dominant frequency which is defined as the frequency of the maximum FRF amplitude. The peak acceleration is then calculated for each mode above 9 Hz up to 20 Hz and summed to obtain the total response. The guide acknowledges that the transient response cannot be compared to the limits for continuous vibrations and thus the equivalent sinusoidal peak acceleration (ESPA) is computed; the ESPA is a product of the RMS of the acceleration response over one footstep period and $\sqrt{2}$ (ratio of peak-to-RMS acceleration for a sinusoid). A summary of the considered modes, response measures and recommended criterion for the three aforementioned guides are shown in Table 2-4. Note for CCIP-016 and SCI P354, the parameter from which the RF is calculated is shown in parentheses.

Table 2-4 *Summary of considered modes, response measures and recommended criterion for CCIP-016, SCI P354 and AISC DG 11.*

Guide	f_c (Hz)	Resonant response $f_1 < f_c$		Transient response $f_1 > f_c$		Criterion
		Modes	Measure	Modes	Measure	
CCIP-016	10.5	< 15 Hz	RF $(a_{w,p})$	< 2 × f_1	RF(v_{rms})	RF < 8 RF<4*
SCI P354	10	< 12 Hz	RF$(a_{w,rms})$	< 2 × f_1	RF$(a_{w,rms})$	RF < 8
AISC DG11	9	< 9 Hz	a_p/g	< 20 Hz	a_{ESPA}/g	<0.5%g

Note: * reduced limit for premium quality open-plan offices and open-plan offices with corridor close to mid-span.

2.6.2.3 HIVOSS

HIVOSS (Feldmann 2008) is commonly used in Europe for the assessment of steel-concrete composite floors and follows the one-step RMS (OS-RMS) method developed from a research project conducted by Sedlacek et al. (2006). The OS-RMS value is the RMS over the time-history response of one footstep and does not consider the walking path i.e. the excitation point is kept fixed. Based on investigations of OS-RMS value of 700 people at the entrance of a building in Delft, statistical distributions were obtained and correlated for the step frequency and body mass (Feldmann et al. 2009). From this data, a cumulative probability distribution was calculated and the 90th percentile value, referred to as the OS-RMS90 was proposed for design. Thus, it is one of the only vibration design methods that incorporates a probabilistic approach.

The data from the study was used to produce a set of graphs for damping ratios of 1% to 8% from which the designer can obtain the OS-RMS90 based on the frequency and modal mass of the floor. For floors with many dominant modes, the SRSS method is used to obtain the total OS-RMS90 for all relevant modes, although, there is no guidance on how many modes should be considered. One important point of differentiation of HIVOSS from the other previously discussed design guides is that criterion is provided with respect to six floor classes and the floor occupancy. For office floors, the OS-RMS90 boundary for the lowest recommended performance class (Class D) is 0.8 to 3.2 which is equivalent to a RF of 8 to 32.

2.7 Concluding remarks

This chapter presented a review of important literature on the three key areas of vibration serviceability of floors with a focus on timber floors as the transmission path. It is clear that each component (the vibration source, the transmission path and human sensitivity to vibration) has its own complexities. These complexities introduce a number of challenges to vibration serviceability design and are particularly important to consider for timber floors where vibration design is critical. These challenges can be separated into three areas:

1. Idealising the walking force using a deterministic load model:

   The assumptions made when using the deterministic modelling approach have been shown to produce inconsistencies in response prediction (Brownjohn, Racic & Chen 2016; Brownjohn & Middleton 2008; Ellis 2000; Živanovic & Pavic 2009). Consequently, some researchers have recommended that a probabilistic approach to walking load models is more appropriate (Živanović, Pavic & Reynolds 2007b). The main benefit of a probabilistic force model is the ability to provide a range of responses over a population sample which allows the engineer to make an informed decision of the likelihood that a certain response will be exceeded. In addition, there is potential for probabilistic models to be customised with the characteristics of a certain country's population.

2. Disparity between vibration codes and standards in evaluating human exposure to vibration:

   The recommended quantity for evaluation of vibration exposure differs between countries. For example, the British standard BS 6472-1 (2008a) only suggests the VDV while ISO 2631-1 (1997) recommends either the running RMS method or VDV in addition to the general RMS acceleration. Frequency-weighting curves for z-axis (parallel to spine) vibrations vary between standards. Further, the basis of the base curve for human perception of continuous vibrations from which criteria are established remains unclear and interestingly is no longer included in current edition of ISO 2631-2 (2003).

3. Duration of vibration is generally not considered in criteria in current design guides:

   Despite duration being a key factor in human perception (Lenzen 1966; Parmelee & Wiss 1974) and annoyance (Howarth & Griffin 1988), where human the pass-

fail response factor (RF) criterion dominates the approach taken in current vibration design guides. This is in contrast to the approach taken in Japan's vibration guide (AIJES-V001 (2018)) where a factor dependent on vibration duration *T* is used to attenuate the response for vibrations lasting less than 10 s.

In addition to the afore-mentioned issues, there are a number of gaps in relation to floor vibration of long-span ribbed-deck cassette structures which have been identified from the literature review. These include:

- Lack of experimental investigations on the influence of boundary conditions and connections between cassettes:

  A number of experimental investigations have been performed on short-span timber joist floors for use in residential dwellings. However, there is little research around the typical support conditions for a cassette floor used in a commercial building and how these can be modelled. Further, as cassette floors are prefabricated off site and brought to site as individual elements, an understanding of the connections between cassettes is also required for modelling purposes. From studies on CLT panels, it was found that modelling the connections between adjacent panels is imperative for accurate prediction of frequencies and mode shapes (Ussher et al. 2017a).

- Lack of a conclusive vibration design procedure suitable for long-span timber floor structures in commercial buildings:

  There are currently three different design criteria which are deemed to be appropriate for timber floors in commercial buildings. However, the main weakness for two of the methods (Chang et al. 2018; Hamm et al. 2010) is the disregard for the contribution of higher modes which is an important consideration for timber floors due to the susceptibility to modal clustering (Chui 1986; Filiatrault, Folz & Foschi 1990). Although the method proposed by Abeysekera et al. (2018) has merit in terms of proposing performance based criteria (i.e. quality, base and economy choice), it is only stated to be applicable for floors spanning between walls. As such, there is currently no agreed design procedure suitable for long-span timber floors.

- <u>Lack of subjective tests performed on long-span timber floors in commercial buildings</u>

Chang et al. (2018) and Abeysekera et al. (2018) have both noted that tolerance to and acceptability of vibrations in timber floors may be higher than on steel-composite or concrete floors. However, the limited nature of long-span timber floors in practice, particularly in office settings, means that subjective testing to propose more appropriate acceptability criterion is lacking.

The focus of this thesis will be on the first and second aforementioned knowledge gaps in relation to long-span timber floors. Although the third gap deserves attention, it is not within the scope of this thesis.

Chapter 3

Dynamic Testing Methods

3.1 Introduction

Dynamic testing allows an understanding of how a structure or system will behave under a dynamic load. Such information is required in a variety of situations: an aeroplane undergoing atmospheric turbulence, a high rise building subject to wind loading and, in this case, a building floor excited by human walking. Behaviour or 'response' of the structure is attributed to the basic relationship (Ewins 2000) as shown in Figure 3-1. Consequently, vibration testing can be distinguished by two types:

1. Measurement of both the response and input (i.e. modal testing).
2. Measurement of response only (i.e. operational testing).

Response	=	Properties	×	Input

Figure 3-1 *Fundamental relationship of system response*

In this research, estimating modal properties as well as understanding the response of the floor under loading that would be typical in buildings was of interest. These tests were conducted for two main reasons. Firstly, to investigate the effects of support conditions

and cassette-to-cassette connections to the floor modal properties and response to walking excitation. Secondly, to obtain modal properties for use in finite element model calibration and validation which can subsequently be used to investigate the influence of different human walking load models (Chapter 5), modelling of cassette-to-cassette connections (Chapter 6) and parametric studies to investigate the significance of certain design parameters to the floor modal properties and response (Chapter 7).

This chapter first presents the investigated LVL ribbed-deck cassette floor including tests to determine the material properties of the web member. Procedures to determine the modal properties and floor response are then detailed. Finally, the experimental test program, methods and set-up will be summarised.

3.2 The timber cassette floor

3.2.1 Design of the floor

The purpose of the timber cassette design was not to provide an optimised design solution for vibration performance but to present a system which, at minimum, satisfies the limit states of design as per the *Wood Solutions Technical Design Guide 31: Timber Cassette Floors* (Crews & Shrestha 2016). As a result, fire and acoustic performance were not considered. Further, to keep cost efficiency, standard off-the-shelf section sizes were selected. The limit states satisfied were:

1. Short- and long-term ultimate limit state (strength)
2. Short- and long-term serviceability limit state (deflection)
3. 1.0-kN serviceability limit state (current recommended limit for dynamic behaviour)

Load type, load combinations and modification factors for both ultimate and serviceability limit states have been defined in accordance with the AS/NZS 1170.0 (2002) and AS 1720.1 (2010b) standards. The floor was designed to be appropriate for use in a commercial building where a 9 × 9 m grid is a common architectural demand as it suits basement parking layouts and provides flexibility of internal office layouts (Timber Development Association & Forsythe 2015). As a result, web members were 9 m in length. The loading assumed for design was typical for a commercial building and

are presented in Table 3-1. A flange overhang of 95 mm at each end of the cassette was also included to suit typical timber post-and-beam construction practices.

Table 3-1 *Loading assumed for design of timber cassette floor*

Load description	Load (kPa)
Superimposed Dead Load	
Services	0.25
Lighting	0.25
Floor finishes	1.0
Live Load	
Commercial building	3.0

The final geometry of the cassette is shown in Figure 3-2 and consists of a 90 mm thick LVL11 panel (manufactured by Nelson Pine) glued and screwed to three 360 × 63 mm hySPAN® web members (manufactured by Carter Holt Harvey) spaced equidistance apart. A top flange rather than a bottom flange was chosen based on discussions of constructability with industry members. PURBOND® provided the actual bond between the flange and web members while screws (Rothoblaas HBS6160) at 355 mm spacing were used to facilitate clamping action for the glue to set properly. Zabihi (2014) has shown that such a connection can provide a perfect bond and full composite action between web and flange members under both ultimate limit state (ULS) and serviceability limit state (SLS). As such, full composite action was assumed and the flexural stiffness of the section was calculated via the transformed section method.

The 1500 mm wide supporting timber frame was made from two hySPAN® web members screwed together and rigidly connected to the slab on ground through equal angles (three on one side and two on the other at alternating locations). Dynabolts were used to connect the angle to the concrete floor while 100 mm long timber screws were used to connect the angle to the frame. Dynabolts are a proprietary product which have an integrated pull-down section, designed for medium duty anchoring or timber and steel fixtures to concrete, brick or block.

(a)

(b)
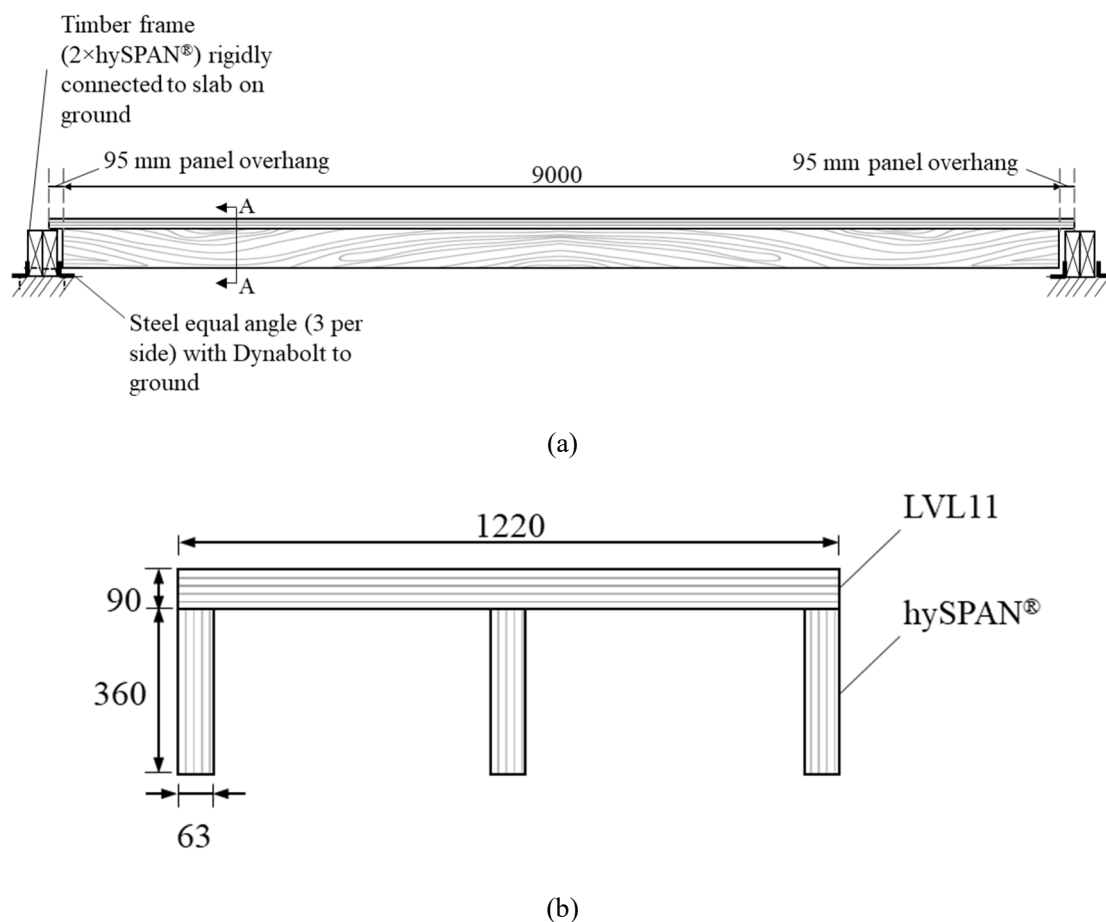
Figure 3-2 *Tested ribbed-deck floor (a) elevation; (b) cross-section A*

The edgewise material properties as provided by the respective manufacturers are provided in Table 3-2. Material testing to obtain the modulus of elasticity parallel to grain and density of the hySPAN® member was conducted. Note that due to laboratory constraints, the material testing of the flange member could not be performed at the same time and had been planned for a later date. However, as will be detailed in Chapter 4 Section 4.5.4.2, the sensitivity of the natural frequencies of the first five modes were less than 7% for a ±10% change in flange material properties. Thus, it was decided that the material testing for the flange member was not required. Material testing of hySPAN® is detailed in Section 3.2.3.
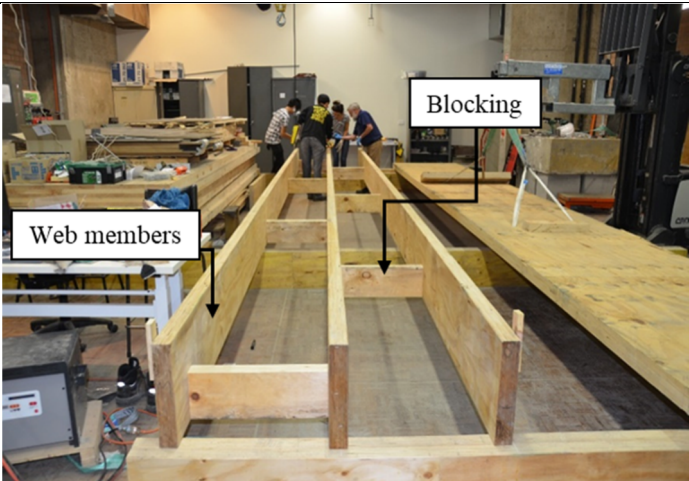
Table 3-2 *Edgewise limit state design characteristic values as per Nelson Pine for LVL11(2016) and Carter Holt Harvey for hySPAN®(2012)*

			LVL11	hySPAN®
Modulus of elasticity	MoE	*MPa*	11000	13200
Modulus of rigidity	G	*MPa*	550	660
Bending strength	*f'b*	*MPa*	38.0	41.0
Tension parallel to grain	*f't*	*MPa*	26.0	25.0
Compression parallel to grain	*f'c*	*MPa*	38.0	41.0
Shear in beams	*f's*	*MPa*	5.0	4.6

3.2.2 Fabrication

Both cassette floors were fabricated at the Timber and Structures Laboratory at the University of Technology Sydney (UTS). The task was challenging due to the enormity of the elements which had to be manoeuvred with the use of forklifts and overhead cranes. It is believed with the correct machinery and process, the cassettes can be efficiently prefabricated at a factory. Table 3-3 briefly describes the fabrication procedure with associated photos.

Table 3-3 *Fabrication procedure for the timber cassettes*

Step	Photo
1	

Web members were laid out at 579 mm centre to centre spacing using pre-cut blocking members. Holes for screws for the panel to joist connection were marked up on the panel and pre-drilled. Four 30 mm diameter holes were also drilled into the panel for ease of lifting with overhead crane or forklift.

2

Once joists were in place, a generous layer of PURBOND® glue was painted over the top surface. Note each joist was painted at the same pace to ensure consistent glue open time (for PURBOND® the specified work time is 45 minutes).

3

The top panel was lifted up with overhead crane, lined up with the joists below and carefully dropped into place using a centreline drawn at mid-span. Once in place, screws were drilled at pre-drilled locations along the joists. Note that the drilling had to be completed within the specified open time for the glue.

4

The cassette was left in place for 24 hours for glue to reach final bond strength.

3.2.3 Determination of material properties of LVL

The purpose of material testing within this research was to obtain definitive properties for use within a finite element (FE) model. Input material properties can influence the dynamic performance of the floor system and thus testing was essential to minimise the number of uncertainties between the experiment and the FE model. As such, only the properties having an influence on the natural frequencies were tested, namely modulus of elasticity and density.

Figure 3-3 *Cross-section of LVL showing veneers*

It is important here to note the nature of wood as a natural material consisting of elongated wood cells (also called fibres) arranged to run parallel to the trunk and glued together by a lignin-rich layer called the middle lamella. The cell wall itself is what provides the strength and stiffness properties of the wood (Harte 2009). Laminated veneer lumber (LVL) is manufactured from thin sheets of wood (also called 'wood veneers') which have been rotary peeled from logs. The wood veneers, shown in Figure 3-3, are glued together using heat and pressure resulting in a product with superior reliability, strength, stiffness and dimensional stability than traditional sawn wood (Harte 2009). Each veneer layer is arranged so that the grain orientation is aligned parallel to the long direction of the member to ensure high strength along the member length (Lam 2009). Consequently, material properties are strongly influenced by the grain direction (orthogonal) where the strength parallel to grain can be up to 10-fold greater perpendicular to grain.

(a) Edgewise   (b) Flatwise
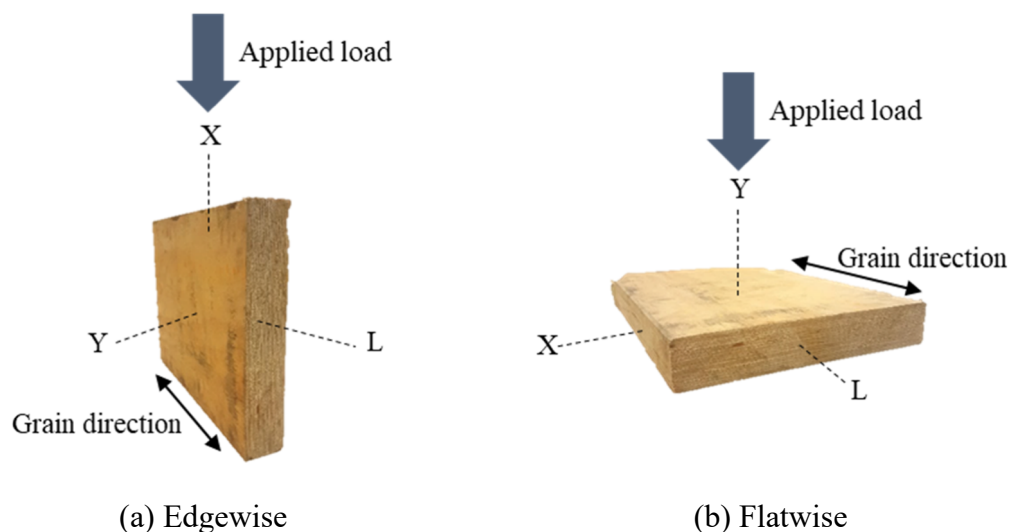
Figure 3-4 *Orientations of laminated veneer lumber*

Both edgewise and flatwise (as shown in Figure 3-4) modulus of elasticity were determined from a four point bending test in accordance with AS/NZS 4357.2 (2006). Ten test specimens (five for edgewise and five for flatwise tests) were cut from a 360 × 63 × 9000 mm hySPAN® sheet. The sheet was from the same batch as the other members used to fabricate the cassette. Although 30 test specimens are typically required as per Clause 5.2 of AS/NZS 4357.2 (2006), it was decided that a smaller sample size was sufficient as the purpose of the property characterisation was not for commercial use. The apparent modulus of elasticity was calculated as per Clause 9.4 of AS/NZS 4357.2 (2006) while the density was calculated as per Clause 2.3 of AS/NZS 4063.1 (2010a). Test specimen dimensions and experimental data from the bending tests are presented in Table A.1 and Figure A.2 (Appendix A), respectively. The mean edgewise and flatwise modulus of elasticity and density obtained from test data as well as the coefficient of variance (CoV) are summarised in Table 3-4.

Table 3-4 *Summary of measured material properties for LVL13*

	MoE (MPa)	CoV (%)	Density (kg/m³)	CoV (%)
Flatwise	12690	2.44	589.1	1.41
Edgewise	12754	2.14		

3.3 Experimental Program

Dynamic tests were conducted in the Timber and Structures Laboratory of UTS. Tests were split into two configurations: single cassette (denoted 'C1' in test name) and double cassette (denoted 'C2' in test name). The test program is summarised in Figure 3-5. Note the results of tests outlined with a blue dashed line were used for finite element model correlation.
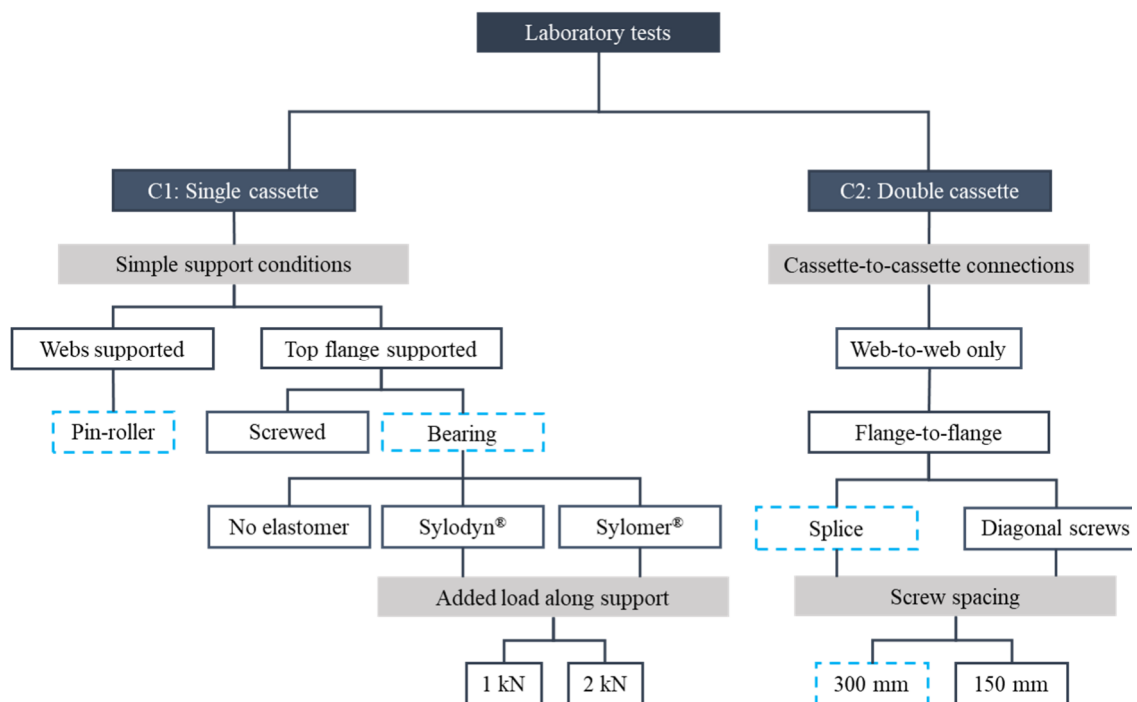
Figure 3-5 *Flowchart of laboratory experiments*

3.3.1 C1: single cassette tests

The purpose of the single cassette tests was to minimise the number of variables which may be caused by additional cassettes and to isolate the influence of various support conditions on the dynamic response of the floor. Investigated boundary conditions were split into two categories: web supported and flange supported. In both cases, a timber frame was used to support the cassette off the ground. The frame was rigidly secured to the laboratory floor using steel brackets as detailed in Section 3.2.1.

The web supported boundary condition involved the web members bearing onto a steel plate and shaft support, as shown in Figure 3-6, which were arranged on the surface of the timber frame. On one end, the plates were arranged to replicate a pin with the indented groove fitted around the shaft to restrict horizontal movement (left image Figure 3-6 (b)).

On the other end, a roller support was replicated by reversing the plates so the shaft was free to move horizontally (right image Figure 3-6 (b)). With the webs bearing on this support, there was no mechanism to stop the ends 'flapping' or bouncing. However, the amplitudes from the impact hammer and walking tests were not expected to be large enough against the self-weight of the cassette. This support condition was used to validate the finite element modelling approach.

(a) C1_Web test set-up
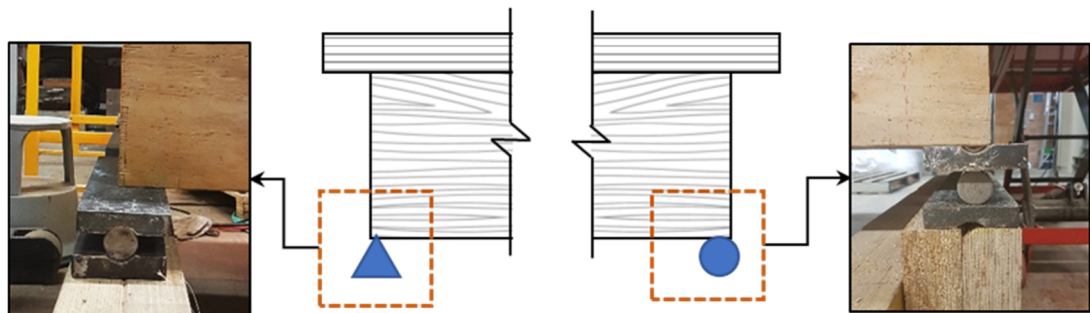
(b) Steel pin and roller used for C1_Web test

Figure 3-6 *Stage C1 web supported test boundary conditions*

The three other simple boundary conditions involved the overhanging flange element supported by the timber frame. This isolates the effect of the flange bearing component of the typical support condition for a ribbed-deck cassette (Figure 2-19). Initial testing revealed that the mode shapes obtained from the flange supported test set-up was highly sensitive to the uniformity of the contact between the top surface of the timber frame support and the underside of the flange. For example, one accelerometer placed on the unsupported side of the cassette at mid-span was picking up the first bending mode while the accelerometer positioned on the opposite unsupported side was not. After a number of different solutions were investigated to avoid the slight level differences, it was decided that a thin plywood veneer would be 'moulded' to the top surface of the timber frame

using a thin layer of cornice plaster, as shown in Figure 3-7; this support configuration will still be referred to as a 'timber frame support' for ease of discussion.

(a) Overview of flange bearing support condition   (b) Detail of plywood solution
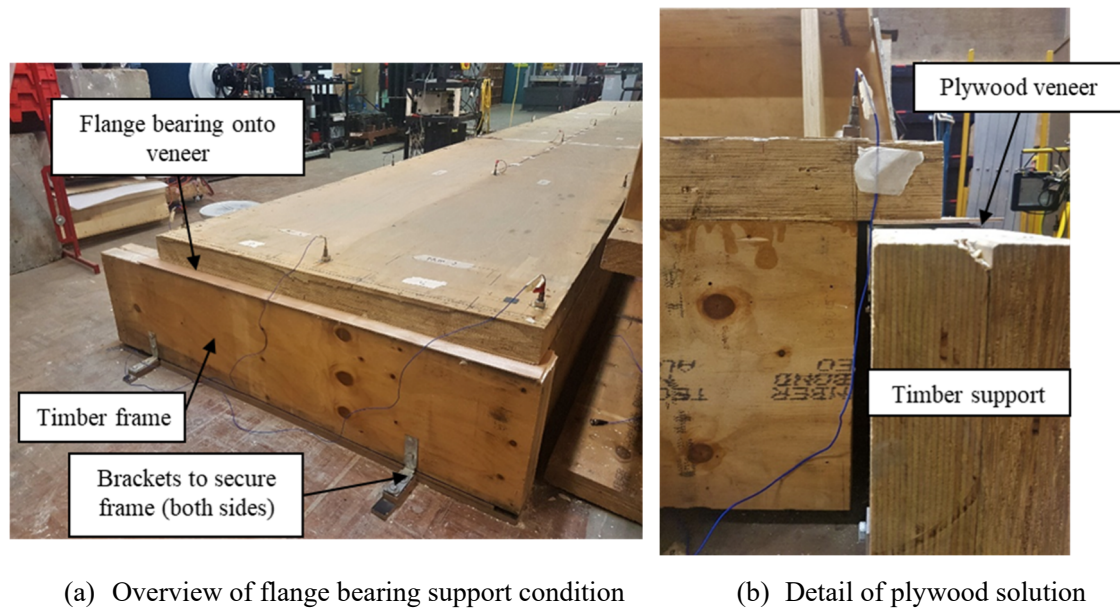
Figure 3-7 *Flange bearing support condition*
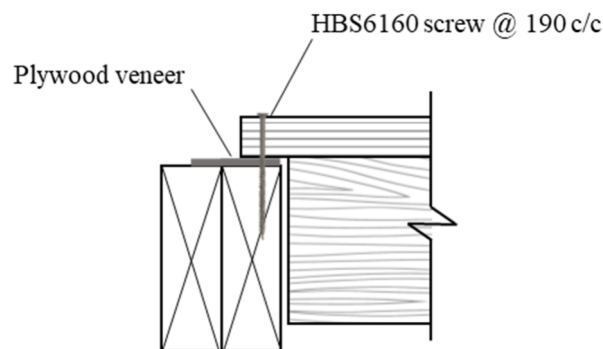
Figure 3-8 *Detail of 'screw' support condition*

Firstly, the boundary conditions with the flange bearing onto the timber frame (denoted by 'flange' in test name) and screwed to the timber frame (denoted by 'screw' in test name) were tested. The detail of the 'screw' support condition is shown in Figure 3-8. For the second stage, the boundary condition involved an elastomer sandwiched between the flange and the supporting timber frame running continuously along the full width of the cassette. This support was similar to the support condition tested by Jarnerö et al. (2015). The polyurethane elastomers, supplied by Getzner, were Sylomer® SR 55 (denoted as 'Smer' in test name) and Sylodyn® NB (denoted as 'Sdyn' in test name) and can be seen in Figure 3-9 (a); both elastomers were 12.5 mm thick. Sylomer has a combination of both spring and damper properties while Sylodyn has stronger spring and

smaller damping properties. Both elastomers are suitable for a wide range of applications including as a vibration isolation element in the rail industry, elastic machine bearing and to minimise footfall noise in buildings including those made from mass timber (Getzner GmbH 2016). The maximum compression loading within the static range of use of both interlayers are shown in Table 3-5. The mass of the floor was 1052 kg which yields a static load of 0.050 N/mm^2 at each support resulting in a ratio of utilisation of 66% and 90% for the Sylodyn and Sylomer interlayer, respectively. The ratio of utilisation is an important consideration when selecting an appropriate elastomer for the design where the elastomer behaves differently depending on whether the loading sits within the static or dynamic range of operation. In the static range of use (within the maximum compression limit), the relationship between the load and deflection of the material is generally linear. When the load surpasses the static range, the elastomer becomes 'softer' and the deflections due to additional static and dynamic loading increases; this range allows for effective vibration isolation (Jarnerö, Brandt & Olsson 2015). The elastomer should be designed so that the permanent static load falls within the static range of use. A test set-up using the Sylomer elastomer is shown in Figure 3-9 (b).

Table 3-5 *Interlayer properties*

			Sylodyn NB	Sylomer SR 55
Manufacturer			Getzner	Getzner
Maximum compression load		*N/mm²*	0.075	0.055
Ratio of utilisation (Static 'S' or Dynamic 'D' range)	0 N	*%*	66 (S)	90 (S)
	1000 N	*%*	79 (S)	108 (D)
	2000 N	*%*	92 (S)	126 (D)
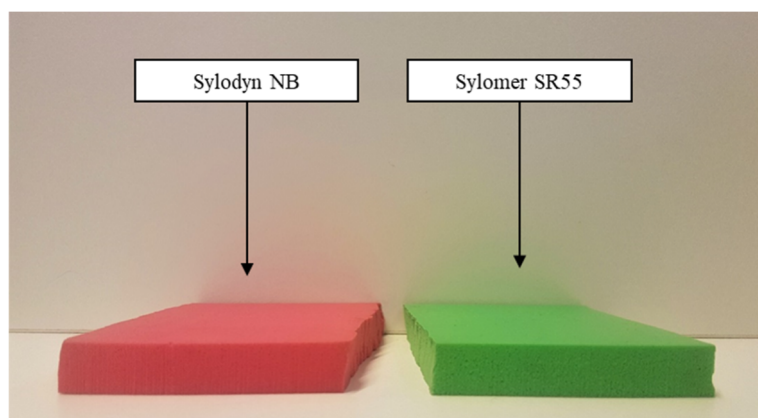
(a) Elastomers used in tests
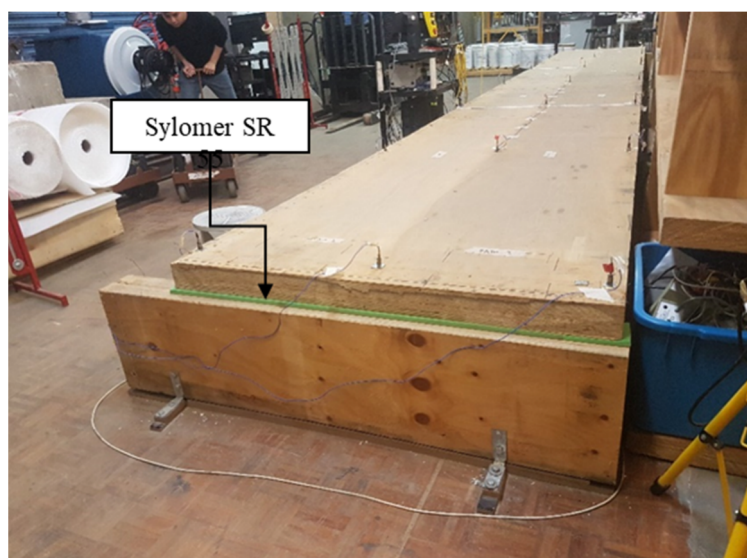
(b) Sylomer support condition

Figure 3-9 *Set-up of simple boundary condition with elastomer*

The effect of added load at support location was also explored to determine the influence of a higher ratio of utilisation of the elastomer to dynamic response. Calibrated 250 N steel plates were stacked over the support between joists to create two additional loading test cases of 1000 N and 2000 N (denoted by 'SdynX' in the test name where 'X' refers to the load at each support), as shown in Figure 3-10. The ratio of utilisation for cases with added load at support is also shown in Table 3-5; as shown, the added load for the Sylomer tests results in the elastomer entering the dynamic range of use. Although the positioning of the plates do not replicate a perfect line load as may be the case from partition walls in a real building, it was deemed that the effect of added mass at supports could still be explored since the loading would be transferred directly to the elastomer on the timber frame. All single cassette tests conducted are summarised in Table 3-6 with note of the reference test case.
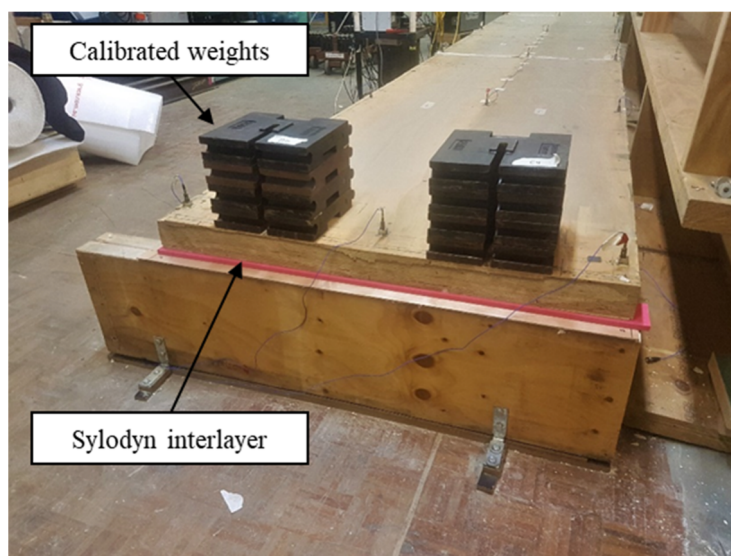
Figure 3-10 *Calibrated weights at support – typical set-up (test C1_Sdyn1500 shown)*

Table 3-6 Summary of single cassette tests

Test name	Support condition		Elastomer	Load (N)	Reference test
	Element	Support Type			
C1_Web	Web	Pin-roller	-	-	-
C1_Flange	Flange	Screwed	-	-	-
C1_Screw	Flange	Bearing	-	-	C1_Flange
C1_Sdyn0	Flange	Bearing	Sylodyn	-	C1_Flange
C1_Smer0	Flange	Bearing	Sylomer	-	C1_Flange
C1_Sdyn1000	Flange	Bearing	Sylodyn	1000	C1_Sdyn0
C1_Smer1000	Flange	Bearing	Sylomer	1000	C1_Smer0
C1_Sdyn2000	Flange	Bearing	Sylodyn	2000	C1_Sdyn0
C1_Smer2000	Flange	Bearing	Sylomer	2000	C1_Smer0

3.3.2 C2: double cassette tests

The purpose of the double cassette tests was to investigate the influence of different cassette-to-cassette connections and screw spacing on the dynamic response of the floor. Thus, all double cassette tests were conducted using the same boundary conditions with webs supported by a pin-roller support condition, as shown in Figure 3-11 (a). Tests first involved a double screw web connection between the adjacent joists, as shown in Figure 3-11 (b) (denoted by 'web' in test name). Two types of flange connections were also investigated: splice connection (denoted by 'Spl' in test name) and diagonal screws

(denoted by 'Diag' in test name). From a constructability perspective, splice connections are more efficient to install than diagonal screws since drilling screws diagonally require a specially angled jig. Nevertheless, both options are used to connect cassettes (Figure 2-15) and therefore were included in testing. Note that in reality, the splice connection would be embedded within the flange to finish flush against the top surface, however due to the higher fabrication demand, the notches were not included and the splice sat on top of the top flange. The diagonal screws were inserted at a 45-degree angle and spaced 11 mm apart from the opposite facing screw. All screw connections were tested with a 300 mm and 150 mm centre-to-centre spacing to investigate the effect of screw spacing on the dynamic behaviour (denoted by 'Splx' in the test name where 'x' refers to the screw spacing). Details of the splice and diagonal screw connections are shown in Figure 3-11 (c) and (d), respectively. All double cassette tests are summarised in Table 3-7 with note of the reference test case.

(a) C2 test set-up
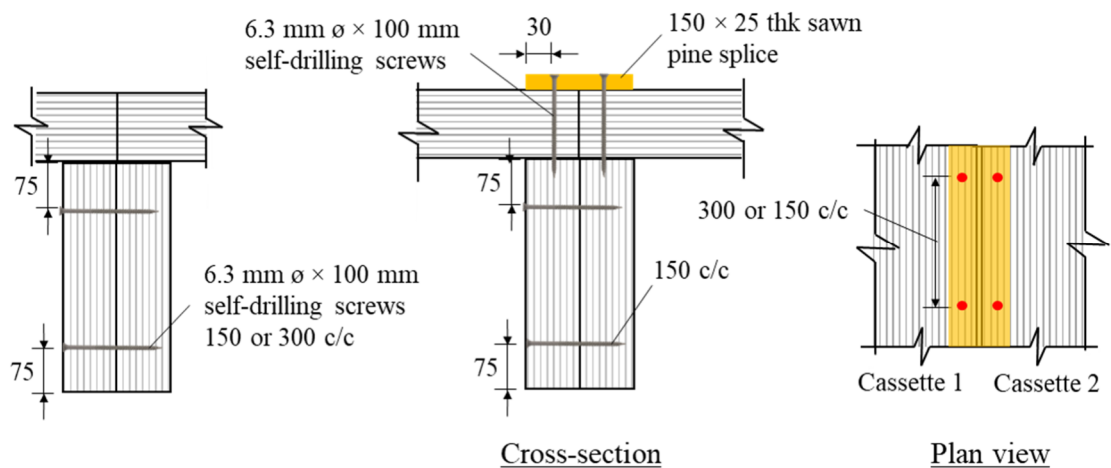
(b) C2_Web   (c) C2_Spl
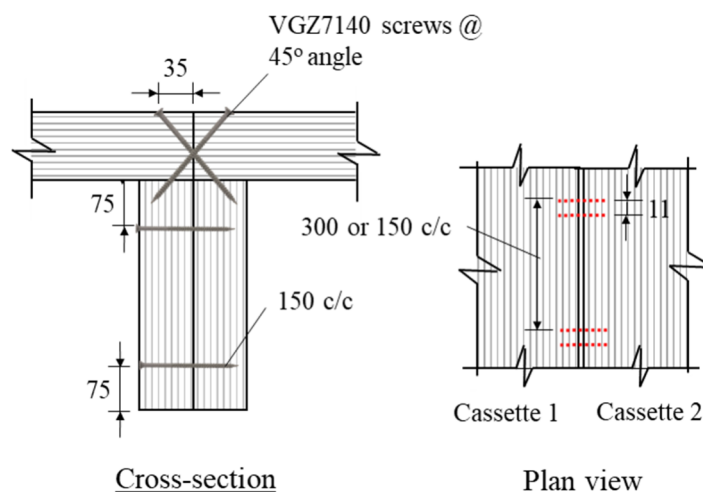
(d) C2_Diag

Figure 3-11 *Double cassette test and connection types*

Table 3-7 *Summary of double cassette tests*

Test name	Web connection		Flange connection		Reference test
	Type	*Screw spacing*	*Type*	*Screw spacing*	
C2_Web300	Web	300	-	-	C1_Web
C2_Web150	Web	150	-	-	C1_Web
C2_Spl300	Web	150	Splice	300	C2_Web150
C2_Spl150	Web	150	Splice	150	C2_Spl300
C2_Diag300	Web	150	Diagonal	300	C2_Web150
C2_Diag150	Web	150	Diagonal	150	C2_Diag300

3.4 Experimental set-up and testing procedure

3.4.1 Test instrumentation and set-up

For single cassette tests, a 21 accelerometer set-up was arranged with seven accelerometers placed equidistance apart on the surface of the top flange along each joist line, as shown in Figure 3-12 (a). For double cassette tests, an 18 accelerometer set-up was arranged with three accelerometers placed equidistance apart along each joist line, as shown in Figure 3-12 (b). The locations of the accelerometers were selected to capture the first two bending and torsion modes.
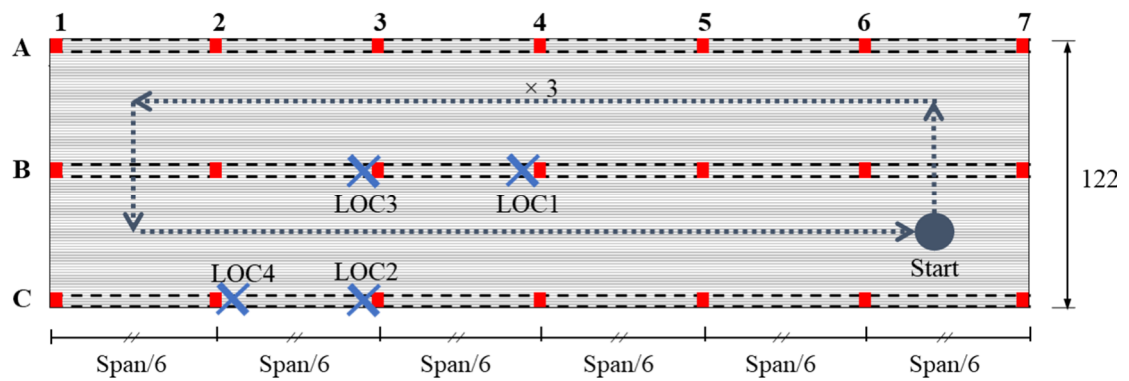
(a) Single cassette tests
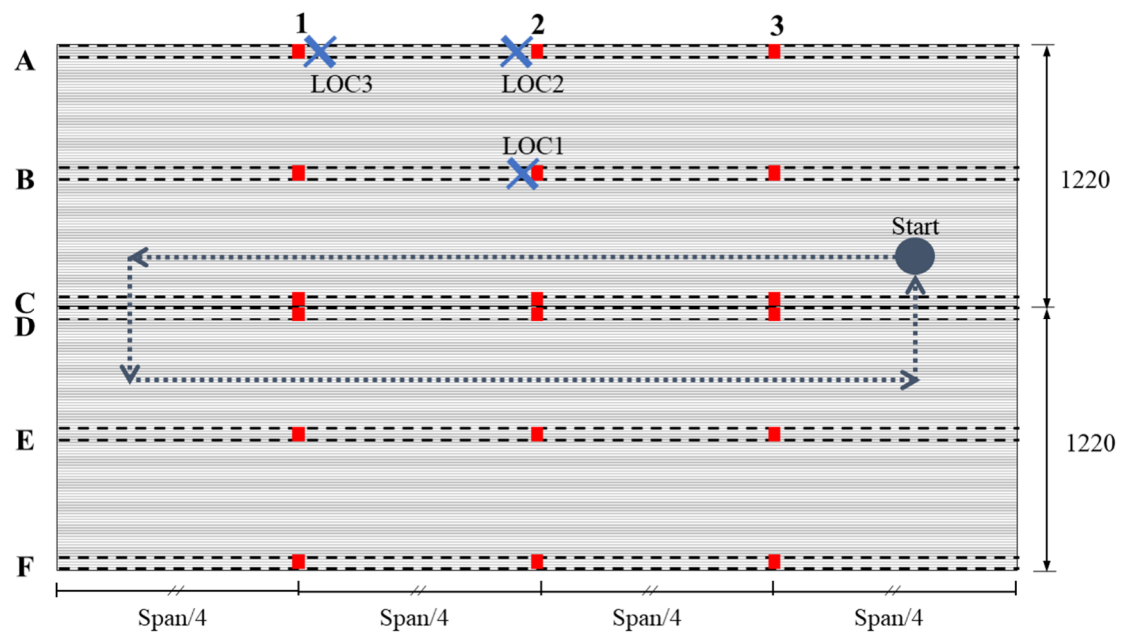
(b) Double cassette tests

Figure 3-12 *Accelerometer set-up plan view (as shown by the red dots), impact hammer locations (as shown by the blue crosses) and walking path (as shown by the dotted arrows). Note 'Start' indicates the location of where the walker started the walking test.*

ICP® ('Integrated Circuit Piezoelectric') accelerometers (model 352C34) from PCB® with sensitivity of 100 mV/g ($\pm$ 10 %), as shown in Figure 3-13 (a), were used to measure the acceleration response of the floor. Each accelerometer was connected to a channel within a multi-channel data acquisition module (National Instruments PXIe-4492) with a resolution of 24 bits. The data acquisition module was slotted into a PXI chassis (PXIe-1073) as shown in Figure 3-13 (b), and connected to a computer where LabVIEW was used to monitor vibrations from each test. This software is shown in Figure 3-13 (c).
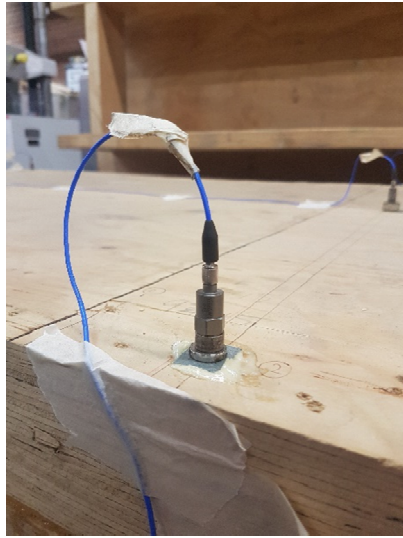
(a) Accelerometer (PCB® model 352C34)
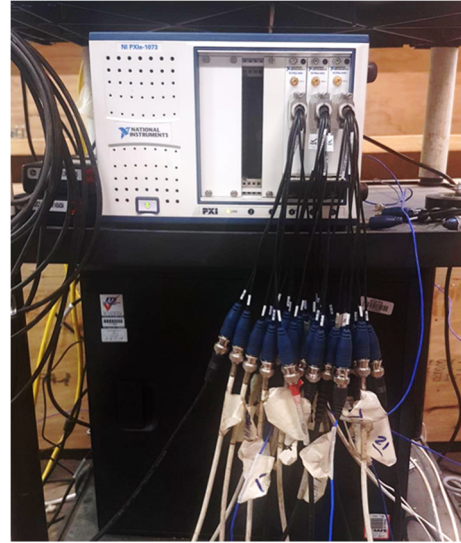
(b) Data acquisition system
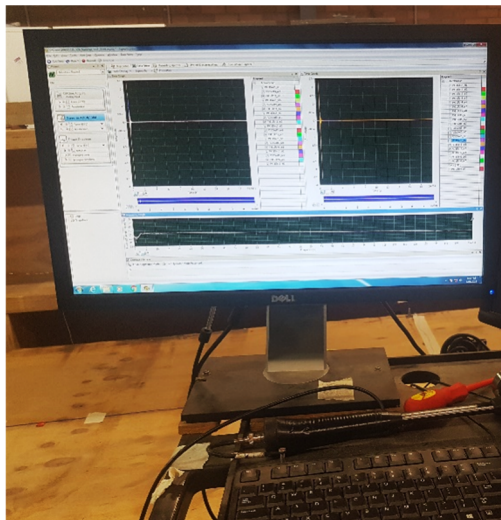
(c) LabVIEW software

(d) Instrumented modal hammer

Figure 3-13 *Test instrumentation*

3.4.2 Impact hammer tests

Due to the lightweight characteristics of the timber cassette, it was decided that an instrumented hammer (PCB model 086D20) would be the most appropriate source of excitation to obtain the modal properties of the floor; this hammer is shown in Figure 3-13(d). Furthermore, the impact hammer was beneficial as it allowed for an efficient testing procedure, which was crucial as there were multiple points of impact (as shown in Figure 3-12) for each test set up.

A soft tip was chosen since the frequency range of interest (0 – 100 Hz) was low. The hammer input was also connected to the data acquisition module. Each test was recorded

with a sample frequency of 1000 Hz for a total of 20000 samples resulting in a total duration of 20 seconds. This sampling frequency was deemed appropriate to eliminate any aliasing effects as the highest frequency of interest was well below the Nyquist frequency of 500 Hz.

For C1 tests, four impact locations were selected as shown in Figure 3-12 (a). Location 1 (LOC1) and 3 (LOC3) were chosen to excite the first and second bending modes, respectively, while Location 2 (LOC2) and 4 (LOC4) were selected to excite the torsion modes. It was important to capture both the torsion and bending modes to investigate the effect of closely spaced modes on the floor response.

For C2 tests, three impact locations were selected as shown in Figure 3-12 (b). Impact at grid C2 was initially attempted, however, it became difficult to impact without making contact with the floor. From a comparison of FRF between grid C2 and LOC1, it was deemed that impacts at LOC1 were acceptable in capturing the first bending mode. Each impact location was struck 10 times and recorded for a length of 20 seconds; from the 10 samples, the best five tests were averaged to produce one FRF for each accelerometer.

3.4.2.1 Post-processing measured data

Before EMA was performed, it was imperative to inspect the quality of both input and output signals for each test sample to check for any random noise and ensure repeatability and reciprocity of the tests. The following were undertaken during the data acquisition as a first pass check before final data was collected:

- A pre-trigger delay was used to ensure that the entire impact excitation signal was captured.
- Any output data samples that were found to have a high degree of noise were deleted and only the five best quality samples were used.
- Input time-domain data showing a 'double hit' were deleted.
- Power spectrum of the input signal was viewed to ensure the energy distribution was equal for the frequency range of interest.

After the final 10 samples were collected for each impact location, the accelerometer response for each sample was overlaid to check the repeatability; a typical graph is shown

in Figure 3-14 (a). Similarly, the FRF for each accelerometer over the 10 samples were also overlaid to check that the peaks were in the same position; a typical graph is shown in Figure 3-14 (b). After the measurement samples were checked, the FRFs were averaged to produce one FRF for each accelerometer for a specific impact location (e.g. LOC1). The coherence graph was viewed to ensure that coherence was above 0.95 at FRF peak locations. To ensure reciprocity, averaged FRFs from each accelerometer due to impact at one location (egg. LOC1) were overlaid to check peak locations and characteristics; the FRF should be similar if not identical between accelerometers.

(a) 10 samples – output time-domain   (b) 10 samples - FRF
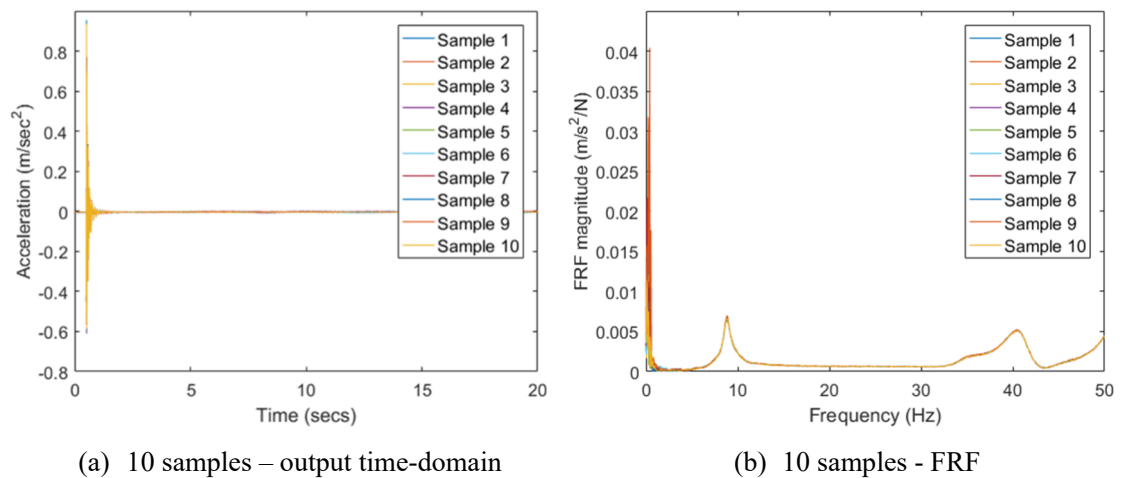
Figure 3-14 *Typical plots for 10 test samples for one accelerometer*

LMS Test.Lab was used to curve fit synthesized FRF to the computed FRF from experimental data. The least-squares complex exponential method was used to obtain the frequency and damping ratios for all modes up to 50 Hz; modes up to 50 Hz were chosen since higher modes have less contribution to human perception (International Standards Organisation 1997). Mode shape coefficients we obtained using the least-squares frequency domain method.

3.4.3 Walking tests

For floors in commercial buildings, a single person walking is generally the most common activity and thus is the main focus for these walking tests. Typically in practice, tested pace frequencies depend on the fundamental frequency of the floor and the consequent resonant or transient response which is assumed to occur. For example, for resonant response floors, only the critical walking pace in which the third or fourth harmonic coincides with the fundamental frequency requires testing (Smith, Hicks & Devine 2009;

Chapter 3

Willford & Young 2006). Modal properties obtained from impact hammer testing revealed the fundamental frequency of the ribbed-deck cassette was generally within a 8.5 – 11 Hz range which is on the border of recommended cut-off frequencies for distinguishing between low- and high-frequency floors (Murray et al. 2016; Smith, Hicks & Devine 2009; Willford & Young 2006). Thus, a range of pace frequencies were tested to ensure both resonant and transient responses were captured. Three pace frequencies were chosen: 1.5 Hz, 2.0 Hz and a walking pace with the fifth harmonic coinciding with the fundamental frequency of the floor (referred to as the 'resonant' pace frequency). The resonant pace frequency was in the range of around 1.6 to 2.1 Hz. Note that a walking pace with the fourth harmonic coinciding with the fundamental frequency was generally over 2.4 Hz and thus was deemed to be too fast for an office scenario (Smith, Hicks & Devine 2009).

Two people with varying masses and heights were selected as test walkers to ensure variability in responses. Note that since the male walker in stage C1 tests was unavailable for stage C2, a different walker with similar mass was selected. Details for each walker are summarised in Table 3-8. To ensure all walking tests were controlled, the pace frequency was played through earphones connected to a mobile phone with a metronome application. Each test subject was then asked to walk individually along a set loop three times with the acceleration response measured at the same accelerometer locations detailed in Figure 3-12. Walking loops for single person walking tests are also shown in Figure 3-12 (a) and (b) for stage C1 and C2 tests, respectively.

Table 3-8 Walker details

Walker	Stage	Gender	Age	Mass (kg)	Height (cm)
1	C1 + C2	F	28	51	165
2a	C1	M	26	78	175
2b	C2	M	28	75	170

3.4.3.1 Post-processing measured data

All response data was frequency weighted to account for the differences in human sensitivity to particular frequencies. The different weighting curves have been detailed in Chapter 2 Section 2.5.1.1. The digital filtering process is performed using specialised

software or can be applied through a MATLAB code by specifying filter coefficients. Rimell and Mansfield (2007) have provided the necessary formulae for all weighting filters defined in ISO 2631-1 (1997) and ISO 2631-2 (2003) and has been used in this research to apply the W_k filter as defined in ISO 2631-1 (1997) to the digital response signal. An example of a filtered response signal in the time and frequency domain is shown in Figure 3-15 (a) and (b), respectively. Figure 3-15 (b) shows the attenuation of amplitudes of higher frequencies due to the frequency weighting filter.
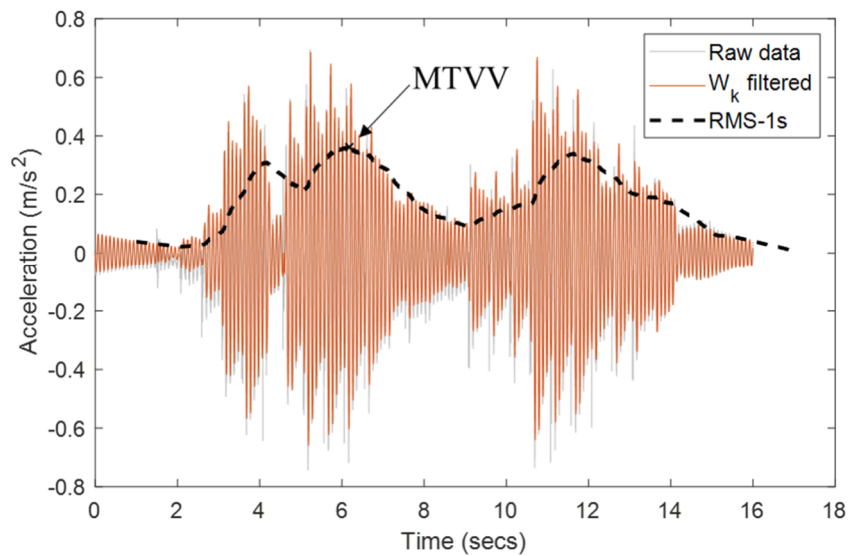
(a) Time-domain acceleration response
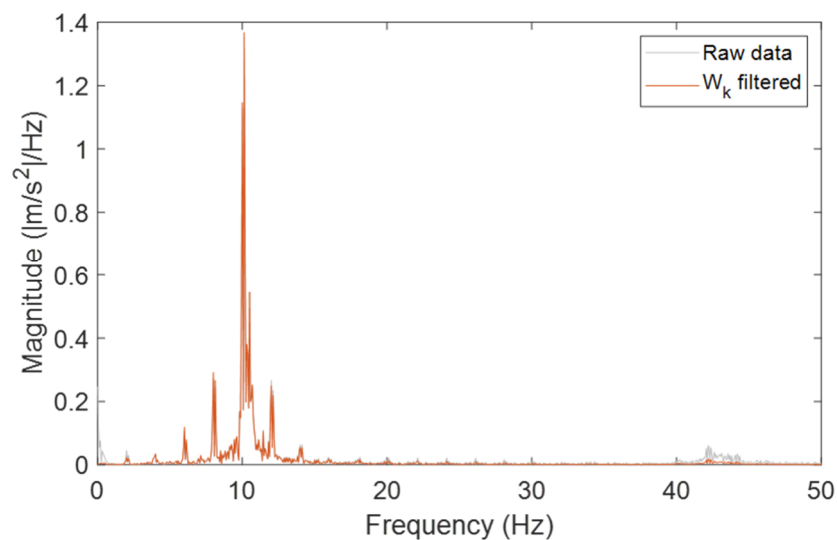
(b) Frequency domain acceleration response

Figure 3-15 *Raw and W_k filtered acceleration response from walking excitation in time and frequency domain.*

3.4.3.2 Evaluating floor response

In this research, floor response to walking excitation was evaluated using two methods:

1. Response factor (RF) based on the maximum transient vibration value (MTVV) divided by the appropriate base curve for human perception. For acceleration response, this is 0.005 m/s^2 while for velocity response the base curve amplitude is 1×10^{-4} m/s; both values are as per ISO 2631-2 (1989).

2. Cumulative distribution of 1 second running RMS floor response amplitudes and resulting running RF.

The first method is based on a procedure defined in ISO 2631-1 (1997) where the MTVV is the highest magnitude of the running root-mean-square average with a time constant of 1 s, as defined in Equation 2.2424. An example of the 1 second RMS (1s RMS) running window and MTVV of an acceleration response is shown in Figure 3-15 (a). In this case, the RF is equal to 72 (i.e. 0.3618 / 0.005 m/s^2). To keep within recommended practices of the CCIP-016 vibration guideline (Willford & Young 2006) and literature (Brownjohn & Middleton 2008; Middleton & Brownjohn 2010), floors classified as 'high-frequency' have been evaluated in terms of their velocity response obtained through integration of the measured acceleration response. Velocity response is generally the preferred measure for these floors for two main reasons. The first is due to the fact that many floors which are 'high-frequency' are extremely stiff and tend to be associated with floors which house vibration-sensitive equipment including optical equipment (Amick 1997), precision lasers or linear accelerators such as those used in particle physics experiments (Seryi 2001). These processes can tolerate limited blurring which is defined as the distance travelled during exposure i.e. velocity (Middleton & Brownjohn 2010). The second reason is due to the fact that after approximately 8 Hz, human perception appears to be constant when expressed as a velocity, as defined in the ISO 2631-2 base curves (International Standards Organisation 1989). When using the velocity response, a frequency weighting is not applied and the 1 s RMS running window is applied on the raw data. Since three walking loops were performed, the evaluated response was averaged to obtain the final response amplitude while the coefficient of variation was computed to check variability between amplitudes.

The second method is based on the study by Živanović et al. (2009) who investigated different walking load models on a beam-and-block floors. She concluded that taking into account only the extreme values of vibration response (i.e. the maximum response) may be misleading when assessing vibration serviceability of floors. Instead, she recommended that a consideration into the duration that the vibration response spends above or below a limit is more appropriate. The duration of vibration response can be obtained by calculating the cumulative distribution of the response as shown in Figure 3-16; the plot has been created using the same response data from Figure 3-15 (a). The MATLAB code used to calculate the cumulative distribution from a number of samples of data is provided in Appendix B. From Figure 3-16, it is revealed that, for example, for 60% of the walking event, the response was less than approximately a RF of 40.
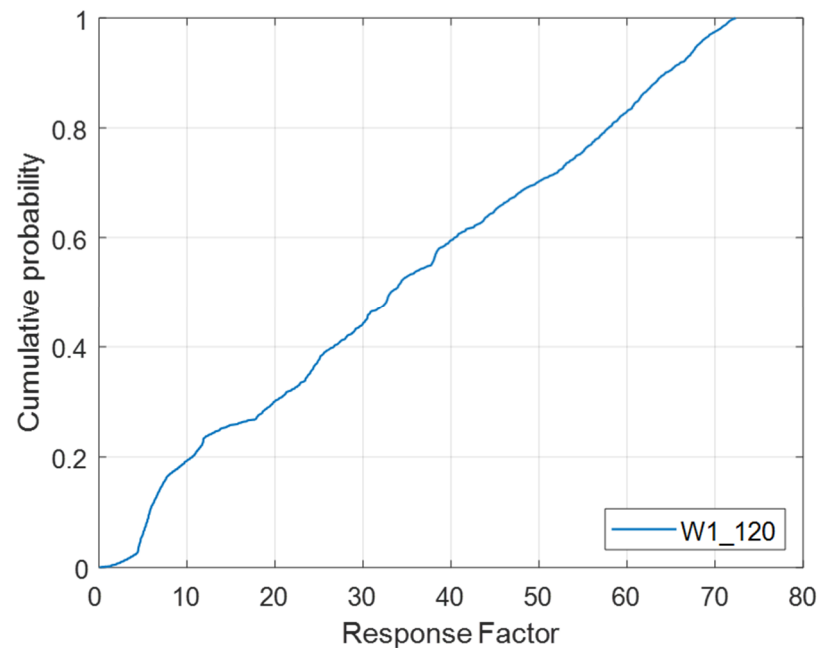
Figure 3-16 *Cumulative distribution of floor response*

In Chapter 7 where parametric studies are undertaken on a multi-cassette floor, a VDV estimate is also calculated using Equation 2.26 to understand the likelihood of adverse comment for the particular floor response. The estimated VDV is compared to the limits in Table 2-3.

3.5 Concluding remarks

This chapter introduced the ribbed-deck cassette floor and details the dynamic tests that have been conducted. These tests include impact hammer tests to obtain the modal

properties of the floor and walking tests under three different pace frequencies to investigate floor response. Experimental modal analysis using LMS Test.Lab software was used to curve fit the analytical transfer function to the measured function to obtain the natural frequencies, mode shape amplitudes and damping ratios for each mode. Experiments involved various configurations including different simple support conditions for single cassette tests and varying cassette-to-cassette connections for a double cassette configuration. Results from these tests are presented and discussed in Chapters 4 - 6.

Chapter 4

Modal Properties of Long-Span Timber Ribbed-Deck Floor: Test Results and Finite Element Model

4.1 Introduction

Computer based analysis methods such as finite element (FE) modelling have had a significant impact to engineering design and product development since the 1960s (Friswell & Mottershead 1995). By representing a physical structure analytically, one can precisely identify potential stress concentrations or predict their dynamic characteristics. However, the FE model is only as accurate as the modelling assumptions and even with the best engineering judgement, differences between analytical results and measurements from the physical structure regularly occur. Particularly in the case of complex civil engineering structures, difficulties in modelling joints, boundary conditions and damping have caused inaccuracies in the model (Modak, Kundra & Nakra 2002). Indeed, results from experimental testing also have limitations related to the number of measured points (and therefore mode shapes), the frequency range and potential errors from noise. Nevertheless, since dynamic tests directly measure the response of the physical structure

without any assumptions, measured results are considered to be more reliable (Visser 1992). FE model updating or calibration is a technique which attempts to minimise the inaccuracies of the model with reference to results from experimental tests. The detailed representation of the structure through the FE model can be retained and thus this approach can be considered as an attempt to combine the best features from both the experimental and analytical model (Modak, Kundra & Nakra 2002).

This chapter has been sectioned into four main parts; the FE modelling approach, description of the initial pre-test FE model for the flange-supported support condition, experimental results from impact hammer tests and the final validated model including the model updating procedure. All numerical models were created using ANSYS (2016) which is a commercially available FE analysis package. The purpose of the validated model was for the investigation of different walking load models with comparison to experimental walking test results which will be detailed in Chapter 5. Further, the updated model will be used in Chapter 6 for a double cassette model to explore modelling of cassette-to-cassette connections, and a multi-cassette model for parametric studies in Chapter 7.

4.2 Finite element modelling approach

4.2.1 General modelling considerations for ribbed-deck floors

4.2.1.1 Orthotropic nature of wood

Due to the orthotropic nature of wood, the modulus of elasticity differs for each direction. These directions are aligned longitudinal to the grain direction (L), radial direction (R) and the tangential direction (T) as shown in Figure 4-1. However, since the differences in properties between the tangential and radial direction are minimal compared to the longitudinal direction (Porteous & Kermani 2007), material properties are usually provided for two directions only: parallel to grain (longitudinal) and perpendicular to grain (radial and tangential). Plate and shell elements in finite element analysis software packages (ANSYS in this study) allow the user to input material properties corresponding to the various axes. Beam elements, on the other hand, only allow material properties associated with the longitudinal axis.
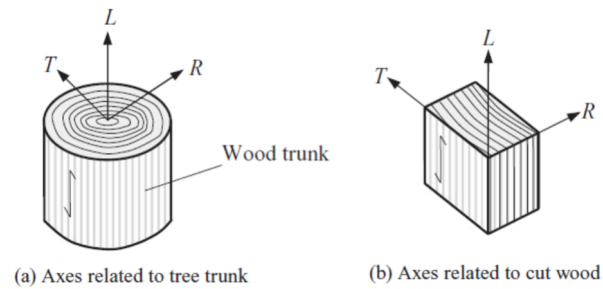
Figure 4-1 *Principal axes of wood (Porteous & Kermani 2007)*

4.2.1.2 Analytical behaviour of a ribbed-deck cassette

Ribbed-deck cassette floors are similar to a lightweight wooden joist floors in the fact that they are made up of similar components: a web element (rib), flange (panel or sheathing) and the connection between web and flange. Smith and Chui (1986) proposed explicit equations to predict the fundamental frequency of wooden joist floors based on the Rayleigh method. The floor was represented as a ribbed plate system with simply-supported edges perpendicular to joist direction and free along edges parallel to the joist direction. It was found that if the sheathing has high rigidity in bending across joists, which may be approached for floors having a large span-to-width ratio, the floor can be assumed to behave as a simply-supported beam (Leissa 1969; Smith & Chui 1986).

Hu (1992) also developed a numerical model for lightweight wooden joist floors as a ribbed plate system. However, unlike Smith and Chui's (1986) approach, the modal synthesis method was used; this meant that the structure was treated as a collection of substructures where the mode shape functions for the complete structure were synthesised from the mode shape functions of the substructures. Such a method eliminates the difficulties in selecting appropriate mode shape functions for a complete system which occurs in the conventional Rayleigh-Ritz method (Hu 1992). Two-dimensional theory of flexural vibration of an orthotropic elastic plate was used to determine the characteristics of the plate. Timoshenko beam theory was adopted to account for the effects of shear deformation and moment of inertia in each rib, which was found to be important for ribs with a high flexural-to-shear rigidity ratio. Semi-rigid connection (nailed or glued) between the plate and the ribs was considered through an effective flexural rigidity expression based on Smith (1980). If the connection is rigid, the standard transformed section solution for full composite action applies.

One of the largest differences of the ribbed-deck floor system from the wooden joist floor is that web members are glued and screwed to the flange. The connection can be assumed to be rigid under serviceable loads (Zabihi 2014) and thus the flexural rigidity of the composite cross-section can be considered. Other points of differentiation from wooden joist floors include:

1. Support condition involves both flange and web supported (e.g. between primary beams in a commercial building) to reduce structural floor depth rather than just web supported;

2. Potentially thicker flange members due to the use of engineered wood products (EWPs) such as LVL or CLT rather than the typical oriented strand board (OSB) and plywood;

3. Ribbed-deck floors are generally prefabricated. As a result, width of each cassette will be influenced by the width of the container/truck as well as consideration of the standard manufactured dimensions of EWPs. This means that for LVL flange members, the along-grain axis will typically align with the web members; this is compared to methods where sheathing is generally placed perpendicular to the web direction.

4.2.1.3 Numerical models of a ribbed plate system

Using ANSYS, Kurian (2000) developed a finite element model of a glued laminated girder bridge in order to accurately predict the analytical behaviour. The bridge deck consisted of a deck supported by three equally spaced girders. Kurian (2000) chose a four-node shell element (SHELL63) to model the deck which has six degrees of freedom at each node. This element can represent the orthotropic properties of wood through defining the longitudinal and transverse moduli of elasticity, shear modulus and major and minor Poisson's ratio.

Initially, a beam element (BEAM4) was used to model the girders, however, this was shown to be inaccurate since the nodes of the element were located in the middle of the cross-section. This translated to inaccuracies in terms of support location. Hence, SHELL63 was chosen to model the girders. Results from both models were used for comparison with experimental results of two bridge decks. Although both models provided a good approximation of the experimental behaviour, the model using the

SHELL63 for the girders was recommended as it was the best idealisation of the bridge. Gerber et al. (2008) also developed an ANSYS model for a timber stressed skin panel. Similarly to Kurian (2000), a shell element was used as the sheathing. However, the I-joist was modelled using two different element types: solid for the flanges and solid-shell for the web.

Steel-concrete composite floors are similar to timber joist floors in that there are two connected components which either act compositely or semi-compositely. A common pattern in the modelling of these floors in ANSYS is that the steel beam is represented by a beam element (BEAM4 or BEAM44) and the concrete topping is represented by a shell (SHELL63 or SHELL181) (Gajalakshmi & Mohaideen 2013; Pavic, Miskovic & Reynolds 2007; da Silva, Vellasco & de Andrade 2008). In most cases, the beam-slab connection is rigid.

4.2.2 Preliminary investigation of appropriate element type

The FE model of the ribbed-deck cassette consists of two main sections: the web and the flange element. When selecting an appropriate element type for each section, comparisons to analytical solutions for element verification as well as comparison to single beam experiments for model validation has been carried out. Mode shapes, natural frequencies and where available, static deflection was compared. Consideration was also given to the element order or shape function (linear or quadratic), mesh size and computation time with the main objective of building a model with an acceptable level of accuracy without excessively long solving times. An overview of the element types provided within ANSYS is shown in Table 4-1.

Table 4-1 *ANSYS element summary table*

Type	Description	Typical elements	
		Linear	Quadratic
Beam	Simple line element which carries axial, bending, shear and twisting forces. Cross section is defined with a real constant.	BEAM4 (Euler-Bernoulli); BEAM188 (Timoshenko)	BEAM189 (Timoshenko)
Shell	Carries in-plane and out-of-plane loads. Thickness is small compared to other dimensions.	SHELL63 (Kirchhoff-Love); SHELL181 (Mindlin-Reissner)	SHELL93 (Kirchhoff-Love)
2D Solid (Plane)	Either plane strain (negligible strain in thickness direction) or plane stress (thickness is free to change depending on stress).	PLANE42; PLANE182	PLANE82; PLANE183
3D Solid	Geometry is fully defined by the element nodes i.e. volumes are created.	SOLID45	SOLID95

Single element tests involve comparing the model results to an analytical solution of one component of the floor system. For the web, beam and shell elements were analysed while for the flange component, various shell elements were analysed. Boundary conditions were taken to be simply-supported. The material properties input into ANSYS are shown in Table 4-2. Note that the ANSYS notation refers to the element local coordinate system as shown in Figure 4-2 where the y-axis is parallel to the elements strong direction. All material properties other than those obtained from material testing as detailed in Chapter 3 were obtained from the manufacturer's data sheet supplied by Carter Holt Harvey (2015) and Nelson Pine (2016) for the web and flange element, respectively. The perpendicular to grain MoE is calculated as 10% of the parallel to grain MoE and the Poisson's ratio is 0.3 which is approximated from the USDA Wood Handbook (Green, Winandy & Kretschmann 2010).
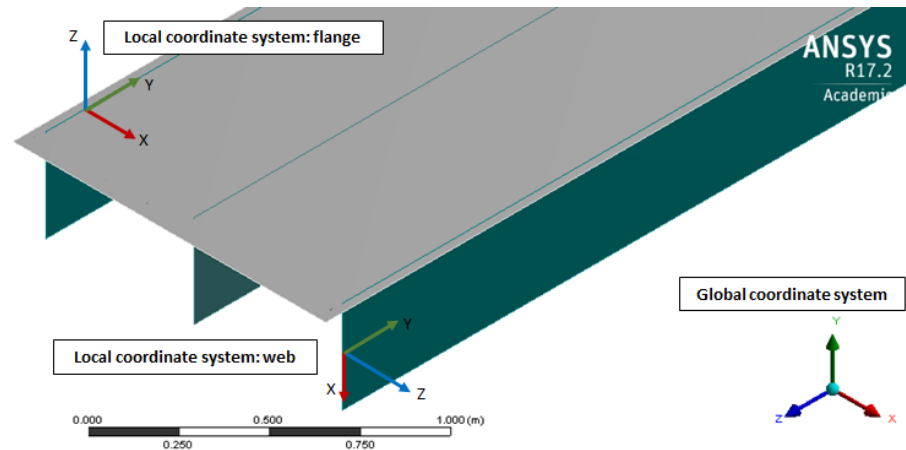
Figure 4-2 *Local and global coordinate system of FE model*

Table 4-2 *ANSYS material property input*

	ANSYS notation		Web element		Flange (SHELL)
			BEAM	SHELL	
Modulus of Elasticity	EX	*MPa*	12754	1275.4	1100
	EY	*MPa*	-	12754	11000
	EZ	*MPa*	-	1275.4	1100
Poisson's ratio	PRXY		0.3	0.3	0.3
	PRXZ		-	-	-
	PRYZ		-	-	-
Density	DENS	*kg/m³*	589.1	589.1	570
Modulus of Rigidity	GXY	*MPa*	660	660	550
	GYZ	*MPa*	-	660	550
	GXZ	*MPa*	-	6.6	5.5

4.2.2.1 Web element

For the web, BEAM4, BEAM188, SHELL63 and SHELL181 were selected for analysis and comparison to an analytical solution. BEAM4 is an uniaxial element based on Euler-Bernoulli beam theory and has six degrees of freedom at each node. BEAM188 is a higher order version of BEAM4 but is based on Timoshenko beam theory and thus includes effects of shear deformation. In order to consider the influence of the orthotropic nature of timber, shell elements were also included. As noted in Kurian (2000), shell elements also provide flexibility in terms of support location. SHELL63 is a four node orthotropic element having both bending and membrane capabilities and is based on Kirchhoff-Love

plate theory. SHELL181 is also a four node orthotropic element but is based on Mindlin-Reissner plate theory and thus includes the effect of shear stress distribution over the thickness. One of the differences of SHELL181 from SHELL63 is that SHELL181 allows the user to define a cross-section whereas for SHELL63 a real constant is used. Note that the full integration method was considered for SHELL181 rather than the default reduced integration method to eliminate hourglass effects as this is recommended for in-plane bending dominated problems (ANSYS Inc 2016). The mesh size was kept constant at 30 mm for all models.

The analytical natural frequency of mode *n* for the first two modes and mid-span deflection were calculated based on the following expressions for a simply-supported beam:

$$f_n = \frac{n^2\pi^2}{2\pi}\sqrt{\frac{EI}{m_l l^4}} \tag{4.1}$$

$$\delta_{mid} = \frac{5}{384}\frac{w_l L^4}{EI} \tag{4.2}$$

where E = modulus of elasticity (N/m^2); m_l = mass per unit length (kg/m); I = moment of inertia (m^4); l = span (m); w_l = load per unit length (N/m).

Both numerical and analytical cases were based on a simply-supported 8.946 m long beam with dimensions 360 x 63 mm (to match the experimental set-up). The modulus of elasticity and density were taken from material tests as described in Chapter 3. It should be noted that Equations 4.1 and 4.2 are based on Euler-Bernoulli beam theory and thus influence of shear deformation was not considered in the analytical case.

Table 4-3 reveals the analytical and numerical solutions for a single web member with various element types for the first three bending modes and mid-span deflection. As expected, BEAM4 was the most accurate element type for the analytical solution. The effects of considering shear deformation is more significant for the second bending mode as shown in results of BEAM188. Using the full integration method, SHELL181 has very little difference to the results using SHELL63 elements.

Table 4-3 *Numerical solutions for simply-supported web for various element types and % error from analytical results*

	f_1 (Hz)	Error (%)	f_2 (Hz)	Error (%)	δ_{mid} (mm)	Error (%)
Analytical	9.491	-	37.963	-	3.499	-
BEAM4	9.491	0.0	37.963	0.0	3.499	0.0
BEAM188	9.343	-1.6	35.758	-5.8	3.603	3.0
SHELL63	9.271	-2.3	34.645	-8.7	3.622	3.5
SHELL181	9.271	-2.3	34.646	-8.7	3.622	3.5

To understand how the numerical and analytical results of a simply-supported beam compare to experimental results, impact hammer tests were undertaken on a single hySPAN® beam with dimensions 360 × 63 mm. The beam spanned 8.946 m between a steel shaft and plate pin and roller boundary condition. The pin boundary is shown in Figure 4-3 while for the roller condition on the opposite end, the plates were turned upside-down so the shaft was free to roll in the longitudinal direction. It was assumed that self-weight of the beam would outweigh the soft impacts from the hammer and would not cause substantial upward movement at the support ends. Seven accelerometers were positioned equidistant apart on the top of the beam, as shown in Figure 4-4, to ensure the first two bending modes were captured. Two impact locations were chosen: at accelerometer 4 (LOC1) and accelerometer 3 (LOC2). Ten samples were collected for each impact and an average FRF for each location was calculated to identify the first two modes.

Figure 4-3 Steel shaft and plate pin boundary condition
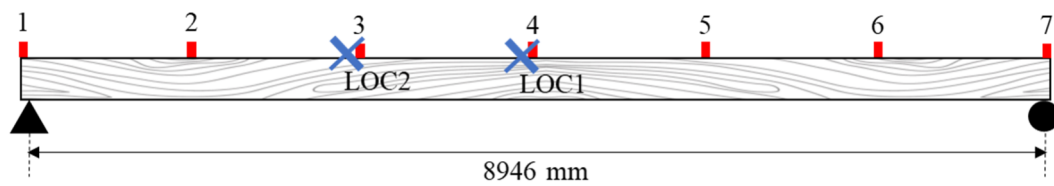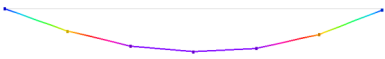
Figure 4-4 *Accelerometer layout and impact locations*

Table 4-4 shows the frequencies for the first two modes obtained from the LMS Test.Lab software which are used to compare against the FE results as shown in Figure 4-5. The frequencies differ from the ideal pin-roller (PR) boundary condition which is to be expected particularly since there is no restraint in the positive vertical direction (i.e. away from the ground) and friction between elements is not considered. As a result, a fix-fix case was also analysed numerically for the same models to obtain an upper bound frequency limit. As shown in Figure 4-5, BEAM188, SHELL63 and SHELL181 all appear to be appropriate element types for the web. However, to allow for investigation into the influence of considering orthotropic behaviour of timber beams, SHELL181 was selected to model the web elements.

Table 4-4 *Natural frequency of the first three modes obtained from LMS Test.Lab*

Mode	f (Hz)	Mode shape
1	10.049	
2	37.506	
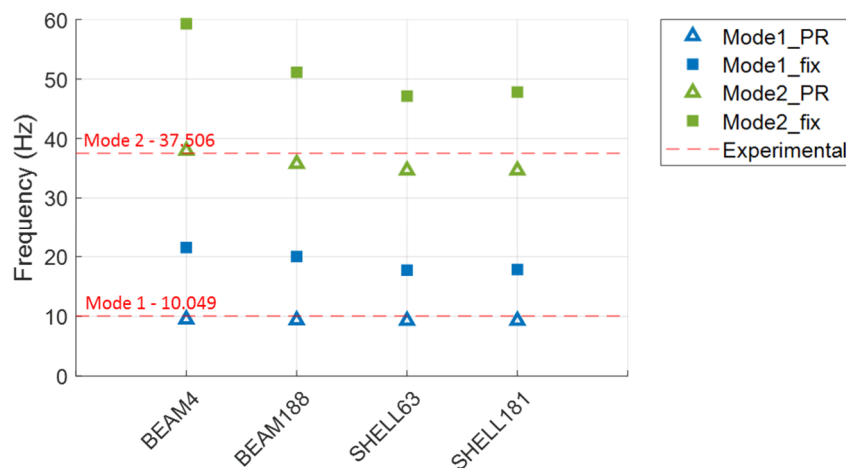
Figure 4-5 *Experimental vs numerical results for the first two bending modes under PR and fix-fix boundary conditions*

4.2.2.2 Flange element

One of the advantages of SHELL181 over SHELL63 is the capability to offset location of the nodes in the section. By default, the nodes are located in the middle of the section, however, these can be relocated to the top or bottom surface of the section. This becomes important when connecting web to flange and ensuring the full second moment of inertia is accounted for. Due to these reasons, SHELL181 has been chosen as the panel element.

4.2.3 Modelling approach validation of ribbed-deck floor

Based on the element investigation detailed in Section 4.2.2, an FE model of the ribbed-deck cassette was created. The results of this model were compared to the experimental results of the web-supported pin-roller boundary condition set-up (C1_Web). The purpose of this investigation was to validate the modelling approach of the cassette using shell elements.

4.2.3.1 Model overview

An overview of the elements used for the web and flange sections for the preliminary model is shown in Figure 4-6. On the basis of the assumption that the section acts compositely under serviceable loads, the coincident nodes at the intersection between flange and web were merged to create a rigid connection. The model only considers the self-weight of the cassette and no additional loading was applied. Material properties as per Table 4-2 were used. A static analysis was first solved to ensure the model was

properly constrained. Following the static analysis, a modal analysis was conducted to obtain the first five non-spurious modes (i.e. modes which are expected to be seen in reality) under 50 Hz; modes up to 50 Hz were chosen since higher modes have less contribution to human perception (ISO 1997). A spurious (non-physical) mode shape was considered as one in which only the web members were moving out-of-plane; an example of a spurious mode is shown in Figure 4-7.
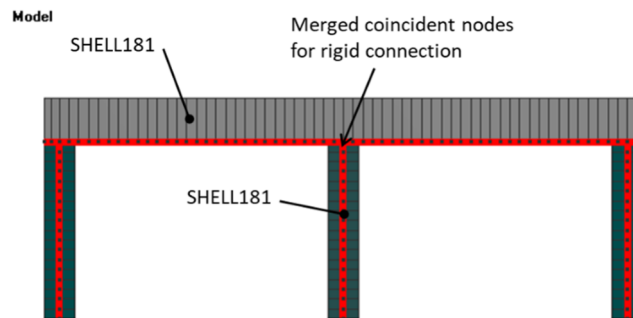
Figure 4-6 *Preliminary FE model overview of element type*
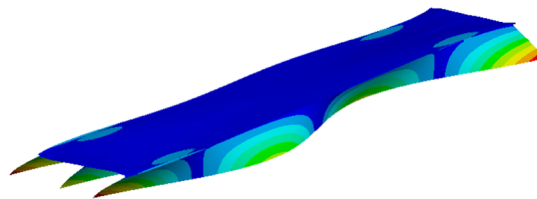
Figure 4-7 *An example of a spurious (non-physical) mode*

4.2.3.2 Boundary conditions

The physical boundary conditions used in the test set-up consisted of the ends of the web members sitting on a steel shaft and plate system similar to that shown in Figure 4-3. The fact that the web members were simply bearing onto the steel plate means that the only restraint in the lateral (x-axis of global coordinate system) and longitudinal (z-axis of global coordinate system) directions is the friction between the timber web and steel plate. Further, the web members are still free to lift off the supports. These factors need to be taken into account when comparing the FE model results to the experimental results.

As such, two different boundary condition configurations were considered in the model: an 'ideal' and a 'spring' pin-roller configuration. The 'ideal' pin-roller condition is shown in Figure 4-8(a) and has one end of the web members restrained translationally in the x-, y- and z-directions while the other end is restrained in the x- and y-directions. The 'spring' pin-roller configuration, shown in Figure 4-8(b), has the same directions restrained as the

'ideal' condition, except that instead of a complete constraint, springs in the form of COMBIN14 elements were used for each direction. COMBIN14 is a spring-damper element with no mass and can be defined as having longitudinal or torsional capability in one, two or three dimensional applications (ANSYS Inc 2016). The element allows user input of real constants for the stiffness and damping coefficient, although in this case only the stiffness was used. Stiffness values of 1×10^5 N/m, 1×10^8 N/m and 1×10^6 N/m for the x-, y- and z-direction were used, respectively; these values were determined based on manual tuning. The purpose of this configuration was not to correlate with experimental results but to highlight the differences in results from an 'ideal' boundary condition configuration.

(a)   (b)
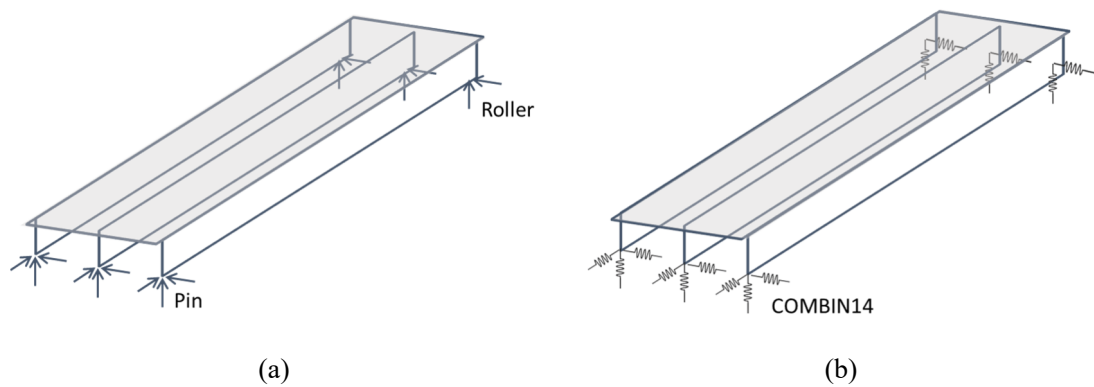
Figure 4-8 *(a) 'Ideal' pin-roller boundary condition configuration; (b) 'Spring' boundary condition configuration*

4.2.3.3 Mesh Size

Convergence with mesh refinement is an important consideration in finite element modelling. As the mesh is refined, the numerical solution converges towards results of the corresponding mathematical model (Cook 1995). An appropriate mesh size is selected when two iterations of meshes give very similar results. In this study, the sizes of the elements were chosen to be 10, 20, 30, 50, 75, 100 and 150 mm and were uniform along the span. The results of mesh sensitivity for mid-span deflection and frequency of the first five modes for the 'ideal' boundary condition are shown in Figure 4-9. From the analyses, it was observed that a mesh size of 20 mm was appropriate for accurate results (annotated in Figure 4-9). Frequency differences between a 10 mm and 20 mm mesh size ranged from less than 1% for modes 1 and 4, with the largest difference being for Mode 2 with 2.5% difference. This was deemed an acceptable trade-off between accuracy and computation time where a mesh size of 10 mm had four times more elements than a mesh

size of 20 mm. Mid-span deflection difference between a 10 mm and 20 mm mesh size was less than 1%.
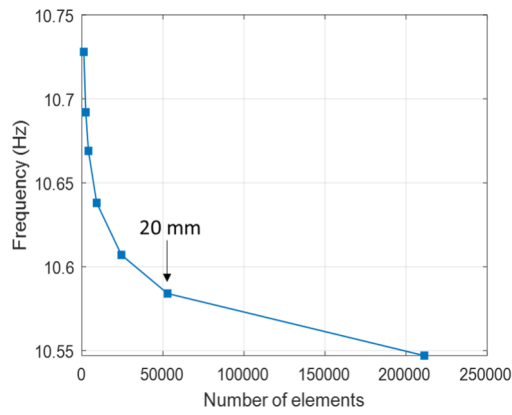
(a) Mode 1
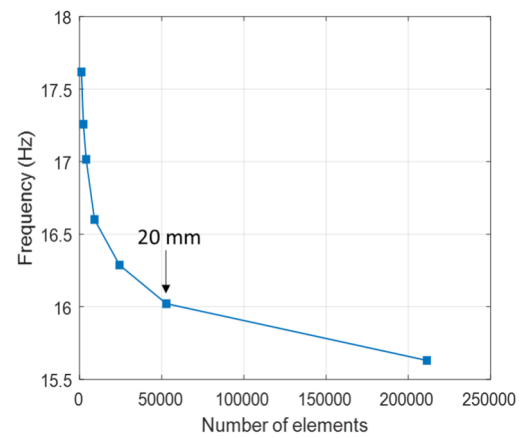
(b) Mode 2
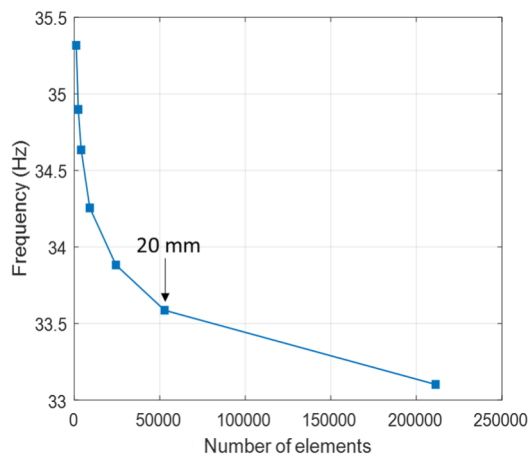
(c) Mode 3
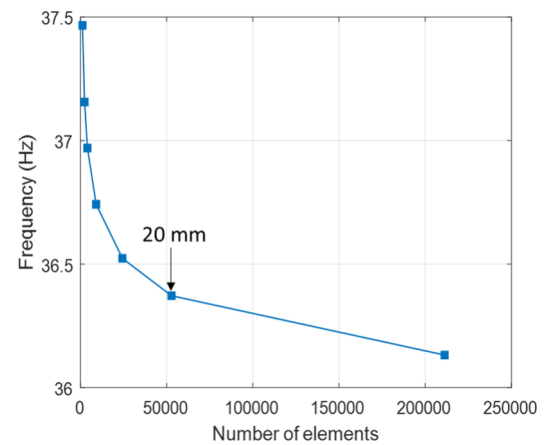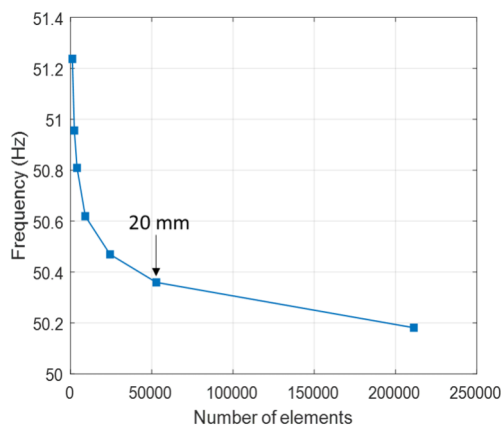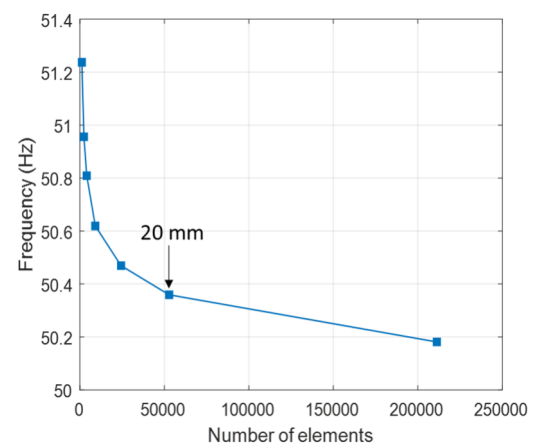
(d) Mode 4

(e) Mode 5

(f) Mid-span deflection

Figure 4-9 *Sensitivity study of mesh size and frequency of first five modes and mid-span deflection*

4.2.3.4 Comparison of FE model to experimental results for approach validation

The natural frequencies and mode shapes were extracted from the ANSYS model for both boundary condition configurations and shown in comparison with experimental results in Table 4-5. One factor which supports the modelling approach of the cassette is the matching sequence of mode shapes between the model and experiment. However, the second mode of the 'ideal' model looks slightly different from the same mode of both the experimental result and 'spring' FE model. This is due to the complete translational restraint at the support which causes the joists to warp. The influence of the additional stiffness is also revealed in the natural frequency error shown in Table 4-6 where the 'ideal' model overestimates the frequency of the second mode by 27.2%. The introduction of the springs reduces the error to -6.2% highlighting the influence of different boundary condition assumptions on the modal properties of the floor. The 'spring' model also reduces the error of the fourth mode from 4.7% to 1.8%, although for mode 3, the error increased from 8.1% to 11.8%. It is also important to note the symmetry of the mode shapes produced from the FE model which is a result of the assumption that the material properties are consistent between web members and along the flange. Asymmetry of the experimental mode shapes will be further discussed in Section 4.3.

Table 4-5 *Comparison of mode shapes between FE model and experimental*
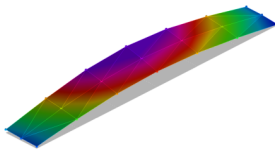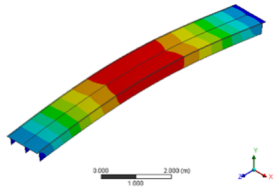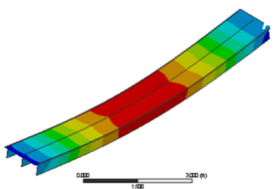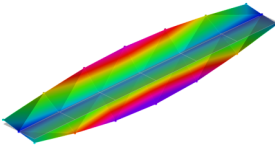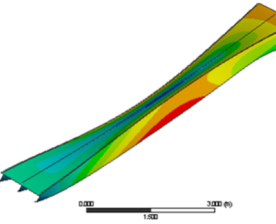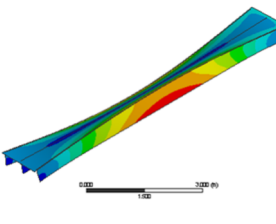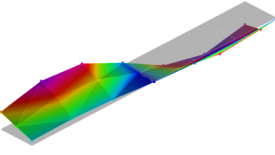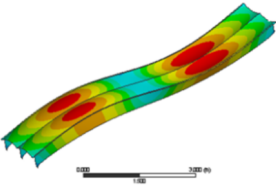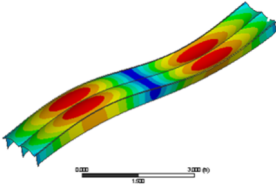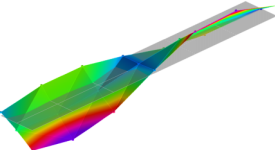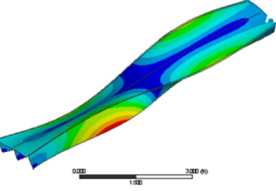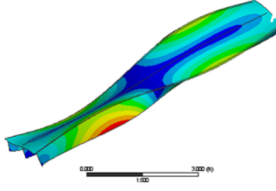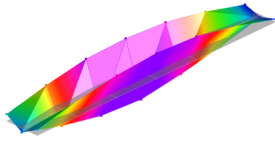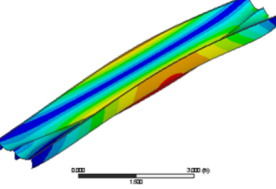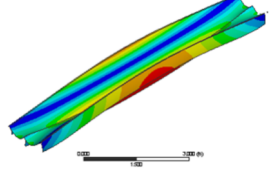
Mode		Experimental	FE model	
			Ideal	Spring
1	Bending			
2	Torsion			
3	Bending			
4	Torsion			
5	Lateral Bending			

Table 4-6 *Natural frequency error from experimental natural frequencies*

Mode	Experiment f (Hz)	'Ideal' FEM f (Hz)	Error (%)	'Spring' FEM f (Hz)	Error (%)
1	10.68	10.58	-0.9	10.66	-0.2
2	12.60	16.02	27.2	11.82	-6.2
3	31.07	33.59	8.1	34.73	11.8
4	34.74	36.37	4.7	35.38	1.8
5	41.77	50.36	20.6	48.97	17.2

4.3 Impact hammer test results

Figures 4-10 and 4-11 show the sum of Frequency Response Functions (FRFs) across all the accelerometers at each impact location for the bearing and screwed support conditions, respectively; the peaks have been annotated corresponding to each mode shape. The natural frequencies, damping ratios and mode shapes are shown in Table 4-7. Note that the web members are not shown in the mode shape images since accelerometers were placed on the top surface of the flange. Frequency estimation over the different impact locations resulted in a coefficient of variation (CoV) of less than 0.2% while for damping estimation the CoV was less than 5%.

Comparing the FRFs of both support conditions, there is a similar pattern of four distinct peaks for modes 1, 2, 4 and 5 and a smaller peak for mode 3. Mode clusters appear in two locations: around the 10 – 12 Hz range and again at the 32 – 34 Hz range. As detailed in Chapter 2 Section 2.4.2, closely spaced modes are a common phenomenon in timber floors due to the highly orthotropic nature of the system with stiffness in one direction being significantly greater than the other (Chui 1986; Filiatrault, Folz & Foschi 1990). As a result, modal interaction may occur, particularly for the first cluster of modes, which can negatively affect the vibration performance through the amplification of the floor response. Further, modes 1 and 2 may be excited by the fifth harmonic of a person walking at a pace of 2.1 Hz or 2.3 Hz, respectively, which is very close to the average walking pace of a human (2 Hz). It is expected that these modes will have the highest contribution to the response during human walking.

Comparison of the frequencies and damping ratios of each mode between the two boundary conditions indicates that the addition of screws has minimal effect on the modal properties. A calculation of the fundamental frequency of the system using the equation for a simply-supported beam of uniform cross-section (Equation 4.1) results in a frequency of 10.51 Hz, considering that the section is fully composite. This equates to a <1% error to the experimentally obtained fundamental frequencies from both boundary conditions suggesting the appropriateness of the theoretical equation for single-span ribbed-deck floors. It is important to note that damping ratios remained at approx. 1% for all modes except for a slight increase for the second bending mode; the 1% damping ratio

aligns with the Eurocode 5 (European Committee for Standardisation 2004) recommendation for residential timber floor systems.
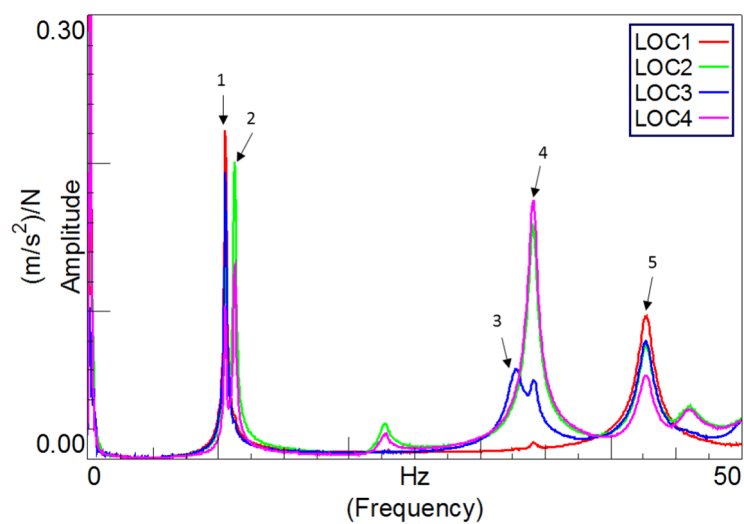
Figure 4-10 *Plot of sum of FRFs for all impact location points for bearing support condition*
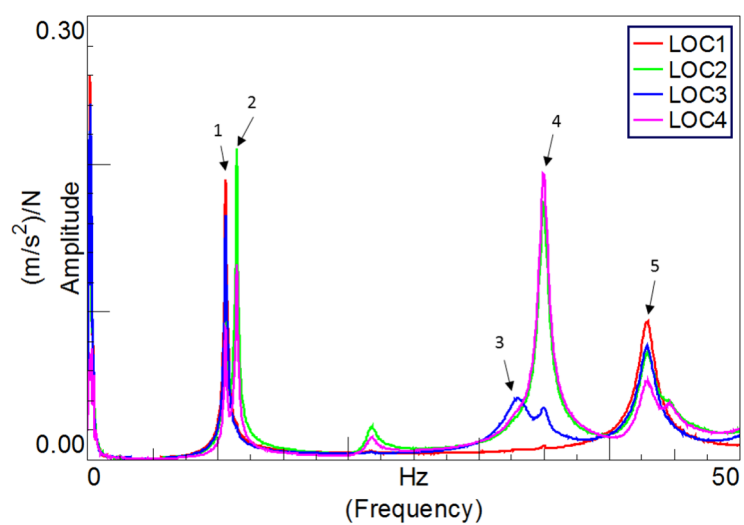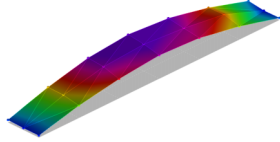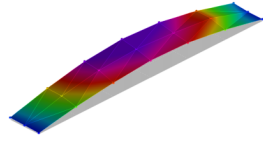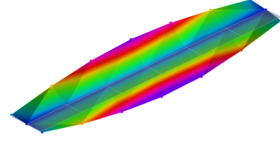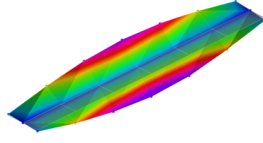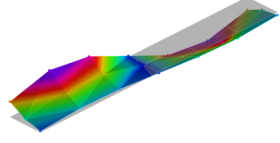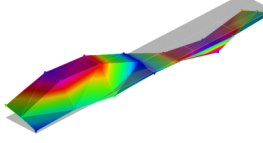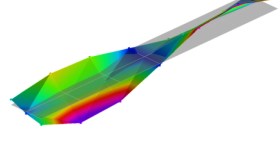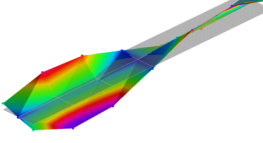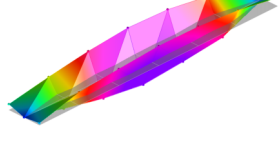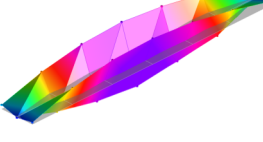
Figure 4-11 *Plot of sum of FRFs for all impact location points for screwed support condition*

Table 4-7 Frequency, damping ratios and mode shapes for simple boundary condition tests

Mode	C1_Flange		C1_Screw	
	f (Hz)	*ξ (%)*	*f (Hz)*	*ξ (%)*
1: Bending	10.50	0.71	10.56	0.81
2: Torsion	11.21	0.69	11.40	0.71
3: Bending	32.73	1.69	32.97	2.91
4: Torsion	34.09	1.08	34.96	0.91
5: Lateral Bending	42.70	1.34	42.89	1.36

On closer inspection of the mode shapes as shown in Table 4-7, it was noticed that there is a slight asymmetry about the longitudinal axis of the floor. For the bending modes, the side corresponding to grid line A (GL A), as shown in Figure 4-15, had a higher deformation while for torsion modes, the opposite side had a higher deformation. This asymmetry was also observed in mode shapes produced by Jarnerö et al. (2015) for a prefabricated CLT flange and glulam beam floor system, although no reason for the asymmetry was reported. For this research, it was believed that inconsistencies of material properties between joists may be the cause, especially since the MoE of LVL can vary by up to +/- 10% of the reference value (Buchanan 2007). Whilst this variation is expected

during production over a period of a year, the normal variation within a batch would be less than 5%. Nevertheless, in this investigation +/- 10% variation was considered as there was no certainty that all web members came from the same batch.

Static deflection tests were performed for the flange bearing boundary condition with two laser displacement transducers set up at mid-span (in line with grid 4): one measuring the top surface of the flange along grid A (referred to as 'Web A') and the other at grid C (referred to as 'Web C'). Calibrated 0.25 kN weights were then placed at mid-span (centred about grid 4) in sets of two (0.5 kN increments) with two placed equidistant between grid A and B and the other two placed equally between B and C. Deflections at seven increments (1 kN to 4 kN) were recorded to produce a load deflection curve as plotted in Figure 4-12. Figure 4-12 also shows a theoretical deflection curve obtained from a finite element model of the cassette using three MoE cases for the joists: reference MoE obtained from material tests (12754 MPa), an MoE 10% greater ('E+10%') and an MoE 10% lower ('E-10%') than reference. The weights were assumed to as act as two point loads at mid-span. As shown in Figure 4-12, the load-deflection curve for Web A is very close to the theoretical. However, Web C sits well below the E+10% curve indicating it is actually much stiffer than Joist A and may explain why mode shapes are asymmetrical.
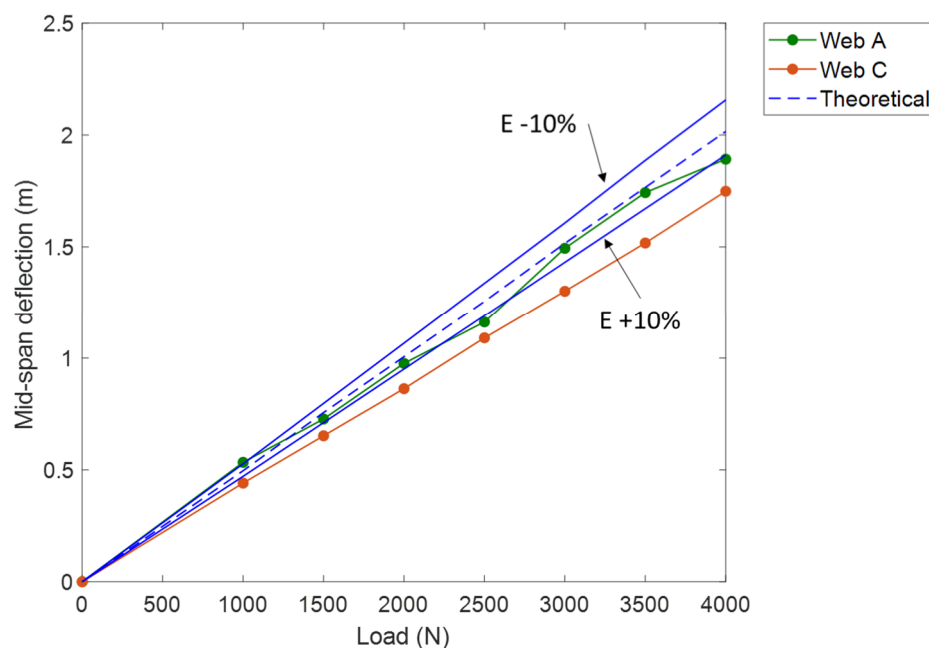
Figure 4-12 *Static deflection test load-deflection curve for Joist A and C*

4.4 Initial finite element model

4.4.1 Experimental boundary condition

The initial FE model consists of the same element types and material properties as described in Section 4.2.3. The boundary conditions were changed to reflect the flange-supported experiment where the overhanging portion of the flange bears onto the timber frame. The support condition is shown in Figure 4-13 both experimentally and the FE model; the red lines indicate the outline of the web member and interface with the flange. As shown in the photo in Figure 4-13, there is a small gap between the frame and web element resulting in a total bearing width of approx. 85 mm. In the numerical model, the mesh size means that the support nodes must be within 76 mm from the edge of the overhang (based on a 19 × 20 mm mesh size in the panel overhang section of the model). To numerically represent the experimental boundary condition, a small sensitivity study was performed to determine which row of nodes within the 76 mm portion should be restrained. Note that only one row of nodes (63 nodes) were considered to be restrained at one time since restraining a number of rows or the complete five rows within the 76 mm portion would create a rotational restraint which would not be seen experimentally. For the sensitivity study, each row of nodes was translationally restrained in the x-, y- and z-directions; the same condition was mirrored on the support on the opposite side of the cassette. The results of the natural frequencies of the first five modes from translationally restraining each row, as annotated in Figure 4-14, are shown in Table 4-8.
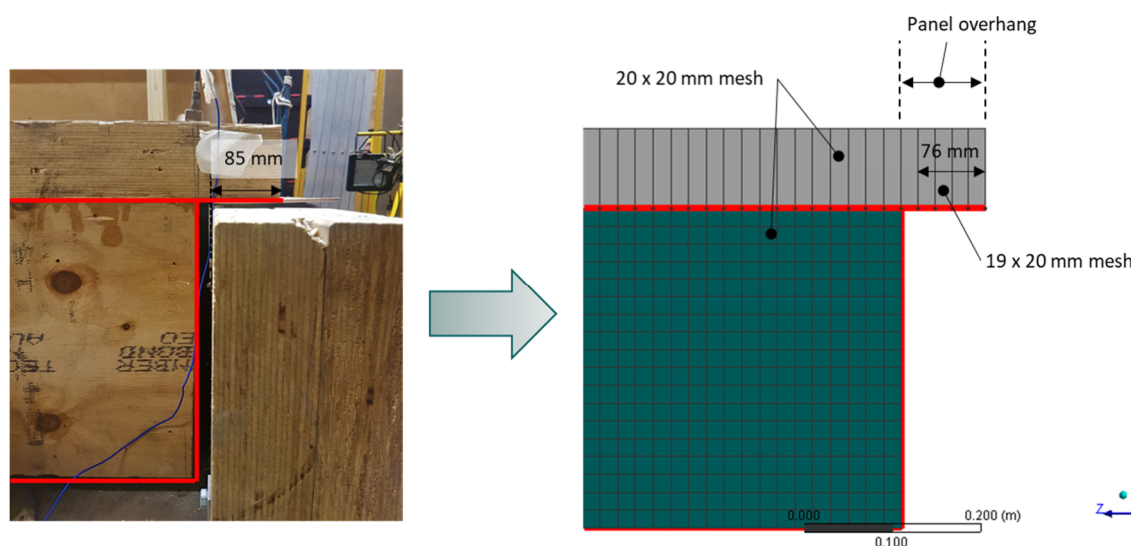
Figure 4-13 *Detail of flange bearing onto timber frame*
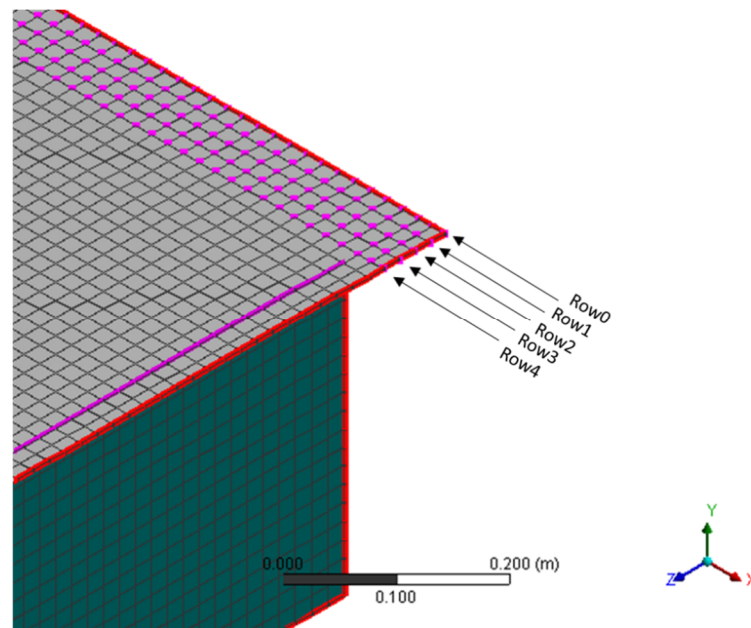
Figure 4-14 *Row names for each row within the panel overhang portion of model. Identical row names for the opposite support.*

Table 4-8 *Summary of natural frequencies for each restrained row within 76 mm (Row0 – Row4) and the measured natural frequency with mode order in parentheses*

FE Mode	Natural frequency (Hz)					
	Measured	Row0	Row1	Row2	Row3	Row4
1: Bending	10.50 (1)	10.35	10.51	10.67	10.85	11.03
2: Torsion	11.21 (2)	11.07	11.27	11.48	11.70	11.95
3: Torsion	34.09 (4)	31.20	31.74	32.28	32.86	33.48
4: Bending	32.73 (3)	33.31	34.00	34.70	35.44	36.27
5: Lat. bending	42.70 (5)	49.31	49.38	49.45	49.51	49.58

It is important to remember that restraining the complete row translationally would be the upper limit and therefore cannot be any stiffer in regard to the boundary conditions. As such, through comparison with the measured natural frequencies (as reproduced in Table 4-8 for ease of comparison) of the first two modes, Row0 would not be an appropriate location to simulate the experimental boundary condition. Further, results from restraining Row4 were deemed too stiff as an initial model. Therefore, Row1 – Row3 were selected as an appropriate starting point for the boundary conditions of the initial model; any of these rows would be acceptable.

Another point for consideration in setting up the boundary conditions to represent the experimental condition is the time taken to set up each spring element as part of the future model updating procedure. As the geometry was developed in ANSYS ADPL (2016) and then imported into ANSYS Workbench (2016), spring elements would need to be manually created for each translational degree-of-freedom and for each node. This process would have to be repeated for each modelled cassette. Consequently, one cassette would result in 378 manual operations (2 support lines × 63 nodes × 3 degrees-of-freedom) which would be time consuming, particularly in the later stages of the research where eight cassettes would be numerically modelled (Chapter 7). Subsequently, a reduced number of restrained nodes in the row were considered and compared to the total row results. Spacing between the restrained nodes were taken as 40 mm (29 nodes), 80 mm (15 nodes) and 150 mm (9 nodes); these models will be referred to as Row*-*sp* where * is the row number and *sp* is the spacing.

Table 4-9 Natural frequencies for first five modes considering reduced number of restrained nodes for Row1 – Row3

Model	Natural frequency (Hz) – FE mode				
	Mode 1	Mode 2	Mode 3	Mode 4	Mode 5
Row1-40	10.40	11.07	31.13	33.28	49.29
Row1-80	10.36	11.00	31.02	33.07	49.24
Row1-150	10.33	10.93	30.93	32.89	49.19
Row2-40	10.59	11.31	31.83	34.17	49.38
Row2-80	10.56	11.26	31.76	34.02	49.34
Row2-150	10.53	11.21	31.69	33.89	49.30
Row3-40	10.78	11.57	32.54	35.08	49.46
Row3-80	10.77	11.53	32.49	34.97	49.43
Row3-150	10.74	11.49	32.44	34.87	49.39

Table 4-9 reveals the natural frequencies for the first five modes when considering a reduced number of restrained nodes for Row1 – Row3. The difference between restraining the whole row and 9 nodes was less than 3.3%, 2.4% and 1.9% for Row1, Row2 and Row3, respectively. Subsequently, reducing the number of nodes restrained was deemed as an acceptable compromise between accuracy and time. As shown, reducing the number of restrained nodes along Row1 resulted in natural frequencies for

the first and second modes to be less than the measured results indicating that these models would not be appropriate for the initial model.

Therefore, models with nodes restrained along Row2 and Row3 were deemed as the best candidates for an initial model. It should be noted here that any of the models for Row2 and Row3 would have been an acceptable starting point as further model updating would be performed on the spring stiffness and material properties. However, it is important to select the best initial model with consideration to how closely it represents the experimental set-up.

As shown in Figure 4-13, the flange was not restrained against uplift (y-direction) and friction between the flange underside and the top surface of the timber frame would be the only restraint for the lateral axes (x- and z-directions). It was anticipated that spring elements, similar to those used in Section 4.2.3.2, with defined stiffness' would be used in the model updating procedure. As a result, it was deemed to be more appropriate to select the row which produces a stiffer result and subsequently allowing for greater variation when selecting and appropriate spring stiffness. Therefore, Row3-150 was considered as the best starting point for the initial model. The final support node locations and details are illustrated in Figure 4-15 and Figure 4-16.
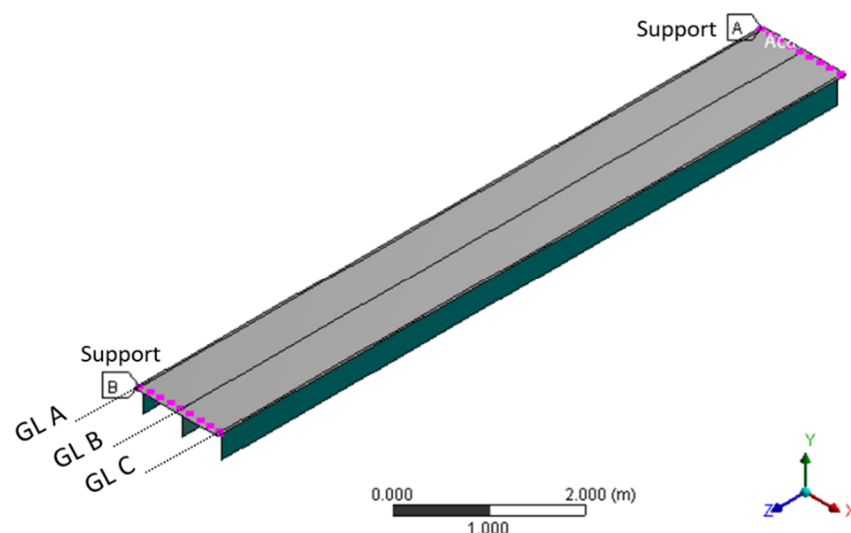
Figure 4-15 *Isometric view of FE model of cassette with support node locations highlighted*
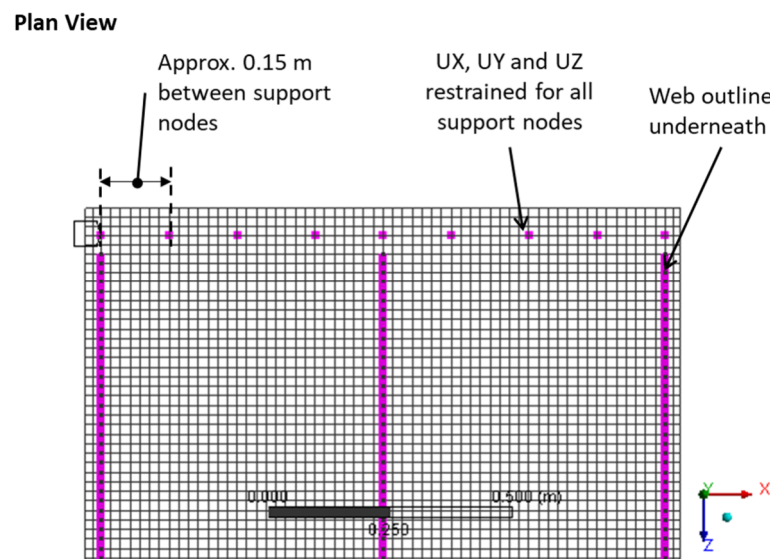
Figure 4-16 *Plan view of Support A from Figure 4-15. Support B is identical.*

4.4.2 Design boundary condition

The aforementioned boundary condition, as detailed in the previous section, is specific to the experiment conducted for this research with the primary goal of having a calibrated FE model which can be used for further investigation. It is not a suggested approach for a design situation where efficiency and accuracy need to be balanced. In a design scenario, it is likely that a pin connection would be used at the location where the floor is supported by the primary beams. Thus, it is of interest to investigate how closely the measured natural frequencies compare to such a model. In this case, the screw case (C1_Screw) natural frequencies (as detailed in Table 4-7) were compared with results in Table 4-8. The screws were inserted at 40 mm from the edge which is approximately at the mid-point of the bearing width. As shown, Row1 which lies at 19 mm from the edge results in the closest match to the measured results with approx. -0.5% and -1.1% error for mode 1 and 2, respectively. Row2 which lies at 38 mm from the edge also had a very small errors of 1.1% and 0.7% for mode 1 and 2, respectively.

This indicates that modelling the floor with a pin-pin boundary condition along the location of where the floor is secured to the surrounding frame provides a sufficiently accurate modelling approach for the floor. It is important to highlight however that the higher modes may have a higher margin of error and in this case, modes 3 and 4 have switched order between the numerical and experimental results. Nevertheless, the contribution of these higher modes to the floor response will be smaller.

4.5 Finite element model updating of initial model

The process of model updating originated in the mechanical and aerospace engineering industries where structures or parts subject to dynamic loads were prototyped and further analysed using a validated FE model based on results from modal tests. The procedure typically consists of identifying key parameters (inputs) which influence the modal properties, manual tuning by trial and error and, if required, automatic model updating using specialised software to further minimise the differences (Živanović, Pavic & Reynolds 2007a).

Numerous automatic or formalised model updating techniques exist (Friswell & Mottershead 1995) and are typically split into two categories: direct methods which directly updates the stiffness and mass matrices and, the more preferred, iterative method which updates structural parameters having a clear physical significance. The manual tuning procedure is essential as a first-pass check to obtain a relatively close analytical model which can be used as a starting point for the automated model updating. If the differences between experimental and numerical results are too large, the automatic model updating may cause results to diverge and/or produce unrealistic parameter changes (Živanović, Pavic & Reynolds 2007a). Once the numerical and experimental results match with an acceptable level of accuracy, the FE model is 'validated'.

For civil engineering structures, application of automatic model updating is still relatively recent. Building a 'prototype' is rare where the only chance to test the structure is generally after it has been built. Consequently, the benefits of an updated model are not realised as immediately as would be the case for product refinement in the mechanical and aerospace industries (Brownjohn & Xia 2000). As such, one of the main motivations of having a validated model is its use for further investigations of structure behaviour. Examples include analysing the dynamic behaviour to time-dependent loads such as earthquakes (Dumanoglu, Brownjohn & Severn 1992) or footfall impacts (Ussher et al. 2017b). Other motivations include parametric studies to understand which parameters influence the modal properties of floor (Ebadi, Doudak & Smith 2017) and condition assessment of structures (Brownjohn et al. 2001; Hashim, Ibrahim & Razak 2013).

4.5.1 Correlation analysis for model updating

The aim of FE model updating is to minimise the differences between the FE model and experiment. It is essentially an optimisation problem which can be expressed by the following objective function (Kim & Park 2004):

$$\text{minimise} \quad \boldsymbol{F(x)} = \{F_1(\boldsymbol{x}), F_2(\boldsymbol{x}), \dots, F_n(\boldsymbol{x})\}$$

$$\text{subject to} \quad \boldsymbol{g(x)} \leq 0, \qquad\qquad\qquad\qquad\qquad (4.3)$$

$$\boldsymbol{x}_{min} \leq \boldsymbol{x} \leq \boldsymbol{x}_{max}$$

where $F_i(\boldsymbol{x})$ is the i-th objective function; $g(\boldsymbol{x})$ is a constraint vector; $\boldsymbol{x}$ is a vector of design variables $(x_1, x_2, \dots, x_k)$; and $\boldsymbol{x}_{min}$ and $\boldsymbol{x}_{max}$ are the lower and upper constraints of the design variables vector, respectively. As the iterative method is preferred over the direct method of model updating, the design variables x are iteratively modified within the set limits to minimise the objective function. This method provides an important connection between the updating procedure and the physical structure where the parameter boundaries are generally guided by engineering judgement.

The most common objective functions to minimise are the natural frequency error and the Modal Assurance Criterion (MAC) error. The natural frequency error (NF_{ERROR}) for mode i is expressed as:

$$NF_{ERROR,i} = \frac{f_i^{FE} - f_i^{exp}}{f_i^{exp}} \times 100 \qquad\qquad (4.4)$$

where f_i^{FE} and f_i^{exp} refer to the numerically obtained and experimentally obtained natural frequencies in Hz, respectively.

The MAC provides a measure of consistency (degree of linearity) between estimates of a modal vector (Allemang 2003); for example, between modal vectors obtained experimentally and numerically. A MAC value close to 1 indicates that the mode shape vectors from the two sources are consistent whereas a MAC value of 0 indicates no consistent correspondence. The MAC only indicates consistency between sources and does not provide information on the validity or orthogonality of the mode shapes. The MAC of the i-th mode of the FE model compared to the j-th mode of the experiment can be calculated as follows:

$$MAC_{ij} = \frac{\left(\{\varphi_{FE,i}\}^T \{\varphi_{exp,j}\}\right)^2}{\{\varphi_{FE,i}\}^T \{\varphi_{FE,i}\}\{\varphi_{exp,j}\}^T \{\varphi_{exp,j}\}} \tag{4.5}$$

where $\varphi_{FE,i}$ and $\varphi_{exp,i}$ refer to the numerically and experimentally obtained mode shape vector, respectively. The diagonals in the MAC matrix (i.e. MAC_{11}, MAC_{22} and so on) indicate the correlation between the same mode from the FE model and experiment.

As the aim of the objective function is to minimise the sub-functions, this research reports the $MAC_{ERROR,ij}$ which is calculated by subtracting the MAC value reported in Equation 4.5 from 1:

$$MAC_{ERROR,ij} = 1 - MAC_{ij} \tag{4.6}$$

This means that a lower *MAC$_{ERROR}$* indicates a closer linear relationship between numerically and experimentally obtained mode shapes.

4.5.2 Correlation between initial FE model and experimental results

Table 4-10 shows the NF_{ERROR} and MAC_{ERROR} between the experimental results and initial FE model for the matching modes; the mode order is shown in parentheses. As shown, all five modes in the experiment were identified in the initial FE model. However, the order of the second bending and torsion modes were reversed. This indicates that the boundary condition assumption may not be accurately representing the experimental boundary condition. Except for the second bending mode, all other modes were overestimated by the model with an *NFerror* ranging from 2.3% for the first bending mode up to 15.7% for the lateral bending mode. The second bending mode was underestimated by 4.8%. The *MAC$_{ERROR}$* shown in the last column of Table 4-10 indicates that the first bending and torsion mode shapes as well as the lateral bending mode correlated well with the experimental mode shape. A possible reason for the higher *MAC$_{ERROR}$* values for the second bending and torsion modes may be the asymmetry in the experimental mode shapes.

Table 4-10 *Correlation between experimental results and initial FE model*

Mode type	f^{exp} (Hz)	f^{FE} (Hz)	NF_{ERROR} (%)	MAC_{ERROR}
Bending	10.50 (1)	10.74 (1)	2.3	0.01
Torsion	11.21 (2)	11.49 (2)	2.5	0.01
Bending	32.73 (3)	34.87 (4)	6.5	0.29
Torsion	34.09 (4)	32.44 (3)	-4.8	0.24
Lat. Bending	42.70 (5)	49.39 (5)	15.7	0.04

4.5.3 Forming the objective function for automatic model updating

If the objective function only includes a single sub-objective function $F_1(\boldsymbol{x})$, as is the case for conventional model updating, the objective function is generally formulated as a weighted sum of the natural frequency error and mode shape error for each mode *i*:

$$F_1(\boldsymbol{x}) = \sum_i^n w_{f,i} NF_{ERROR,i} + \sum_i^n w_{\varphi,i} MAC_{ERROR,ii} \qquad (4.7)$$

where *n* = total number of modes considered and $w_{f,i}$ and $w_{\varphi,i}$ are the weighting factors for the frequency error and MAC error, respectively. Selection of weighting coefficients can depend on the confidence levels in the measured data where a higher weighting is given to data with a high degree of confidence. For example, confidence in the measured natural frequencies is typically higher than for mode shapes (Živanović, Pavic & Reynolds 2007a). Further, measured natural frequencies of higher modes are not usually measured with the same accuracy as lower ones (Wu & Li 2004). Although the ability to apply a weighing factor is powerful, it can be difficult to quantify as it is based on the analyst's judgement and experience and is often project specific. Thus, a multi-objective function approach has been suggested (Jin et al. 2014; Kim & Park 2004; Perera & Ruiz 2008) to avoid the weighting coefficient so that several objective terms can be minimised simultaneously as follows:

$$F_1(\boldsymbol{x}) = NF_{ERROR,i}; \; F_2(\boldsymbol{x}) = MAC_{ERROR,ii} \qquad (4.8)$$

The multi-objective function approach aims to find a set of preferred solutions or 'candidate points' called the Pareto optimal front or Pareto curve. The curve is made up of feasible candidate points, also called 'non-dominated solutions', by which the objective function cannot be improved without degradation of the other objective function values (Jin et al. 2014).

To simplify the optimisation problem for this research and also considering that there was higher confidence in the measured natural frequency data, it was deemed sufficient that only the natural frequency error was minimised. The *MACerror* was then used as a check on the updated model for comparison to the initial FE model. As such, the objective function for this research can be formulated as follows and considers the first five modes i=1 to 5 so that there are five individual sub-objective functions, as shown in Equation 4.9. The target responses refer to the measured experimental natural frequencies.

$$F(x) = \{NF_{ERROR,1}, NF_{ERROR,2}, NF_{ERROR,3}, NF_{ERROR,4}, NF_{ERROR,5}\} \tag{4.9}$$

4.5.4 Updating parameter selection

Selection of the updating parameters, as shown by vector x in Equation 4.3, is a crucial step in the model updating process. Essentially, only uncertain parameters should be chosen and the sensitivity of those selected parameters to the target responses should be determined. Examples of input parameters which have a degree of uncertainty include model geometry, material properties and boundary conditions.

4.5.4.1 Parameter identification

As the dimensions of the cassette are known, only uncertainty in the material property and boundary conditions were considered. The elements of the web members and flange were treated as separate substructures and, for simplicity, each web was assumed to have the same material properties as other web members. This means that varying the material property in one element of the web subsequently modified all other web elements. Out of a total of 22 input parameters for the combined material properties of both the flange and web, only 12 were selected as an updating parameter. The selected parameters were based on the following engineering judgements:

- MoE in the element y-direction is the largest contributor to the stiffness of the cassette and thus was selected as a parameter for both flange and web.
- MoE in the element x-direction was included to investigate the significance of considering LVL as an orthotropic material in an FE model.
- The effect of the MoE in the element z-direction (i.e. out of plane) was considered to be negligible in adding to the stiffness of the section as the thickness of both the flange and web members was not large.

- The majority of shear stresses will occur in the web members and thus the shear modulus in the flange was not considered; the effect of GXZ and GYZ were considered to be negligible.
- The natural frequency is directly related to the mass of the structure and therefore the density of both materials were considered.
- Despite studies showing that the Poisson's ratio had no significant effect on response (Crews 2002), Poisson's ratio was still included as a check.

For the support stiffness, each direction of translational restraint was treated as one parameter i.e. varying the stiffness in the y-direction (KTy) of one support point also varied KTy at other support points simultaneously. The support stiffness was applied via a COMBIN14 element as discussed in Section 4.2.3.2. For simplicity, rotational restraints were not considered. Based on findings in Section 4.2.3.4, translational support stiffness was considered to have a large influence on the modal properties. All 12 selected parameters are shown in Figure 4-17.
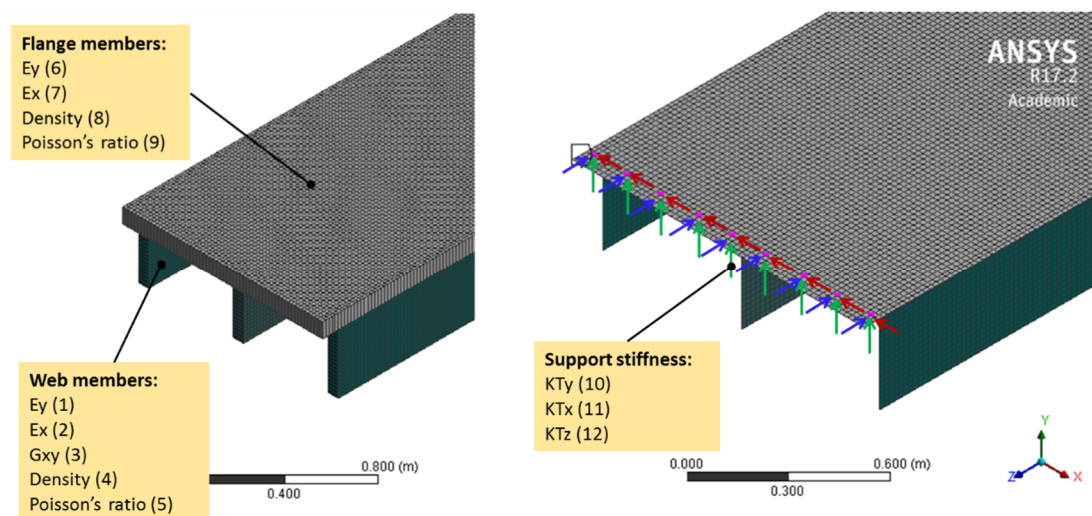
Figure 4-17 *Uncertain parameters in the FE model*

4.5.4.2 Parameter sensitivity

The simplest form of parameter sensitivity is to assess the influence of each parameter independently while keeping all other parameters constant or fixed. This is referred to as 'local' sensitivity (Crick, Hill & Charles 1987) or 'one-at-a-time' sensitivity analysis (Hamby 1994). Differential analysis (also referred to as the direct method) is the most fundamental of sensitivity techniques and forms the backbone of nearly all sensitivity analysis procedures (Hamby 1994). The method is based on partial differentials to

calculate a sensitivity coefficient S_{ij} for each target response R_i ($i = 1,2,…,m$) to a certain change in parameter P_j ($j = 1,2,…,n$):

$$\boldsymbol{S} = \left[S_{ij} \right] = \left[\frac{\delta R_i}{\delta P_j} \right] \qquad (4.10)$$

The above equation assumes that the there is no correlation between input parameters and that the higher ordered partials are negligible (Hamby 1994). If we assume that the input-output relationship is linear, Equation 4.10 can be approximated by the ratio of the finite difference in output from the base case over the difference in input from the base case (Downing, Gardner & Hoffman 1985):

$$\boldsymbol{S} = \left[S_{ij} \right] = \left[\frac{\Delta R_i}{\Delta P_j} \right] \qquad (4.11)$$

The model output with which all parameters are held constant defines the 'base case' scenario. It must be emphasised here that Equation 4.11 is based on neglecting non-linearities and so is only valid for small changes in the input parameter which is typically accepted as 1% (Downing, Gardner & Hoffman 1985). Indeed, the natural frequency is not linearly related to material properties such as density and modulus of elasticity. However, the objective of calculating the sensitivity coefficient in this research was not to obtain precise quantities of sensitivity but to understand the general influence of certain input variables to the response outputs. To compare the parameters to one another, the sensitivity index shown in Equation 4.11 was normalised by multiplying by the ratio of the base response over the base input parameter (Živanović, Pavic & Reynolds 2007a):

$$S_{n,ij} = \frac{\Delta R_i}{\Delta P_j} \frac{P_j}{R_i} \qquad (4.12)$$

Here, the 'base' scenario for the ribbed-deck cassette model is the response when input parameters correspond to those defined in Table 4-2. Table 4-11 shows the lower and upper limits of each input parameter calculated as a percentage of the 'base' scenario. For the support stiffness parameters, the model was first analysed iteratively with an extremely flexible (1×10^2 N/m) to stiff (1×10^{12} N/m) spring for each direction independently. For very flexible springs in the z- and y-directions, the model output (natural frequencies and mode shapes) did not represent the experimental behaviour of

the structure. Therefore, the lower bound limit in Table 4-11 represents the spring stiffness with which the mode shapes begin to represent those measured from the experiment. A spring stiffness of 1×10^{12} N/m for all directions produced a very similar result to the case where pin-supports were used.

Table 4-11 Upper and lower limits considered for sensitivity analysis

No.	Parameter (Unit)	Member	Base value x	x_{min} (%x)	x_{max} (%x)
1	EY (MPa)	Web	12754	11479 (-10%)	14029 (+10%)
2	EX (MPa)	Web	1275.4	1148 (-10%)	1403 (+10%)
3	GXY (MPa)	Web	660	594 (-10%)	726 (+10%)
4	Density (kg/m^3)	Web	589.1	530.2 (-10%)	648.0 (+10%)
5	PRXY	Web	0.3	0.27 (-10%)	0.315 (+5%)
6	EY (MPa)	Flange	11000	9900 (-10%)	12100 (+10%)
7	EX (MPa)	Flange	1100	990 (-10%)	1210 (+10%)
8	Density (kg/m^3)	Flange	570	495 (-10%)	605 (+10%)
9	PRXY	Flange	0.3	0.27 (-10%)	0.315 (+10%)
10	KTy (N/m)	Support	1×10^{12}	1×10^{6}	1×10^{12}
11	KTx (N/m)	Support	1×10^{12}	1×10^{2}	1×10^{12}
12	KTz (N/m)	Support	1×10^{12}	1×10^{5}	1×10^{12}

(1) Influence of material properties

Figures 4-18 and 4-19 show the normalised sensitivity coefficients for the material property input parameters when varied f rom x_{min} to x and from x to x_{max}, respectively, with respect to each response output. The properties associated with the web member have been denoted with '_1' at the end while properties associated with the flange member have been denoted with '_2' in the legend. Note that for consistency, the sequence of mode shapes in the x-axis of the graph aligns with the sequence from experimental measurements rather than the initial FE model. A negative sensitivity coefficient means that the output decreased as a result of the change in parameter. A common trend between both graphs is that EX, GXY and PRXY of the web members have small influence which indicates that modelling the webs as isotropic members may

have been sufficient for this case. The lateral bending mode had a high sensitivity to the EX and EY properties of the flange as well as to the flange Poisson's ratio which was an interesting finding. As expected, changes in density of both the web and flange members have a large influence to all modes. In relation to the flange material properties, the largest change in natural frequency due to the change in parameter was 6.9% for mode 5 when the Poisson's ratio was increased by 5%. All other changes were less than 3.8% and thus it was deemed that further material testing on the flange was not required.
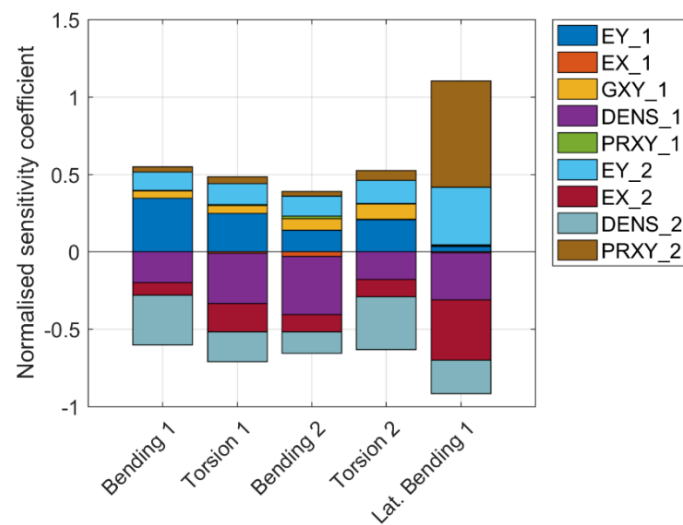
Figure 4-18 *Normalised sensitivity coefficient of varying material property parameters to x_{min} with respect to each response output*
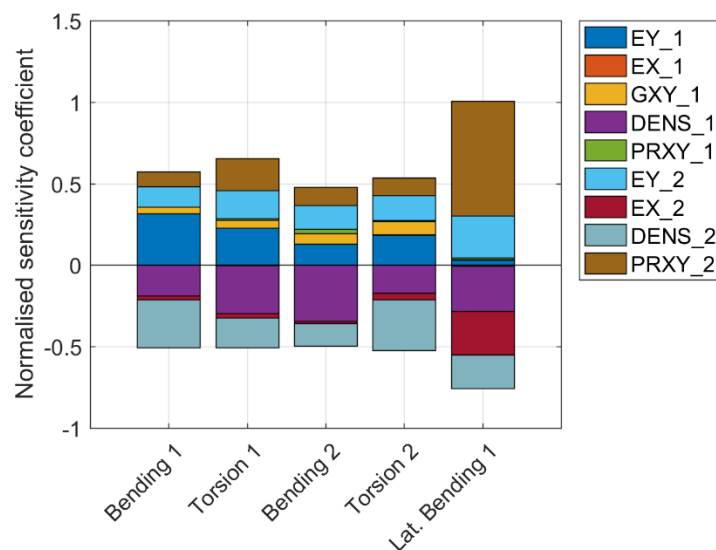
Figure 4-19 *Normalised sensitivity coefficient of varying material property parameters to x_{max} with respect to each response output*

(2) Influence of support stiffness

Figure 4-20 shows the normalised sensitivity coefficient for each support stiffness parameter compared to each mode. It is clear that the stiffness in the y-direction (vertical) had the largest influence on all output values, particularly the second bending mode. The z-direction (longitudinal) stiffness had a higher effect on the first torsion mode while the second torsion mode was highly sensitive to the x-direction stiffness. In fact, KTx values less than approximately 1.1×10^6 N/m caused a switch in the sequence of the second bending and torsion modes. This indicates that the complete restraint in the x-direction for the initial FE model did not accurately reflect the boundary condition in the experiment resulting in the mismatch of mode order.
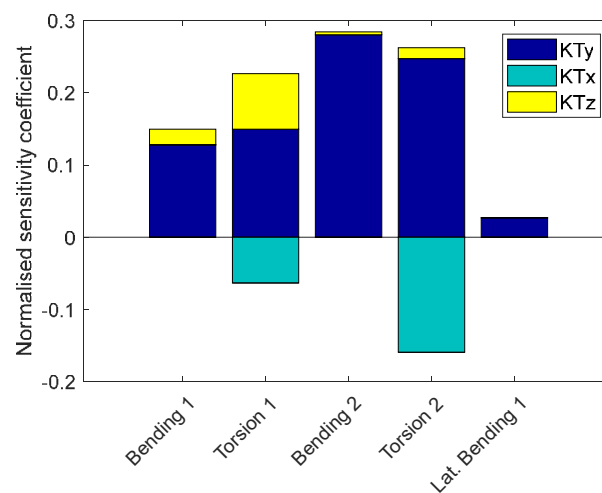
Figure 4-20 *Normalised sensitivity coefficient of support stiffness parameters with respect to each response output*

4.5.5 Updated FE model

Before the automatic updating was performed, the initial FE model was manually tuned to get a closer match to the experimental results with a particular focus on obtaining the correct sequencing of mode shapes. Manual tuning of the support stiffness found that a spring stiffness of 1.8×10^7 N/m, 1×10^2 N/m and 1×10^6 N/m for KTy, KTx and KTz, respectively, provided this match. The correlation between the tuned FE model and the experimental results is shown in Table 4-12; the mode order is shown in parentheses. The *MAC~ERROR~* values have slightly improved for modes 3 to 5 when compared to the initial FE model results.

Table 4-12 *Correlation between experimental and tuned FE model*

Mode type	f^{exp} (Hz)	f^{FE} (Hz)	NF_{ERROR} (%)	MAC_{ERROR}
Bending	10.50 (1)	10.40 (1)	-0.95	0.01
Torsion	11.21 (2)	11.34 (2)	1.17	0.01
Bending	32.73 (3)	33.65 (3)	2.80	0.27
Torsion	34.09 (4)	33.92 (4)	-0.50	0.23
Lat. Bending	42.70 (5)	49.25 (5)	15.34	0.03

Automatic updating was then conducted using the Multi-Objective Genetic Algorithm method within the ANSYS Workbench Response Surface and Response Surface Optimisation module which is based on the multi-objective function approach detailed in Section 4.5.3. The candidate points were extracted using a goal-based, weighted, aggregation-based decision ranking technique which combines the collection of objectives for *m* output parameters into a single weighted objective function, ϕ, as follows:

$$\phi = \sum_{i=1}^{n} w_i N_i + \sum_{j=1}^{m} w_j M_j \tag{4.13}$$

where N_i and M_j are the normalised objectives for the input and output parameters, respectively and w_i and w_j are the weighting factors. As there were no objectives for the input parameters, Equation 4.13 reduces to just consider the output parameters. The weighting factors are defined for a 'Higher', 'Default' and 'Lower' Importance level as follows:

$$w_i = w_j = \begin{cases} 1.000, & \text{if the Importance is Higher} \\ 0.666, & \text{if the Importance is Default} \\ 0.333, & \text{if the Importance is Lower} \end{cases}$$

Based on the sensitivity study, only input parameters EY_1, DENS_1, EY_2, EX_2, DENS_2 and PRXY_2 were used. The same importance was initially placed on all target responses, however, due to the close proximity of mode 3 and 4, a higher importance was placed on mode 3 to keep the mode sequence. A higher importance was also placed on the first mode. The final input parameter values and parameter change from the initial model are listed in Table 4-13.

Table 4-13 *Final input parameter values for updated model*

No.	Parameter (Unit)	Member	Base value x	Updated value x_u	% change
1	EY (MPa)	Web	12754	13369.4	4.8%
2	EX (MPa)	Web	1275.4	N/A	No change
3	GXY (MPa)	Web	660	N/A	No change
4	Density (kg/m³)	Web	589.1	598.6	1.6%
5	PRXY	Web	0.3	N/A	No change
6	EY (MPa)	Flange	11000	10118.7	-8.0%
7	EX (MPa)	Flange	1100	1115.7	1.4%
8	Density (kg/m³)	Flange	570	563.9	-1.1%
9	PRXY	Flange	0.3	0.277	-7.8%

Table 4-14 reveals the correlation of the updated FE model to the experimental results along with the modal masses of the updated FE model, M_i^{FE}, calculated using the extracted total sum of the kinetic energy for each mode. As shown, the largest *NF$_{ERROR}$* occurs for the fifth mode at 5.8% which is a significant change from the tuned FE model where the *NF$_{ERROR}$* was 15%. As the natural frequency of modes 1 – 4 were already quite close in the tuned FE model, there were only small improvements for the first torsion and second mode. Mode 1 and 4 in fact increased in *NF$_{ERROR}$* by 0.03% and 0.6% respectively, however this trade-off was accepted as the *NF$_{ERROR}$* was still approximately 1%. There were no improvements in the *MAC$_{ERROR}$*.

Table 4-14 *Correlation between experimental and updated FE model*

	Updated FE				
Mode type	f^{exp} (Hz)	f^{FE} (Hz)	M_i^{FE} (kg)	*NF$_{ERROR}$* (%)	*MAC$_{ERROR}$*
Bending	10.50 (1)	10.40 (1)	472.7	-0.98	0.01
Torsion	11.21 (2)	11.28 (2)	80.2	0.60	0.01
Bending	32.73 (3)	33.44 (3)	399.6	2.18	0.27
Torsion	34.09 (4)	33.71 (4)	50.2	-1.11	0.23
Lat. Bending	42.70 (5)	45.17 (5)	193.0	5.78	0.03

A summary of the model updating procedure as discussed throughout this chapter has been illustrated using a flowchart as shown in Figure 4-21.
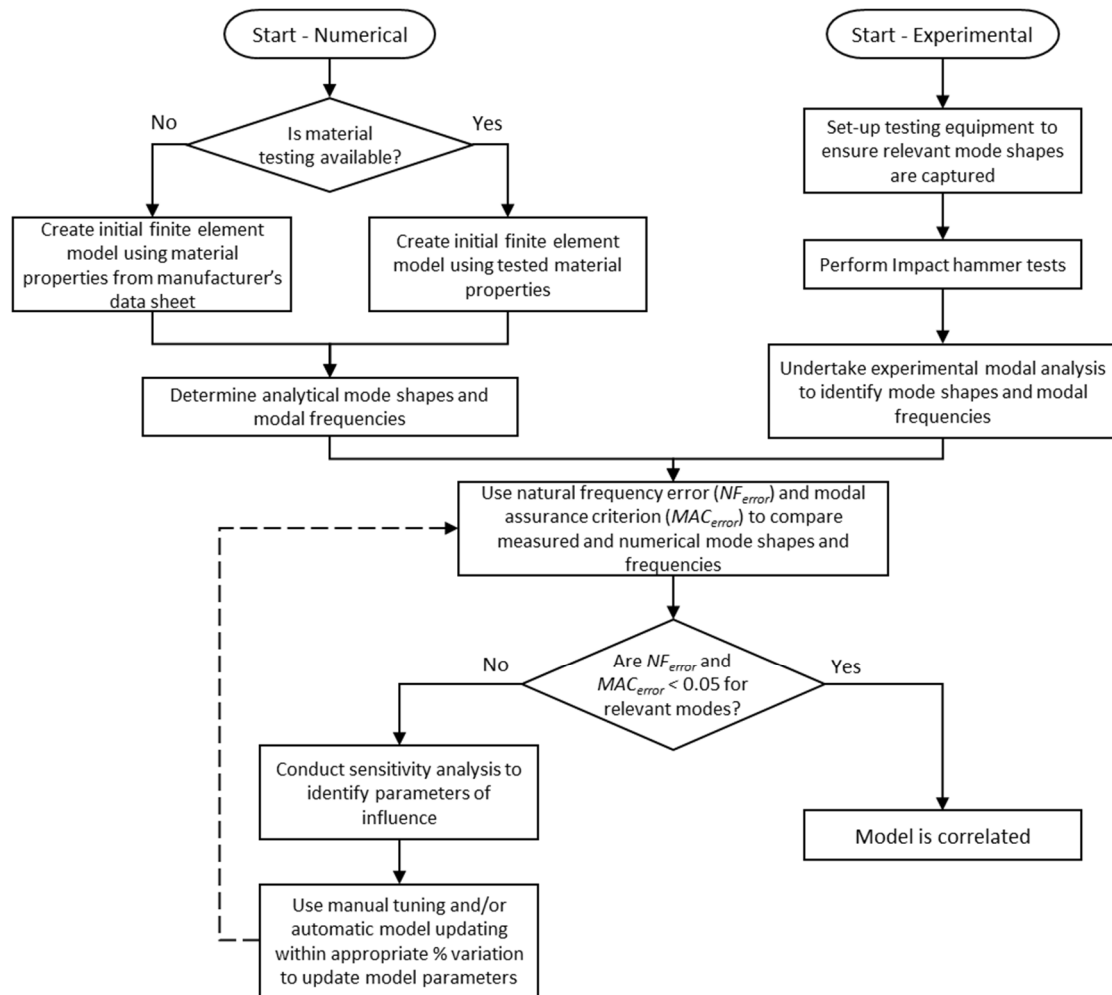
Figure 4-21 *Flowchart for model updating procedure*

4.6 Concluding remarks

This chapter presented a validated FE model of a single 9 m spanning ribbed-deck cassette with flange bearing boundary conditions based on results from impact hammer testing. Correlation analysis was used to determine the most influential properties and automatic model updating was performed using ANSYS Workbench. The validated FE model had a NF_{ERROR} of less than 1% for the first bending and torsion modes, less than 2.2% for the second bending and torsion modes and less than 6% for the first lateral bending mode (mode 5) and therefore was deemed as an acceptable representation of the experiment. The following conclusions can be drawn from the test results, FE model and model updating process:

- When developing an FE model for model updating purposes, modelling of boundary conditions plays a key role in not only the frequency values but also in the sequencing of the mode shapes. As a result, support conditions represented by spring elements should be considered.

- When developing an FE model for a design scenario, modelling the floor with a pin-pin connection at the location of where the flange bearing section is secured to the surrounding timber frame would be sufficiently accurate.

- A sensitivity analysis showed that the most influential properties on the natural frequency of the first five modes were EY and DENS of the web member and EY, EX, DENS and PRXY of the flange member. This suggests that considering the orthotropic nature of LVL used as web members in a cassette may not be relevant, however, it must be considered for the flange member.

- The first lateral bending mode of the cassette was highly sensitive to the Poisson's ratio of the flange member in the x-y plane. This was not expected and further analysis or tests are recommended to understand why this is the case.

- The addition of the screws at supports had minimal effect on the modal properties of the system.

- The first bending mode of a single cassette with flange bearing onto a primary beam can be calculated accurately using the theoretical equation of a simply-supported beam with uniform cross-section. The cross-section can be considered to be a composite section for vibration serviceability.

Chapter 5

Walking-induced Vibration of Long-Span Timber Ribbed-Deck Floor

5.1 Introduction

One of the other key elements of an effective vibration design procedure, in addition to accurate prediction of modal properties, is the accurate response prediction due to walking-induced vibration. Investigations of walking load models have been undertaken on footbridges (Li et al. 2010; Živanović, Pavic & Reynolds 2007b), long-span steel structures (Setareh & Lovelace 2010), long-span steel-concrete composite floors (Nguyen et al. 2011; Pavic et al. 2003; Willford, Young & Field 2006) and beam-and-block floors (Živanović & Pavić 2009). However, there is limited research on the applicability of numerical walking load models on long-span timber floor systems. Furthermore, there is some uncertainty among design engineers on the applicability of current vibration design guides to long-span timber floor systems.

In this chapter, using the validated FE model from Chapter 4, a comprehensive investigation has been conducted into the accuracy of response prediction using three different walking load models. These models include a recently suggested single footfall

force model considering inter- and intra-subject variability of walking (Chen, Ding & Zivanovic 2019), a continuous walking load function as a Fourier series of five harmonics (Živanović, Pavic & Reynolds 2007b) as well as the commonly used effective impulse approach included in many current design guidelines (Murray et al. 2016; Smith, Hicks & Devine 2009; Willford & Young 2006).

The aim of this chapter is therefore to evaluate the accuracy and impact of current existing and two innovative load models in terms of representing the measured floor responses and as a result, to propose the most suitable approach. Although frequency-domain load models have been the focus of recent research (Bassoli et al. 2018; Brownjohn, Racic & Chen 2016; Brownjohn, Pavic & Omenzetter 2004; Chen, Xu & Zhang 2014), only time-domain load models have been considered here as it is the same approach taken in current vibration design guidelines. The chapter introduces the load models to be investigated and then presents the predicted responses using each load model with comparison to experimental results.

5.2 Walking load models

Idealisations of the complexities of walking are important in saving time and resources to solve a design problem only if the mathematical function is able to predict the response with sufficient accuracy i.e. avoiding large overestimations and underestimations. As discussed in Chapter 2, deterministic time-domain load models (Section 2.3.3.1) disregard the variabilities which exist in human walking and assume a certain floor behaviour based on the fundamental frequency of the floor. For low-frequency floors (generally with a fundamental frequency less than 10 Hz), the floor is supposed to undergo a resonant response with the amplitude building up from each consecutive footstep. On the other hand, high-frequency floors (generally with a fundamental frequency greater than 10 Hz) are supposed to undergo a transient response with the response from each footstep decaying to close to zero before the next footstep arrives. However, there have been a number of research advancements which have identified that some of these assumptions may lead to inaccuracies in response prediction. These can be grouped as follows:

1. The appropriateness of a cut-off frequency: studies have shown that a degree of resonant amplification can still be caused by energy at harmonics above the fourth

multiple (Brownjohn & Middleton 2008; Ellis 2000). This means that the effective impulse approach adopted in current guidelines can underestimate floor response for floors with fundamental frequency in the range up to 15 Hz and possibly higher (Brownjohn & Middleton 2008). Furthermore, there have been floors which are classified as 'low-frequency' but have high-frequency modes with low modal masses which can be excited by footstep impulses (Brownjohn, Racic & Chen 2016). Another study has shown that floor classification and subsequent response prediction is particularly unreliable for floors which sit on the borderline of the cut-off frequency (Živanović & Pavić 2009). Possible solutions have been proposed including increasing the cut-off frequency to 14 Hz (A. S. Mohammed, Pavic & Racic 2018), using a response spectrum approach which can predict response for any floor types with a natural frequency of 1 – 20 Hz (Brownjohn, Racic & Chen 2016) and a probabilistic force model combining both approaches from low- and high-frequency floors (Živanović & Pavić 2009). Another option would be to use a single footfall trace model such as that proposed by Chen et al. (2019) and detailed further as Load Model 2.

2. <u>Probabilistic (stochastic) rather than deterministic approach:</u> The deterministic force model approach neglects the inter-subject variability within a population. Through statistical descriptions of walking parameters including subject body weight, pace frequency, stride length, DLFs and phase angle, the vibration response from a large number of people can be generated. Intra-subject variability can also be considered in a similar manner. From this approach, a probability distribution and corresponding cumulative distribution function can be obtained and used to investigate the probability that the response will exceed a certain value. This is in contrast to the pass/fail approach currently adopted in some guidelines. CCIP-016 is the only guide which applies a somewhat probabilistic approach to the DLFs by proposing a 'design' DLF with a 25% chance of exceedance. Other models have been proposed in literature including Živanović et al. (2007b), Racic and Brownjohn (2011) and Chen et al. (2019).

3. <u>Influence of intra-subject variability:</u> from inspection of a continuously measured walking force signal such as that measured by Racic and Brownjohn (2011) (Figure 2-14), it can be seen that although the continuous force is near-periodic, imperfections exist between left and right footfalls as well as between steps made

by the same foot. These imperfections induce intermediate harmonic load amplitudes, also called 'subharmonics', which are created from a 'leaking' of energy into adjacent frequencies from the perfectly periodic signal (Sahnaci & Kasperski 2005). These sub-harmonics are not accounted for in the Fourier series load model for continuous walking (Equation 2.20) which can lead to an overestimation of response particularly when higher harmonics coincide with the floor vibration modes (Brownjohn, Pavic & Omenzetter 2004). Using Brownjohn et al.'s (2004) data, Živanović et al. (2007b) was, to the author's knowledge, the first to analyse the dynamic load factors of the sub-harmonics and develop a time-domain continuous force model which includes these effects. This load model has been included in this investigation and will be detailed as Load Model 3.

Considering the three aforementioned deficiencies of the deterministic walking load models adopted in current guidelines, the vibration response in this study was predicted using two novel probabilistic walking models from literature, as well as the effective impulse response adopted in current guidelines for high-frequency floors. The effective impulse response was taken since the measured fundamental frequency of the long-span ribbed was found to be 10.50 Hz (longitudinal bending). Although on the borderline, this classifies the floor as 'high-frequency' based on cut-off frequencies suggested by current design guidelines (Murray et al. 2016; Smith, Hicks & Devine 2009; Willford & Young 2006). The three load models are as follows:

- Load Model 1 (LM1): Effective impulse response as defined in the Concrete Centre (CCIP-016) (Willford & Young 2006), Steel Construction Institute (SCI P354) (Smith, Hicks & Devine 2009) and American Institute of Steel Construction (AISC DG 11) (Murray et al. 2016) design guides.
- Load Model 2 (LM2): Chen et al.'s (2019) stochastic single footfall trace loading function.
- Load Model 3 (LM3): Živanović et al.'s (2007b) continuous loading function Fourier series considering five harmonics and subharmonics.

5.2.1 Response evaluation procedure

For this investigation, root-mean-square (RMS) amplitudes are presented both for simulated and measured results. Depending on the load model, as will be discussed in the

next three sections, the RMS amplitudes were obtained either by evaluating the maximum RMS amplitude from a running 1 second RMS (1s RMS) averaging window, also referred to as the maximum transient vibration value (MTVV), or over a period of $1/f_p$. The RMS amplitudes were then converted to a response factor by dividing the RMS value by the respective baseline value of human perception (R=1) as defined in ISO 10137 (2007) for RMS acceleration and ISO 2631-2 (1989) for RMS velocity, depending on the load model. The measured response factor is calculated in the same manner as the predicted response factor i.e. if the predicted response factor is calculated using RMS velocity, the measured response factor is also calculated using RMS velocity where the velocity time-history was integrated from the acceleration time-history data. The response factor was used as the main evaluation measure in this investigation as it is commonly used in design practices and recommended in guidelines CCIP-016 and SCI P354. Where appropriate, the cumulative distribution of the floor response has also been calculated based on the MATLAB code in Appendix B. Note the acceleration time-history was frequency-weighted by the W_k weighting as per ISO 2631-1 (1997).

5.2.2 Load Model 1

Load Model 1 (LM1) follows the 'effective impulse' approach developed by Arup (Willford, Young & Field 2006) who found that the response of high-frequency floors is governed by the initial peak amplitude from the impulsive heel-strike component of the footstep, as shown in Figure 2-11; the heel-strike component has been shown to contain energy in the range of frequencies between 10 – 75 Hz (Kerr 1998; Simon et al. 1981).

As detailed in Chapter 2 Section 2.3.3.1, an equation for the design 'effective impulse', I_{eff}, in Ns of each footstep was derived using footstep measurements from Kerr (1998); this equation is reprinted in Equation 5.1 for ease of reference. The peak velocity response for a particular mode using the effective impulse method would predict the same response as if the footfall time history was directly applied (Pavic & Willford 2005).

$$I_{eff} = A \frac{f_p^{1.43}}{f_n^{1.3}}$$
(5.1)

where f_n = natural frequency of mode of interest (Hz) and f_p = pace frequency (Hz).

The effective impulse approach is adopted in the three main design guides for floor vibration including CCIP-016, SCI P354 and AISC DG11, although with slightly different coefficients *A* and procedures to calculate floor response. The CCIP-016 guide recommends a design effective impulse where *A* is a coefficient equal to 54 which was derived for a 25% chance of exceedance. The effective impulse in SCI P354, with coefficient *A* equal to 60*Q*/700 (where *Q* is the walker weight in N), incorporates factors provided in EN 1990 Annex C (British Standards Institution 2002) and results in an 18% larger effective impulse for a 76 kg person than the design I_{eff} listed in CCIP-016.

In AISC DG11, the coefficient *A* in Equation 5.1 is equal to *Q*/17.8 which, for a 76 kg person, would be equivalent to 42. This is the same as the mean effective impulse provided in CCIP-016. Unlike CCIP-016 which recommends calculation of the effective impulse for the fastest anticipated walking pace only (Willford & Young 2006), the effective impulse in AISC DG11 is recommended to be calculated as the 5th – 9th integer division of the dominant mode. The dominant mode is determined by conducting a harmonic analysis of a unit sinusoidal force for a frequency range from 1 Hz below the fundamental frequency to 20 Hz including at all natural frequencies within this range. Further, rather than a velocity response, SCI P354 and AISC DG 11 suggest an acceleration response should be calculated with SCI P354 providing frequency-weighting factors as per W_b weighting provided in BS 6841 (1987). All guides follow the modal superposition method where the response is calculated for each relevant mode and summed using the square-root sum of squares (SRSS) method.

In a design scenario when the walking path is unknown, the effective impulse would be applied at points of maximum amplitude for each mode as this would produce the worst case response. However, in this case, the accelerometer locations (response nodes) and the walking path are known. Therefore, the excitation node was selected at the mid-span node in line with the walking path used in the experiment where the test subject was directed to walk approximately along the centreline between the two web members, as shown in Figure 5-1.
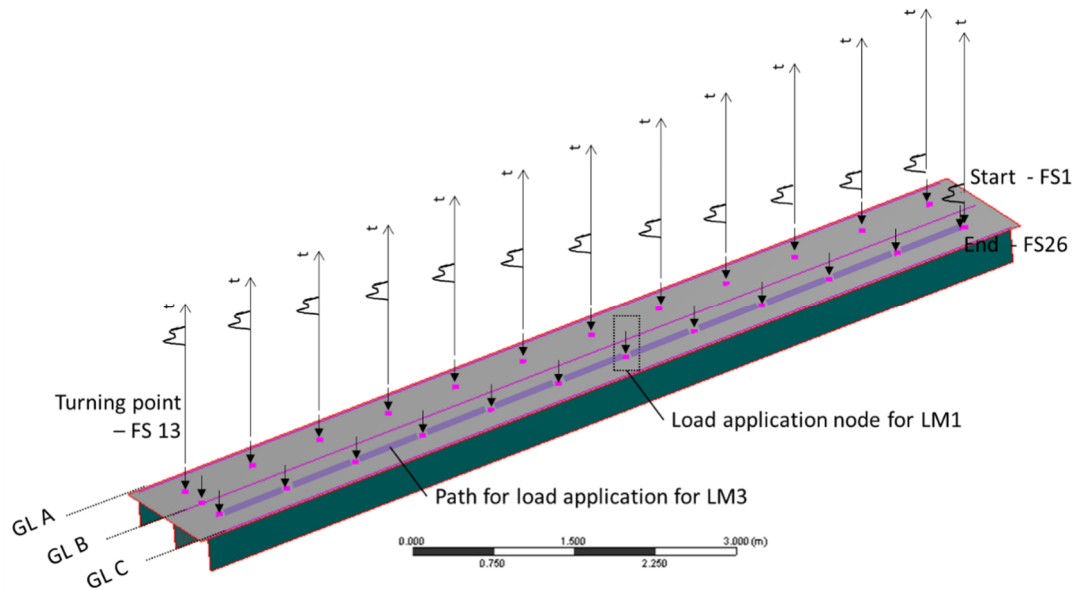
Figure 5-1 *Node locations for each footstep for LM2 (shown temporally for the first 13 footsteps) and the load application node for LM1 and path for LM3*

The method of response prediction using the effective impulse method for CCIP-016 and SCI P354 methods follow the procedures specified in the respective guidelines. The method can be summarised as follows:

1. Calculate the effective impulse for all modes up to 20 Hz (mode 1 and 2) using the respective effective impulse equation and experimentally obtained modal frequencies. The calculated effective impulse using each guide are shown in Table 5-1 for reference. The mass of the walker was 78 kg to represent Walker 2a (referred to as W2a).

2. Extract the mass-normalised mode shape amplitudes from the validated numerical model for each relevant mode at both the load application and response nodes.

3. Calculate the time-history response (acceleration response for SCI P354 and velocity response for CCIP-016) for one footstep following the equations provided in the respective guidelines for each mode.

4. Use the modal superposition method as suggested in the respective guidelines to calculate the total response. The RMS amplitude was calculated over a period of $1/f_p = 1/2.1 = 0.476$ s and divided by the respective baseline (R=1) curve values to obtain the response factor.

The procedure for the AISC DG 11 approach was as follows:

1. Apply a unit sinusoidal force at the load application node for all natural frequencies up to 20 Hz (mode 1 and 2) as well as 30 other frequencies between 9 Hz and 20 Hz.

2. Extract the acceleration FRF magnitudes and determine the dominant frequency at the response location.

3. For each experimentally obtained modal frequency under 20 Hz, calculate the effective impulse using a 2.1 Hz step frequency. Note in a design situation, the step frequency would be determined based on the dominant frequency for that response location however in this case a blanket 2.1 Hz step frequency was taken to compare with experimental results. The calculated effective impulses for each mode are shown in Table 5-1 for reference.

4. The peak acceleration and acceleration time history of each mode was calculated using equations provided in Section 7 of AISC DG 11.

5. Use the modal superposition method as suggested in AISC DG 11 to calculate the total response. The RMS amplitude was calculated over a period of $1/f_p = 1/2.1 = 0.476$ s and divided by the respective baseline (R=1) curve values to obtain the response factor.

Table 5-1 *Calculated effective impulse for each relevant mode*

Guide	I_{eff} (Ns)	
	Mode 1	Mode 2
CCIP-016	7.339	6.740
SCI P354	8.913	8.187
AISC DG11	5.842	5.366

5.2.3 Load Model 2

In one of the most recent studies on human footfall load models, Chen, Ding and Živanović (2019) developed a single footfall trace (SFT) model which considers the randomness of human walking. The load, $F(t)$, for the duration of each footstep (FS), T_f, is expressed as a Fourier series function for a total n harmonics as follows:

$$F(t) = Q \left[A_0 + \sum_{h=1}^{n} A_i \sin \left(\frac{2\pi i}{T_f} t + \phi_i \right) \right] \tag{5.2}$$

where Q = walker weight (N); A_0 = mean value of the weight normalised force; A_i = DLF of an SFT for the i-th harmonic; T_f = duration of a single footfall (s); and ϕ_i = phase angle for the i-th harmonic.

This model differs from the single pedestrian continuous loading function (as per Equation 2.20) as it is a mathematical function for a single footstep and does not include the double support phase. As a result, A_0 is taken as approx. 0.80 rather than 1.0 for continuous loading functions. It is important to note that the DLF for a SFT differs from that of a continuous load function.

The stochastic nature of walking was considered through the inclusion of an inter-subject and intra-subject variability coefficient based on a normal probability distribution using a mean and standard deviation are then applied to the DLF and phase angles. These probability distributions were calculated from the statistical results of kinematics and kinetics tests of 73 volunteers (59 males and 14 females) using a motion capturing system and two force plates. The motion capturing system consisted of 10 infrared cameras which recorded the spatial trajectories of the anatomical landmarks (e.g. legs, foot, pelvis, torso, arm and head) through reflective markers attached to each participant's body. The mean DLFs and phase angles for a given pace frequency have been reproduced in Table 5-2 (Chen, Ding & Zivanovic 2019).

The advantage of LM2 is that a walking load function can be calculated for a large number of pedestrians. However, for this research, only five sets (i.e. representing five walkers) of the intra-subject variability coefficients for the DLFs and phase angles were used i.e. the DLF and phase angles changed between each footstep; these sets will be referred to

as 'SetN' where N is the set number. The inter-subject variability coefficient was not considered as the same walkers were used for all walking tests and the walker weight was known while the intra-subject variability for the walking frequency was set to 1.0 since walking tests were performed with a metronome. To investigate the response when intra-subject variability coefficients for DLF and phase angles are not considered (i.e. the DLF and phase angles are constant between footsteps), another loading set referred to as 'NoIntra' was also analysed.

Table 5-2 *Mean DLFs and phase angles at given walking frequency as per Chen, Ding and Živanović (2019)*

Harmonic	DLF	Phase angle (rad)
1	$0.2080f_p^2 - 0.9373f_p + 1.1998$	$0.1730f_p^2 - 0.4087f_p - 0.2936$
2	$0.1714f_p + 0.0025$	$0.0296f_p - 0.5275$
3	$0.0129f_p + 0.1216$	$0.0815f_p - 0.6305$
4	$0.0188f_p + 0.0235$	$0.0955f_p - 0.5477$
5	0.0364	-0.3563
6	0.0214	-0.4004
7	0.0146	-0.3863
8	0.0114	-0.0851

The procedure for the numerical application and analysis of the SFT load was as follows:

1. Using the procedure described by Chen et al. (2019), the SFT load was calculated for the mass of W2a at a pace frequency of 2.1 Hz.

2. The timing and overlapping of each step was calculated based on the equations provided by Chen et al. (2019).

3. As the step length of the walker was not measured, a reasonable assumption of the step length was decided based on Pachi and Ji's (2005) research. From 800 measurements of men and women walking naturally on footbridges and shopping centre floors, it was found that men generally have a larger step-length than women where a mean value of 0.75 m and 0.67 m was recorded for men and women, respectively. Therefore, a step length of 0.76 m was assumed so as to coincide with the 20 mm mesh size of the model.

4. Each SFT was applied in ANSYS as a time varying nodal force at the approximate location of where each heel strike would occur; this is shown temporally (for the

first 13 footsteps as an example) and spatially in Figure 5-1. The walking loop from experimental tests is mirrored in the numerical model as a closed-loop path starting at footstep 1 (FS1) and ending at FS26; gridline A, B and C are denoted as 'GL A', 'GL B' and 'GL C', respectively. The width of the walking base was neglected, i.e. each footstep was assumed to be in line with the others, and the path was positioned mid-way between the joists, as was instructed to the walker in experimental tests.

5. A transient analysis (using the modal superposition method) was undertaken within the ANSYS software to obtain the velocity time-history at all nodes coinciding with accelerometer locations, as appropriate for evaluation of high-frequency floors (Ohlsson 1991; Pavic et al. 2003). The transient analysis was linked to the modal analysis results which meant that all five modes were considered. However, since modes 3 and 4 have mode shape amplitudes close to 0 at locations A4 and C4, only modes 1, 2 and 5 would have contributed to the floor response.

6. A running 1s RMS averaging window was applied across the total response using a MATLAB code and the MTVV was obtained for response factor (RF) calculation.

The five calculated loading sets considering intra-subject variability as well as the 'NoIntra' case normalised by walker weight is shown in Figure 5-2 for the first two steps as an example; note the variability in the shape of each footstep between sets caused by the intra-subject variability coefficient.
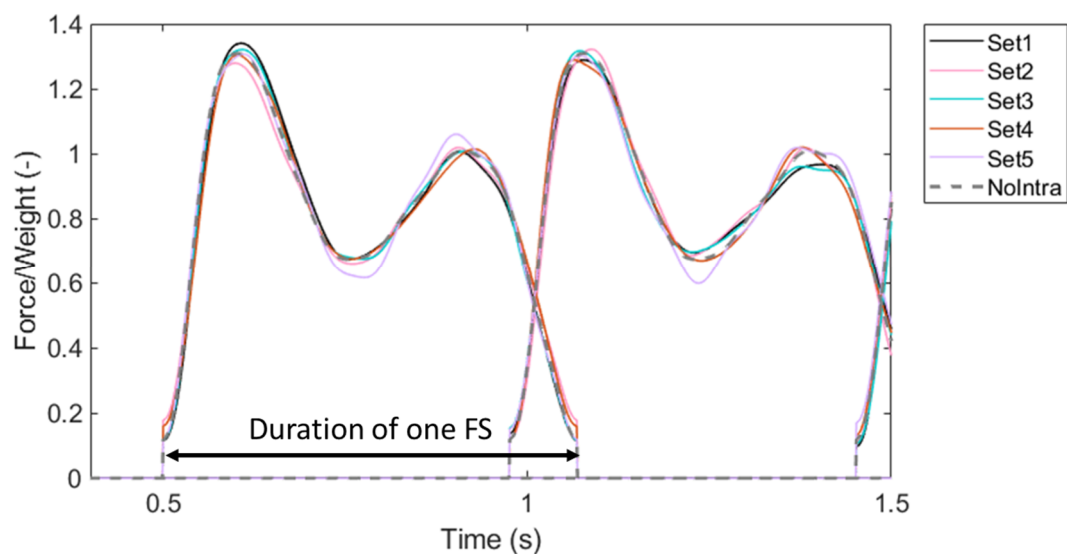
Figure 5-2 *Single footfall traces applied to the FE model as per Chen et al.* (2019)

5.2.4 Load Model 3

The final load model is based on Živanović, Pavić and Reynolds (2007b) research who extended the work of Kerr (1998) and Brownjohn et al. (2004) to develop a time-domain continuous force function which includes the DLFs for the fifth contributing harmonic and five subharmonics. Rather than considering only the frequency content of the force spectrum at the harmonic values (i.e. at integer multiples of the walking frequency), the 'leakage' of energy around each harmonic and subharmonic has been included using a spectrum width of $0.5f_p$. The proposed load model was primarily developed to estimate the response of footbridges, however has the potential to also be used on slender floor structures (Živanović, Pavic & Reynolds 2007b). It has been verified using an imaginary 3 degree-of-freedom (DOF) footbridge simulation model and one as-built footbridge.

For this research, two variations of this load model have been considered: 'basic' and 'advanced'. The 'basic' model uses the mean DLF values for the (sub)harmonics (as reprinted in Table 5-3) and does not consider the energy leakage. The 'advanced' model includes the statistical distributions for the DLFs and frequency content for the full spectrum from $0.25f_p - 5.25f_p$. Both models use Equation 5.3 to generate the walking load where the force is first constructed in the frequency domain and then reconstructed in the time domain. In Equation 5.4, $\bar{f}_j$ is the frequency ratio between the current frequency line and the pace frequency, α_i is the DLF for i-th harmonic, φ_i is the phase angle for the i-th harmonic and $\bar{\alpha}_i(\bar{f}_j)$ and $\theta(\bar{f}_j)$ is the normalised DLF amplitude and phase angle, respectively, for the current line in the spectrum as detailed in (2007b); note superscript s denotes the same parameters for the subharmonic.

$$F(t) = \sum_{i=1}^{5} F_i(t) + \sum_{i=1}^{5} F_i^S(t) \tag{5.3}$$

where:

$$F_i(t) = Q\alpha_i \sum_{\bar{f}_j=i-0.25}^{i+0.25} \bar{\alpha}_i(\bar{f}_j)\cos\left(2\pi\bar{f}_jf_pt + \theta(\bar{f}_j)\right) \tag{5.4}$$

$$F_i^S(t) = Q\alpha_i^S \sum_{\bar{f}_j^S=i-0.75}^{i-0.25} \bar{\alpha}_i^S(\bar{f}_j^S)\cos\left(2\pi\bar{f}_j^Sf_pt + \theta(\bar{f}_j^S)\right) \tag{5.5}$$

Table 5-3 *Dynamic load factors for harmonics and sub-harmonics as per Živanović et al.* (2007b)

(Sub)harmonic	α_i	α_i^S
1	$-0.2649f_p^3 + 1.3206f_p^2 - 1.7597f_p + 0.7613$	$0.026\alpha_1 + 0.0031$
2	0.07	$0.074\alpha_1 + 0.01$
3	0.05	$0.012\alpha_1 + 0.016$
4	0.05	$0.013\alpha_1 + 0.0093$
5	0.03	$0.015\alpha_1 + 0.0072$

One of the main advantages of Živanović et al. (2007b) method is the probabilistic approach where the procedure can be programmed to create the loading of a number of pedestrians or walkers, thus generating a large variation of responses based on the statistical distributions of the DLF and phase angles. The cumulative distribution of the response can then be used to determine the probability that a certain response level will be surpassed. Although Živanović et al. (2007b) suggests the response from 2000 pedestrians, the 'advanced' model will be generated for 100 individuals with identical mass and pace frequency (2.1 Hz). A summary of the features for the 'basic' and 'advanced' model are shown in Table 5-4 while an example of the 'basic' and 'advanced' continuous load function considering a 78 kg subject walking at a 2.1 Hz walking pace is shown in Figure 5-3.

Table 5-4 *Summary of 'basic' and 'advanced' LM3*

	Basic	Advanced
Frequency content;	$0.5\,f_p - 5\,f_p$;	$0.25\,f_p - 5.25\,f_p$;
interval (Hz)	$0.5\,f_p$	$f_p/80$ as per Živanović et al. (2007b)
DLF	Mean values as per Živanović et al. (2007b)	Normal distribution as per parameters provided in Živanović et al. (2007b)
Phase angles	Uniform distribution with interval [-π, +π] as per Živanović et al. (2007b)	Uniform distribution with interval [-π, +π] as per Živanović et al. (2007b)
Step length (m)	0.76 (to match LM2)	0.76 (to match LM2)

The procedure of application of LM3 to the numerical model was as follows:

1. Extract the natural frequencies, modal mass and mode shape amplitudes from the numerical model for mode 1 and 2. Calculate the modal stiffness and damping coefficient.

2. Generate the 'basic' and 'advanced' loading models using the respective equations and parameters noted in Table 5-4.

3. Calculate the modal force for each vibration mode by multiplying the generated time domain force by the mode shape amplitude.

4. The modal force, mass, stiffness and damping is input into the dynamic equation of motion and the modal response (acceleration, velocity and displacement) for each vibration mode is calculated based on the Newmark integration method. This procedure is provided in Živanović (2006) *Multi Harmonic Multi Mode* script.

5. The modal superposition method was used to calculate the total response.

6. A running 1s RMS averaging window was applied to the time-history response and the maximum transient vibration value (MTVV) was obtained for response factor calculation. Note that Živanović et al. (2007b) recommend calculation of the root-mean-square over the total duration that the walker is on the floor. However, the 1 s RMS averaging window was used here to directly compare to experimentally obtained responses and the other two load models.
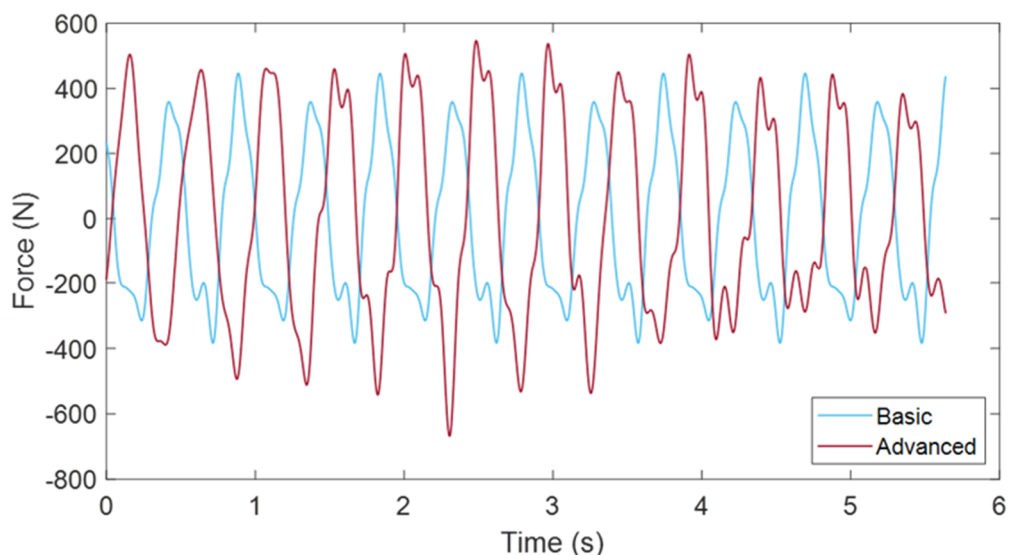
Figure 5-3 *LM3 'basic' and 'advanced' load function for a 78 kg person at a 2.1 Hz walking pace*

5.3 Comparison of simulated and measured results

As noted in Section 3.4.3, walking tests for single cassette tests were conducted using W1 and W2a. To induce floor resonance, both walkers walked at 2.10 Hz pace frequency which is the fifth integer division of the fundamental frequency (found as 10.50 Hz from impact hammer tests). The Fast Fourier Transform (FFT) of the frequency-weighted measured floor response for W1 and W2a at accelerometer locations B4 (LOC1), C3 (LOC2), B3 (LOC3) and C2 (LOC4) are shown in Figure 5-4 below. These response locations were chosen to illustrate the frequency content as each location captures one of the five modes obtained from impact hammer testing. The harmonics and modes have been annotated where visible. Figure 5-4 shows that the response has very little frequency content in the higher modes (modes 3 to 5); only modes 1 and 2 had been excited with mode 1 dominating the response. As a result, node locations along the mid-span coinciding with accelerometer A4, B4 and C4 of the laboratory specimen were selected as the locations of interest.

The results reported below are in relation to these node locations which will be referred to as 'A4', 'B4' and 'C4', as appropriate. Both the maximum response factor (RF) and, where applicable (for LM2), the probability distribution and cumulative distribution of response for the walking event are presented.

(a)

(b)
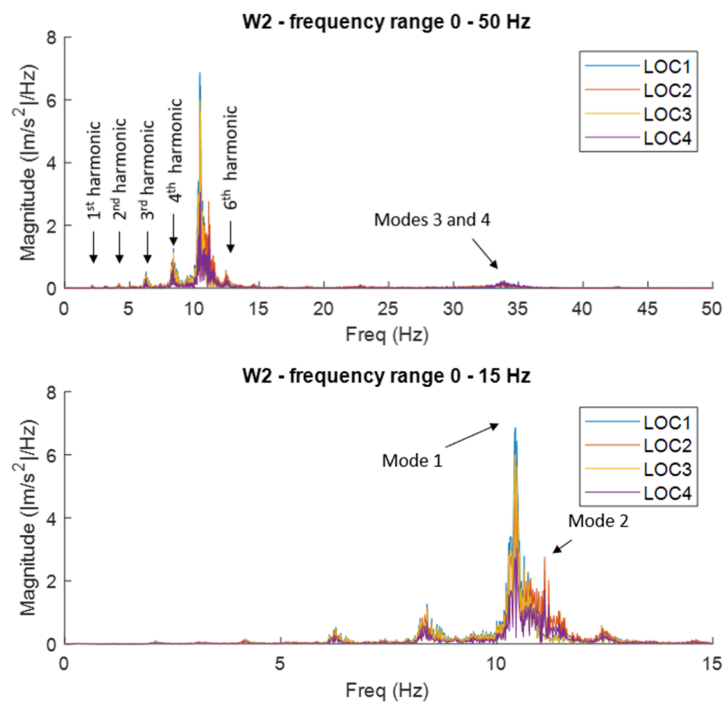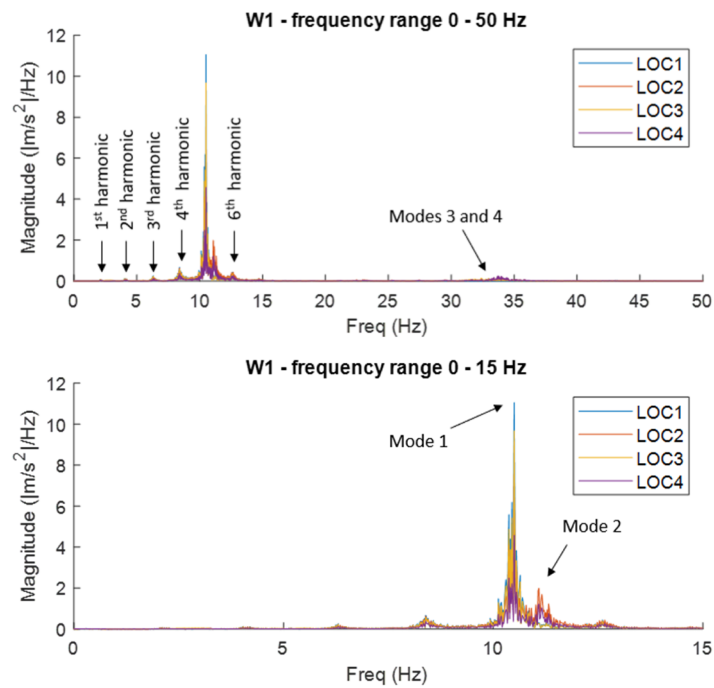
Figure 5-4 *Fast Fourier Transform (FFT) of the Wk frequency-weighted measured acceleration response for frequency range of 0 – 50 Hz and 0 – 15 Hz at locations LOC1, LOC2, LOC3 and LOC4 for (a) W1 and (b) W2a.*

5.3.1 Maximum response

Table 5-5 shows the summary of maximum transient vibration values from the measured acceleration and integrated velocity results for the three response nodes; the coefficient of variance over the three loops has also been noted. The walker location when the maximum response occurred for each walking loop is also noted in Table 5-5 where applicable; this is denoted as either 'adj' for adjacent to the accelerometer or 'opp for opposite side of the accelerometer.

In most cases, the maximum response occurred when the walker was on the opposite side of the cassette. Although this behaviour may be amplified due to the fact that the walking tests were conducted on a single cassette with two sides unsupported, it is still believed to be an important observation which may be more relevant to narrow pedestrian structures including pedestrian bridges or possibly for floors with an unsupported edge. Table 5-6 reveals the predicted response amplitudes at the node corresponding to accelerometer A4, B4 and C4 for the three load models.

Table 5-5 *Summary of measured acceleration and integrated velocity amplitudes for both walkers at pace frequency equivalent to the fifth integer of the fundamental mode (2.1 Hz)*

Walker	Node	a_{MTVV} (m/s^2)	RF	v_{MTVV} (m/s)	RF	CoV	Walker Loc.		
							Loop 1	Loop 2	Loop 3
	A4	1.0625	212	0.0161	161	0.08	Opp.	Adj.	Opp.
W1	B4	0.8302	166	0.0127	127	0.03	-	-	-
	C4	0.7132	143	0.0108	108	0.07	Opp.	Adj.	Adj.
	A4	0.9140	183	0.0139	139	0.11	Opp.	Opp.	Opp.
W2a	B4	0.7616	152	0.0118	118	0.08	-	-	-
	C4	0.7252	145	0.0110	110	0.07	Opp.	Adj.	Opp.

Table 5-6 *Predicted response at location A4, B4 and C4 based on the three load models*

		Accelerometer Location					
		A4		B4		C4	
Method	Response	Amplitude	RF	Amplitude	RF	Amplitude	RF
Load Model 1							
CCIP-016	v_{RMS} $(\times 10^{-3}\,\text{m/s})$	8.90	89	9.26	93	14.77	148
SCI P354	$a_{RMS}\,(\text{m/s}^2)$	0.73	146	0.74	148	1.22	244
AISC DG 11	$a_{RMS}\,(\text{m/s}^2)$	0.48	96	0.49	97	0.80	160
Load Model 2							
NoIntra		16.16	162 (Opp.)	15.33	153	16.59	166 (Opp.)
Set1		15.11	151 (Adj.)	15.13	151	16.17	162 (Opp.)
Set2	v_{MTVV} $(\times 10^{-3}\,\text{m/s})$	18.78	188 (Opp.)	17.13	171	18.60	186 (Opp.)
Set3		19.69	197 (Opp.)	17.86	179	17.33	173 (Adj.)
Set4		18.04	180 (Adj.)	18.43	184	20.72	207 (Opp.)
Set5		16.05	160 (Opp.)	14.90	149	15.59	156 (Opp.)
Load Model 3							
Basic	v_{MTVV} $(\times 10^{-3}\,\text{m/s})$	19.66	197	18.07	181	17.54	175
Advanced – W1	v_{MTVV} $(\times 10^{-3}\,\text{m/s})$	Figure 5-9 (a)		Figure 5-9 (c)		Figure 5-9 (e)	
Advanced – W2a	v_{MTVV} $(\times 10^{-3}\,\text{m/s})$	Figure 5-9 (b)		Figure 5-9 (d)		Figure 5-9 (f)	

5.3.1.1 Response analysis – LM1

The response prediction using LM1 is calculated from the RMS amplitude over a period of $1/f_p$, as shown as t_{RMS} in Figure 5-5. Results from LM1 reveal that there is a large variation in response prediction between the design guidelines. SCI P354 predicted the highest response where the maximum response of 1.22 m/s^2 was 15% greater than the maximum measured response of 1.06 m/s^2. On the other hand, AISC DG 11 predicted a maximum response of 0.80 m/s^2 which was an underestimation of approx. 25%. CCIP-016 provided the closest prediction to the measured response (obtained from the integrated acceleration response) where there was a slight underestimation of 8%.

(a)

(b)
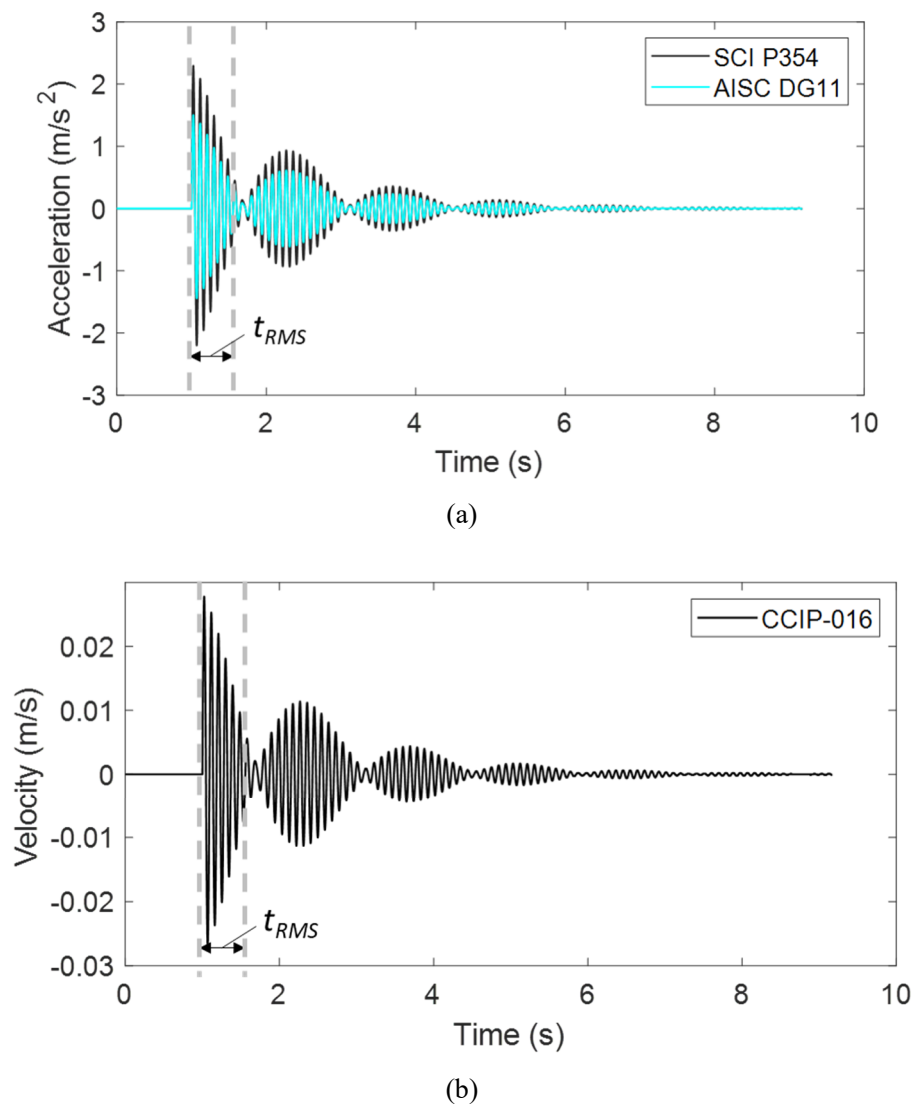
Figure 5-5 *Simulated (a) acceleration and (b) velocity response (sum of both modes) of one footstep at C4 for a 78kg walker at 2.1 Hz walking pace based on three vibration design guides*

5.3.1.2 Response analysis – LM2

Unlike LM1, the step-by-step SFT of LM2 allowed the full time-history of the walking loop to be obtained. A comparison of the simulated velocity time-history at A4 and B4 for the 'NoIntra' case overlaid with the velocity responses integrated from the measured acceleration response from W1 and W2a are shown in Figures 5-6 and 5-7, respectively. Comparing Figures 5-6 and 5-7, it can be seen that while the response from LM2 'NoIntra' accurate represents the floor behaviour measured from both walkers, the RMS-1s amplitudes were closer to that of W1. As shown in Table 5-6, the maximum simulated response based on the 'NoIntra' loading which occurred at C4 had an error of less than 2.9% compared to the measured result.

Results of Sets 1 to 5 indicate that considering the intra-subject variability of the DLF and phase angle of the walker can produce a range of results based on the statistical distributions of the intra-subject variability coefficients. In this case, the five sets predicted a response factor ranging from 151 – 197 for A4, 149 – 184 for B4 and 156 – 207 for C4. It is important to remember that these five sets of loading were based on the same walker mass of 78 kg. If this model was to be expanded further, the same analysis procedure for a larger sample of walkers (statistical distribution of walker mass and pace frequency can also be included) could be conducted. This would mean the probability distribution of the floor responses can be calculated, allowing for a more informed decision on how the floor will respond.
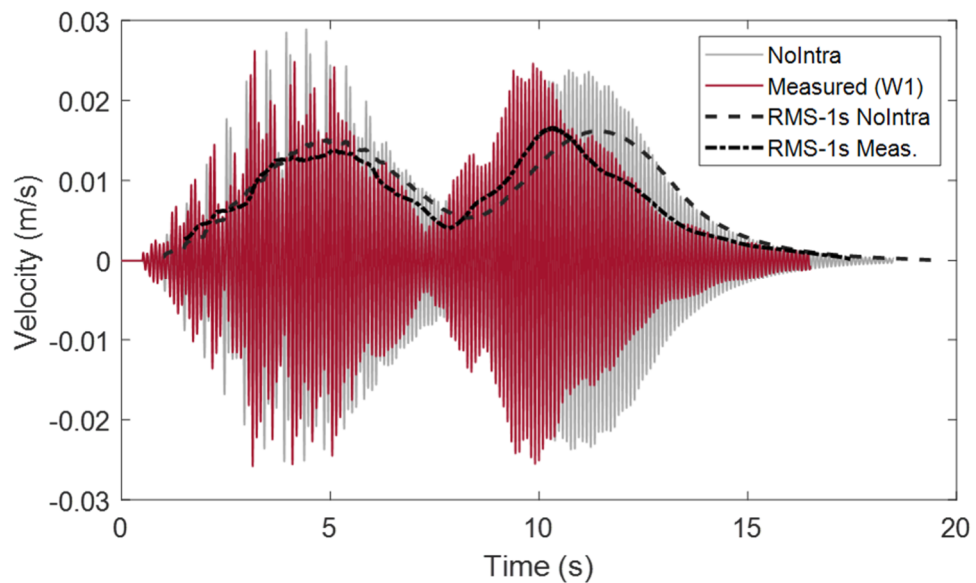
(a) Response at A4
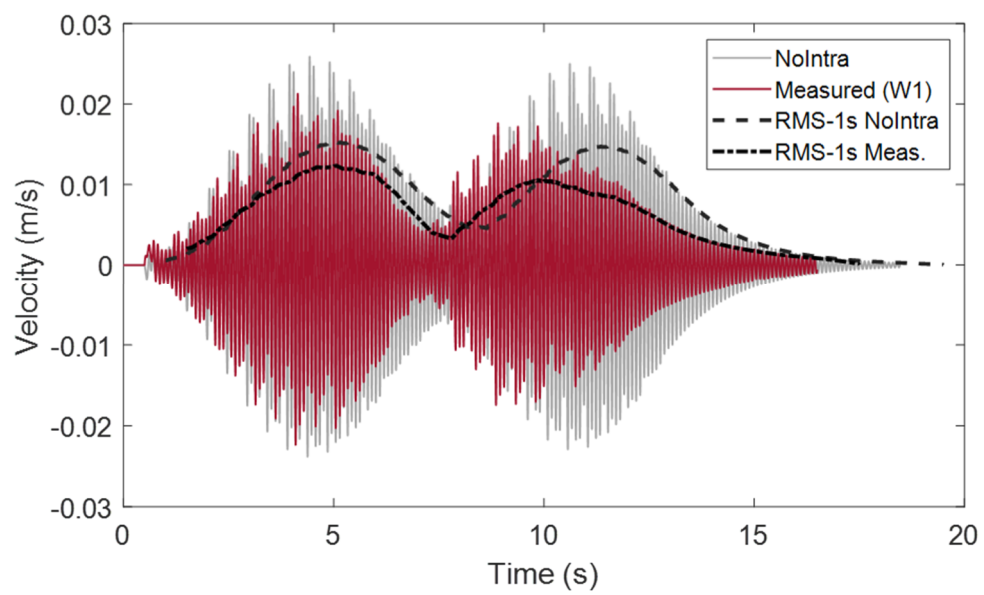
(b) Resonse at B4

Figure 5-6 *Simulated (NoIntra) vs measured time history response for W1 showing similarities in time-history response.*
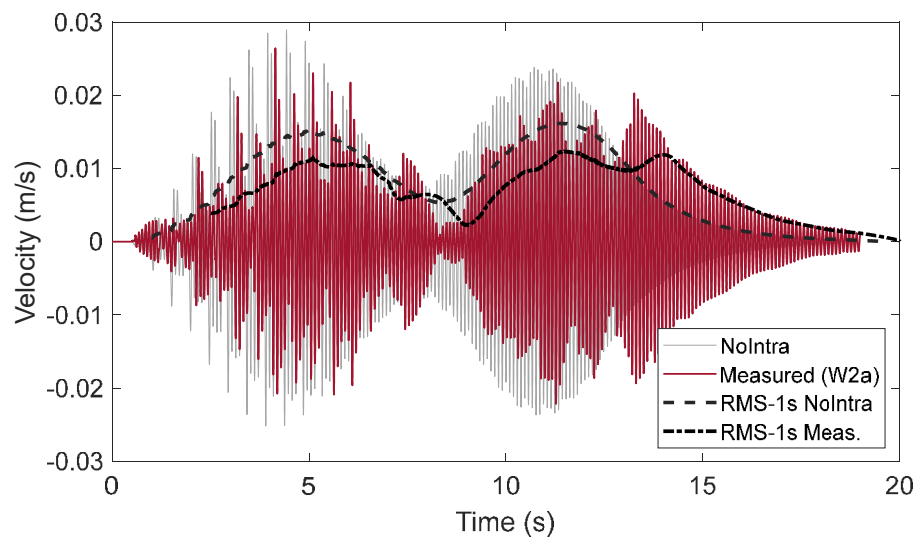
(a) Response at A4
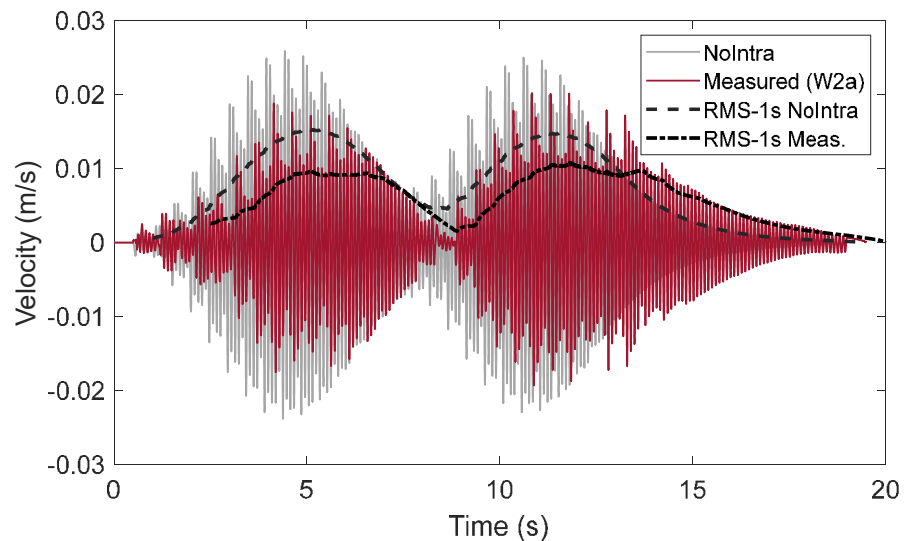
(b) Resonse at B4

Figure 5-7 *Simulated (NoIntra) vs measured time history response for W2a showing similarities in time-history response.*

Table 5-6 also reveals that the simulated response is generally symmetric about the centreline of the cassette whereas there is a large variation (50% for W1 and 26% for W2a) between the measured responses at A4 and C4. Initially, it was believed that the possible asymmetry in measured response between A4 and C4 may be due to the turning manoeuvre which occurs when the walker needs to change direction to complete the walking loop; this action of turning while walking is a complex task and has shown to significantly decrease the walking frequency (Shkuratova et al. 2004). Although an additional FS is included at the turn location (FS 14), the numerical model does not

capture walker deceleration and each footstep loading is applied at the exact same frequency. However, when investigating the walker location which caused the maximum response for accelerometers along GL A, as noted in Table 5-5, for the majority of cases these occurred when the walker was on the opposite side (i.e. walking along gridline C). This meant the walker was able to continue along the second half of the path at the assigned walking pace.

The hypothesis then changed to the experimental mode shape amplitudes which in Chapter 4, were found to be asymmetrical due to the higher stiffness of the web member along GL C (from here on referred to as Web C). As noted in Chapter 4, for simplicity, the validated model assumed all joists had the same material properties and thus the asymmetrical mode shapes were not captured. Therefore, to check the hypothesis, the modulus of elasticity (MoE) in the parallel to grain direction for Web C was increased by 10% of the measured MoE from material testing (new MoE = 14029 MPa) and 'NoIntra' loading was re-analysed (this case is referred to as 'NoIntra_C'). This change is a 5% difference to the MoE of the joist along GL A (referred to as Web A) found through the model updating procedure (13369 MPa). As shown in Table 5-7, the difference between response at A4 and C4 is now approx. 10% compared to 3% for the 'NoIntra' case which suggests that the variability in parallel to grain MoE between joists may be the cause of the observed asymmetry of the floor response. Further, comparison to original 'NoIntra' results reveal that a 5% variability of MoE between joists has caused an increase of response by 13% for B4 and 17% for A4. Such results indicate the significance of having accurate parallel to grain MoE for the web members in the prediction of floor response in long-span ribbed-deck floor systems.

Table 5-7 Simulated response for 'NoIntra_C' with MoE parallel to grain increased by 5% for Web C

Node		NoIntra_C	% diff. to NoIntra
A4	RF	186	15%
	Location	Adj.	
B4	RF	173	13%
	Location	-	
C4	RF	167	1%
	Location	Opp.	

5.3.1.3 Response analysis – LM3

For LM3, the excitation nodes were selected as one half of the closed loop which meant that the simulated time history response could only be compared to the measured response of the walker traversing along GL C. A comparison of the measured and simulated response using the 'basic' load model is shown in Figure 5-8. These figures, together with the maximum response shown in Table 5-6 reveal that LM3 'basic' lies on the conservative side where the maximum predicted response (RF = 197) is approx. 23% greater than the maximum measured response. Similarly to LM2, the resonant response on the opposite side of the location of the walker is effectively captured.

For the 'advanced' model, two cases were considered: a walker mass equivalent to W1 (51 kg) and W2a (78 kg). The cumulative probability of MTVV velocity of W1 at response nodes A4, B4 and C4 is shown in Figure 5-9 (a), (c) and (e) while Figure 5-9 (b), (d) and (f) show the probability for W2a at A4, B4 and C4, respectively. A line indicating the measured results for the respective walker is also shown to indicate where the response sits in terms of a sample of 100 pedestrians with the same mass. These plots provide the engineer with an insight as to the likelihood of a certain response occurring (similar to if LM2 were to be extended for a larger sample) which is an important consideration when vibration design is critical. Further, although not included in this research, the step frequencies for each pedestrian can also be varied based on a statistical distribution (Živanović et al. (2007b) suggests a mean of 1.87 Hz and standard deviation of 0.186 Hz).

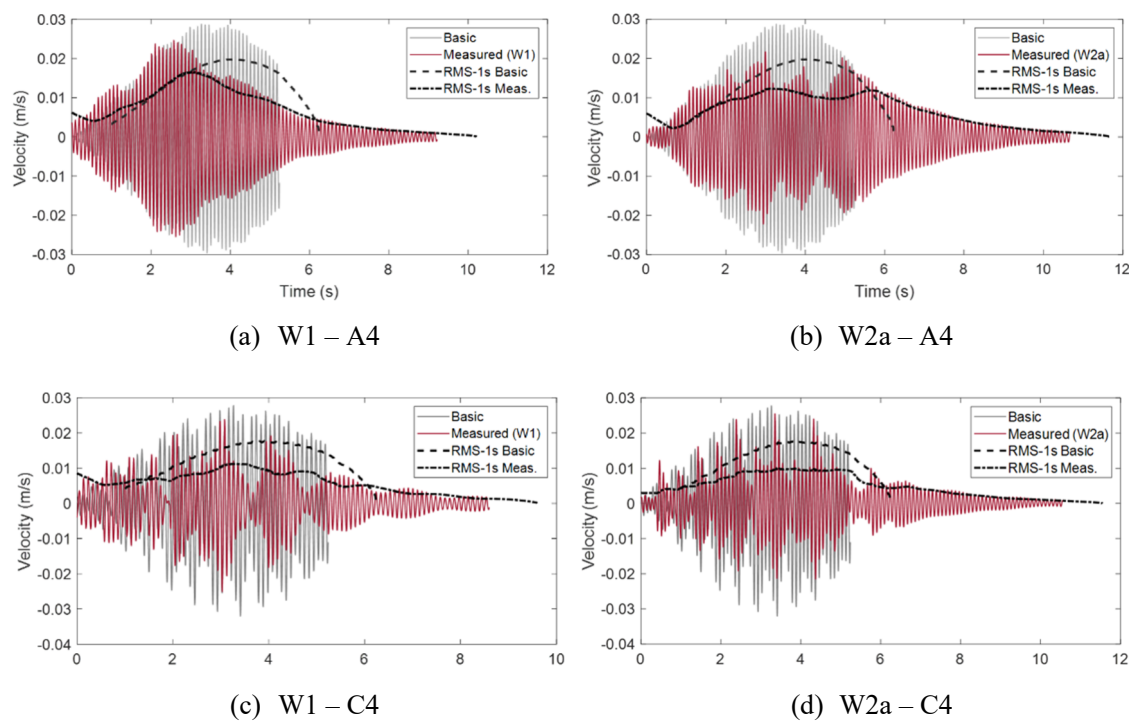(a) W1 – A4

(b) W2a – A4

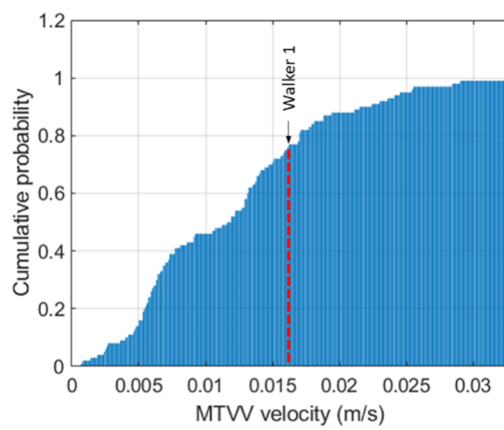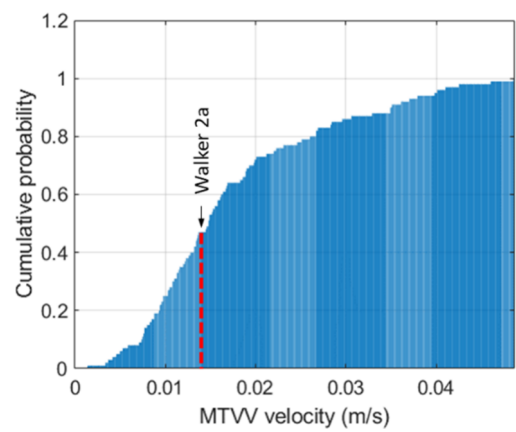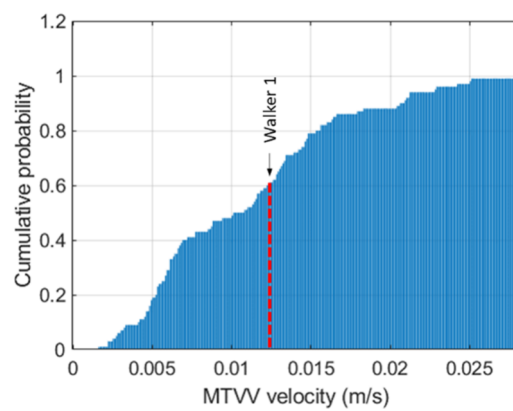(c) W1 – C4

(d) W2a – C4

Figure 5-8 *Simulated vs measured time-history response using LM3 Basic*

(a) W1 – A4

(b) W2a – A4

(c) W1 – B4
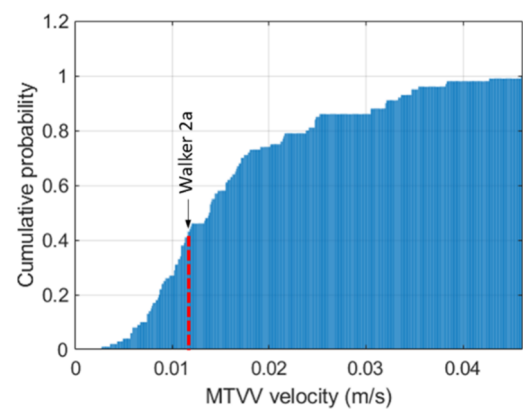
(d) W2a – B4
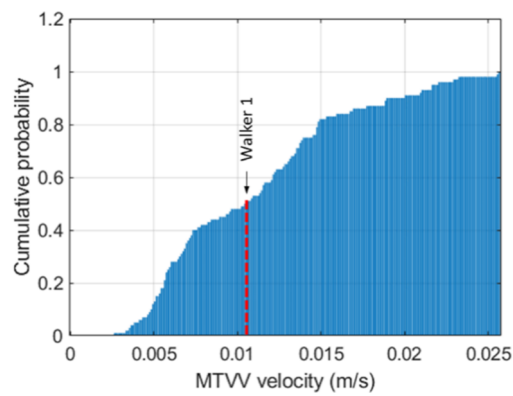
(e) W1 – C4
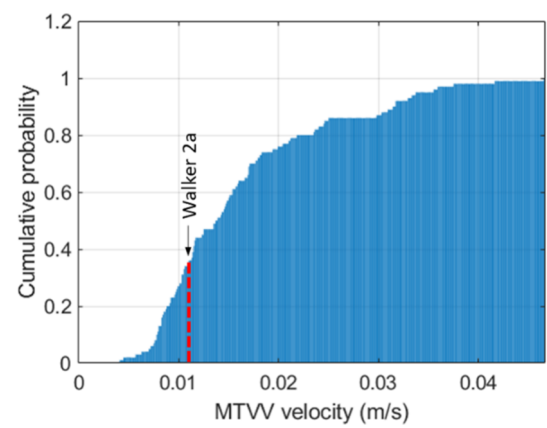
(f) W2a – C4

Figure 5-9 *Cumulative distribution plots of MTVV velocity based on LM3 'Advanced'*

5.3.2 Distribution of floor response

In Section 5.3.1, the maximum amplitude of the floor response was obtained for comparison to the measured results; this is a common approach adopted in current design guides. However, basing the vibration design of a floor on the maximum response disregards the fact that that the maximum response may only occur for a very short period of time. This is illustrated in Figures 5-6 and 5-7 where the maximum response is usually at a peak of the running 1s RMS averaging window.

Investigation into the distribution of the floor response over the complete walking event provides further insight into the percentage of time that the vibration amplitudes stay above or below a certain level; the significance of which needs to be understood in the context of the functional requirements of the floor. A comparison of the measured and simulated distribution of the floor response for the total walking event using LM2 is shown Figure 5-10; the cumulative distribution plots have been calculated only for the time that the walker was on the floor. LM2 was used here since this is the only load model which gives the time history response for the total walking loop. As shown in Figure 5-10, the cumulative distribution of all simulated loading sets are fairly similar for all response nodes. Cumulative distributions calculated from measured results also show similarities to simulated results, particularly for A4. The significance of using these plots during design is that they reveal the duration of certain amplitudes occurring during the walking event. For example, for W1 at A4, the RF will be less than approximately 130 for 80% of the walking event or, in other words, for approx. 10.7 s.
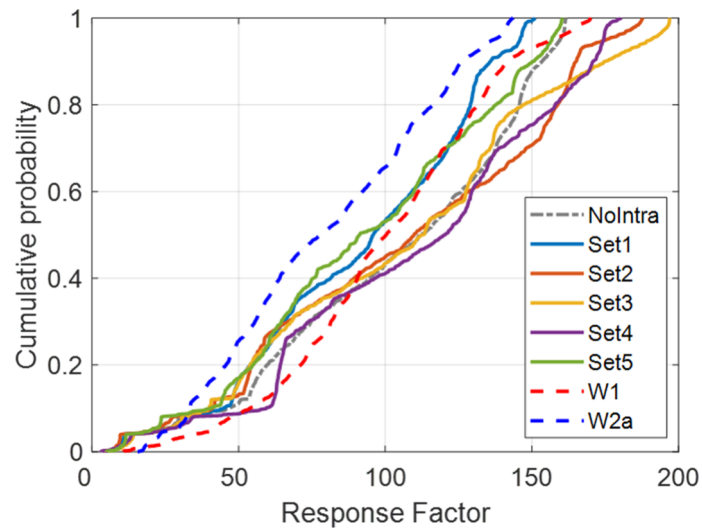
(a) Cumulative distribution – A4
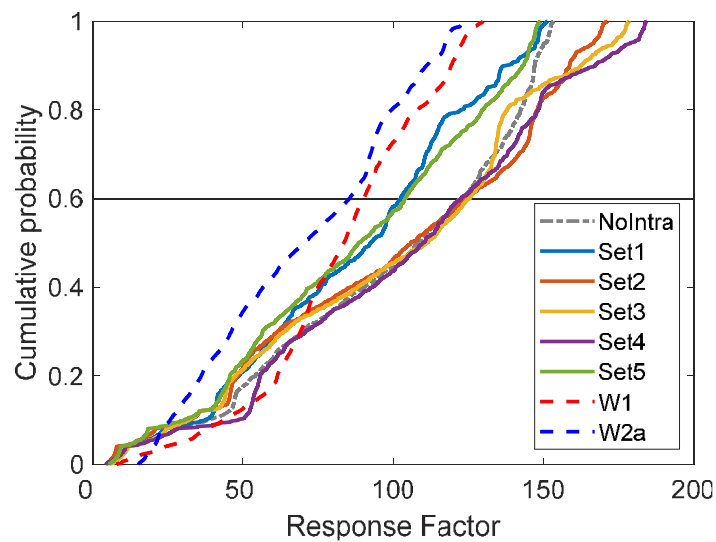
(b) Cumulative distribution – B4
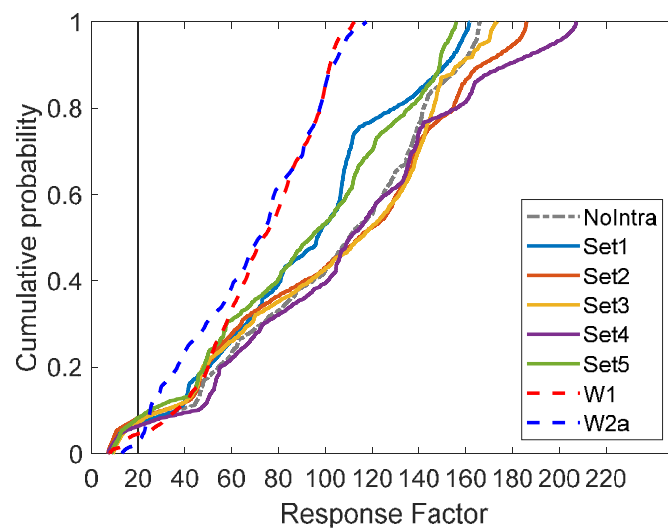
(c) Cumulative distribution – C4

Figure 5-10 *Probability and cumulative distribution plots comparing LM2 and measured results*

5.4 Discussion

It is clear from these investigations that selecting an appropriate load model is crucial in the design process for long-span timber floors. Firstly, the results of LM1 show that the adequacy and appropriateness of following commonly used floor vibration design guides to predict the response of the timber cassette floor remains questionable. Despite the tested floor being classified as a 'high-frequency' floor by all guides, it is apparent from the measured time-history from W1 and W2a shown in Figure 5-6 and Figure 5-7, respectively, that the floor response when the walker is adjacent to the accelerometer cannot be explicitly classified as either completely "resonant" or completely "transient"; there is certainly evidence of resonant response build-up between each footstep. This may explain why the predicted response was underestimated using the AISC DG 11 and CCIP-016 effective impulse approach (which assumes a transient floor response) and over-estimated using the LM3 'basic' model (which assumes a resonant floor response with the fifth harmonic of the walking pace). Considering the pass-fail approach suggested in current vibration guidelines, such inaccuracies (or misconception) could result in the floor being deemed unacceptable for design. This highlights the advantage of a step-by-step load model such as LM2 or the probabilistic approach of LM3 'advanced' which avoids an initial assumption on floor behaviour.

In addition, using a load model which provides a complete time-history of the floor response allows a design engineer to consider the duration that the floor response may surpass a certain limit. The duration may be obtained through calculation of the cumulative distribution of the response for a particular walking event, as detailed in Section 5.3.2. Consequently, a more realistic comprehension of the liveliness of the floor can be obtained and used to assist in performance assessment. For example, a response which surpasses the recommended limit only for a very short period may be deemed acceptable. A similar recommendation was also made by Živanović et al. (2009) who studied four identical classroom floors constructed from a beam-and-block system; the fundamental frequency of these floors ranged from 8.2 to 8.7 Hz. The duration of floor responses have already been considered in Japan's most recent vibration design standard AIJES-V001-2018 (Architectural Institute of Japan 2018) which adopts a reduction factor if the duration of vibration is less than 10s.

The probabilistic approach explored through LM3 'advanced' is also another appropriate option for evaluation of long-span timber floors. Rather than evaluating floor performance on a single maximum value from an 'average' walker, the probabilistic approach allows an assessment of the probability of a certain response occurring for a specific walking event considering a larger sample of walkers. The importance of considering inter-subject variability within the load model is shown through the measured responses where W1 consistently produced a higher response despite being 27 kg lighter than W2a. This is likely due to W1 being a more effective walker, an assumption supported by Figure 5-9 (a) which shows that W1 was in the top 25% of the population of 100 people. The effectiveness of W1 may also explain why the CCIP-016 method (which is designed to have a 25% chance of exceedance) slightly underestimates the maximum response by 8%. This slight underestimation is also supported by research undertaken by Mohammed et al. (2018) who found that the CCIP-016 effective impulse load model slightly underestimated the vibration response for higher pacing rates (2.2 and 2.4 Hz).

However, for a probabilistic approach to be implemented into a design guide, acceptable probabilities of perception need to be agreed upon and appropriately qualified. These may be presented as a range of probabilities based on the required performance level and floor occupancy, similar to the approach of HIVOSS (Feldmann et al. 2008) (another floor vibration design guide from Europe for steel-framed floors) where RF ranges are provided for six floor classes. For example, a premium quality office building may demand that only 10 – 20% of occupants can perceive the vibration while for a more standard office building, 40 – 50% probability of perception may be more appropriate. This information could be presented as an informative part of a design guide or code which users can refer to if the floor design is not satisfied using the maximum amplitude approach.

Despite the accuracy of LM2, a drawback of the step-by-step load model is its time-consuming nature of applying each footstep individually in an FE model and then conducting a transient analysis to obtain the full time-history response. This can be avoided by superimposing multiple SFT to generate a continuous footstep loading function with a duration equivalent to the time taken for the walker to cross the floor, as suggested in Chen et al. (2019). Using this continuous loading function, a similar

approach to Živanović et al. (2007b) procedure can be followed where extracted mode shape amplitudes can be used to determine the floor response.

Finally, it is worthwhile addressing the limitations of the experimental study in regards to the limited sample size. Although a larger sample size of measured results would have produced a more definitive result on the appropriateness of each load model, this was unfortunately not within the scope of this research. In saying this, small data sets have been used by two notable studies on the applicability of walking load models on a long-span steel-concrete composite floor (Pavic et al. 2003) and beam-and-block floors (Živanović & Pavić 2009). In Pavić et al. (2003) experimental work, two pedestrians (one male and one female) were used to obtain floor response for comparison to numerical results obtained from three different load models. Similarly, walking tests conducted by Živanović & Pavić (2009) included only two test subjects, although this limitation was acknowledged. Živanović & Pavić (2009) were able to expand their data set by including the measured walking forces from experiments conducted by Brownjohn et al. (2004). These measured force time histories were generated by 10 test subjects on an instrumented treadmill. In lieu of physical test results from a large number of pedestrians, a similar approach to that by Živanović & Pavić (2009) would be beneficial in expanding this research. Nevertheless, the measured responses from the two walkers (W1 and W2a) can still be used as a basis in assessing the suitability of the different load models in a qualitative, if not quantitative sense.

5.5 Concluding remarks

Using the validated FE model of Chapter 4, this chapter investigated three load models in terms of their vibration response prediction to walking excitation on a long-span timber ribbed-deck floor. The three walking models were: the effective impulse method suggested in current vibration design guidelines (LM1), a single footfall trace model proposed by Chen et al. (2019) (LM2), and Živanović, Pavić and Reynolds' (2007b) multi-harmonic probabilistic continuous force model (LM3). Response predictions were compared to the results from walking tests on a single cassette with flange bearing boundary conditions. From the results of the investigation, the following conclusions are drawn:

- The choice of walking load model greatly influences the predicted response of a long-span timber cassette floor.

- The measured floor response revealed neither a completely transient nor resonant response which may explain why LM3 over-estimated the maximum response while the effective impulse approach of AISC DG11 and CCIP-016 under-estimated the maximum response.

- The Chen et al. (2019) single footfall trace model most accurately predicted the maximum measured response, the cumulative distribution of response and mirrored the behaviour of experimental walking tests where the floor exhibited both transient and resonant behaviours depending on the location of the walker; the maximum response generally occurred when the walker was on the opposite side of the accelerometer rather than adjacent.

- With regard to the most widely used current vibration design guides, the CCIP-016 effective impulse approach provided the closest match to the measured response, although with a slight under-prediction of 8%. The accuracy of this model should be confirmed using the measured response from other test configurations.

- The inclusion of inter- and intra-subject variability in Chen et al. (2019) (LM2) and Živanović et al. (2007b) load model (LM3) allows for a large number of responses to be generated efficiently. This means that the design engineer can follow a probabilistic approach to floor vibration assessment which may have more merit for the design of long-span timber floors where vibration design is critical.

Further testing on a larger sample of long-span timber floors, preferably in-situ, is recommended to validate the findings from this investigation.

Chapter 6

Factors Affecting Dynamic Behaviour of Long-Span Timber Ribbed-Deck Floors

6.1 Introduction

When incorporating a single cassette into a building, design variables such as connections to adjacent cassettes and an inclusion of an acoustic interlayer (elastomer) with damping properties will influence the floors modal properties and response to walking. The limited number of long-span cassette floors in practice means that the effect of these design variables are not readily understood and thus it was of interest to investigate these within a laboratory setting so as to isolate the design variable of interest.

This chapter builds upon the previous chapters by first presenting the experimental results (both modal properties and floor response to walking) for the final boundary condition of the single cassette set-up and the double cassette floor tests. These tests will be referred to by their test names as detailed in Chapter 3 which have been reprinted in Tables 6-1 and 6-2 for the single and double cassette tests, respectively, for ease of reference. The second part of this chapter uses the modal properties obtained from the double cassette tests to develop and calibrate an FE model using ANSYS software. The objective of

developing this model is for use in a parametric study which will be detailed in Chapter 7.

Table 6-1 *Summary of single cassette tests referenced in this chapter*

Test name	Support condition		Elastomer	Added load over support (N)
	Element	*Support Type*		
C1_Flange	Flange	Bearing	-	-
C1_Sdyn0	Flange	Bearing	Sylodyn	-
C1_Smer0	Flange	Bearing	Sylomer	-
C1_Sdyn1000	Flange	Bearing	Sylodyn	1000
C1_Smer1000	Flange	Bearing	Sylodyn	1000
C1_Sdyn2000	Flange	Bearing	Sylodyn	2000
C1_Smer2000	Flange	Bearing	Sylomer	2000

Table 6-2 *Summary of double cassette tests referenced in this chapter*

Test name	Web connection		Flange connection	
	Type	*Screw spacing (mm)*	*Type*	*Screw spacing (mm)*
C2_Web300	Web	300	-	-
C2_Web150	Web	150	-	-
C2_Spl300	Web	150	Splice	300
C2_Spl150	Web	150	Splice	150
C2_Diag300	Web	150	Diagonal	300
C2_Diag150	Web	150	Diagonal	150

6.2 Influence of elastomer at support

As detailed in Chapter 3 Section 3.3.1, the final simple support condition that was tested involved placing an elastomer between the underside of the overhanging flange and the rigid timber support. The investigated elastomers were Sylodyn® and Sylomer® which are commonly used as acoustic interlayers for timber frame buildings in Europe. These results have been compared with the C1_Flange case.

6.2.1 Modal properties

Figure 6-1 and 6-2 show the plots of the sum of FRF's for all accelerometers for each impact location for the flange bearing onto the Sylodyn® and Sylomer® layer, respectively. The peaks corresponding to the mode shapes are annotated. The ratio of utilisation of the Sylodyn and Sylomer were 66% and 90%, respectively, and both were in the static range of use. The natural frequencies, damping ratios and mode shapes obtained from experimental modal analysis using LMS Test.Lab are shown in Table 6-3. Frequency estimation over the different impact locations resulted in a coefficient of variation (CoV) of less than 0.3% while for damping estimation the CoV was less than 7.5%.

Comparison to the sum FRF's of the C1_Flange tests, shown as grey plots in Figures 6-1 and 6-2 for ease of comparison, reveals an increased number of peaks under 50 Hz from five to eight. Modes 3 and 4 have shifted down by approximately 10 Hz while additional modes have appeared around the 35 – 45 Hz range introducing further clustering of modes. There is also a distinct difference in the shape of the FRF between the C1_Sdyn0 and C1_Smer0 tests which highlights the variabilities between the Sylodyn and Sylomer material. The material make-up of Sylomer is a combination of a spring and damper while Sylodyn is highly elastic with stronger spring and smaller damping properties. The higher damping characteristics of the Sylomer is evident in Figure 6-2 which shows significantly smaller amplitudes (approx. seven times less than C1_Flange for mode 1), wider peaks (indicating larger damping) and even causing some modes to be less pronounced, namely modes 3, 5 and 6. As shown in Table 6-3, these modes correspond to the second torsion, third torsion and third bending mode where movements or 'flapping' at the supports was particularly high.

Interestingly, the addition of elastomer decreased the frequency of the first and second modes by approximately 2 Hz and 1 Hz for Sylodyn and Sylomer, respectively. Although not a significant reduction, the first two modes are now within the 8 – 10 Hz range which will make the floor likely to be excited by the fourth harmonic of walking rather than the fifth as per the C1_Flange tests. However, the beneficial aspect of the elastomer inclusion is the increase in damping for all modes, particularly with the Sylomer. For ease of comparison, a plot of the damping ratios for the C1_Flange, C1_Sdyn0 and C1_Smer0 test cases is shown in Figure 6-3; this graph reveals that the addition of the Sylomer interlayer increases the damping ratio for modes 1 and 2 by over six- and nine-fold, respectively. Further, damping ratios for the bending modes at mode 4 and 6 for both Sylomer and Sylodyn cases are distinctly higher than other modes which may be a result of the larger movement at the supports and can be observed in the mode shapes shown in Table 6-3. A sharp drop in damping ratio is observed for both elastomers for mode 7, corresponding to the first lateral bending mode, with little difference to the C1_Flange test; similar findings were also reported in findings by Jarnerö et al. (2012). Whether the benefit of increased damping ratio outweighs the addition of modes and lowering of the fundamental frequency will be investigated through walking test data.

Figure 6-1 *Plot of sum of FRFs for all impact location points for flange bearing onto Sylodyn support condition. Grey FRF plots refer to single cassette C1_Flange tests from same impact locations.*
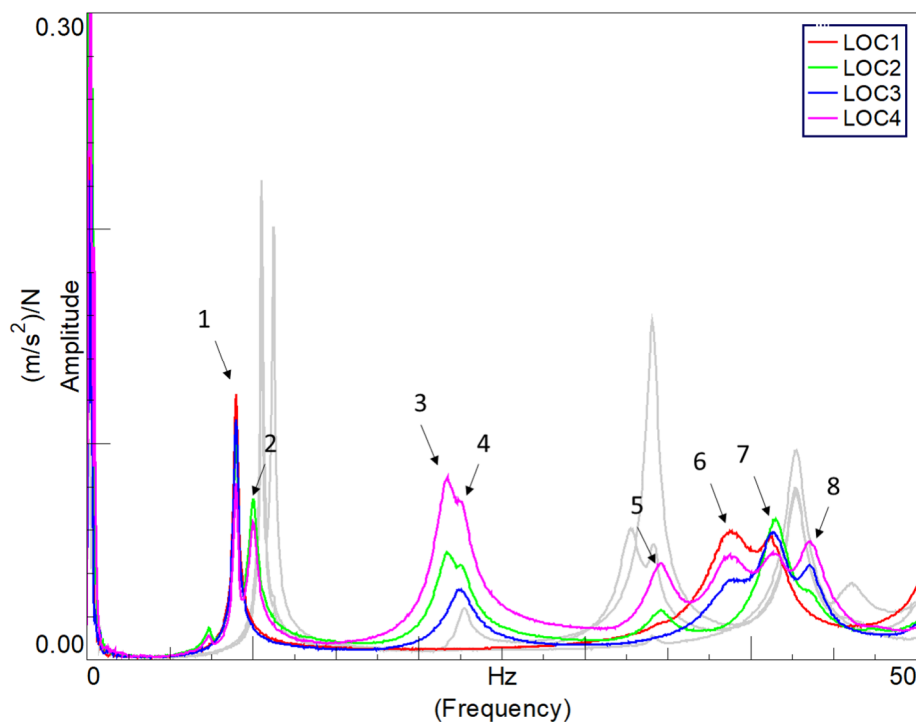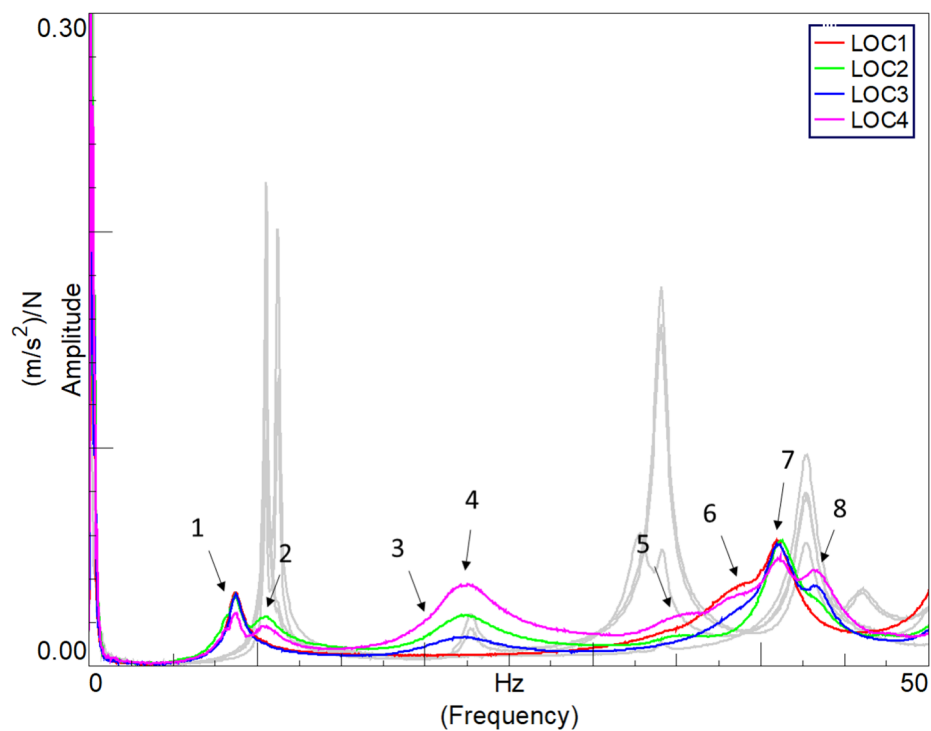
Figure 6-2 *Plot of sum of FRFs for all impact location points for flange bearing onto Sylomer support condition. Grey FRF plots refer to single cassette C1_Flange tests from same impact locations.*
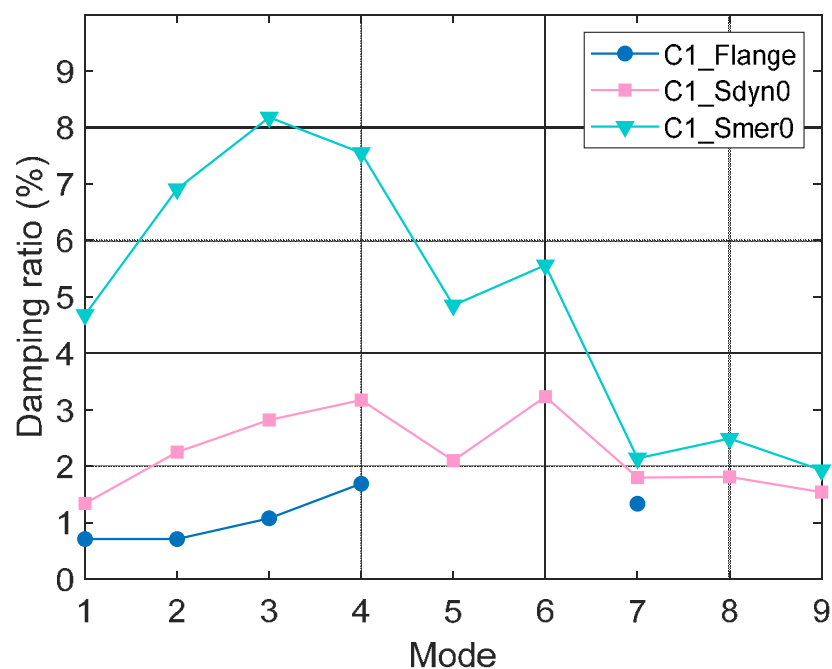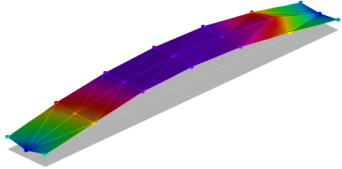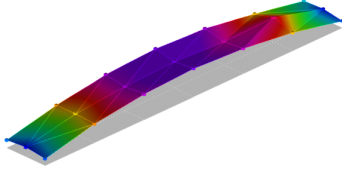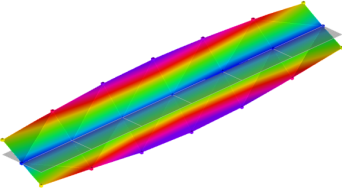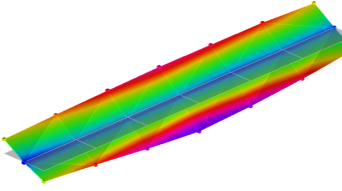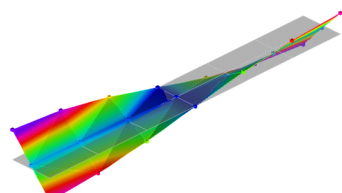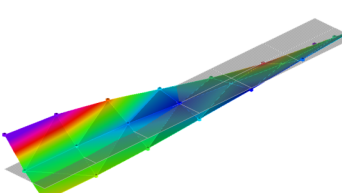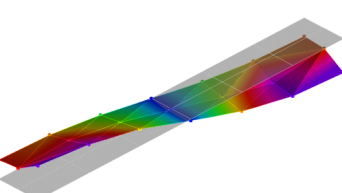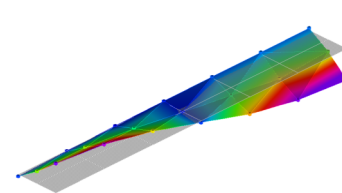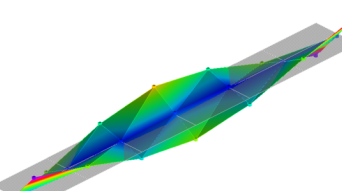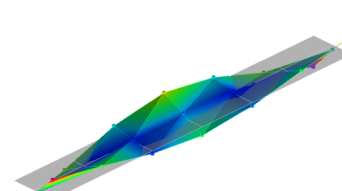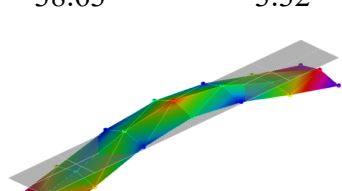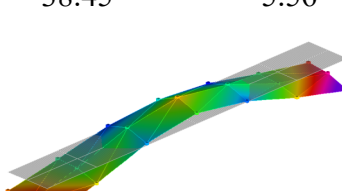
Figure 6-3 *Comparison of damping ratios between C1_Flange, C1_Sdyn0 and C1_Smer0 tests*

Table 6-3 *Modal properties of flange supported boundary condition with addition of elastomer*

Mode	C1_Sdyn0		C1_Smer0	
	f (Hz)	*ξ (%)*	*f (Hz)*	*ξ (%)*
1	8.94	1.34	8.68	4.68
2	9.98	2.25	10.30	6.91
3	21.56	2.82	20.50	8.18
4	22.42	3.17	22.29	7.55
5	34.50	2.10	34.72	4.85
6	38.63	3.32	38.45	5.56
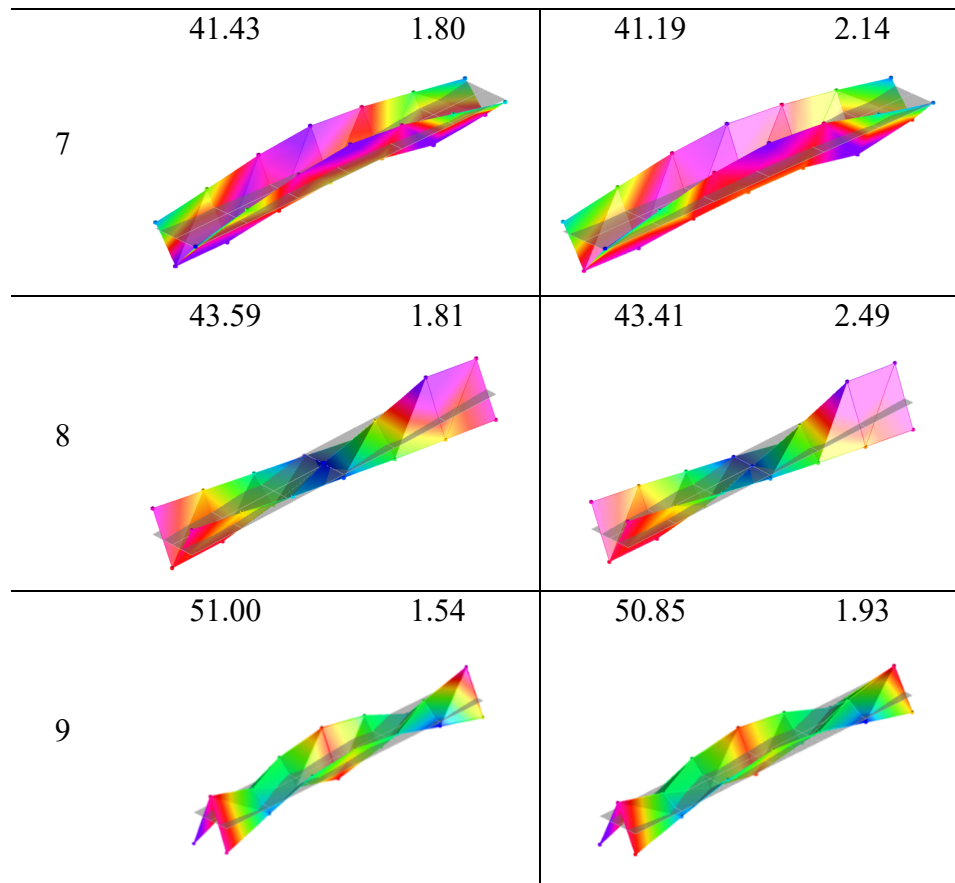
6.2.2 Floor response to walking

6.2.2.1 Maximum response

The maximum frequency-weighted response for each accelerometer averaged over the three walking loops for the C1_Sdyn0 and C1_Smer0 tests are shown graphically as response factor (RF) contours in Figures 6-4 and 6-5 for W1 and W2a, respectively. The contours have been created using Kearney's (2018) MATLAB function which allows consistent colour scales. For ease of comparison, a colour scale matching the maximum response of the walking pace over both C1_Sdyn0 and C1_Smer0 tests has been used.

As shown in Figures 6-4 and 6-5, the maximum response occurs at accelerometer A4 or C4 (grid lines noted in image). However, in a typical building floor scenario, there would be multiple connected adjacent cassettes, and thus the response at accelerometer B4 was of interest. Figure 6-6(a), (b) and (c) shows the response at B4 for elastomer tests for a walking pace of 1.5 Hz, 2.0 Hz and fifth integer of the first bending mode (referred to as

'R' Hz), respectively; the reference case of C1_Flange is also shown for ease of comparison. It is clear that in almost every case the inclusion of an elastic interlayer significantly reduces the response of the floor, particularly for the Sylomer interlayer. For walking frequencies of 1.5 (Figure 6-6(a)) and 2.0 Hz (Figure 6-6(b)), the reduction of response from C1_Flange test condition ranges from 14% to 44% for C1_Sdyn0 tests and a significant 34% to 52% for C1_Smer0 tests. However, the most substantial difference in response occurred for C1_Smer0 tests when the walker was walking at a pace equivalent to the fifth integer division of the first bending mode (Figure 6-6(c)) where the RF reduced from 166 to 36 for W1 (78% reduction) and 152 to 69 for W2a (61% reduction). Interestingly, the only test where the inclusion of the elastic interlayer resulted in a higher response at accelerometer B4 was for W2a at 1.5 Hz pace frequency, although there is no clear reasoning behind this. Further tests with a larger sample of walkers at varying pace frequencies would help to clear these discrepancies.
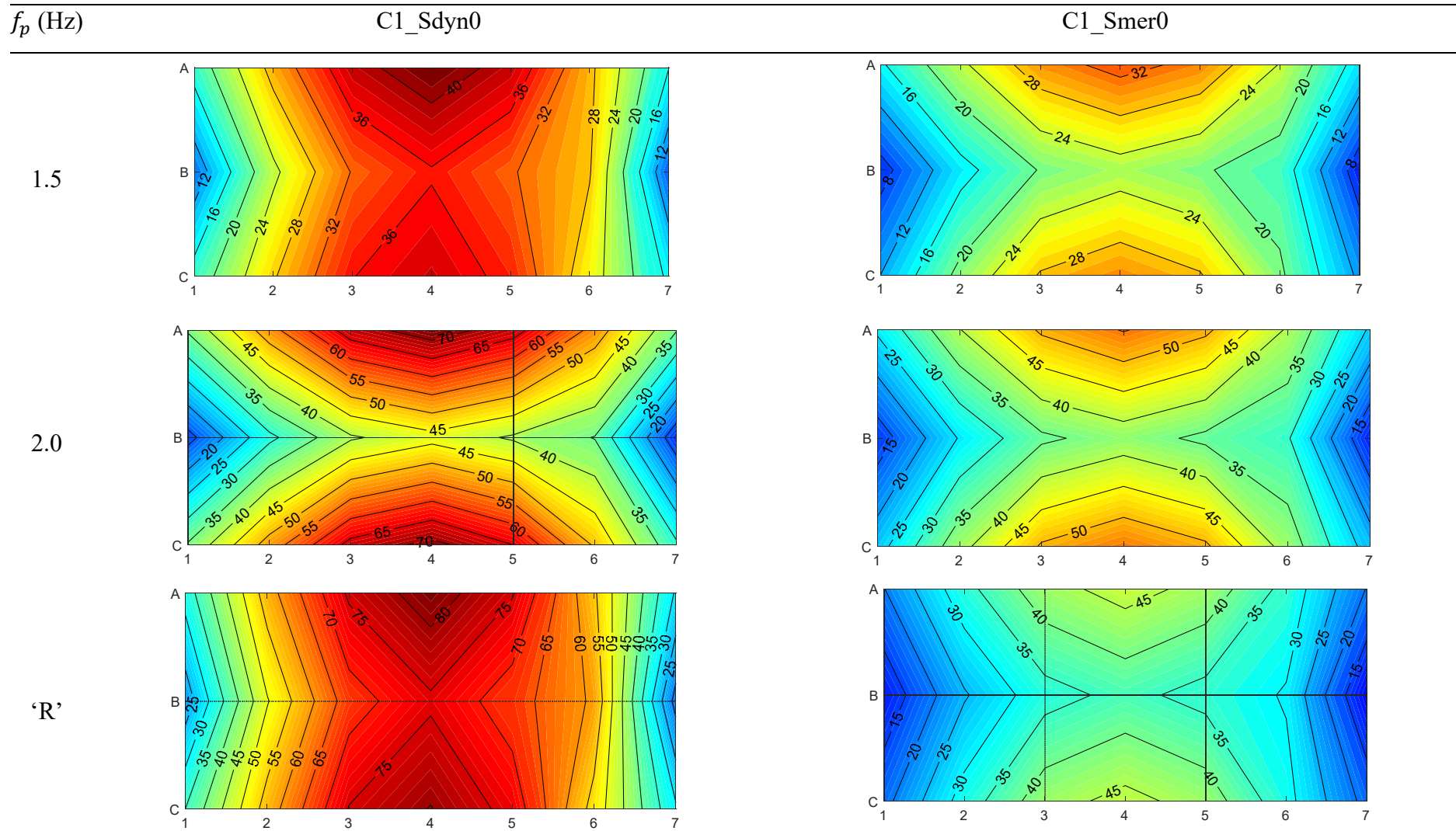
Figure 6-4 *Maximum response factors from W1 walking tests with elastic interlayer*

f_p (Hz)	C1_Sdyn0	C1_Smer0
1.5		
2.0		
'R'		
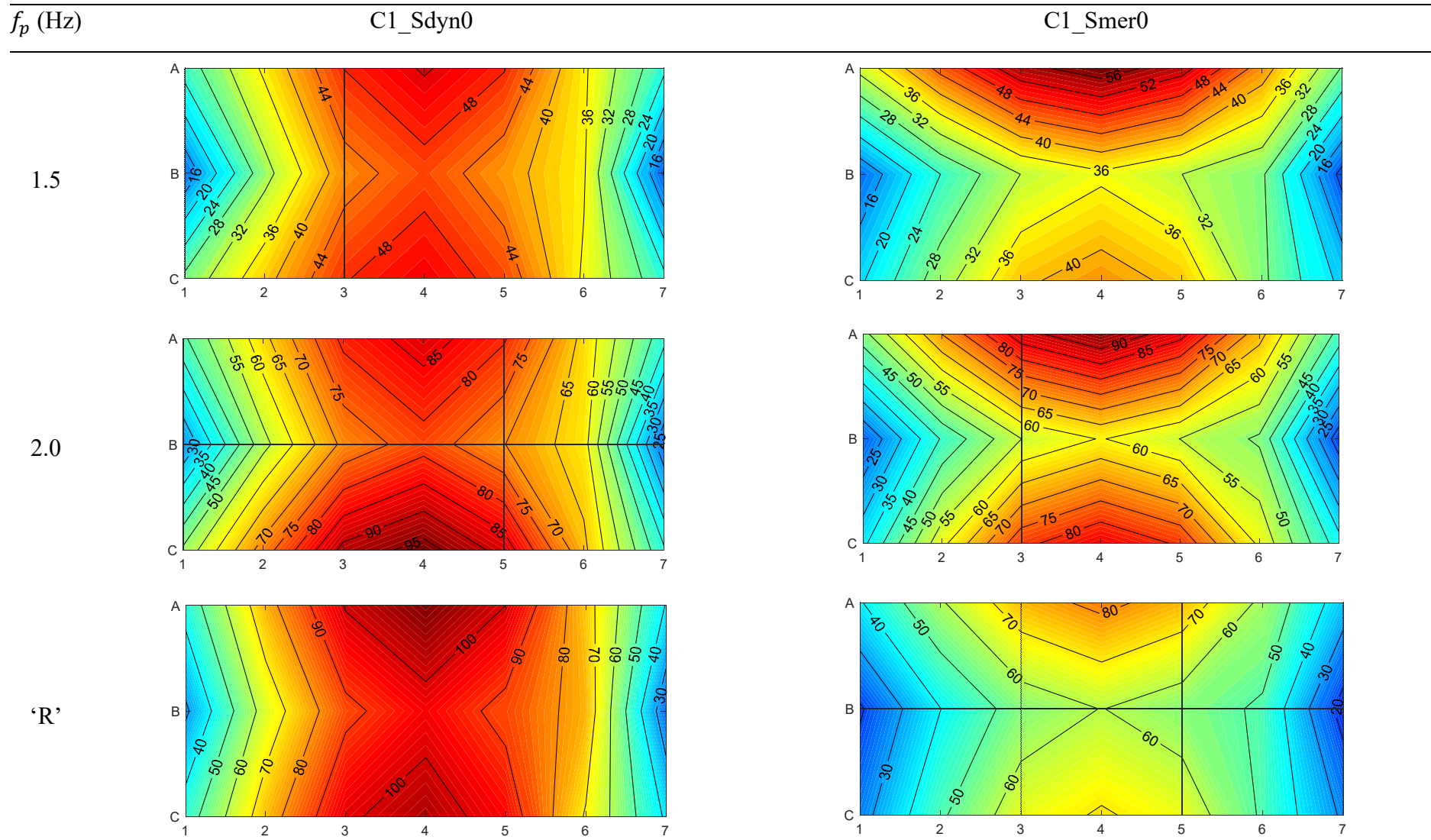
Figure 6-5 *Maximum response factors from W2a walking tests with elastic interlayer*

(a) 1.5 Hz

(b) 2.0 Hz

(c) 'R' Hz
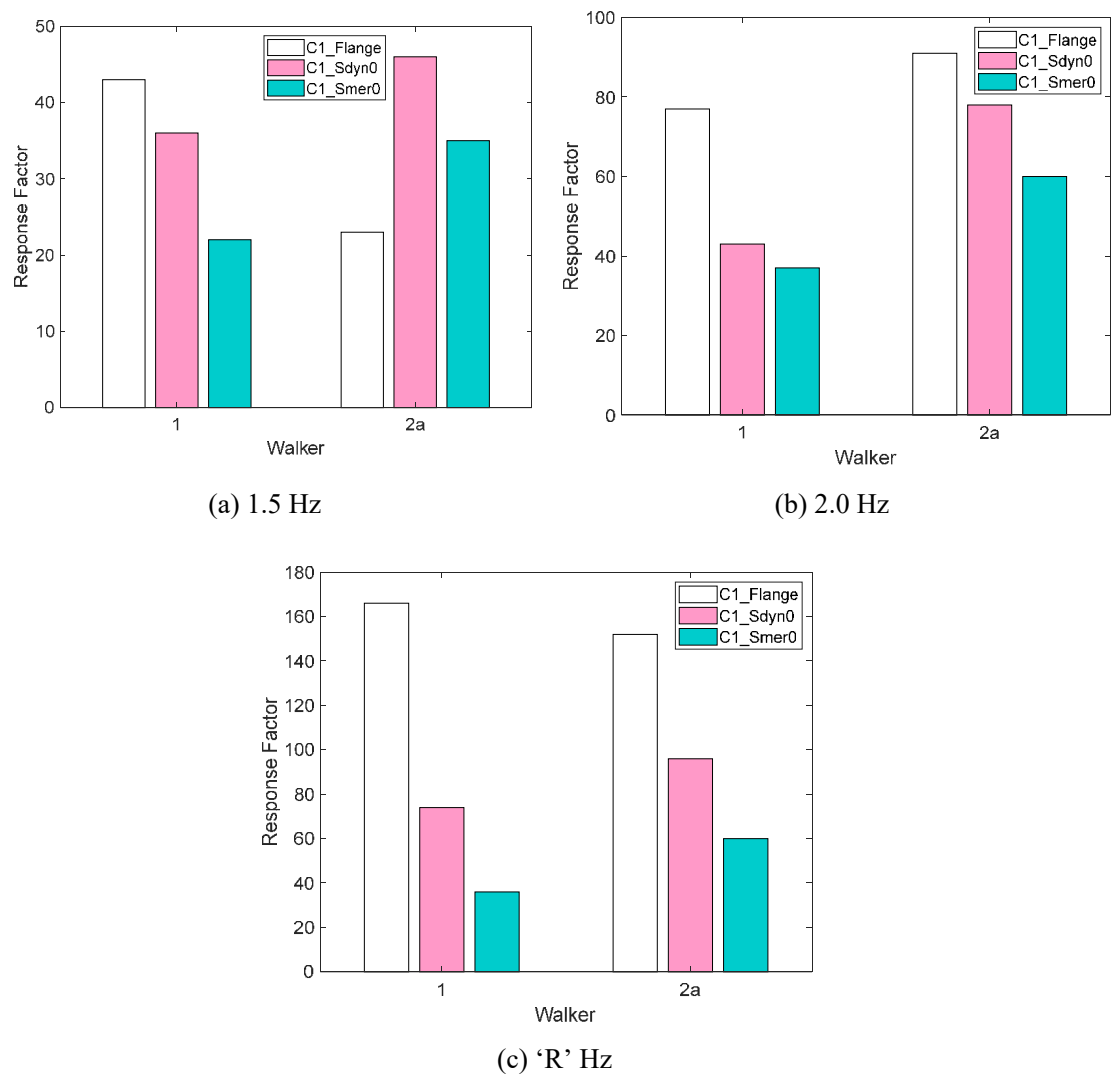
Figure 6-6 *Maximum response at B4 for all double cassette walking tests for walking pace*

6.2.2.2 Cumulative distribution of response

The cumulative distribution can be used to determine the percentage of time the RF surpasses a certain value and has potential to be a useful tool in assessing floor performance (Pavic & Zivanovic 2007; Živanovic & Pavic 2009). The cumulative distribution of the floor response for one walking loop for accelerometer B4 is shown in Figures 6-7, 6-8 and 6-9 for pace frequencies 'R' Hz, 2 Hz and 1.5 Hz, respectively. The distribution plots also include the C1_Flange test results, shown in grey, for ease of comparison. Note the acceleration response from both walkers have been merged (refer to Appendix B for the MATLAB code). The influence of the Sylomer interlayer on the distribution of response is clear for 2 Hz and 'R' Hz tests where for 80% of the time of the walking loop, the response factor is less than approximately 50 and 44, respectively.

In contrast, for the C1_Flange test, there is an 80% probability that the RF will be less than 60 and 120 for the 2 Hz and 'R' Hz walking tests, respectively. These results present a case for consideration of an elastic interlayer support condition which increases the floor damping ratio. Further walking tests undertaken on a larger scale floor set-up (not just a single cassette) and preferably in-situ would be required to further confirm these findings.
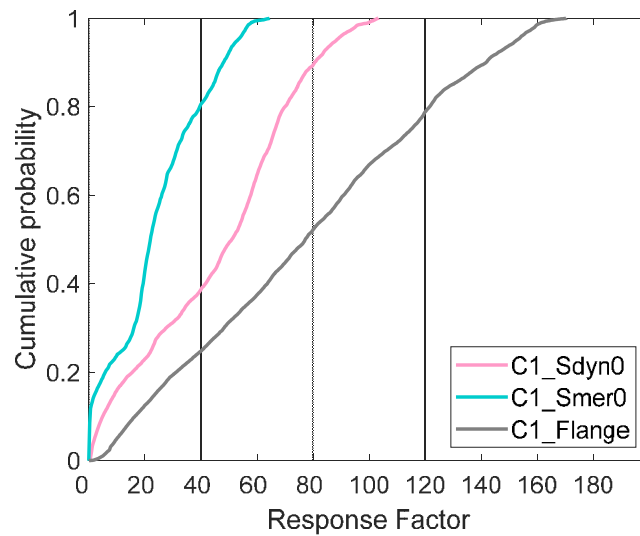
Figure 6-7 *Cumulative distribution functions for the RF at accelerometer B4 for all double cassette tests at pace frequency equal to fifth integer division of first bending mode.*
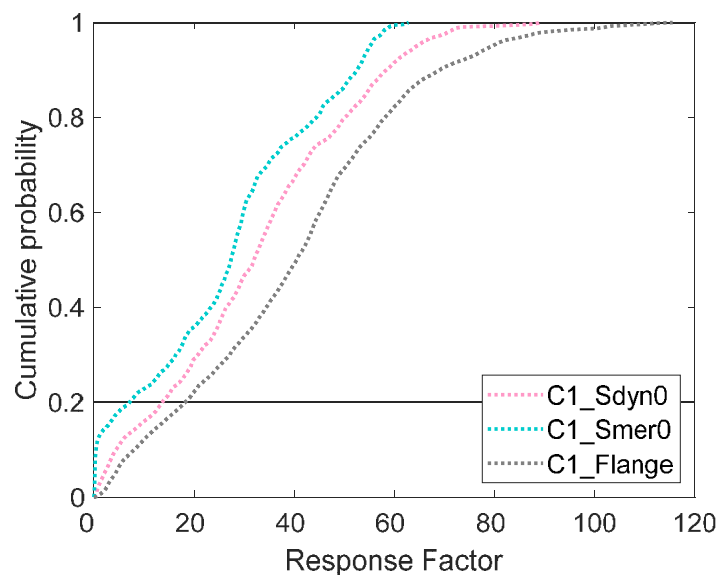
Figure 6-8 *Cumulative distribution functions for the RF at accelerometer B4 for all double cassette tests at pace frequency of 2 Hz.*

189
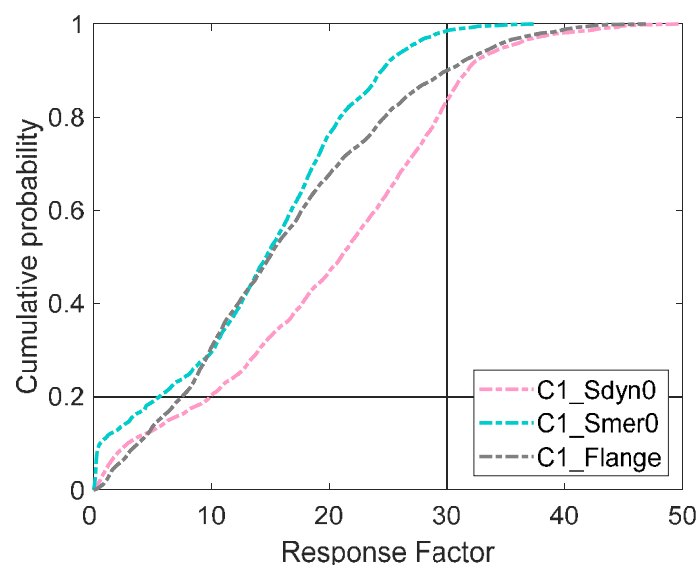
Figure 6-9 *Cumulative distribution functions for the RF at accelerometer B4 for all double cassette tests at pace frequency of 1.5 Hz.*

6.3 Influence of higher ratio of utilisation of elastomer

A higher ratio of utilisation of the elastomers occurs when additional loading is placed over the support locations. Examples of additional loading in an office building may be from partition walls, book cases or filing cabinets. As an extension of the C1_Sdyn0 and C1_Smer0 tests, these tests investigated the effect of increasing the ratio of utilisation of the elastomer by placing additional loading in the form of calibrated steel plates along the support location. Two loading cases for each support side were considered: 1000 N and 2000 N.

6.3.1 Modal Properties

Tests were first conducted with a 1000 N additional loading at each support end (C1_Sdyn1000 and C1_Smer1000) resulting in a 79% and 108% utilisation of the Sylodyn and Sylomer elastomers, respectively. This meant that the Sylomer material had surpassed the static linear-elastic portion of the load-deflection curve and was now within the dynamic range of use. The second set of testing involved adding an additional 1000 N loading at each support end resulting in a total 2000 N load (C1_Sdyn2000 and C1_Smer2000); this resulted in a 92% and 126% utilisation of the Sylodyn and Sylomer elastomer, respectively.

The sum FRF's based on impact LOC4 for all Sylodyn and Sylomer tests are shown in Figure 6-10; sum FRF's for the tests with no mass as well as the C1_Flange support condition are also shown for ease of comparison. The associated natural frequencies and damping ratios for all modes up to 50 Hz are shown in Tables 6-4 and 6-5; matching mode shapes have been grouped together where possible for ease of comparison. The modes that were either not found (for Sylodyn and Sylomer tests) or are not relevant (for C1_Flange tests) are indicated by a dash (-). Typical mode shapes for all eight modes, based on C1_Smer1000 tests as an example, are shown in Figure 6-11.

Figure 6-10 and Table 6-4 reveals that the first added mass test of 1000 N reduced the natural frequencies, particularly for mode 7 where the natural frequency decreased by approx. 9 Hz; FRF amplitudes for the higher modes were also noticeably reduced. These effects became more pronounced as the second set of added mass was placed at the supports. This results in the behaviour of the floor becoming increasingly more complex where some modes which were originally obtained from tests with no additional mass became non-existent or extremely difficult to find. For most modes, the added mass resulted in either negligible change or a slight increase to the damping ratio compared to the tests with no added mass.
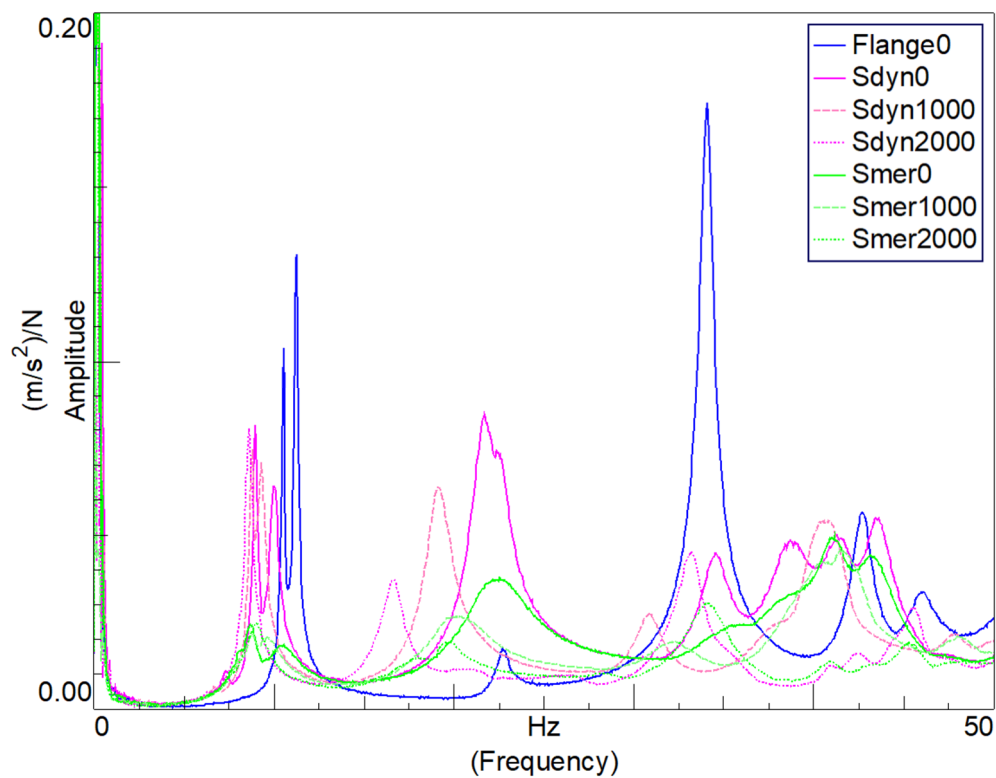
Figure 6-10 *Sum FRF amplitude for impact LOC4 for all added mass tests*

Table 6-4 *Natural frequencies for all modes under 50 Hz for all added mass tests with covariance across all impact locations shown in italicised parentheses*

	Natural Frequency (Hz)							
Mode	1	2	3	4	5	6	7	8
C1_Sdyn1000	8.74	9.25	18.86	19.27	29.28	30.86	40.42	48.03
	(0.01)	*(0.00)*	*(0.01)*	*(0.04)*	*(0.14)*	*(0.01)*	*(0.17)*	*(0.07)*
C1_Sdyn2000	8.39	8.57	16.64*	15.94*	23.76	27.18	33.16	44.35
	(0.08)	*(0.06)*	*(0.17)*	*(N/A)*	*(0.25)*	*(1.95)*	*(0.35)*	*(0.07)*
C1_Smer1000	8.74	9.67	18.93	20.33	30.06	-	40.29	48.42
	(0.01)	*(0.02)*	*(0.07)*	*(0.01)*	*(N/A)*		*(0.18)*	*(0.04)*
C1_Smer2000	8.64	8.85	18.79	-	-	-	34.17	44.83
	(0.01)	*(0.03)*	*(0.05)*				*(0.17)*	*(0.24)*

Note: If CoV is N/A, the mode was only found from the FRF of one impact location; *denotes modes that have switched from Figure 6-11.

Table 6-5 *Damping ratio for all modes under 50 Hz for all added mass tests with covariance across all impact locations shown in italicised parentheses*

Mode	Damping ratio (%)							
	1	2	3	4	5	6	7	8
C1_Sdyn1000	1.55	2.14	3.11	3.56	3.47	2.36	1.77	1.48
	(1.87)	*(0.66)*	*(0.91)*	*(0.00)*	*(5.92)*	*(3.60)*	*(1.76)*	*(3.31)*
C1_Sdyn2000	1.95	2.15	3.33*	3.66*	2.69	4.11	2.14	1.50
	(0.36)	*(4.58)*	*(4.10)*	*(N/A)*	*(7.46)*	*(0.00)*	*(7.27)*	*(0.47)*
C1_Smer1000	4.36	7.37	8.37	8.01	6.54	-	2.58	1.96
	(4.22)	*(5.18)*	*(4.59)*	*(4.50)*	*(N/A)*		*(7.83)*	*(4.17)*
C1_Smer2000	6.34	5.54	9.50	-	-	-	3.39	2.49
	(0.45)	*(3.32)*	*(1.94)*				*(11.86)*	*(0.28)*

Note: If CoV is N/A, the mode was only found from the FRF of one impact location; *denotes modes that have switched from Figure 6-11.

Mode 1   Mode 2   Mode 3

Mode 4   Mode 5   Mode 6

Mode 7   Mode 8
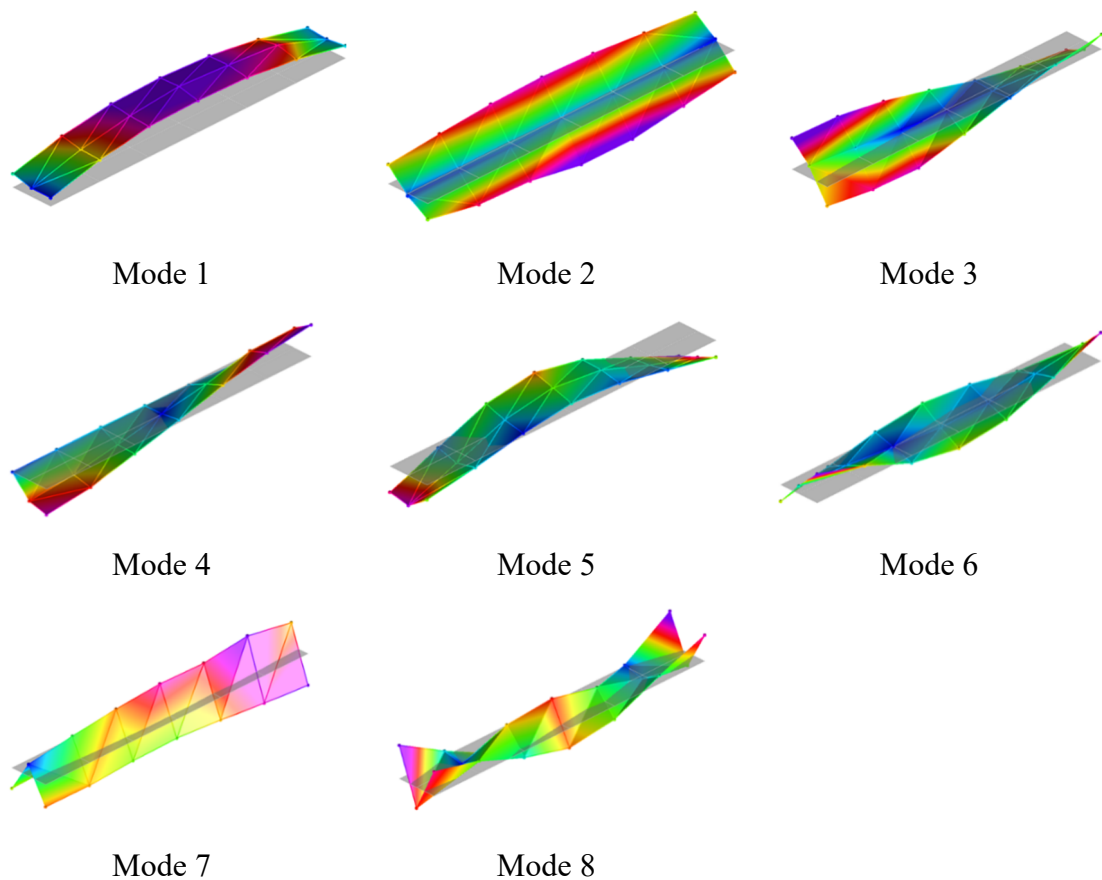
Figure 6-11 *Typical mode shapes for all modes under 50 Hz. Figures are from C1_Smer1000 test.*

6.3.2 Floor response to walking

6.3.2.1 Maximum response

Figures 6-12 and 6-13 reveal the maximum RF contours based on W1 tests and averaged over the three walking loops for the additional load tests with the Sylodyn and Sylomer interlayer, respectively. For ease of comparison, the contours have been plotted with a colour scale matching the maximum response for the particular walking pace for both 1000 N and 2000 N added load.

Figure 6-14 reveals the maximum RF at accelerometer B4 for test cases with elastomer and additional load at support. As shown, the results indicate that, for a walking pace of 1.5 Hz and 'R' Hz, placing additional loading above the support so as to increase the ratio of utilisation of the elastomer further reduces the floor response. This trend was not particularly clear for the 2 Hz walking test, although further walking tests would help to clarify this result.

f_p (Hz)	C1_Sdyn1000	C1_Sdyn2000
1.5		
2.0		
R		
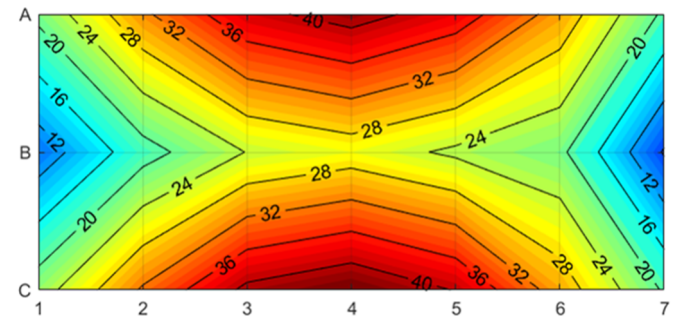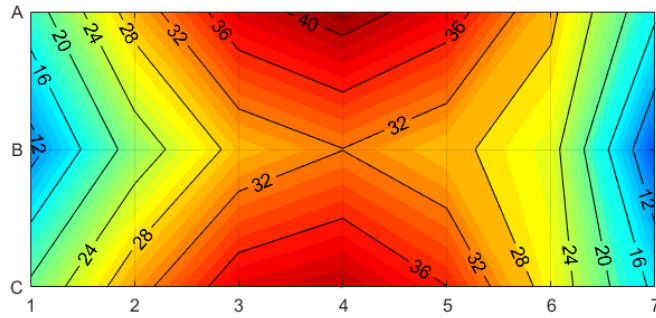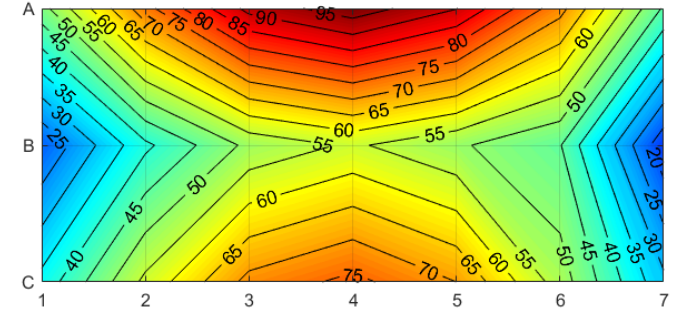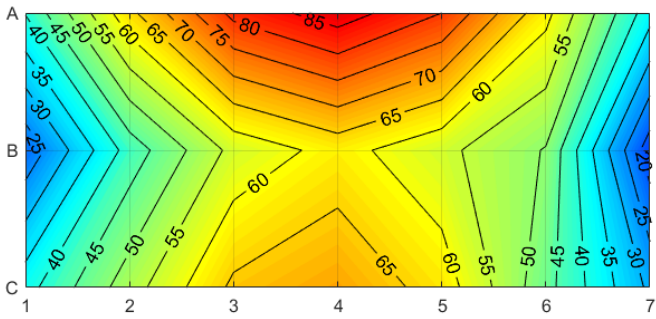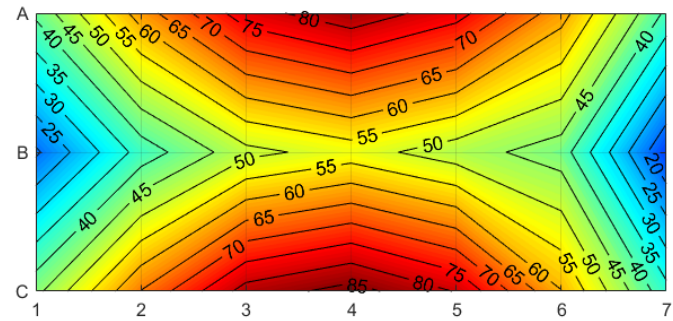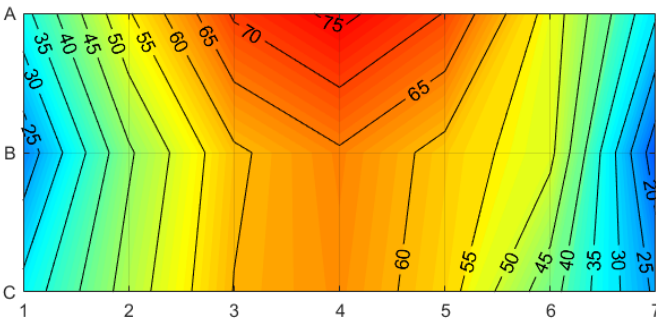
Figure 6-12 *Maximum response factor contours for W1 walking tests for C1_Sdyn1000 and C1_Sdyn2000 tests*

f_p (Hz)	C1_Smer1000	C1_Smer2000
1.5		
2.0		
R		
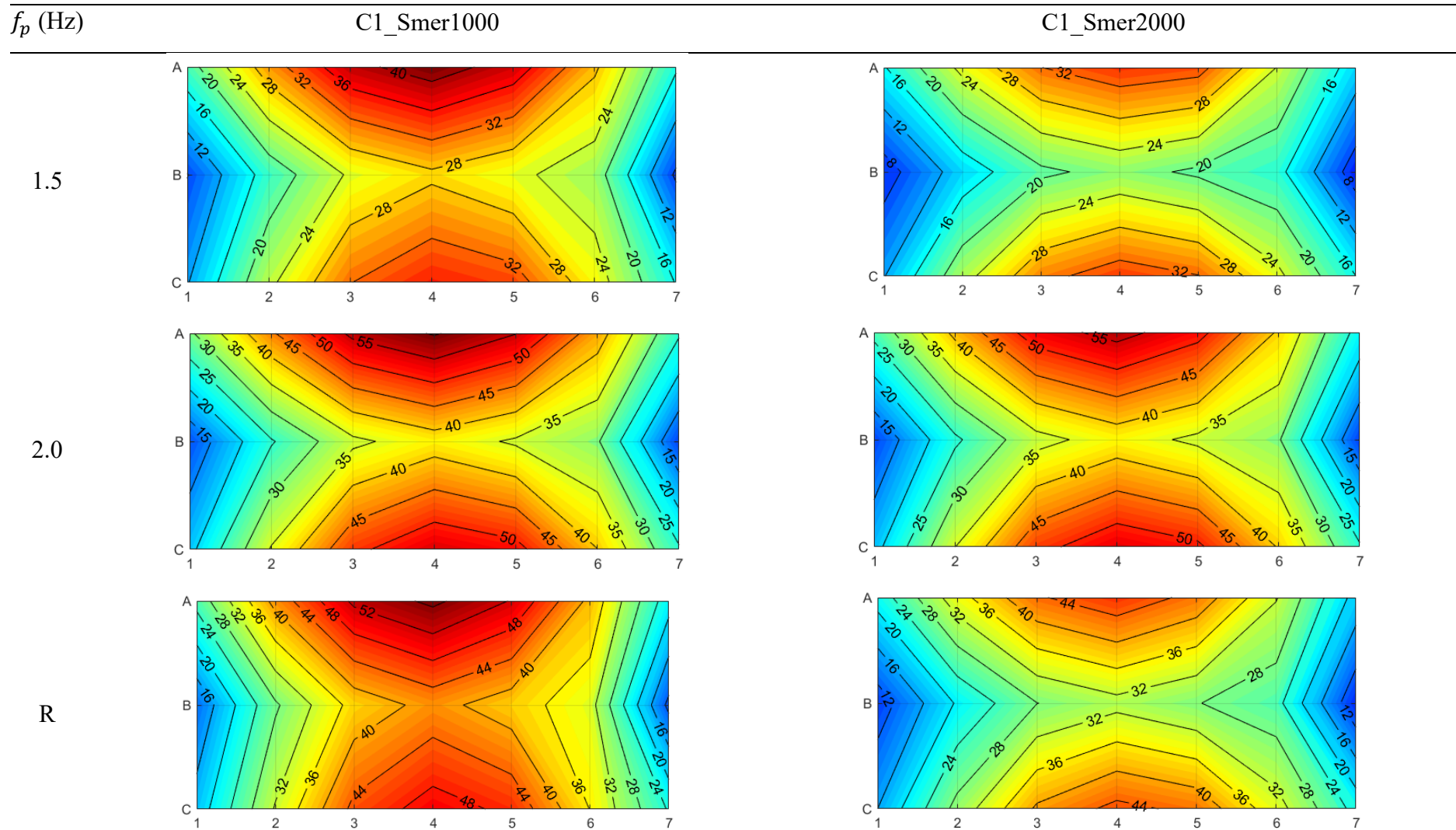
Figure 6-13 Maximum response factor contours for W2a walking tests for C1_Smer1000 and C1_Smer2000 tests

196
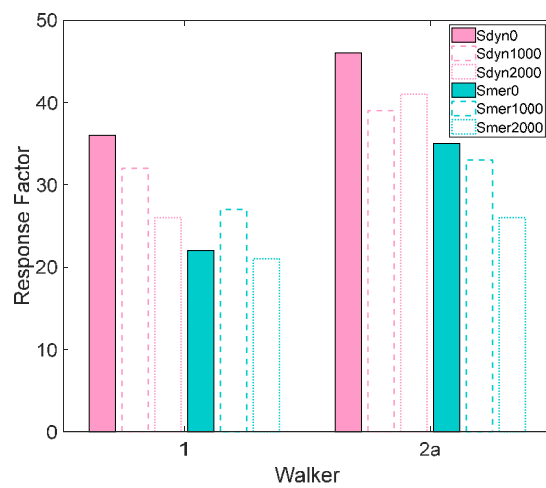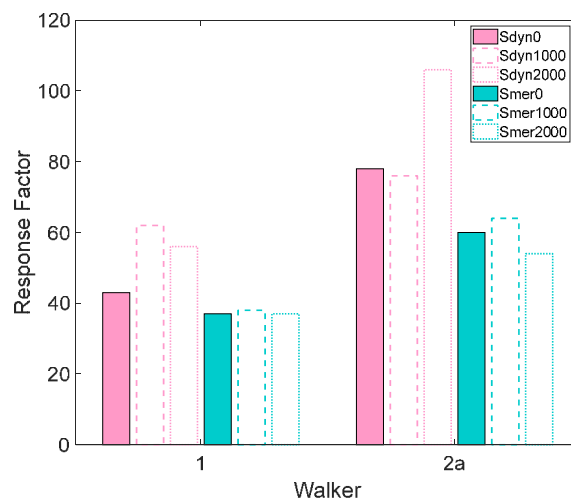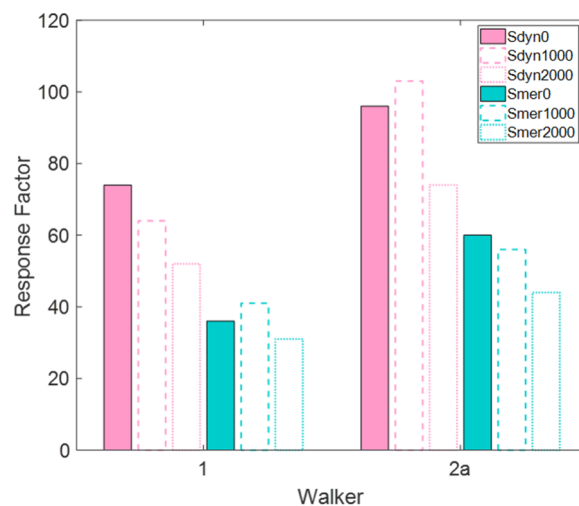
(a) 1.5 Hz

(b) 2.0 Hz

(c) 'R' Hz

Figure 6-14 *Maximum response at B4 for all Sylodyn and Sylomer walking tests for walking pace (a) 1.5 Hz; (b) 2.0 Hz; (c) 'R' Hz*

6.3.2.2 Cumulative distribution of response

Figures 6-15, 6-16 and 6-17 show the cumulative distribution of the floor response for one walking loop for accelerometer B4 for walking paces of 'R' Hz, 2 Hz and 1.5 Hz, respectively. As shown, these plots reveal that a higher ratio of utilisation of elastomer at support locations shifts the cumulative distribution of response slightly to the left for walking tests at 1.5 Hz and 'R' Hz; this indicates that there is a higher probability that the response will fall below a certain limit compared to the case with no additional loading. For example, for walking test at 'R' Hz with the Sylomer interlayer, the probability that the response will be less than RF of 40 increases from approximately 80% to 99% when adding the 2000 N along the support. This indicates that positioning furniture or partition walls along the support location can increase the ratio of utilisation of the elastomer underneath and subsequently improve the floor response. However, care needs to be taken so that the ratio of utilisation of elastomer remains in the static range of use under ultimate static design loads since the material may stiffen over time if the elastomer is in the dynamic range.
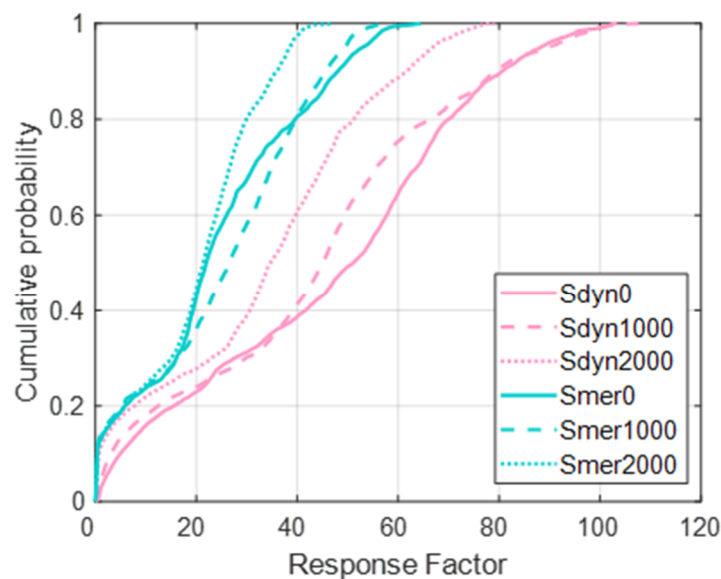
Figure 6-15 *Cumulative distribution functions for the RF at accelerometer B4 for all additional mass tests with elastomer at pace frequency equal to fifth integer division of first bending mode.*
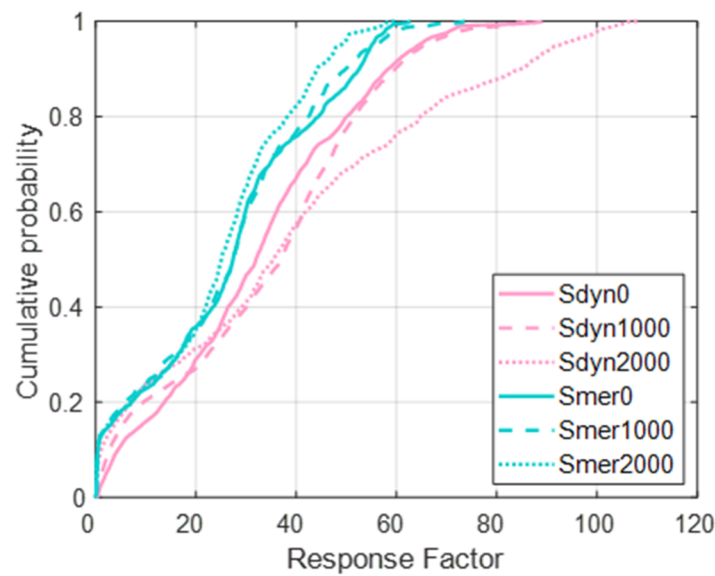
Figure 6-16 *Cumulative distribution functions for the RF at accelerometer B4 for all double cassette tests at pace frequency of 2 Hz.*
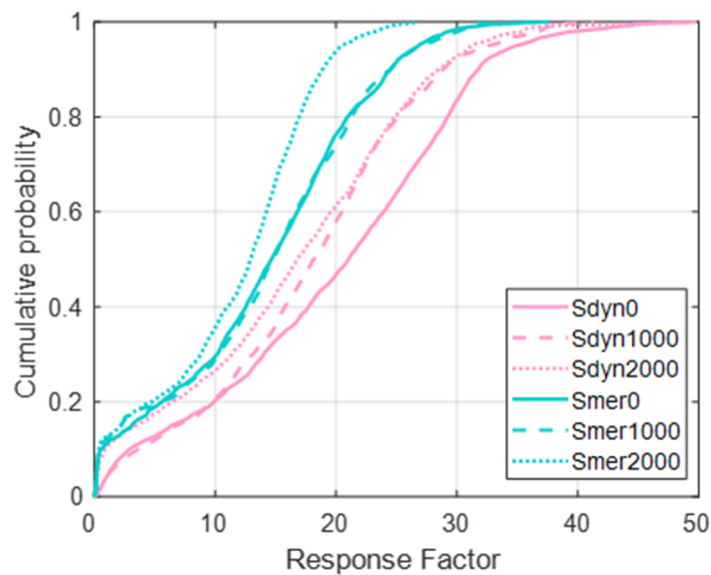
Figure 6-17 *Cumulative distribution functions for the RF at accelerometer B4 for all double cassette tests at pace frequency of 1.5 Hz.*

6.4 Influence of cassette-to-cassette connections

The single cassette tests discussed in Chapter 4, 5 and Section 6.2 and 6.3 above were essential in understanding how various boundary conditions influence the dynamic behaviour without the contribution of other variables. These tests meant that two shorter sides were supported while the other two longer sides were free to move. In practice, however, these cassettes will be integrated into a larger structure with adjacent cassettes. Common practice to connect adjacent cassettes together would include a combination of

web-to-web connections and a flange-to-flange connection in the form of splice or diagonal screws. Investigating how these connections influence the dynamic behaviour is imperative for accurate finite element modelling.

6.4.1 Modal properties

Figure 6-18 reveals the sum FRF amplitude for impact location 3 for all double cassette tests with associated natural frequencies and damping ratios obtained from LMS Test.Lab shown in Tables 6-6 and 6-76-7, respectively. Note for Figure 6-18, 'C2_' has been removed from test names in the legend. The peaks corresponding to the mode shapes are annotated. The FRF plot reveals that connecting a second cassette adjacent to a single cassette increases the number of modes under 50 Hz from five to nine, although the first mode appears to indicate a discontinuity between the two cassettes. The natural frequency of mode 2 which appears to be the first bending mode of both cassettes, as shown in Figure 6-19, remains at 10.68 Hz which matches the fundamental frequency of the single cassette tests. This indicates that the additional mass is in proportion to the additional stiffness gained from connecting a second cassette. The mode shapes shown in Figure 6-19 (based on C2_Spl300 test as an example) also reveals that the type of mode for modes 1, 5, 6 and 8 are unclear; it is particularly difficult to differentiate mode 5 and 6 as either the second bending or torsion mode. This will be investigated further through a finite element analysis. The most significant difference out of all modes between the single and double cassette tests is the decrease of the first lateral bending mode from 41.77 Hz (mode 5) for the single cassette to approx. 20 Hz (mode 4) for the double cassette tests.

One noticeable trend is the minimal effect to modal properties when the screw spacing is reduced form 300 mm centre to centre (c/c) to 150 mm c/c. The additional screws introduced for C2_Web150 and C2_Spl150 tests appears to increase the stiffness of the floor system although the increase is 0.5% very slightly at most. There also appears to be very little difference in modal properties between the two flange-to-flange connection types. The addition of the flange connection appears to only have a notable change to the first lateral bending mode with an increase in natural frequency of 7% and 3% for the splice and diagonal screw connection, respectively. The damping ratio for all modes

remained within the range of 1 – 2% which indicates the cassette-to-cassette connections had minimal effect to the structural damping.

Table 6-6 Natural frequencies for all modes under 50 Hz for all double cassette tests with covariance across all impact locations shown in italicised parentheses

	Natural frequency (Hz)								
Mode	1	2	3	4	5	6	7	8	9
Web300	9.78	10.68	11.22	19.91	27.30	32.73	36.86	43.50	48.78
	(0.13)	*(0.01)*	*(0.01)*	*(0.02)*	*(0.27)*	*(0.06)*	*(0.01)*	*(1.28)*	*(0.06)*
Web150	9.69	10.66	11.23	19.91	27.31	32.87	37.07	43.77	49.01
	(0.60)	*(0.34)*	*(0.03)*	*(0.32)*	*(1.30)*	*(0.20)*	*(0.08)*	*(1.61)*	*(0.01)*
Spl300	9.91	10.69	11.27	21.17	27.93	32.80	37.17	43.98	49.17
	(0.20)	*(0.33)*	*(0.02)*	*(0.26)*	*(0.49)*	*(N/A)*	*(0.03)*	*(0.10)*	*(0.01)*
Spl150	9.91	10.69	11.28	21.28	27.91	32.91	37.29	44.10	49.34
	(0.09)	*(0.04)*	*(0.06)*	*(0.21)*	*(0.23)*	*(0.19)*	*(0.02)*	*(0.15)*	*(0.10)*
Diag300	9.91	10.68	11.19	20.93	27.60	32.38	37.06	43.76	48.71
	(0.81)	*(0.31)*	*(0.27)*	*(0.39)*	*(1.32)*	*(2.64)*	*(0.08)*	*(0.07)*	*(0.02)*
Diag150	9.14	10.52	11.03	20.51	25.87	31.79	37.07	43.29	48.75
	(0.07)	*(0.03)*	*(0.11)*	*(0.10)*	*(0.17)*	*(0.49)*	*(0.69)*	*(0.20)*	*(0.06)*

Note: If CoV is N/A, the mode was only found from the FRF of one impact location.

Table 6-7 Damping ratio for all modes under 50 Hz for all double cassette tests with covariance across all impact locations shown in italicised parentheses

	Damping ratio (%)								
Mode	1	2	3	4	5	6	7	8	9
Web300	1.7	0.9	0.8	1.3	1.7	1.6	1.6	1.5	1.4
	(4.12)	*(0.00)*	*(1.40)*	*(4.55)*	*(6.27)*	*(7.73)*	*(2.60)*	*(8.60)*	*(6.14)*
Web150	2.2	1.1	0.8	1.5	2.1	1.3	1.5	1.5	1.5
	(4.14)	*(2.38)*	*(1.68)*	*(1.16)*	*(2.79)*	*(0.75)*	*(1.40)*	*(0.79)*	*(1.43)*
Spl300	1.6	1.0	0.8	1.3	1.1	1.2	1.5	1.2	1.4
	(3.75)	*(6.67)*	*(1.28)*	*(5.56)*	*(4.64)*	*(N/A)*	*(0.92)*	*(9.59)*	*(3.62)*
Spl150	1.9	0.9	0.8	1.3	1.4	1.4	1.5	1.2	1.6
	(3.36)	*(0.00)*	*(2.44)*	*(2.54)*	*(4.87)*	*(4.06)*	*(1.38)*	*(5.29)*	*(3.66)*
Diag300	1.8	0.9	0.9	1.3	2.0	1.0	1.5	1.7	1.3
	(3.02)	*(6.34)*	*(5.16)*	*(3.88)*	*(10.55)*	*(7.52)*	*(6.51)*	*(7.26)*	*(9.00)*

Diag150	1.4	1.1	0.8	1.3	1.3	1.2	1.4	1.5	1.6
	(4.21)	*(2.47)*	*(5.01)*	*(0.77)*	*(5.41)*	*(3.45)*	*(1.09)*	*(1.12)*	*(3.54)*

Note: If CoV is N/A, the mode was only found from the FRF of one impact location.
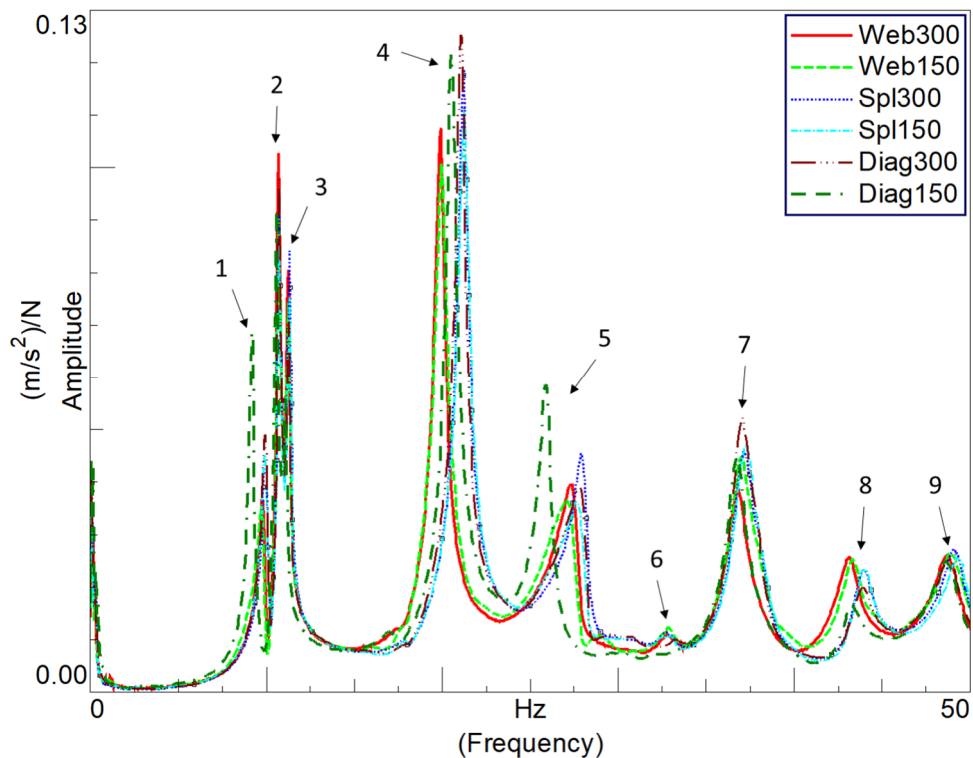
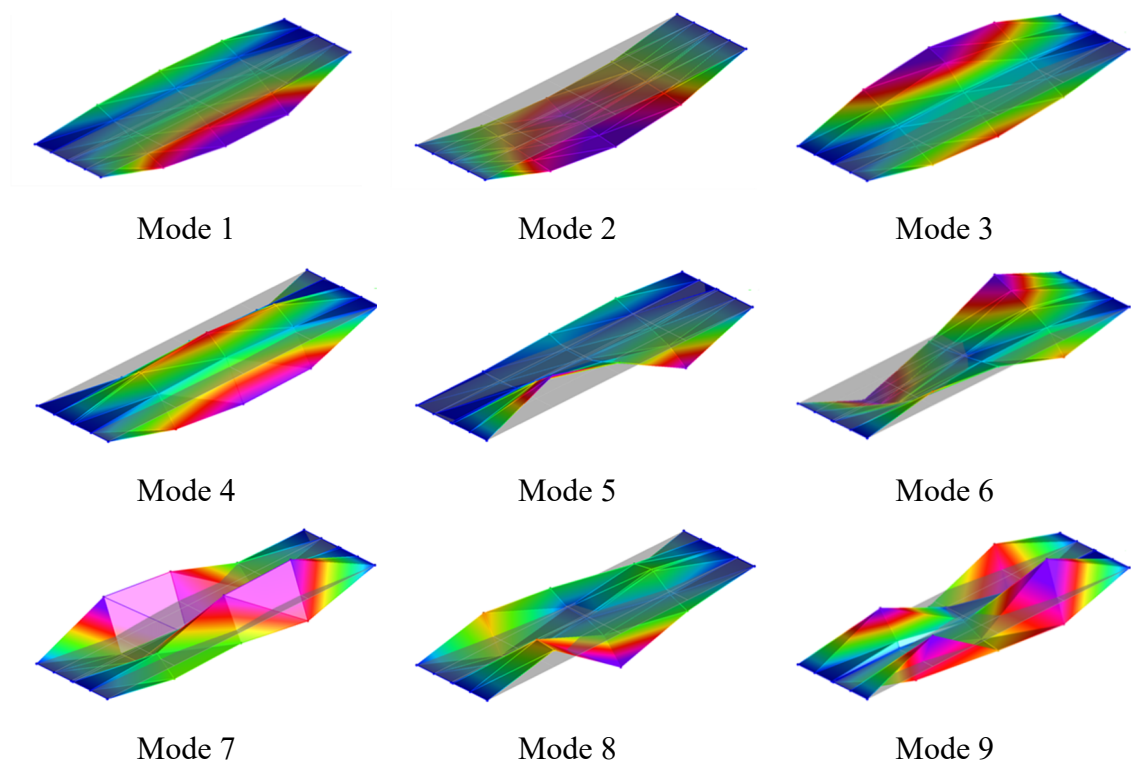**Figure 6-18** *Sum FRF amplitude for impact LOC3 for all double cassette tests*

Mode 1   Mode 2   Mode 3

Mode 4   Mode 5   Mode 6

Mode 7   Mode 8   Mode 9

Figure 6-19 *Typical mode shapes for all modes under 50 Hz. Figures are from C2_Spl300 test, as an example.*

6.4.2 Floor response to walking

6.4.2.1 Maximum response

The RF contours from the maximum frequency-weighted response for each accelerometer averaged over the three walking loops for the C2_Web, C2_Spl and C2_Diag tests are shown in Figures 6-20, 6-21 and 6-22, respectively. Note only results from Walker 1 (W1) are shown here; similar to the observation of the measured responses for C1A_Flange test detailed in Chapter 5, W1 was found to be a more synchronised walker and generally resulted in higher responses than Walker 2b (W2b) despite being 24kg lighter. For reference, maximum response due to W2b are shown in Appendix C. The RF contour plots have been grouped by pace frequency and connection configuration. For ease of comparison between screw spacing of 300 mm c/c and 150 mm c/c, the contours have been plotted with a colour scale matching the maximum response of the walking pace over the two screw space configurations.

As shown in Figures 6-20, 6-21 and 6-22, the maximum response occurred at accelerometers at grid reference A2 or F2 (grid lines noted in image). However, in a typical building floor scenario, there would be multiple connected adjacent cassettes, and thus the response of accelerometers at grid C2 and D2 were of focus. These accelerometers lie along the joist line on each side of the interface of the two joining cassettes and generally had a response within 5% of the other (maximum difference was 6.9%). Figure 6-23(a), (b) and (c) shows the response at C2 for Web150 and all flange-to-flange connection tests for both walkers for a walking pace of 1.5 Hz, 2.0 Hz and 'R' Hz, respectively. Note 'C2_' has been removed from test names in the legend to avoid confusion. The addition of the flange connection (either as splice or diagonal screws) generally reduces the maximum response at C2, however there was no clear trend of the extent of the influence. For example, with the addition of the diagonal crews at 300 mm c/c, the maximum response when walking at a pace of 1.5 Hz reduced by 13% and 38% for W1 and W2b, respectively, while for a pace frequency of 2.0 Hz, the maximum

response reduced by 35% and 14% for W1 and W2b, respectively. However, it was clear that when the walkers were walking at 'R' Hz, Diag150 test set-up achieved the lowest response for both walkers.
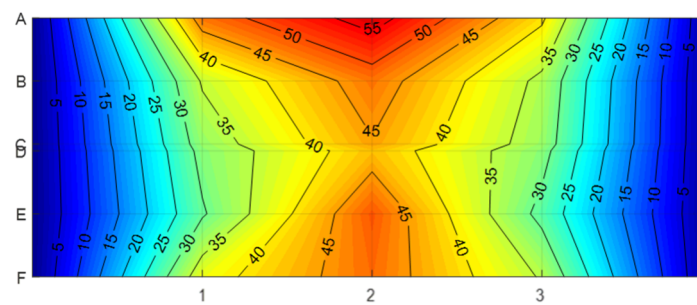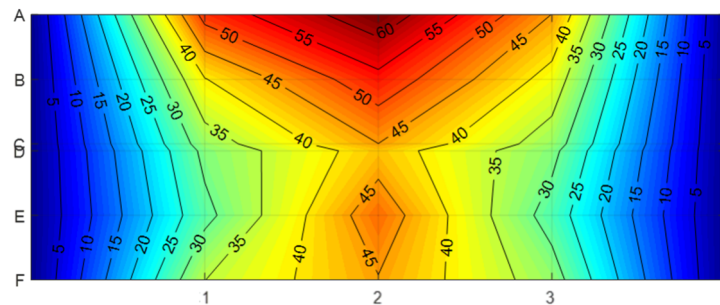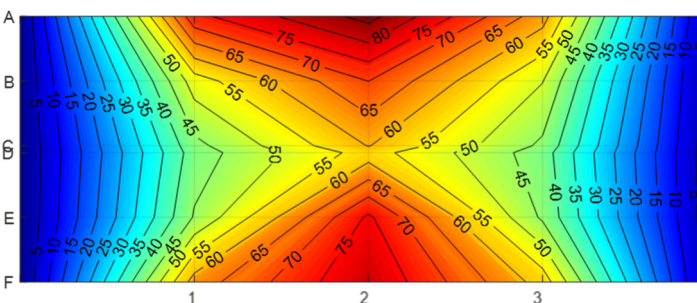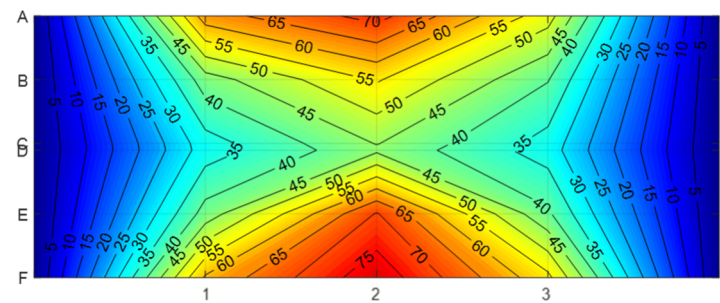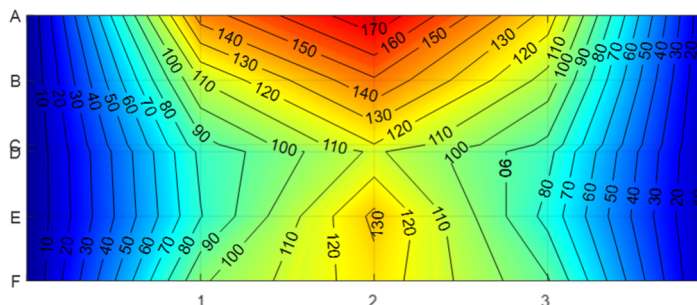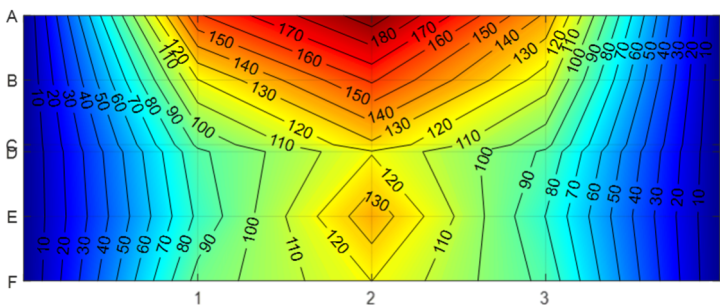
Figure 6-20 *Maximum response factors from W1 walking tests: web-to-web connection*

f_p (Hz)	C2_Spl300	C2_Spl150
1.5		
2.0		
'R'		
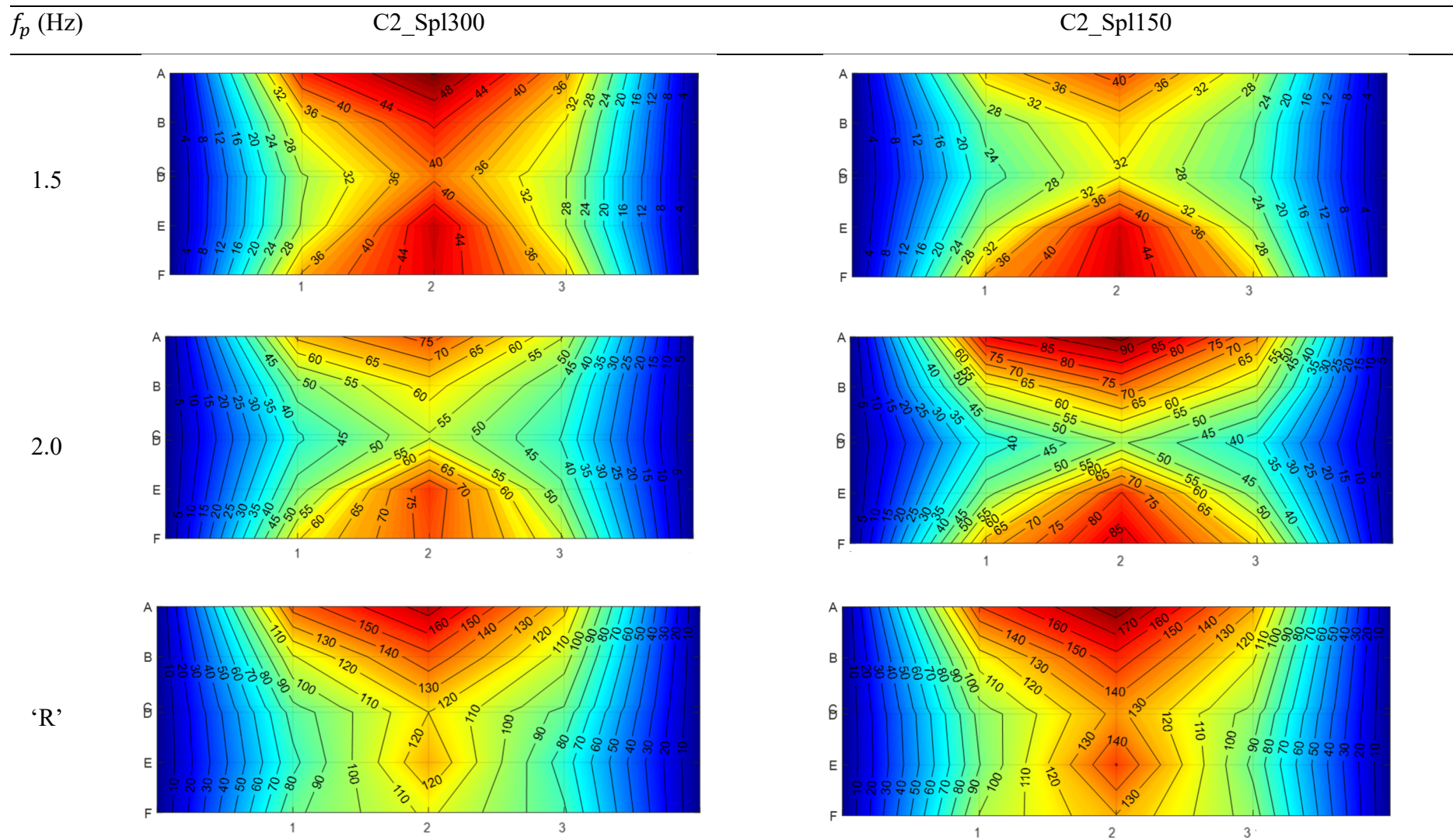
Figure 6-21 *Maximum response factors from W1 walking tests: splice connection between adjacent flanges*

f_p (Hz)	C2_Diag300	C2_Diag150
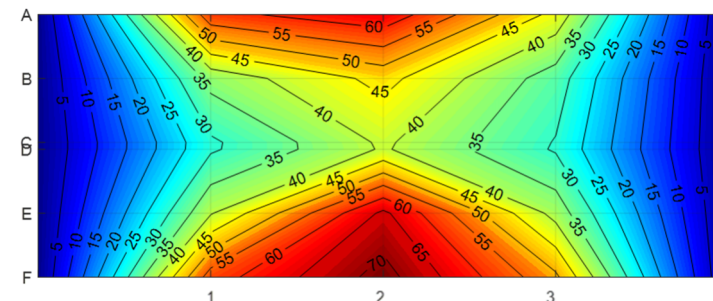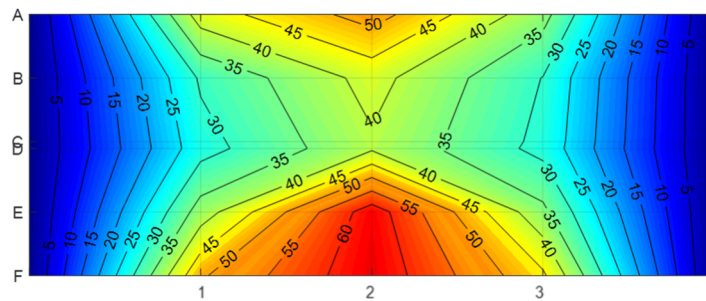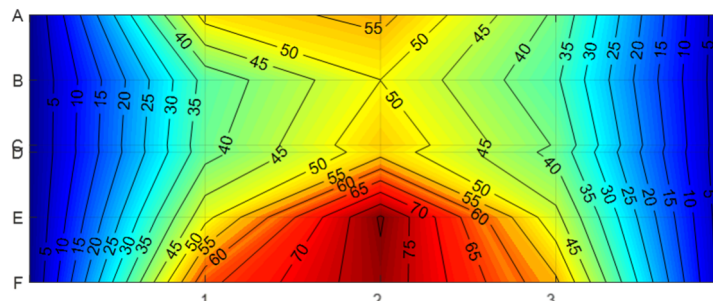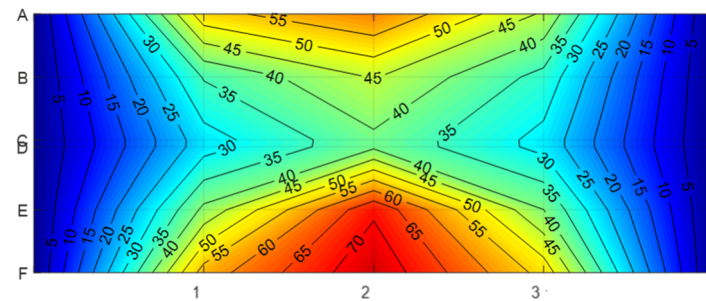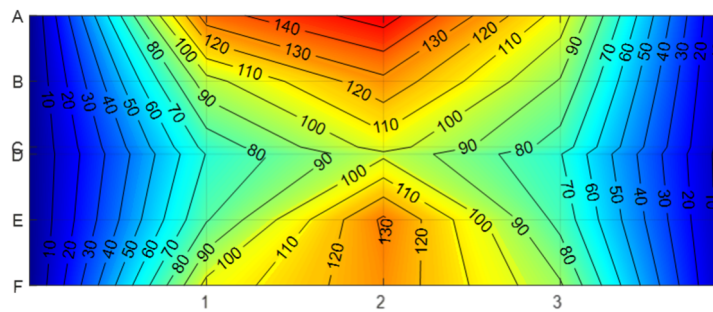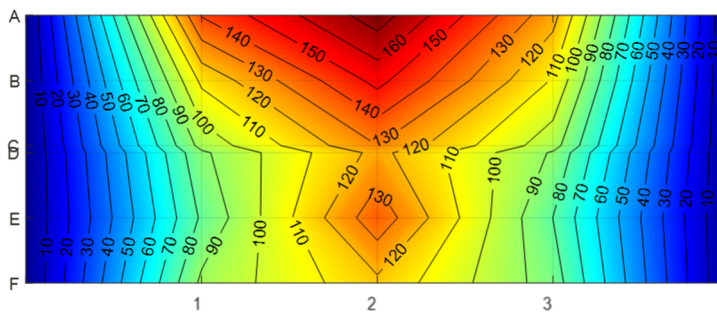
Figure 6-22 *Maximum response factors from W1 walking tests: diagonal screws between adjacent flanges*
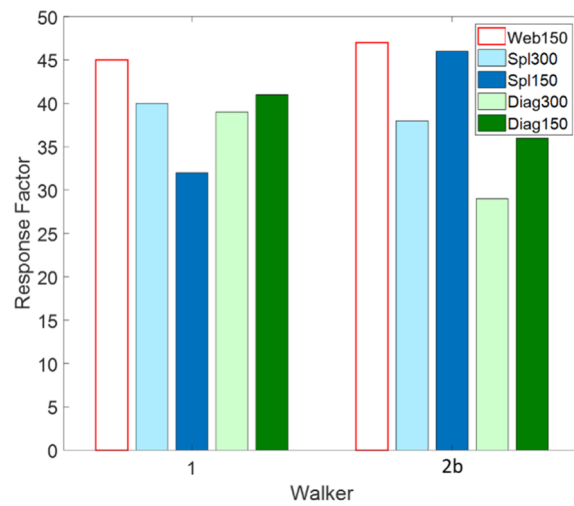
(a) 1.5 Hz
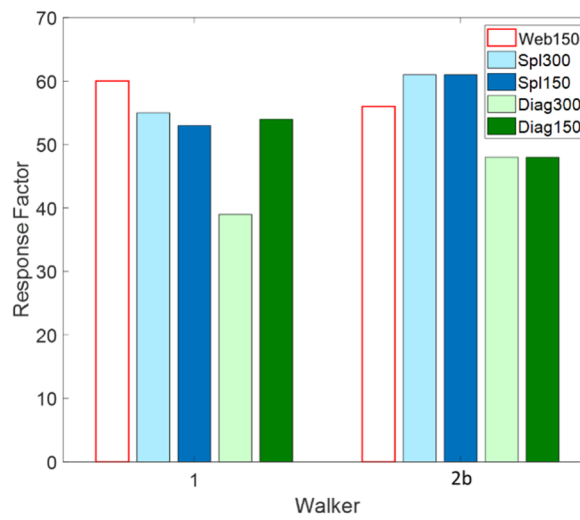
(b) 2.0 Hz
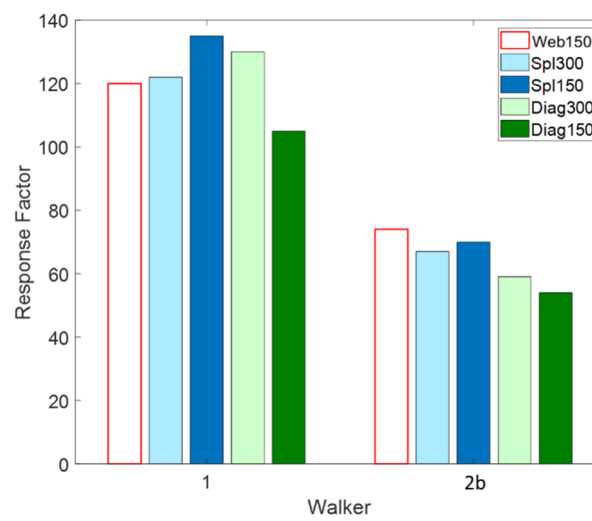
(c) 'R' Hz

Figure 6-23 *Maximum response at C2 for all double cassette walking tests for walking pace (a) 1.5 Hz; (b) 2.0 Hz; (c) fifth integer of first bending mode.*

6.4.2.2 Cumulative distribution of response

Figures 6-24, 6-25 and 6-26 reveal the cumulative distribution at accelerometer C2 for all double cassette set-ups for walking at a pace frequency of 'R' Hz, 2 Hz and 1.5 Hz, respectively. Note the acceleration response from both walkers have been merged and running 1s RMS amplitudes for all walking loops are included. These plots reveal very little difference between the distributions of responses for a walking pace of 1.5 Hz. However at pace frequencies of 2 Hz and 'R' Hz, the responses using the diagonal screw connection (either at 150 mm or 300 mm spacing) appear to be lower for longer periods of time than the splice connection. In addition, there seems to be little influence of different screw spacing on the distribution of response.
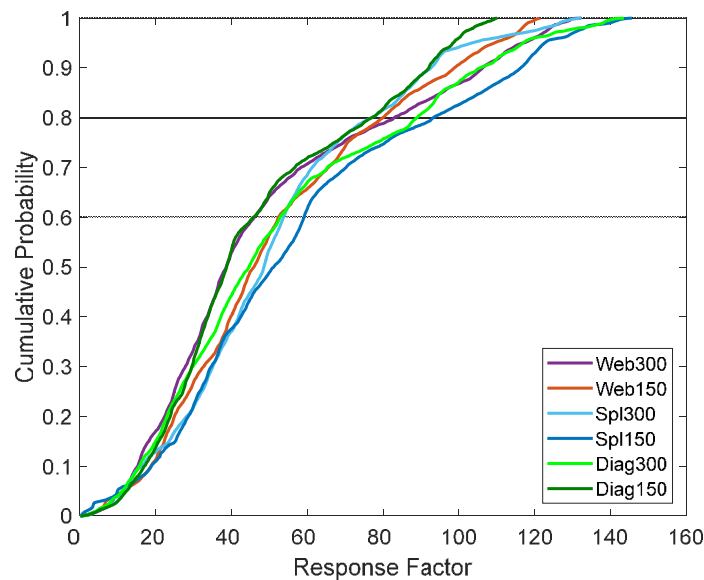
Figure 6-24 *Cumulative distribution functions for the RF at Accelerometer C2 for all double cassette tests at pace frequency equal to fifth integer division of first bending mode.*
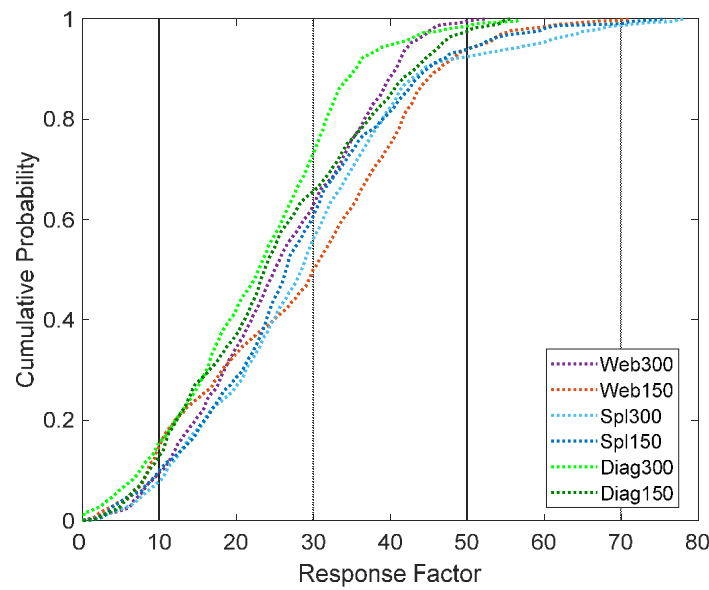
Figure 6-25 *Cumulative distribution functions for the RF at Accelerometer C2 for all double cassette tests at pace frequency of 2 Hz.*
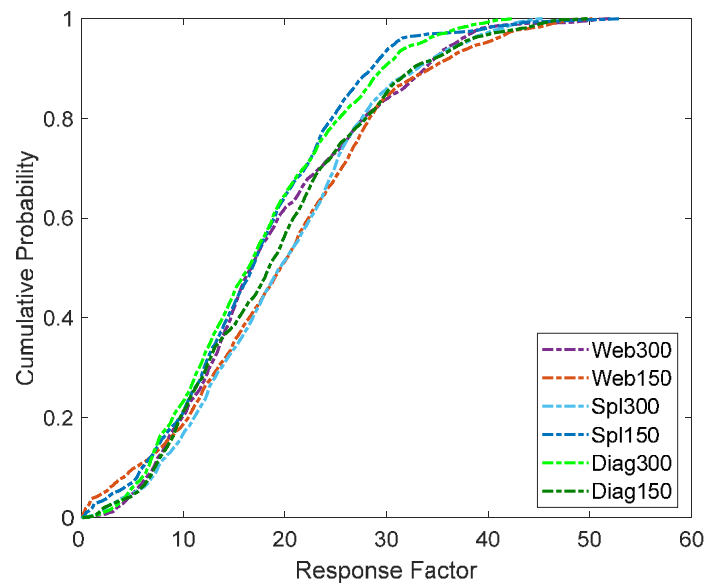
Figure 6-26 *Cumulative distribution functions for the RF at Accelerometer C2 for all double cassette tests at pace frequency of 1.5 Hz.*

6.5 Double cassette finite element model

In Chapter 4, an FE model for a single cassette under flange bearing boundary conditions was validated with modal properties obtained from impact hammer test results. The updated input parameters included the parallel to grain Modulus of Elasticity (MoE) and density of the web members and both parallel to grain and perpendicular-to-gain MoE, density and Poisson's ratio of the flange member. Using these same updated material

210

properties from the single cassette model, a FE model of two adjacent ribbed-deck cassettes (from here on referred to as the 'double cassette model') was created in ANSYS.

6.5.1 Model overview

The element types used for the flange and web were identical to those used for the single cassette model, namely SHELL181. The web elements were positioned at the centreline of the section so that when the element shape was turned on, the thickness of the shell elements at the interface were aligned, as shown in Figure 6-27. The flange nodes at the interface were coincident.
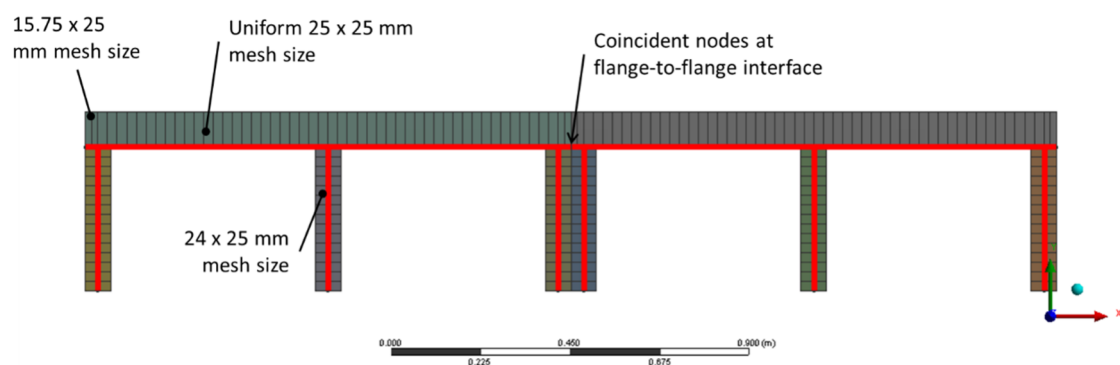
Figure 6-27 *Double cassette model overview*

Along the length of the cassette, the mesh size for the double cassette model was increased to 25 mm from 20 mm in the single cassette model. This size was selected to ensure the spacing of the nodes were consistent or within a reasonable proximity to the spacing of the screw connections in the experimental set-up. For the depth of the web members, however, the 360 mm web depth meant that a mesh size of 24 mm was required. For reference, the mid-span deflection and fundamental frequency for the first five non-spurious modes under 50 Hz for a mesh size of 10, 20, 25, 50 and 100 mm are shown in Figure 6-28. As shown, there is a very small difference (< 0.5%) between results from a mesh size of 20 mm and 25 mm. Further, the difference in natural frequencies between a 10 mm and 25 mm mesh size was less than 2% across all modes and thus was deemed an acceptable mesh size.
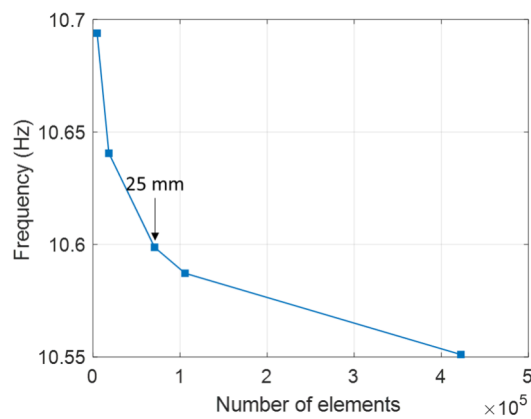
(a) Mode 1
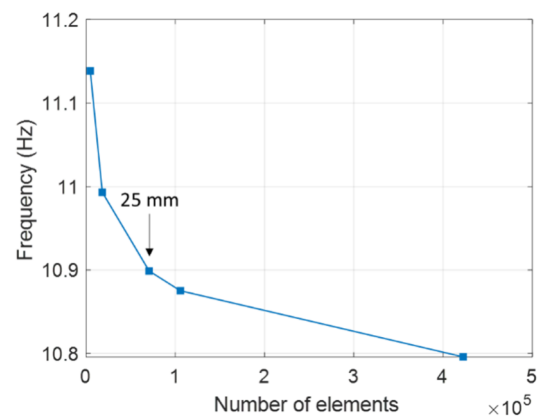
(b) Mode 2
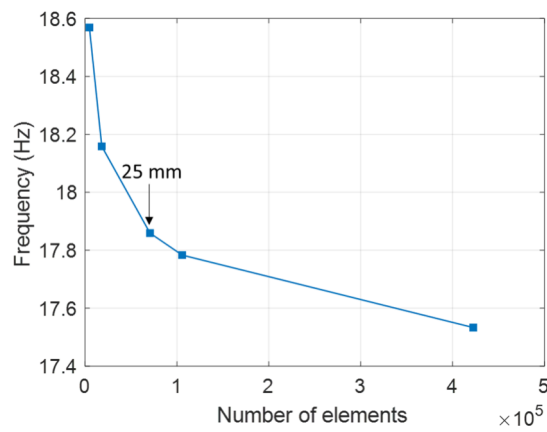
(c) Mode 3
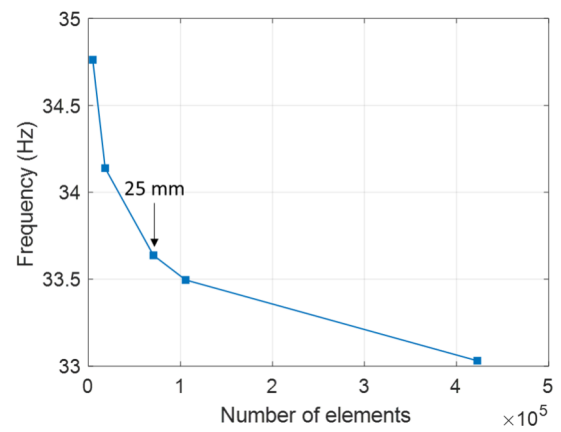
(d) Mode 4
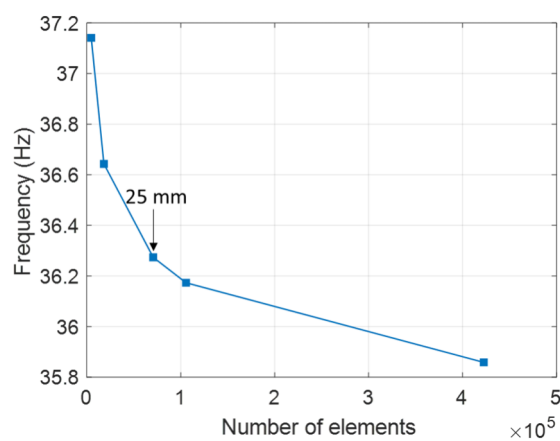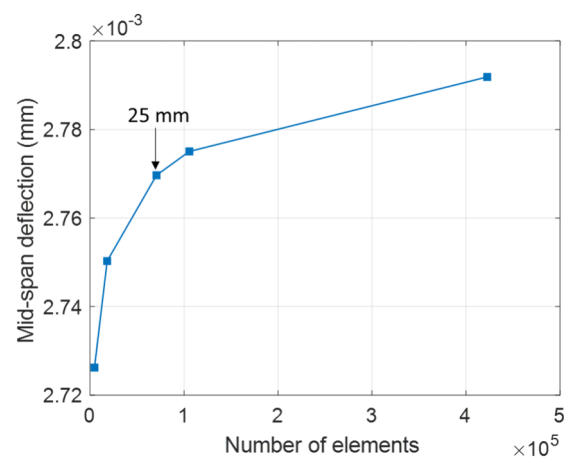
(e) Mode 5

(f) Deflection at mid-span

Figure 6-28 *Sensitivity study of mesh size and frequency of first five modes and mid-span deflection*

6.5.2 Preliminary investigation of screw connections between adjacent cassettes

6.5.2.1 Modelling approach

Modelling two adjacent cassettes introduces an additional modelling consideration in the form of the screw connection between adjacent web and flange members. As detailed in Chapter 3 Section 3.3, experimental tests were first undertaken with the web-to-web connection only (one row of 6.3 mm diameter × 100 mm self-drilling screws at upper and lower web) with screw spacing of 300 (Figure 6-29(a)) and 150 mm c/c. Keeping the web-to-web connection at 150 mm c/c, the effect of a flange-to-flange screw connection was tested in the form of a splice (Figure 6-29(b)) and diagonal screws (Figure 6-29(c)) at a spacing of 300 and 150 mm c/c.

(a)   (b)

(c)

Figure 6-29 *Photo of (a) web-to-web connection at 300 mm c/c; (b) splice connection between flanges with screws at 150 mm c/c; (c) plan view of diagonal screw connections at 150 mm c/c (arrows indicate screw locations).*

Before investigating the modelling aspect of the screws, it is important to first understand the purpose of the connection itself. In ultimate limit state design, web-to-web connections are required not only for shear transfer to form floor diaphragm action but also to ensure that the two joists do not separate during fire exposure (Gerber, Crews & Shrestha 2012). The flange-to-flange connections may be added to provide additional shear transfer to the system. As floor vibration design is only concerned with serviceable rather than ultimate loads, stress concentrations at screw locations or within the screw is not of concern here. As such, both the web-to-web and flange-to-flange screws can be reasonably assumed to act as elastic springs limited by its stiffness in three translational directions. Similar modelling approach have been taken for connecting cross-laminated timber (CLT) floor slabs. For example, in studies on the dynamic behaviour of steel-timber composite floors (Hassanieh et al. 2019), spring elements were used to model the inclined double screws for the CLT-to-CLT slab connection with serviceability stiffness taken as 85% of the static stiffness values based on connection tests conducted by Loss et al. (2016). For half-lap connections, Ussher et al. (2017a) also used zero-length, zero-mass springs with stiffness values in the x-, y- and z-directions based on load-slip tests by Sheikhtabaghi (2015).

In ANSYS, the MATRIX27 element is suitable to represent the screw behaviour as it is an arbitrary element whose geometry is undefined but whose elastic kinematic response is specified by stiffness, damping or mass coefficients in matrix form (ANSYS Inc 2016). The MATRIX27 element differs from the COMBIN14 element used for the flange bearing support condition in that MATRIX27 can be used to connect two coincident nodes (i.e. the direction of action is not defined by the nodal coordinate directions). For this case, only values for the stiffness matrix were input i.e. mass and damping associated with the screw were not considered. The slip modulus (K_{ser}) per shear plane per screw fastener under service load has been calculated as follows as per Eurocode 5 (European Committee for Standardisation 2004):

$$K_{ser} = \rho_m{}^{1.5}d/23 \qquad (6.1)$$

where ρ_m = density of the timber element (kg/m³) and d = diameter of the screw (mm). Based on Equation 6.1, the x-, y- and z-direction translational stiffness values for the MATRIX27 element were calculated as 4.011 kN/mm, respectively. Note, the x-, y- and

z-axis refer to the local element axis which coincide with the global coordinate system as shown in Figure 6-30.
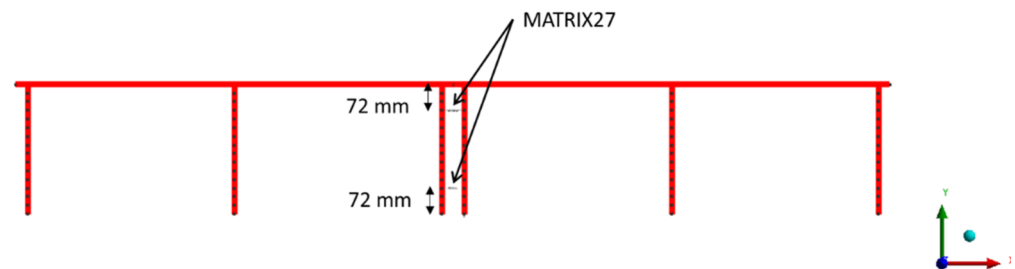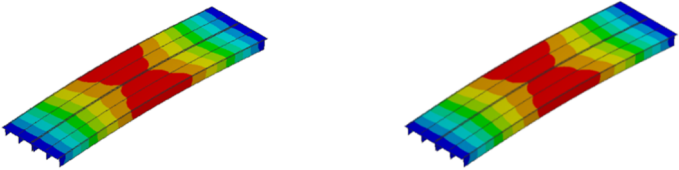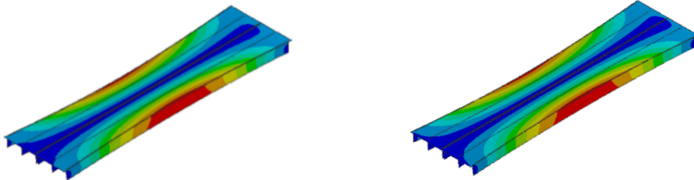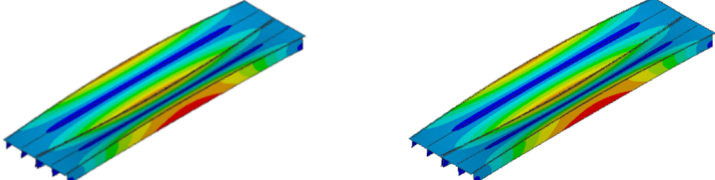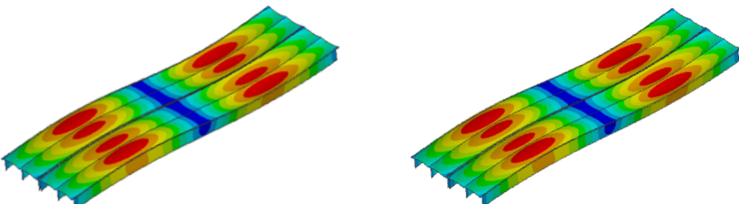
Figure 6-30 *Spring elements at web-to-web screw connection locations*

Another modelling option for the screws would be to simply couple the respective nodes in the translation degrees of freedom only. Coupling specific degrees of freedom for two nodes causes the results calculated for one node to be the same as the other and can be used to model various joint and hinge effects (ANSYS Inc 2016). In essence, this would create an infinitely stiff link between the nodes on each web member defined by the constrained degrees of freedom and would be an upper-bound result for the screw connection.

To mirror the experimental tests, a double cassette model with only web-to-web screws was analysed first. The web-to-web screws were positioned at 72 mm below and above the top and bottom edges of the web member, as shown in Figure 6-30; this was as close to the experimental set-up as possible where the screws were at a 75 mm distance. The spacing of the screws were set as 300 mm. All non-spurious modes and corresponding natural frequencies under 50 Hz for the screws as springs (from here on referred to as 'S-w300' model where 'w' refers to the web-to-web connection and '300' is the spacing) and coupled nodes (from here on referred to as 'C-w300' model) are shown in Figure 6-31 with the mode shape order in parentheses; the % error between natural frequencies has also been calculated. Modes which are common between the models have been presented together for ease of comparison. Similar to the boundary condition investigated in Chapter 4 Section 4.2.3.2, a COMBIN14 'spring' pin-roller configuration was used with x-, y- and z-direction stiffness values of $1{\times}10^5$ N/m, $1{\times}10^8$ N/m and $1{\times}10^6$ N/m, respectively; these values are identical to those used in in Chapter 4 Section 4.2.3.2.

As shown in Figure 6-31, there is very little difference (< 1.8% error) in natural frequency between the S-w300 and C-w300 model which indicates that it is not necessary to model the web-to-web screws with defined translational stiffness properties for modal analysis. As such, nodes for the double cassette model will be coupled translationally where web-to-web screws are used in experimental tests.

	Natural Frequency (Hz)		
Mode (*m,n*)	S-w300	C-w300	% Error
1,1	10.672 (1)	10.672 (1)	0.0
1,2	11.103 (2)	11.131 (2)	-0.3
1,3	15.530 (3)	15.809 (3)	-1.8
2,1	34.655 (4)	34.660 (4)	0.0
2,2	34.821 (5)	34.892 (5)	-0.2

| 1,4 | 37.511 (6) | 37.881 (6) | -1.0 |

| 2,3 | 38.072 (7) | 38.165 (7) | -0.2 |

| 1,5 | 46.490 (8) | 46.589 (8) | -0.2 |

| 2,4 | 48.461 (9) | 48.872 (9) | -0.8 |
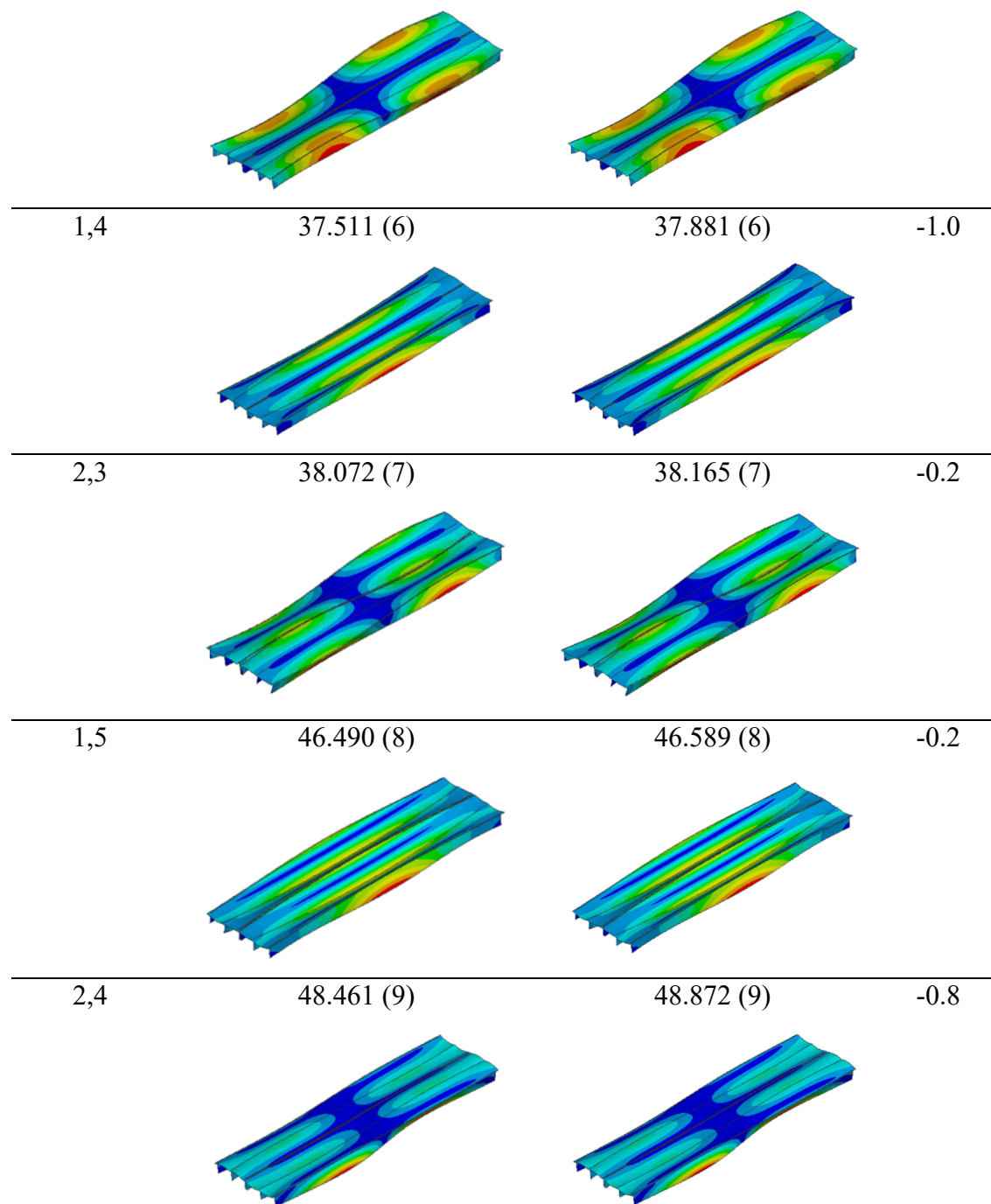
Figure 6-31 *Comparison of mode shapes and natural frequency between 'S-w300' and 'C-w300' model with mode shape order in parentheses. Note m and n refer to the degree of curvature in the longitudinal and transverse directions, respectively.*

6.5.2.2 Screw spacing

Experimental testing also involved varying screw spacing from 300 mm c/c to 150 mm c/c. To understand the influence of the web-to-web screw spacing on the natural frequency and mode shapes of all non-spurious modes under 50 Hz, a second model was

analysed with nodes coupled at 150 mm c/c (from here on referred to as 'C-w150') in line with the top and bottom web connection rows as illustrated in Figure 6-30. Note that although the nodes are coupled at the screw locations, the friction between the adjacent surfaces of the web members, as would exist in reality, was not modelled. Consequently, as a reference case, another model where all nodes between adjacent web members were coupled (from here on referred to as 'C-w') was analysed; this is, in essence, as if the adjacent web members are 'glued' together and no separation can occur.

As shown in Table 6-8, which shows the natural frequencies for all modes up to 50 Hz for both models, there is minimal additional stiffness gained from modelling a closer screw spacing. This result also aligns with experimental test results between C2_Web300 and C2_Web150 test cases as detailed in Section 6.4.1. However, when comparing to the reference case C-w, the coupling of all adjacent web nodes largely influences mode 3 and, to a lesser extent, mode 7; this means that assuming no separation between adjacent web members increases the transverse stiffness and consequently the natural frequencies of modes with high deformation at the connection interface (as shown in Figure 6-31). Nevertheless, since experimental tests for flange-to-flange connections were undertaken with web connections at 150 mm c/c, web-to-web connections were numerically modelled with the same spacing.

Table 6-8 *Natural frequencies for all non-spurious modes under 50 Hz for C-w and C-w150 with % error of C-w150 from C-w and C-w300 model*

Mode	Natural Frequency (Hz)		C-w150 % error from	
	C-w	C-w150	C-w	C-w300
1	10.682	10.672	-0.1	0.0
2	11.138	11.132	-0.1	0.3
3	18.186	15.924	-12.4	0.7
4	34.681	34.665	0.0	0.0
5	34.937	34.897	-0.1	0.2
6	37.938	37.895	-0.1	1.0
7	40.874	38.221	-6.5	0.2
8	45.535	46.638	2.4	0.1
9	48.994	48.891	-0.2	0.9

6.5.2.3 Flange-to-flange connection

To investigate the influence of the flange-to-flange connection in conjunction with the web-to-web connection, three additional models were analysed representing the splice connection in experimental tests: all flange nodes coupled ('C-w150-f'), flange nodes coupled at 300 mm c/c ('C-w150-f300') and at 150 mm c/c ('C-w150-f150'). In all flange connection models, the web-to-web connection was modelled as translationally coupled nodes at 150 mm c/c based on findings in Section 6.5.2.1 and also to replicate experimental tests.

The natural frequency results for all modes up to 50 Hz for all flange-to-flange connection models are shown in Table 6-9. Comparing C-w150-f300 to C-w150, modelling of the flange connection in addition to the web connection mainly influences modes 3 and 7 by 9.2% and 3.9%, respectively. The increase in natural frequency for the first lateral bending mode (mode 3) with the flange-to-flange connection was also found in experimental tests. Reducing the screw spacing to 150 mm c/c had negligible effect to the natural frequencies which is a similar finding to experimental tests. These results indicate that considering the flange-to-flange connection (as translationally coupled nodes) is relevant for the FE model, although the spacing may not be particularly important. For example, even when C-w150-f300 was compared to C-w150-f, there was only an additional 1.9 % and 2.2 % increase in natural frequencies of modes 3 and 7, respectively.

Table 6-9 *Natural frequencies for all non-spurious modes under 50 Hz for C-w150-f300 and C-w150-f150 with % error of C-w150-f300 from C-w150 and C-w150-f150 models*

| Mode | Natural frequency (Hz) | | | C-w150-f300 % error from | | |
	C-w150-f	C-w150-f300	C-w150-f150	C-w150	C-w150-f	C-w150-f150
1	10.681	10.680	10.680	0.1	0.0	0.0
2	11.390	11.312	11.361	1.6	-0.7	-0.4
3	17.733	17.395	17.584	9.2	-1.9	-1.1
4	34.677	34.670	34.674	0.0	0.0	0.0
5	35.057	34.998	35.034	0.3	-0.2	-0.1
6	37.951	37.929	37.942	0.1	-0.1	0.0

7	40.628	39.715	40.176	3.9	-2.2	-1.1
8	45.492	45.392	45.454	-2.7	-0.2	-0.1
9	49.112	49.027	49.078	0.3	-0.2	-0.1

6.5.2.4 Considering the rotational stiffness of flange-to-flange connections

Under ultimate loads, timber screw connections between floor slabs or cassette systems are assumed to act as ideal pin connections with no rotational stiffness. Such an assumption is prudent for strength design, however, considering rotational stiffness under serviceable loads and subsequently in vibration design, may prove beneficial in designing a more efficient floor structure. Considering rotational stiffness of the connections in steel-framed floors is common with the assumption that strains under serviceable loads are not large enough to overcome the friction (Smith, Hicks & Devine 2009). Although there is limited information on the rotational behaviour of timber-to-timber diagonal inclined screws and splice connections, a recent study found that CLT half-lap joints have some degree of rotational stiffness which can be considered in design (Macpherson et al. 2018). Therefore, it was of interest to investigate the effect on the natural frequencies if the flange-to-flange connection was assumed to have rotational stiffness about the z-axis (as per the axes in Figure 6-30). In this case, the flange-to-flange connection nodes were coupled rotationally about the z-direction as well as translationally coupled in all three directions; this model is referred to as 'C-w150-f300r'. As shown in Table 6-10, considering the z-direction rotational stiffness has a large influence on the first lateral bending mode, increasing the frequency by nearly 16% or approx. 3 Hz. There was minimal influence for all other modes.

Table 6-10 Natural frequencies for all non-spurious modes under 50 Hz for C-w150-f300r with % error from C-w150-f300.

	Natural Frequency (Hz)	% error from
Mode	C-w150-f300r	C-w150-f300
1	10.691	0.1
2	11.312	0.0
3	20.144	15.8
4	34.749	0.2
5	34.999	0.0

6	37.928	0.0
7	40.529	2.0
8	45.874	1.1
9	49.028	0.0

6.5.3 Correlation of FE model to measured modal properties

Based on the preliminary investigation of modelling both web-to-web and flange-to-flange connections, an initial FE model was created which included translationally coupled web-to-web connections at 150 mm c/c and flange-to-flange connections at 300 mm c/c (C-w150-f300). The results from the FE model (Table 6-9) were compared to the measured results of the C2_Spl300 test for the following reasons:

- As detailed in Section 6.4.1, modal properties of C2_Spl300 were very similar to C2_Spl150, C2_Diag300 and C2_Diag150 tests.
- It is very unlikely in construction that web-to-web connection would be used on its own.
- Comparing the constructability of the splice to the diagonal screw connections, the splice connection would be quicker to implement on-site as it does not require a jig to guide the screws at a certain angle.

The measured natural frequencies up to 50 Hz for C2_Spl300 test case and the *NFerror* and *MACerror* compared to C-w150-f300 model is shown in Table 6-11; the mode order from measured results is shown in parentheses. Although the measured modal properties were detailed in Section 6.4.1, the natural frequencies have been reproduced here for ease of comparison.

The purpose of the model updating procedure is to obtain a sufficiently validated model for use in a multi-cassette model to investigate the effect of certain parameters on the modal properties and floor response (Chapter 7). As such, higher importance was placed on correlating modes which were less than approx. 20 Hz (i.e. FE modes $1-3$). As shown in Table 6-11, natural frequencies of modes 1 and 2 were very close to measured results with an *NFerror* of less than 0.5%; *MACerror* was also small indicating that the measured mode shapes are similar to those identified in the FE model. However, despite high mode shape correlation of FE mode 3 to the experimental mode 4 (first lateral bending mode), the *NFerror* was still significant. Consequently, the measured natural frequencies and mode shape amplitudes were compared to the C-w150-f300r model as it was found in the preliminary investigation that considering the rotational stiffness about the z-direction of the flange-to-flange connection influenced the first lateral bending mode; these results are also listed in Table 6-11. As shown, introducing the z-direction rotational stiffness

222

reduces the *NFerror* to less than 5% which is a reasonable correlation to the measured result. The *MACerror* also reduced to 0.03 from 0.05. Although of lower importance, FE modes 6 and 9 also had low *NFerror* at 2% and 0.3%, respectively, as well as a low *MACerror* at 0.32 and 0.16, respectively. The highest dissimilarities in both natural frequencies and mode shape occurred when comparing FE modes 4, 5 and 7 with experimental modes 5, 6 and 8. However, the uncertainty of these modes were also highlighted in Section 6.4.1 where the mode shapes were difficult to identify. Additional model updating in the form of adjusting the spring stiffness' of the pin-roller boundary condition may further improve the accuracy of the numerical model. However, it was deemed that since the *NFerror* for the modes less than 20 Hz were less than 1%, the accuracy of the C-w150-f300r model was sufficient enough.

The MAC diagram comparing the numerical and measured mode shapes is shown in Figure 6-32; the mode numbers correspond to the mode order obtained experimentally and numerically, as detailed in Table 6-11. Experimental mode 1 was not numerically identified while FE mode 8 was not experimentally identified and therefore were not included in the diagram. Figure 6-32 reveals that experimental mode 6, which visually looks like both cassettes are active, has in fact a moderate correlation to both mode 4 (MAC value = 0.52) and 5 (MAC value = 0.49). In the FE model, modes 4 and 5 were only separated by approx. 0.3 Hz which may mean these modes were too close to distinguish in experimental testing and post-processing. Nevertheless, it was deemed that due to the high correlation for the first three modes, the C-w150-f300r was an acceptable model to be used for investigation of walking response and subsequent parametric studies.
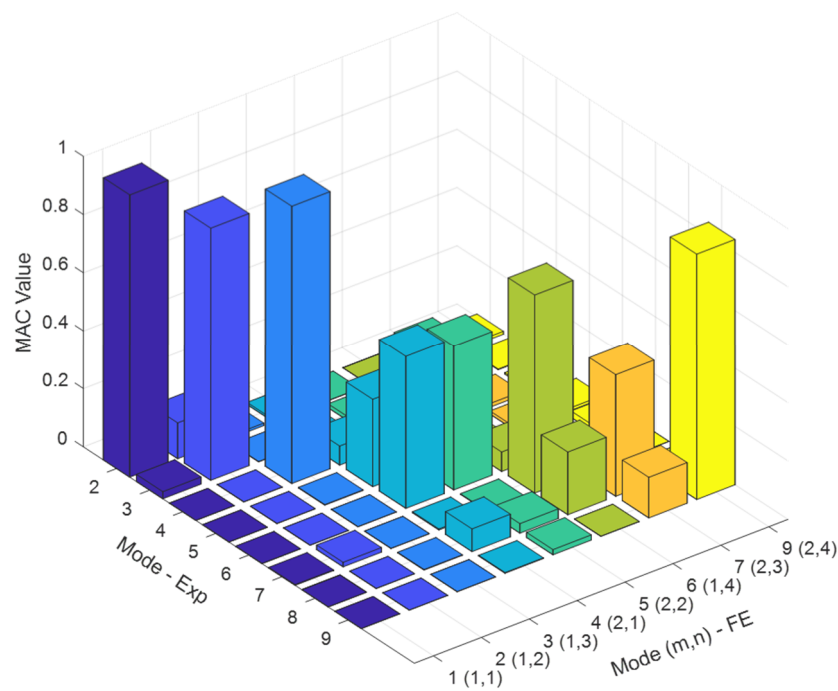
Figure 6-32 *MAC diagram for eight common modes obtained experimentally and numerically in C-w150-f300*

Table 6-11 *Correlation between Spl300 and numerical models C-w150-f300 and C-w150-f300r*

FE mode (*m,n*)	f^{exp} (Hz)	C-w150-f300		C-w150-f300r	
		NFerror (%)	*MACerror*	*NFerror (%)*	*MACerror*
-	9.911 (1)	-	-	-	-
1 (1,1)	10.691 (2)	-0.1	0.03	0.0	0.03
2 (1,2)	11.275 (3)	0.4	0.13	0.4	0.13
3 (1,3)	21.17 (4)	-17.8	0.05	-4.8	0.03
4 (2,1)	32.797 (6)	5.7	0.59	6.0	0.59
5 (2,2)	27.931 (5)	25.3	0.48	25.3	0.48
6 (1,4)	37.173 (7)	2.0	0.32	2.0	0.32
7 (2,3)	43.976 (8)	-9.7	0.58	-7.8	0.58
8 (1,5)	-	-	-	-	-
9 (2,4)	49.167 (9)	-0.3	0.16	-0.3	0.16

Note: *m* and *n* refer to the degree of curvature in the longitudinal and transverse directions, respectively.

6.5.4 Simulated walking response and comparison to measured results

As an additional investigation into accuracy of the numerical model, the walking loads deemed to most accurately predict the floor response from Chapter 5 were applied to the C-w150-f300r double cassette model. These models included the Chen et al. (2019) single footfall trace load function (LM2) which provided the complete time-history response, and the CCIP-016 effective impulse method (LM1). The predicted floor response were compared to measured results as detailed Section 6.4.1.
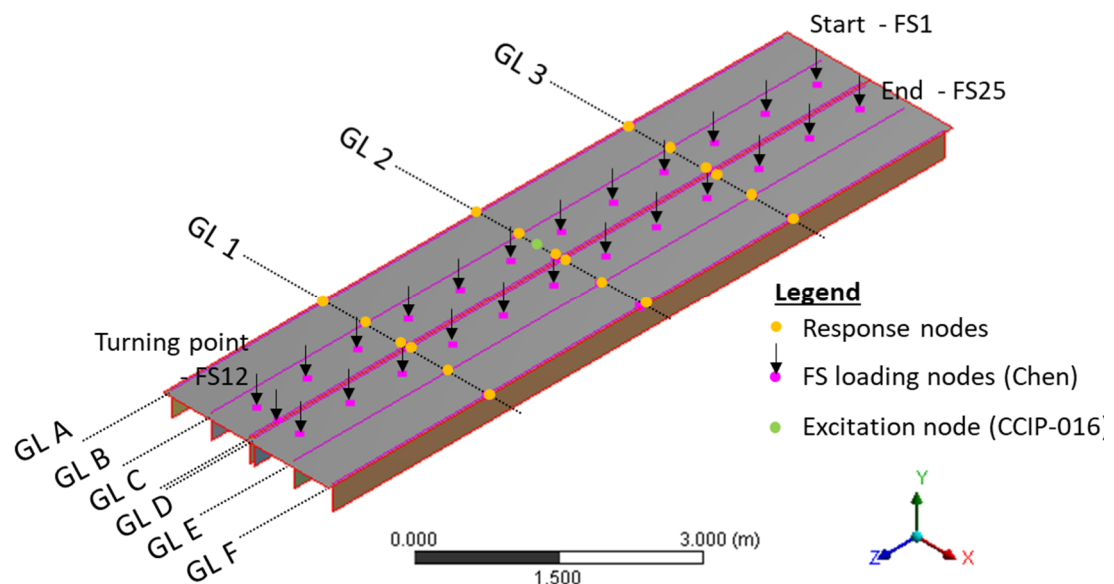
Figure 6-33 *Overview of walking path, footstep loading and response nodes on double cassette model*

Figure 6-33 reveals the walking path set in the numerical model with a step length of 0.75m to coincide with the 25 mm mesh size of the flange member. A walker mass of 75 kg was taken to match the mass of W2b despite W1 generally inducing a higher response due to better synchronisation with the metronome. The walking pace assumed in the numerical model was 2.14 Hz which is the fifth integer division of the first measured bending mode; this is the same walking pace used in experiments. The 'NoIntra' loading from LM2 detailed in Chapter 5 Section 5.2.3 was used i.e. the intra-subject coefficient was set to 1.0. For the CCIP-016 method, the effective impulse was applied along GL 2 between response nodes B2 and C2 and is in line with the walking path; this node is also shown in Figure 6-33.

Since the measured frequency of the first bending mode was 10.69 Hz (and thus would be classified as a 'transient response' floor based on design guides), the maximum transient vibration value (MTVV) from the running 1s RMS averaging window of the velocity time-history response was used to determine the maximum response factor (RF). The CCIP-016 method also uses the velocity response to determine the maximum RF. The measured acceleration response was therefore integrated to obtain the velocity time-history to ensure the evaluated RF were obtained from the same response parameter.

Table 6-12 *Predicted response based on Chen et al. (2019) single footstep loading and measured response at accelerometer C2*

	FE – load model		Measured - walker	
	LM2 'NoIntra'	CCIP-016	W1	W2b
RF	83	49	92	51

The maximum predicted RF at response node C2 (coinciding with accelerometer C2) from both walking load models and the measured results are shown in Table 6-12. As shown, the maximum measured response from both walkers (produced by W1) is 92 which is 12% greater than predicted response using LM2 'NoIntra'. This indicates that the C-w150-f300r is an appropriately validated model. The simulated velocity response and velocity time-history integrated from measured acceleration results is shown in Figure 6-34 (a) and (b) for W1 and W2b, respectively. These plots highlight the effectiveness of W1 in exciting the floor at resonance in comparison to W2b.

On the other hand, the predicted response using the CCIP-016 method significantly under-predicted the floor response by approx. 47%; this was substantially larger than the under-prediction of 8% for the single cassette test as detailed in Chapter 5. These results indicate that assuming a transient floor response is not accurate which is further reinforced through the measured time-history response in Figure 6-34. All modes up to $2 \times f_1 = 21.38$ Hz were included in the CCIP-016 method as per the guideline; these modes are shown in Table 6-13 for reference including the mass-normalised mode shape amplitudes at the response (denoted as $\mu_{r,n}$) and excitation (denoted as $\mu_{e,n}$) nodes for each mode n.
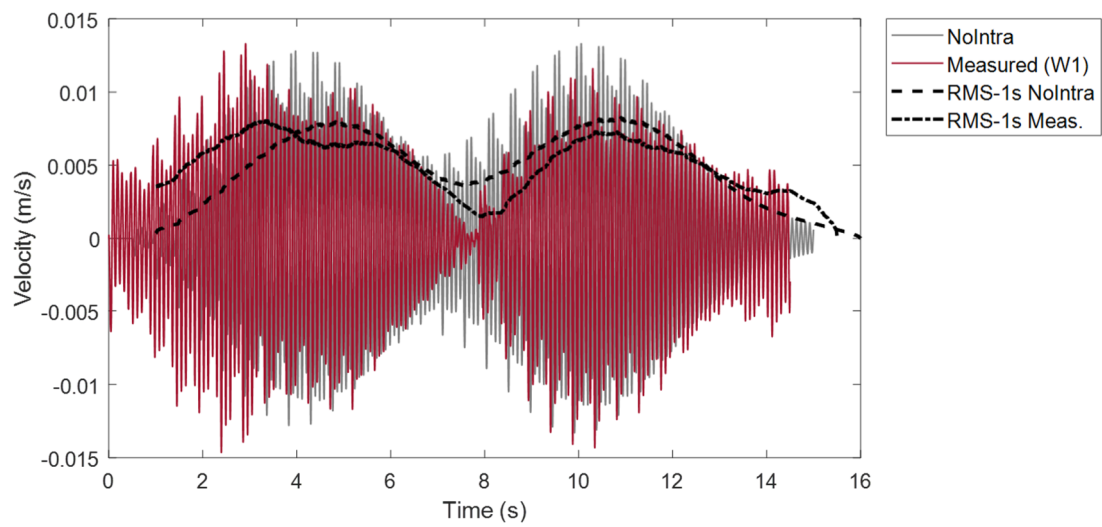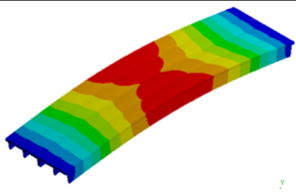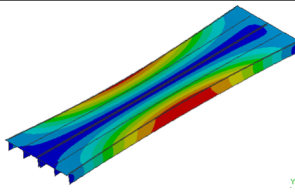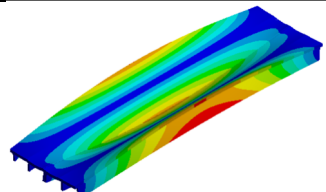
(a) W1
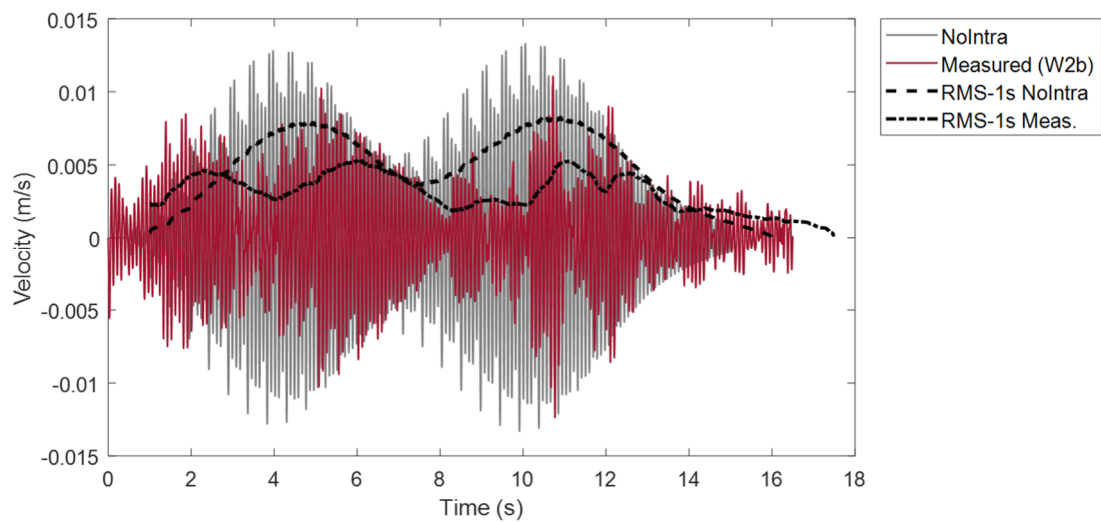
(b) W2b

Figure 6-34 *Simulated velocity response using LM2 'NoIntra' and velocity time-history response integrated from measured acceleration response at C2*

Table 6-13 Summary of modes from C-w150-f300r considered in CCIP-016 method

Mode	1	2	3
Mode shape			
f_n (Hz)	10.691	11.312	20.144
M_n (kg)	845.5	351.3	218.6
$\mu_{r,n}$	0.0316	-7.627×10^{-6}	-0.0433
$\mu_{e,n}$	0.0320	-0.0132	-0.0263

The cumulative distribution of the running RF for LM2 'NoIntra' and running RF based on the velocity response integrated from the measured acceleration results at C2 for the Spl300 test are shown in Figure 6-35. The plot shows similarities between the simulated and experimental results, particularly for W1, which further highlights the appropriateness of Chen et al. (2019) step-by-step walking model.
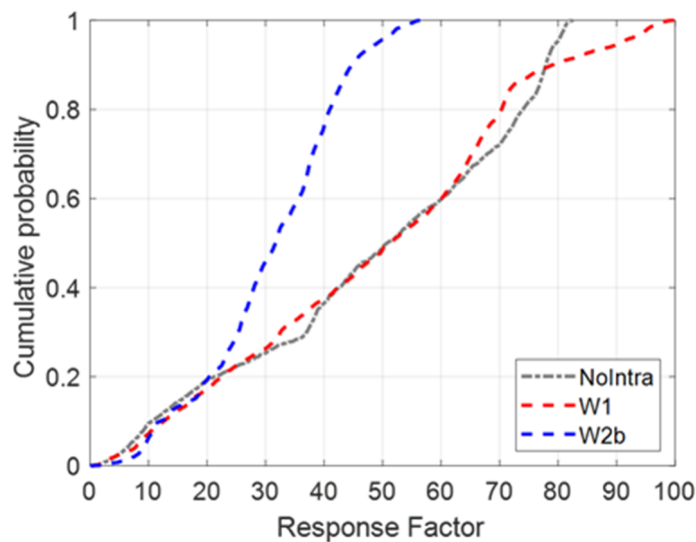
Figure 6-35 Cumulative distribution plot of measured Spl300 ('R' Hz) for both walkers and LM2 NoIntra at C2

6.6 Concluding remarks

This chapter presented the effect of certain design variables on the modal properties and floor response of a timber cassette floor. These design variables included the influence of cassette-to-cassette connections such as a splice or diagonal screws, screw spacing and the addition of an elastic interlayer along the flange bearing support. The following conclusions can be drawn from the experimental investigations:

- There is negligible benefit to modal properties and floor response with reduced screw spacing from 300 to 150 mm c/c for both web-to-web and flange-to-flange connections.

- The addition of the flange-to-flange connection in conjunction with the web-to-web connection provides additional stiffness for the first lateral bending mode, particularly when using a splice connection where natural frequency increased by 7%. For other modes, the differences in the modal properties between using either a splice or diagonal screw connection was negligible.

- From the cumulative distribution of floor response it was observed that the floor response is generally lower for a longer duration of the walking event when using diagonal screws rather than the splice connection. However, no clear trend was observed when comparing the maximum floor response.

- Damping ratio remained within the range of $1 - 2\%$ for all modes regardless of the screw spacing or whether a splice or diagonal screw connection was used.

- The addition of elastic interlayer Sylomer® (90% utilisation under dead load) with the flange bearing support condition significantly increased the damping ratio for modes 1 and 2 to approx. 4.7% and 6.9%, respectively. Consequently, the maximum RF of the accelerometer at the centre of the floor (accelerometer C2) reduced by up to 78%. The Sylodyn® interlayer which has smaller damping properties also resulted in a reduced response although not to the same extent as the Sylomer interlayer.

- Increasing the ratio of utilisation of the elastomer through the addition of added mass along the support ends, in general, further reduces the floor response.

Based on the double cassette tests, a finite element model was developed, and results correlated to measured results the Spl300 test. An investigation into the modelling of the

screw connections between the adjacent webs and flange members resulted in the following conclusions:

- There is negligible difference in natural frequency of all modes when modelling screws as springs with defined translational stiffness properties compared to translationally coupling the nodes. As a result, for simplicity, locations of web-to-web screws can be modelled as translationally coupled nodes rather than a spring element.

- Minimal difference in natural frequencies when considering a reduced screw spacing from 300 to 150 mm c/c in the numerical model.

- Through comparison of measured and numerically obtained natural frequencies, the flange-to-flange connection appears to have some rotational stiffness properties about the axis parallel to the span of the floor. Although, this would need to be confirmed with further connection tests.

In addition, a comparison between measured walking responses and the predicted response using Chen et al. (2019) step-by-step walking load on the calibrated double cassette model provided further evidence of the accuracy of the load model. On the other hand, the CCIP-016 effective impulse method was found to significantly underestimate floor response (by 47%) of the double cassette.

Chapter 7

Numerical Analysis of Multi-Cassette Floor Model and Parametric Studies

7.1 Introduction

A 9 m × 9 m column grid layout is common practice for open-plan commercial buildings in Australia, regardless of the building material. These dimensions are based on architectural demands, car park set-out in the basement levels, flexibility of internal office layout and freedom of worker movement (Timber Development Association & Forsythe 2015). To achieve competitiveness with conventional building materials, this floor grid is often used as a benchmark for timber floor structures.

In this chapter, a full-scale (9.19 m × 9.76 m) multiple cassette numerical model is developed with reference to the calibrated single-cassette floor model in Chapter 4 and the numerical modelling of the cassette-to-cassette connections in Chapter 6. The aim of this chapter is to undertake parametric studies to investigate the influence of common design considerations on the modal properties and floor response under walking excitation. The design considerations include varying damping ratio, increasing stiffness in the direction parallel to the span and increasing the span-to-depth ratio.

7.2 Multiple cassette model

7.2.1 Model overview

Drawing from the calibrated single and double cassette models from Chapters 4 and 6, respectively, a multiple cassette model was developed to investigate the effect of certain design parameters on the natural frequencies and floor response to walking. Eight identical 1.22 m wide cassettes were modelled to create a 9.19 m × 9.76 m floor grid which is similar to a typical commercial building floor grid. The material properties based on the model updating procedure in Chapter 4 were used with each cassette having identical properties. Connections between cassettes were modelled based on the C-w150-f300r model detailed in Chapter 6. This model involved translationally coupling nodes at the upper and lower sections of adjacent web members at 150 mm spacing while coincident flange nodes were coupled translationally in all directions and rotationally about the z-axis (parallel to span) at 300 mm spacing. The calibrated spring support boundary conditions from the flange bearing support detailed in Chapter 4 were used. Similar to the double cassette model, a mesh size of 25 × 25 and 25 × 24 was chosen for the flange and web members, respectively; this resulted in a total of 282,688 elements. An overview of the multiple cassette model is shown in Figure 7-1.
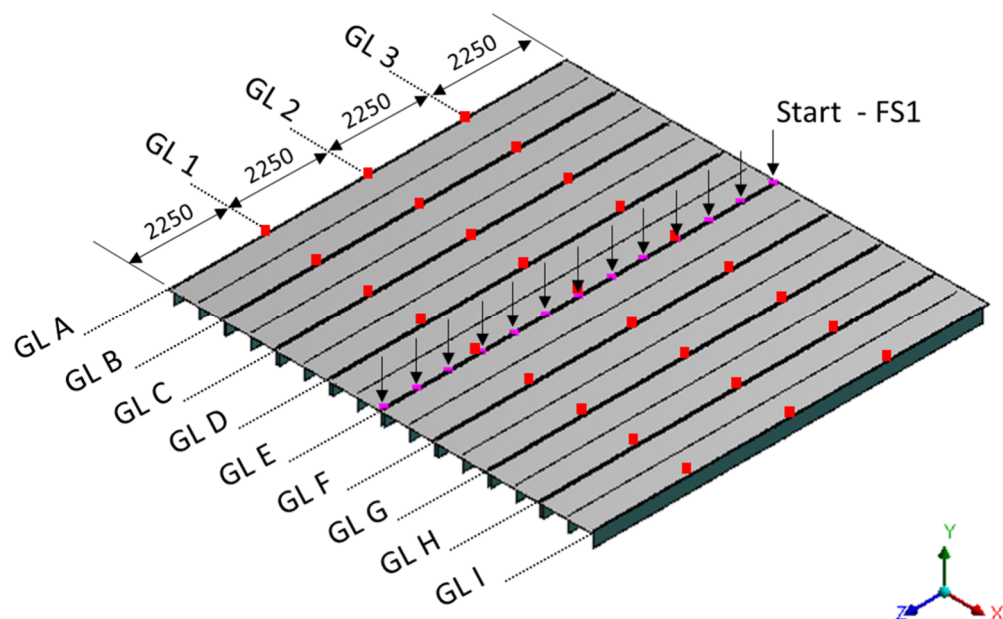
Figure 7-1 *Overview of multiple cassette model including response node locations (red squares) and single footstep loading locations (pink squares with arrows along grid line E).*

7.2.2 Investigated parameters

The three investigated parameters and the reasons behind their selection are listed below with an overview of all analysed models shown in Table 7-1 (to be viewed in conjunction with Table 7-2 for cross-section details). Model 1 has the same cross-section details as the fabricated cassette and is considered as the reference case for all variables; the cross-section is shown in Figure 7-1(a).

1. Increased damping ratio – this was decided as an important parameter based on the results of experiments conducted with the Sylodyn® and Sylomer® interlayers at the supports (as detailed in Chapter 6 Section 6.2) where it was found that an increased damping ratio can influence the floor response. The damping ratios investigated were 1%, 2% and 4%.

2. Reduced joist spacing – having four (386 mm centre-to-centre spacing) rather than three joists (578.5 mm centre-to-centre spacing) per cassette increases the stiffness of the floor in the span direction. The cross-section details of Model 4 are shown in Figure 7-1(b). The frequency of bending modes are expected to increase, however the additional stiffness in the span direction increases the orthotropic behaviour of the system which can lead to closer spaced modes (Smith & Chui 1988).

3. Increased span-to-depth ratio – the current cross-section with 90 × 1220 mm flange and 360 × 63 mm web members results in a total floor depth of 450 mm. However, other off-the-shelf sections would also have an acceptable ultimate limit state design. Two other floor cross-sections were considered, as shown in Figure 7-1(c) and (d), which resulted in a decreased floor depth of 405 mm and 390 mm for Model 5 and 6, respectively. This led to an increased span-to-depth ratio as shown in Table 7-1.

Table 7-1 *Overview of all analysed models for parametric studies*

Model	Variable	Cross-section (Table 7-2)	No. of webs in each cassette	Damping ratio	Span-to-depth ratio
1	Damping ratio	A		0.01	
2		A	3	0.02	20
3		A		0.04	
4	Joist spacing	A	4	0.01	20
5	Span-to-depth ratio	B	3	0.01	22
6		C		0.01	23

Table 7-2 *Summary of cross-sections considered*

Cross-section	Cross-section properties (mm)				Overall floor depth (mm)
	Flange		Web		
	Depth	Breadth	Depth	Breadth	
A	90	1220	360	63	450
B	45	1220	360	63	405
C	90	1220	300	63	390

(a) Model 1

(b) Model 4

(c) Model 5

(d) Model 6
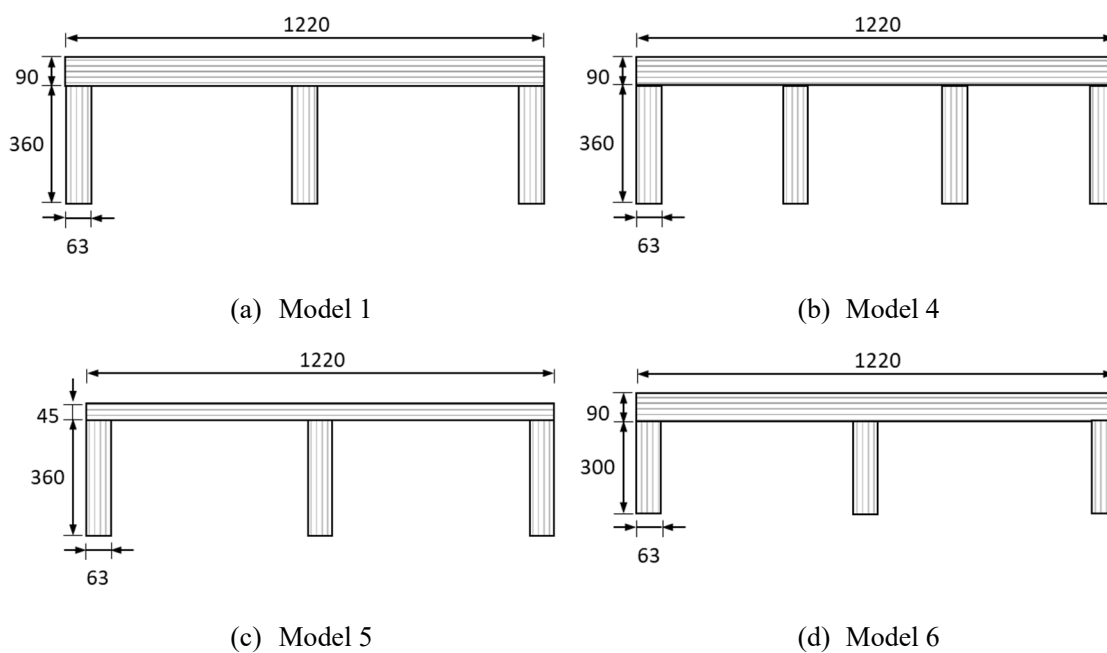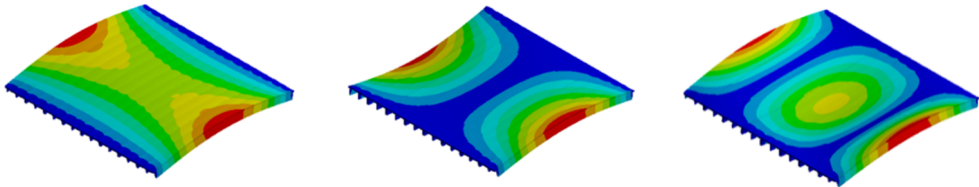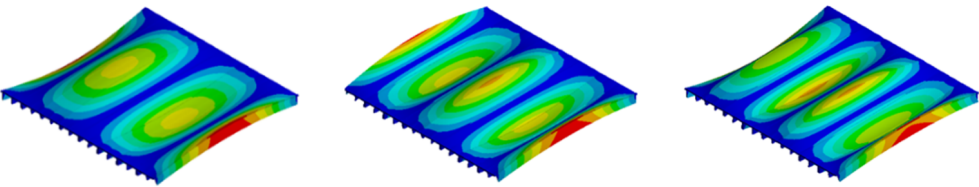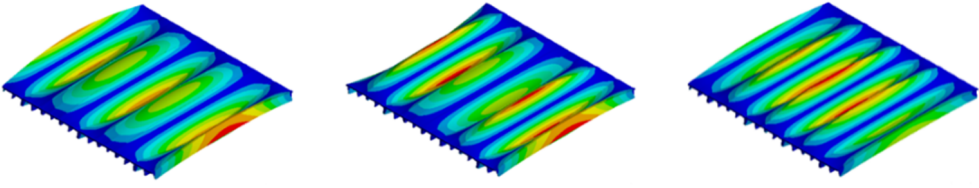
Figure 7-2 *Cross-section details of different models as per Table 7-1*

7.2.3 Modal properties of reference case

A modal analysis of the reference case resulted in a total of 33 non-spurious modes under 50 Hz including nine modes under 30 Hz. These results are in contrast to the five non-spurious modes under 50 Hz with two modes under 30 Hz for the single cassette. The mode shapes, natural frequencies and modal masses associated with each of the nine modes are shown in Table 7-3; modal properties for the common modes between the multiple cassette model and single cassette test are also shown in italics for ease of comparison.

The fundamental frequency of the single cassette (C1_Flange) and Model 1 are close to identical indicating that the ratio of stiffness and mass remained the same as additional cassettes were added. This was in line with findings from the double cassette tests. The ratio of modal mass of the first mode to the total mass of the system was 0.51 and 0.15 for the single cassette and Model 1, respectively. The modal mass for the single cassette is similar to the theoretical equation of the modal mass for a simply-supported uniform beam (i.e. $m/2$), while the modal mass for the multiple cassette model is slightly less than the theoretical equation for a simply-supported plate (i.e. $m/4$). The reduced modal mass for mode 1 is a result of the non-ideal spring boundary conditions. Separation between modes has also decreased from the single cassette where there is just 0.32 Hz between the first and third modes.

Table 7-3 *Overview of modal properties for Model 1 for all modes under 30 Hz. Modal properties for common modes to single cassette tests are also noted in italics for ease of comparison; modal masses were taken from the calibrated FE model.*

Mode	1	2	3
f_n *(Hz)*	*10.50*	*11.21*	*42.70*
M_n *(kg)*	*473*	*80*	*193*
f (Hz)	10.45	10.47	10.77
M_n (kg)	1110	1778	1520

Mode	4	5	6
f (Hz)	11.78	13.55	15.93
M_n (kg)	1506	1321	1063

Mode	7	8	9
f (Hz)	18.59	21.22	23.21
M_n (kg)	943	939	1654

7.2.4 Floor response of reference case

A single footstep load model based on Chen et al. (2019) as detailed in Chapter 5 was applied to the multiple cassette model to simulate a single person walking across the floor along the span direction, as shown in Figure 7-1. Similar to the walking load application for the double cassette model, a 0.75 m step length was assumed resulting in a total 13 footsteps across the floor span. The walker mass was taken as 76 kg representing the mass of an average walker (Smith, Hicks & Devine 2009). The load model considers the effects

of intra-subject variability for the DLF and phase angle of each harmonic as determined using normal distribution parameters. However, for this case only one set of coefficients were used (i.e. one pedestrian) as the objective of this study was to investigate the influence of design parameters on the floor response.

Two step frequencies were considered: an average walking pace of 2 Hz and the fifth integer division of the fundamental frequency (referred to as 'R' Hz). In this case, the first mode was a bending mode, as shown in Table 7-3 resulting in an 'R' of 2.09 Hz. Figures 7-3 (a) and 7-4 (a) show the maximum RF contour for all response nodes (as shown in Figure 7-1) for 2 Hz and 2.09 Hz, respectively. As shown, for both cases, the maximum response occurs at the centre of the floor where the RF reaches 25 and 34 for 2 Hz and 2.09 Hz walking pace, respectively. The 'R' Hz response is approximately 20% of the measured response obtained from walking tests on the single cassette flange bearing set-up (as detailed in Chapter 5). The lower response from the multiple cassette model is a result of the higher modal masses coupled with smaller mode shape amplitudes. Note that since the fundamental mode was less than 10.5 Hz (cut-off frequency recommended by CCIP-016), the RF was calculated from the maximum transient vibration value of the frequency-weighted 1s RMS acceleration rather than the velocity. For consistency, all other RF contour plots presented in this chapter have been obtained using a similar approach.

The total VDV was also calculated using the weighted acceleration response for the single walking event as per Equation 2.26. A 'reasonably busy' environment was considered where one person was assumed to cross the floor every minute over a 8 h work day (Ellis 2001). The colour bands for the contour plots, as shown in Figures 7-3 (b) and 7-4 (b) were selected based on the VDV limits for commercial buildings in BS 6472 (2008a) as shown in Table 2-3. These limits are: $0.4 - 0.8$ m/s$^{1.75}$ for low probability of adverse comment, $0.8 - 1.6$ m/s$^{1.75}$ for adverse comment possible and $1.6 - 3.2$ m/s$^{1.75}$ for adverse comment probable. For values below 0.4 m/s$^{1.75}$, adverse comment is not expected while above the 3.2 m/s$^{1.75}$, adverse comment is very likely. The merit of plotting a VDV contour is that the engineer can directly visualise which the degrees of possibility of adverse comment across the floor plate. As shown in Figure 7-3 (b), a person walking across the floor every minute with a pace frequency of 2.0 Hz will only result in a very

small portion of the floor where adverse comment is possible. Figure 7-4 (b) reveals that for occupants located on the centre and free edges of the floor, adverse comment is possible if a person walks at the fifth integer division of the fundamental frequency.
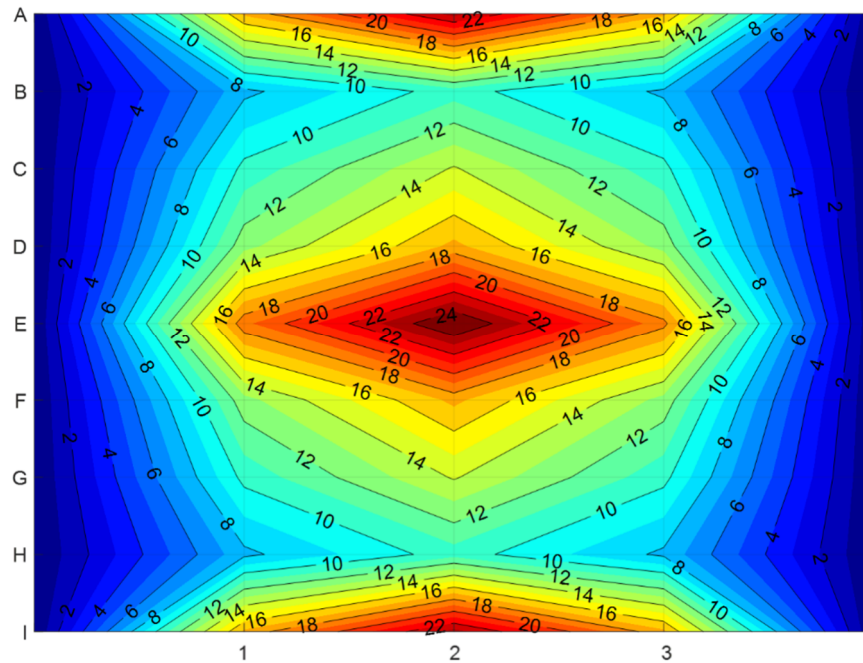
(a) Maximum RF contour plot
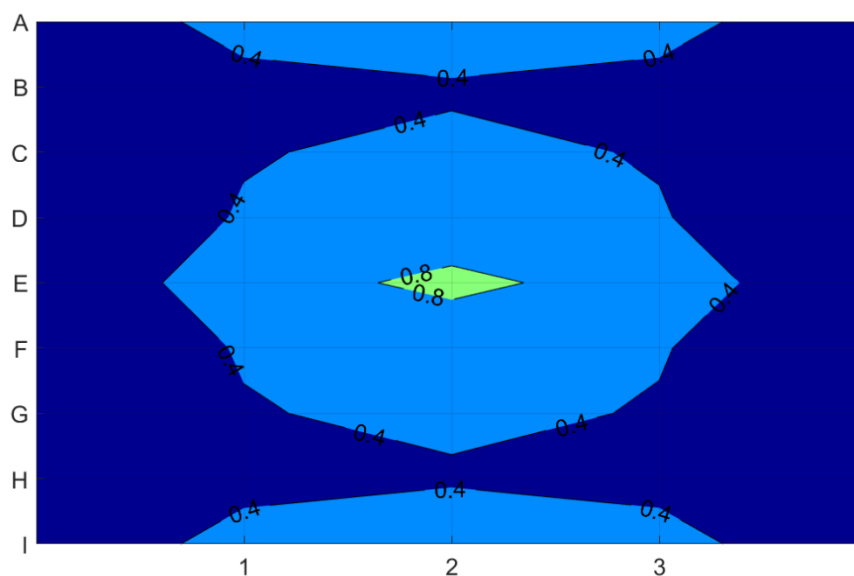
(b) Total VDV contour plot

Figure 7-3 *Model 1 at 2 Hz pace frequency*
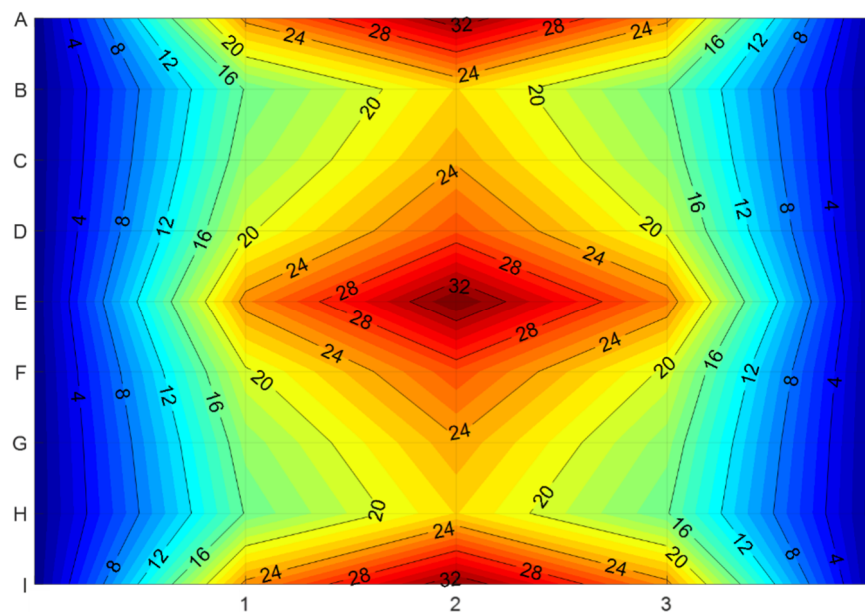
(a) Maximum RF contour plot
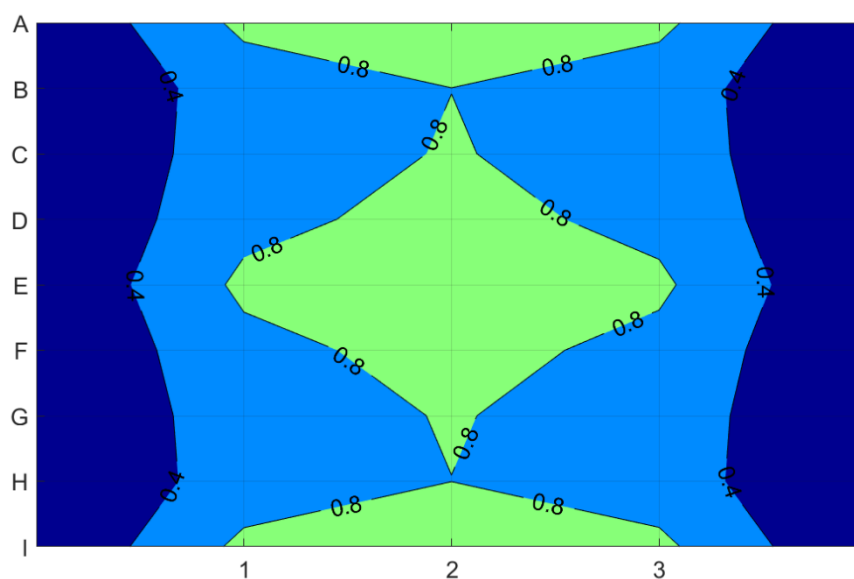
(b) Total VDV contour plot

Figure 7-4 *Model 1 at 2.09 Hz ('R' Hz) pace frequency*

7.3 Influence of higher damping ratio

The same transient analysis performed for Model 1 was also performed for Models 2 and 3 with the damping ratio increased to 2% and 4%, respectively. As the modal properties were the same between the three models, the walking pace was kept consistent at the fifth integer division of the fundamental mode (2.09 Hz). The maximum RF contour plots for

Models 2 and 3 are shown in Figures 7-5 (a) and 7-6 (a), respectively; note for ease of comparison between Models 1, 2 and 3, the contours have been plotted with a colour scale matching the maximum RF across all three models. As shown, the maximum RF reduces by approx. 17% for Model 2 (RF = 28) and 36% for Model 3 (RF = 22) indicating that the damping ratio plays a large role in the floor response for timber cassette floors. A similar result was found in test results with the elastic interlayer at the support locations as detailed in Chapter 6.

Understanding the cumulative distribution of the weighted acceleration response (and RF) provides further insight into the duration that the floor will experience the high levels of vibration. Figure 7-7 shows the cumulative distribution of the floor response as the simulated walker travels across the floor. Based on the 2.09 Hz pace frequency and 0.75 m step length, the duration of the walker traversing the floor is 6.3 s. The plot shows that although the maximum response for Model 1 (considering 1 % damping ratio) is 34, for 70% of the walking duration the response will be less than RF = 28. Similarly, for a 2% damping ratio, the response will be less than 24 for 70% of the time while for a 4% damping ratio, the response will be less than 18 for 70% of the walking duration.

Similarly, the total VDV contour plots as shown in Figures 7-5 (b) and 7-6 (b) reveal that the increasing damping ratio significantly reduces the floor area where adverse comment is possible. Increasing the damping ratio to 2% damping ratio reduces this area from 25% of the total floor area to only 4.3% of the total floor area. A further increase of damping ratio to 4% reduces this area to less than 1% of the total floor area.
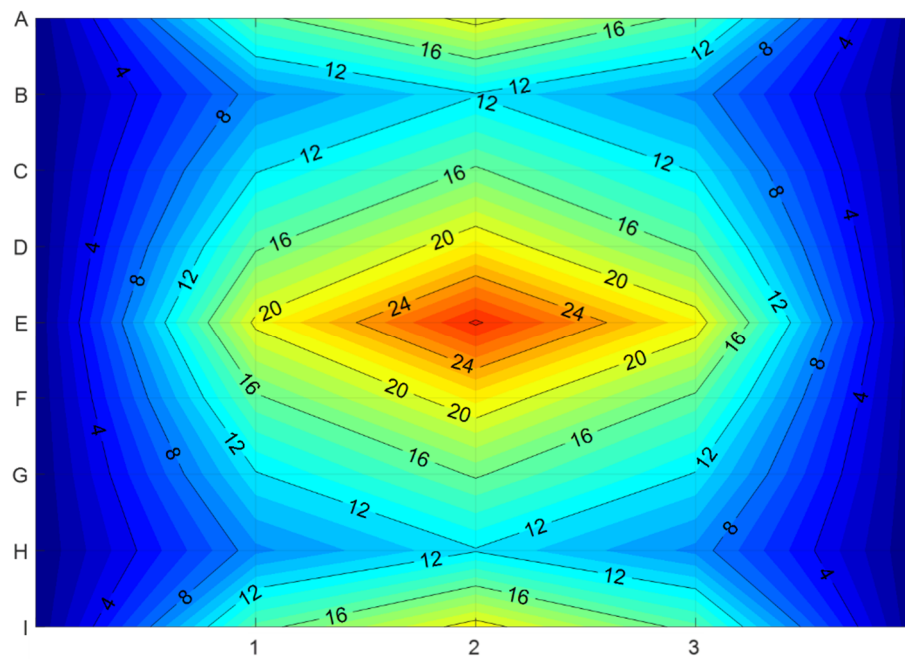
(a) Maximum RF contour plot
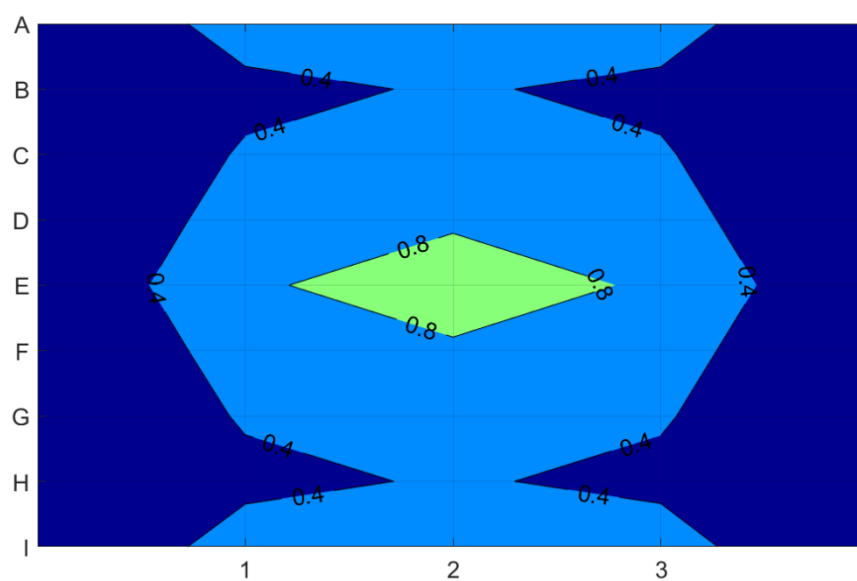
(b) Total VDV contour plot

Figure 7-5 *Model 2 (2% damping ratio) at 2.09 Hz ('R' Hz) pace frequency*

(a) Maximum RF contour plot
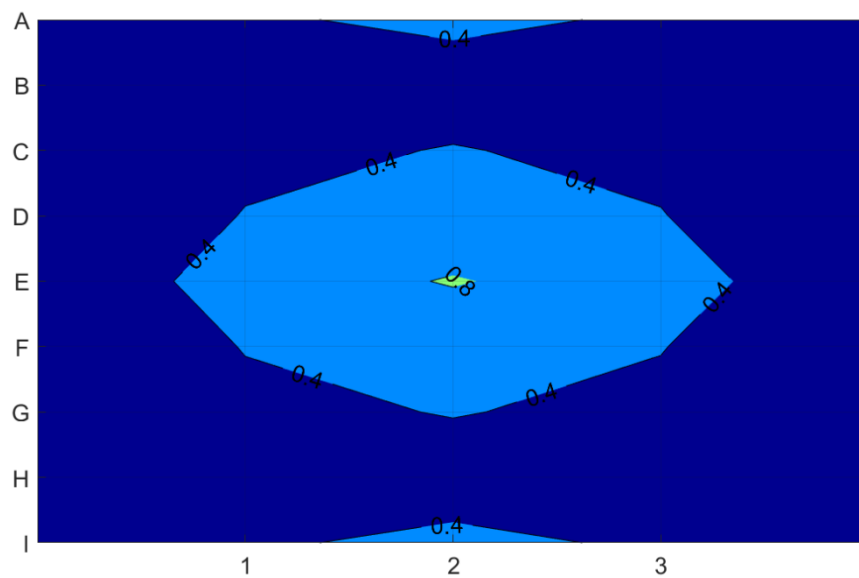
(b) Total VDV contour plot

Figure 7-6 *Model 3 (4% damping ratio) at 2.09 Hz ('R' Hz) pace frequency*
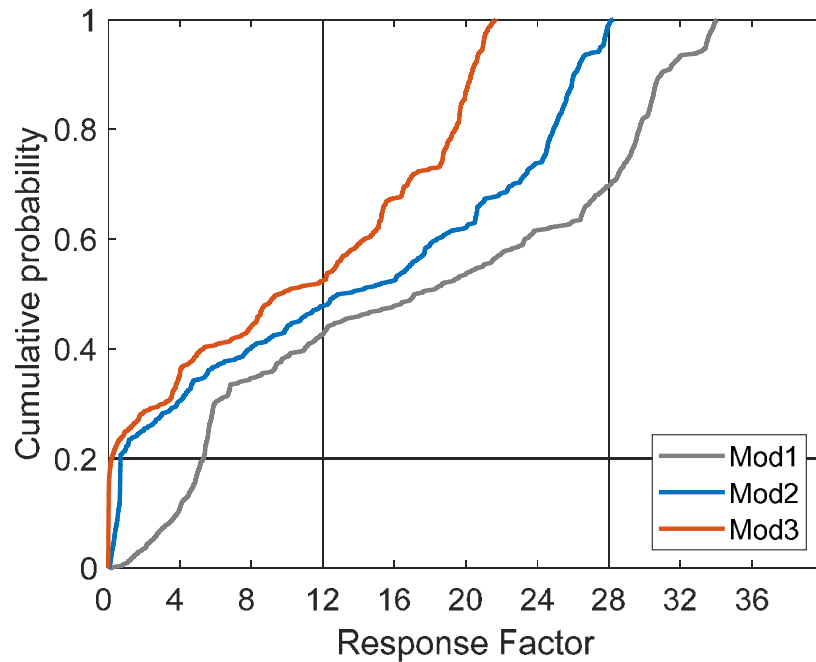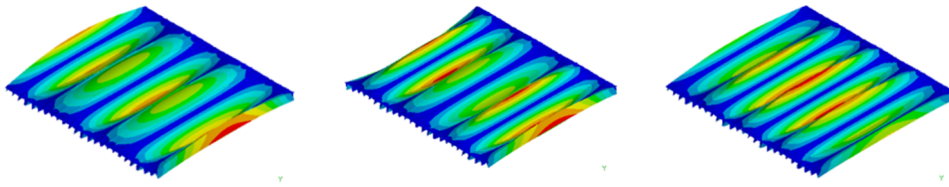
Figure 7-7 *Cumulative distribution of simulated floor response for models with 1% (Mod1), 2% (Mod2) and 4% (Mod3) damping ratio.*

7.4 Influence of increased stiffness parallel to span

The additional joist in the cassette cross-section (Figure 7-2(b)) increases the second moment of inertia by 21% to 3.93×10^9 mm^4 while the mass of each cassette is increased by 11% to 1168 kg compared to the reference case cross-section; this increases the total floor mass to 8462 kg. Therefore, the additional stiffness outweighs the added mass resulting in higher frequencies for the first four modes compared to Model 1, as shown in Table 7-4. However, the disadvantage of additional stiffness in the primary direction means the effects of the orthotropic behaviour become larger and consequently there is a reduction of spacing in natural frequencies; this was also reported by Chui (1986). This is evident through the 0.004 Hz separation between mode 1 and 2 (which have subsequently switched) in Model 4 compared to the 0.014 Hz separation for the same modes in Model 1.

Table 7-4 *Overview of modal properties for Model 4 for all modes under 30 Hz.*

Mode	1	2	3
f (Hz)	10.71	10.71	10.93
M_n (kg)	1185	2750	1137

Mode	4	5	6
f (Hz)	11.82	13.42	15.61
M_n (kg)	1309	1098	865

Mode	7	8	9
f (Hz)	18.10	20.62	22.56
M_n (kg)	764	804	1548

For the transient analysis, two pace frequencies were investigated: 2 Hz and the fifth integer division of the first bending mode ('R' Hz). Walker mass, path and step length were identical to that used for Model 1. Figure 7-8 (a) shows the maximum RF contour plot for Model 4 for the walker at 2 Hz pace frequency. The contours have been plotted with a colour scale matching the maximum RF of Model 1 (as shown in Figure 7-3 (a)) for ease of comparison. As shown, the maximum response for both models occurs at response location corresponding to grid E2 with Model 1 having a maximum RF of 25 and Model 4 having a maximum RF of 22.

However, when comparing Figures 7-8 (a) and 7-9 (a), it can be seen that when walking at 'R' Hz, Model 4 has a higher response (RF = 39 for Model 4 and RF = 34 for Model

1) despite Model 4 having a higher flexural stiffness and modal mass for the first bending mode. Similarly, the VDV contour plot shown in Figure 7-9 (b) shows that the total floor area where adverse comment is probable has slightly increased to approx. 28% compared to the 25% of floor area for Model 1. To investigate this further, a harmonic analysis was conducted on both Model 1 and Model 4 by applying a 1 N sinusoidal load for a frequency range of 0 to 30 Hz including at the specific modal frequencies of the floor. This is similar to the approach recommended in AISC DG 11 when finding the dominant mode. The unit sinusoidal load was applied at E2 and the frequency response amplitudes obtained from the same node. The amplitudes were then frequency weighted using the W_k weighting as per ISO 2631-1 (1997). The resulting FRF plot is shown in Figure 7-10 (a). Although the amplitudes at the modal frequencies appear to be higher for Model 1, when zooming into the range of 8 – 15 Hz as shown in Figure 7-10(b), the amplitudes for the first two modes (at the location of the arrow) for Model 4 are in fact higher than Model 1. This means that, despite Model 4 having a higher fundamental mode and modal mass, when walking at 'R' Hz, the modal amplitudes of the first two modes are higher than Model 1 resulting in a larger response. Further, the amplitude for mode 5 (as annotated in Figure 7-10(b)), is in fact greater than the amplitudes for modes 1 – 3 (due to the lower modal mass), which reinforces that vibration design for long-span timber floors should not be based on the fundamental mode only.
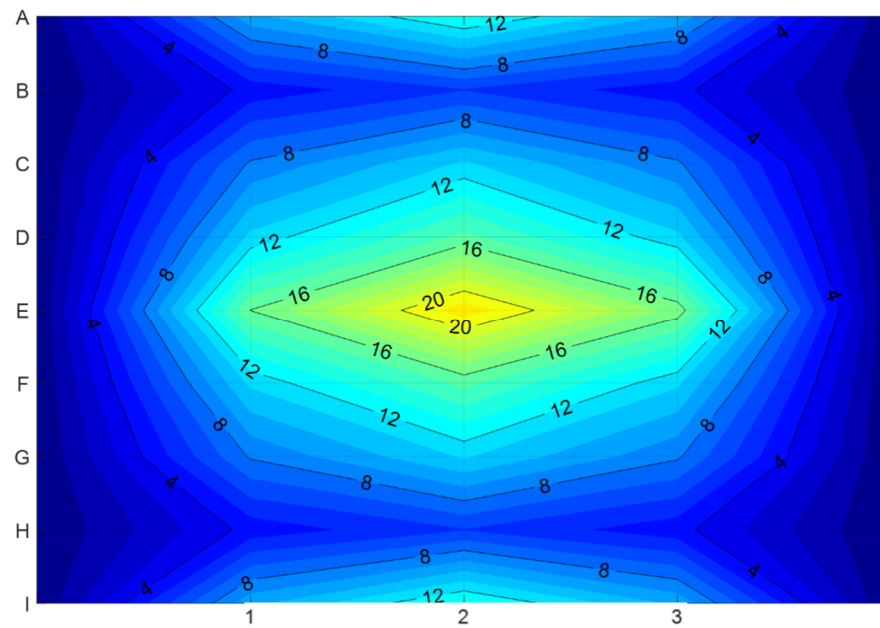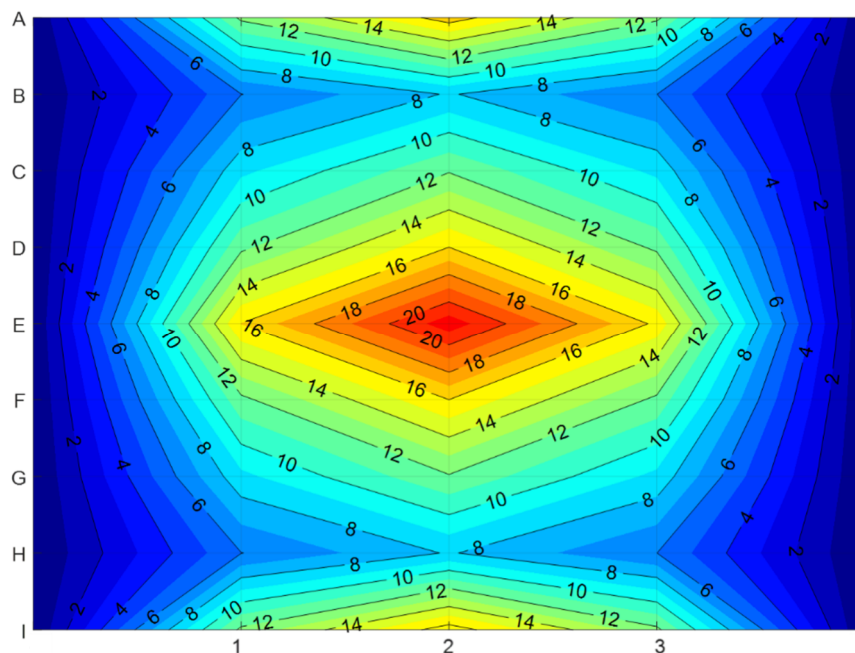

(a) Maximum RF contour plot
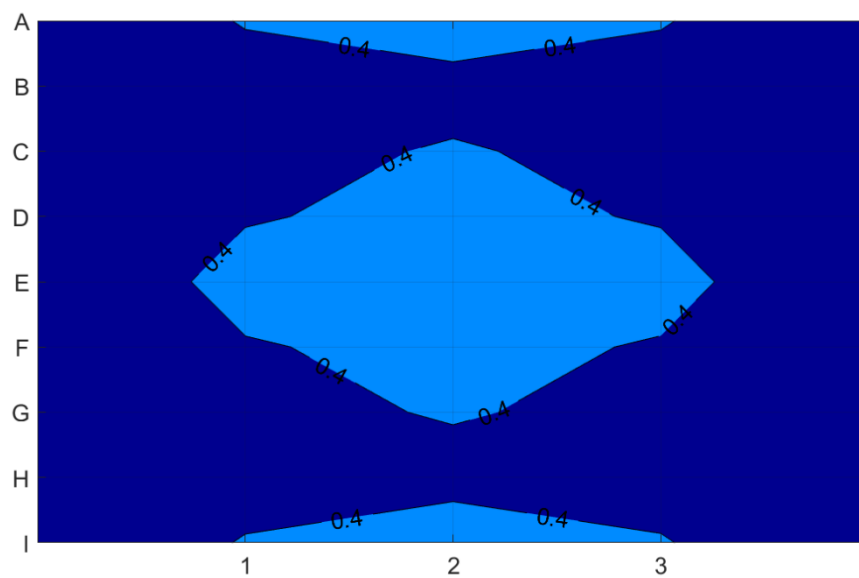
(b) Total VDV contour plot

Figure 7-8 *Model 4 at 2 Hz pace frequency*
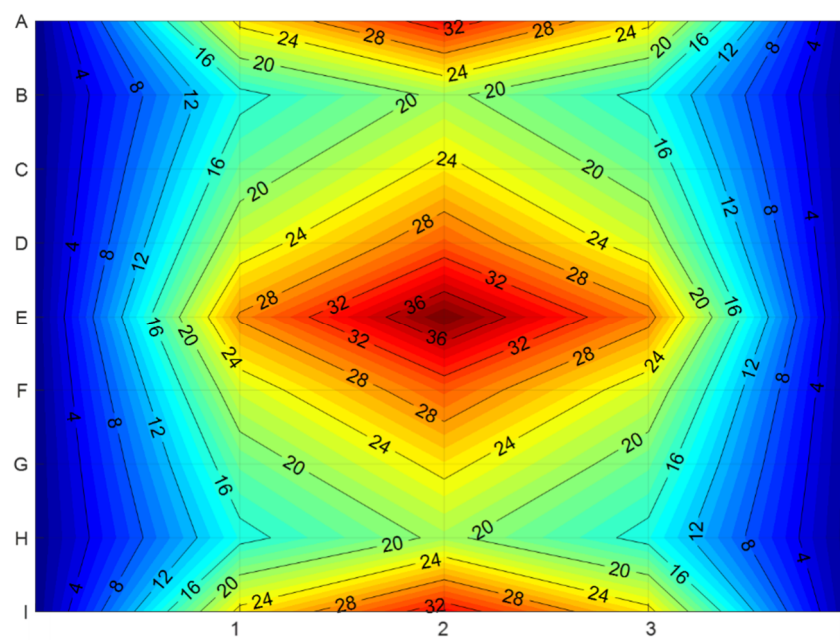
(a) Maximum RF contour plot
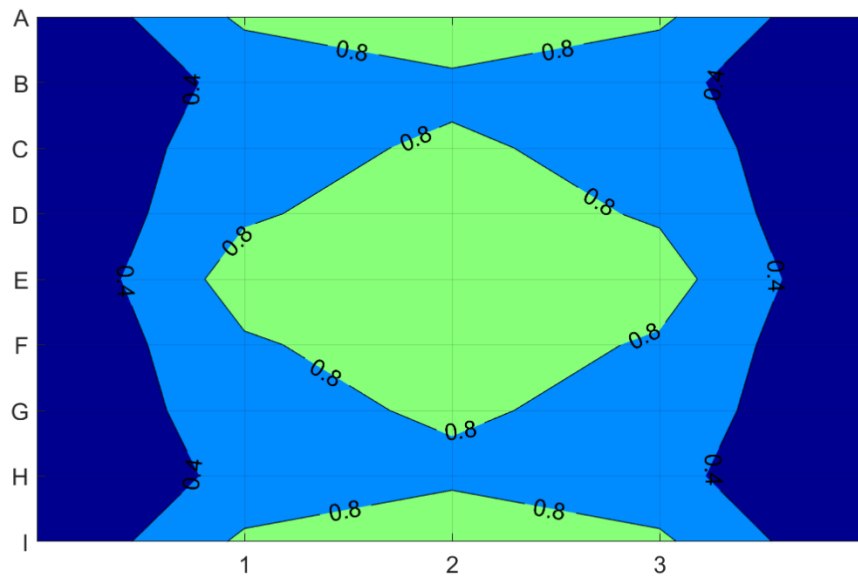
(b) Total VDV contour plot

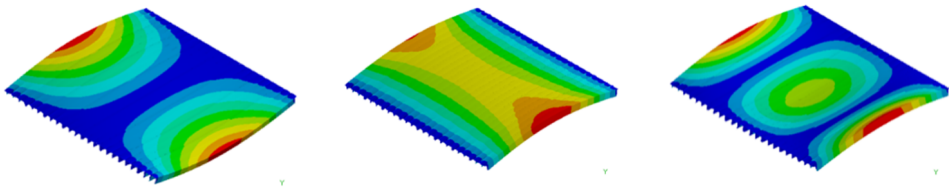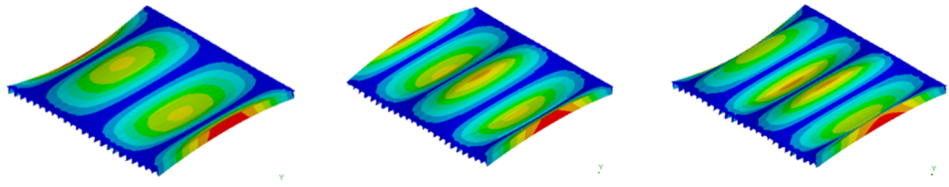***Figure 7-9*** *Model 4 at 2.14 Hz ('R' Hz) pace frequency*

| (a) | (b) |
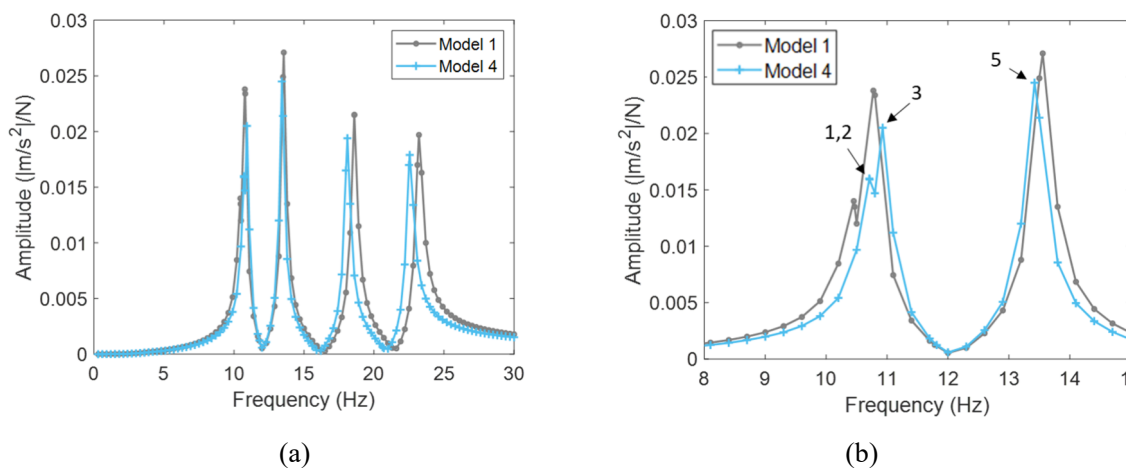
Figure 7-10 *FRF plots at response node E2 for 1 N sinusoidal loading applied at E2 for (a) frequencies between 0 and 30 Hz; (b) 8 to 15 Hz enlarged plot with modes annotated.*

The cumulative distribution of the floor response at node E2, as shown in Figure 7-11, provides further insight to the floor response as the walker crosses the floor. Note label 'Mod*_fp*' in the legend is used to denote result from Model '*' with walking frequency '*' Hz. As shown, when walking at 'R' Hz for Model 4, the plot reveals that the response amplitudes are almost identical to Model 1 for 60% of the time but then begin to diverge due to the higher floor response of Model 4.
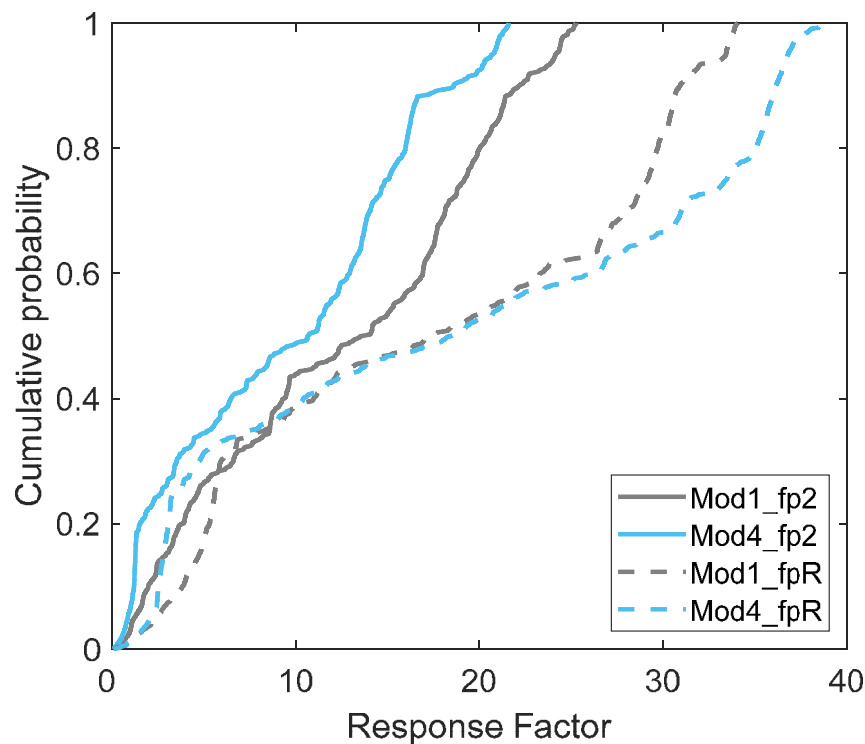
Figure 7-11 *Cumulative distribution of simulated floor response for Model 1 and 4 at 2 Hz and 'R' Hz pace frequencies.*

7.5 Influence of increased span-to-depth ratio

For Model 5, the flange thickness was reduced to 45 mm while the web cross-section was kept the same (360 × 63), resulting in a total floor depth of 405 mm (Figure 7-2(c)). On the other hand, for Model 6, the flange was kept the same as the reference case while the depth of the web member was reduced to 300 mm which resulted in a total floor depth of 390 mm (Figure 7-2(d)). These cross-sections resulted in a span-to-depth ratio for Model 5 and 6 of 22 and 23, respectively, compared to 20 for the reference case. These ratios are similar to those suggested for steel beams where a span-to-depth ratio of 20 – 28 is recommended (Ruddy & Ioannides 2004). The modal properties for Model 5 and 6 are shown in Tables 7-5 and 7-6.

It is clear that halving the depth of the flange member has a detrimental effect on the dynamic behaviour of the floor where the total mass of the floor reduces to 70% of the total mass of Model 1. This results in a significant reduction in modal masses of higher modes when compared to the reference case which means that these modes are more easily excitable. Further, Model 5 has four more modes within the 30 Hz range compared

to the reference where the first six modes are within a range of 2.54 Hz (i.e. 10.12 to 12.66 Hz). Another point to note for Model 5 is the difference in mode shape of the fundamental mode from Model 1 where the highest deflection point now lies in the centre of the floor as opposed to the mid-point along the edges.

By reducing the depth of the web members, the number of modes under 30 Hz remain the same as those for Model 1. However, the fundamental mode decreases by approx. 1.44 Hz to 9.01 Hz making the floor more likely to be excited by a harmonic of the walking frequency.

Table 7-5 *Overview of modal properties for Model 5 for all modes under 30 Hz.*
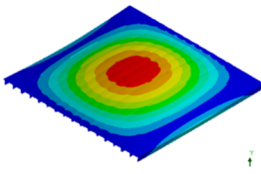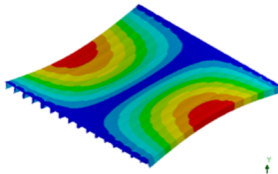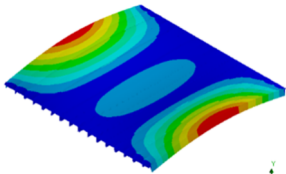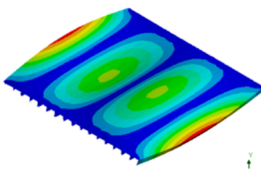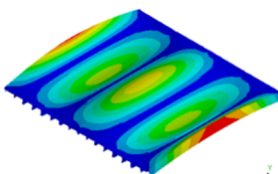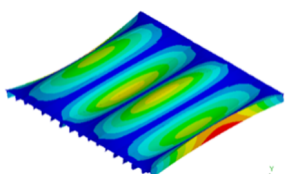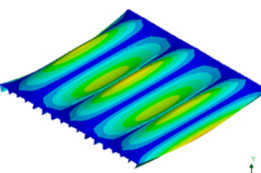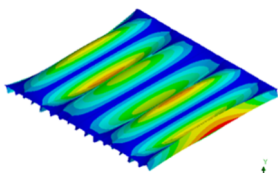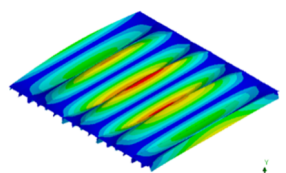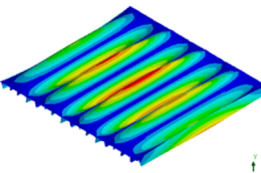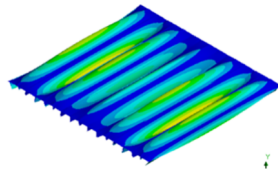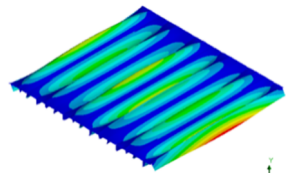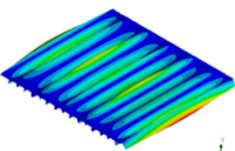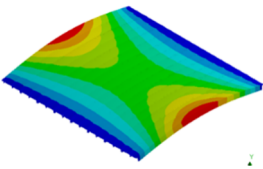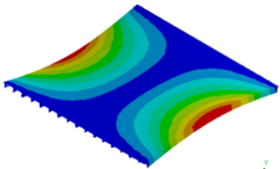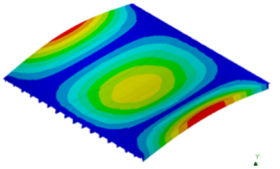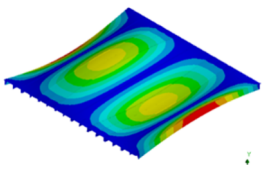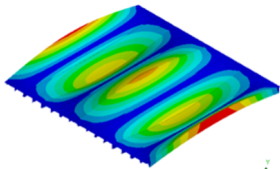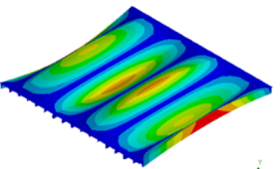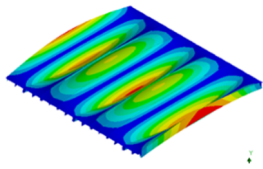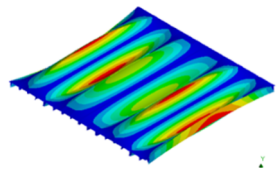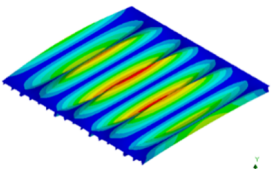
Mode	1	2	3
f (Hz)	10.12	10.17	10.26
M_n (kg)	1245	1301	632

Mode	4	5	6
f (Hz)	10.63	11.45	12.66
M_n (kg)	639	555	378

Mode	7	8	9
f (Hz)	14.16	15.83	17.33
M_n (kg)	304	302	528

Mode	10	11	12
f (Hz)	23.12	24.57	26.54
M_n (kg)	297	135	117

Mode	13		
f (Hz)	28.50		
M_n (kg)	122		

Table 7-6 *Overview of modal properties for Model 6 for all modes under 30 Hz.*

Mode	1	2	3
f (Hz)	9.01	9.04	9.48
M_n (kg)	1627	947	1112

Mode	4	5	6
f (Hz)	10.66	12.66	15.29
M_n (kg)	1110	941	742

Mode	7	8	9
f (Hz)	18.20	21.03	23.14
M_n (kg)	661	713	1250

Similar to Model 4, two pace frequencies were analysed: 2.0 Hz and the fifth integer division of the fundamental frequency. Walker mass, path and step length were identical to that used for Model 1. Figures 7-12 (a) and 7-13(a) show the maximum RF contour plots for the walker at 2 Hz pace frequency for Model 5 and 6, respectively. As shown, there is a significant difference in response between the models with the maximum RF for Model 5 (RF = 78) occurring at E2, being more than three times the maximum RF for Model 6 which occurred at locations A2 and I2 (RF = 24). This is further illustrated in the total VDV contour plot shown in Figure 7-12(b) where adverse comment is 'possible' for approx. 48% of the floor area and 'probable' for approx. 20% of the floor area located at mid-span. These results contrast the VDV contour plot for Model 6 shown in Figure 7-13(b) where adverse comment is 'possible' for only a small (<0.5% floor area) area in the centre of the floor.

This indicates that, rather than reducing the thickness of the flange, reducing the depth of the webs would be more appropriate if the designer wants to increase the structural efficiency of the system. As the flange section holds the majority of the mass of the cassette, a reduction in thickness has detrimental effects on the floor response.

These results are further highlighted when walking at 'R' Hz. For Model 5, the fifth integer of the fundamental frequency is only 0.02 Hz higher than the reference pace frequency of 2.0 Hz. Despite this small difference, Figure 7-14(b) reveals that the floor area for Model 5 where adverse comment is probable has nearly doubled and there is a small area in the centre of the floor where adverse comment is very likely (VDV > 3.2 m/s$^{1.75}$). Inducing resonance in the floor for Model 6 also had a significant effect on the floor response where the unsupported sides of the floor show a larger area of high response than the centre as shown in Figure 7-15(a). If occupants are positioned in these locations, Figure 7-15(b) shows that adverse comment is probable.
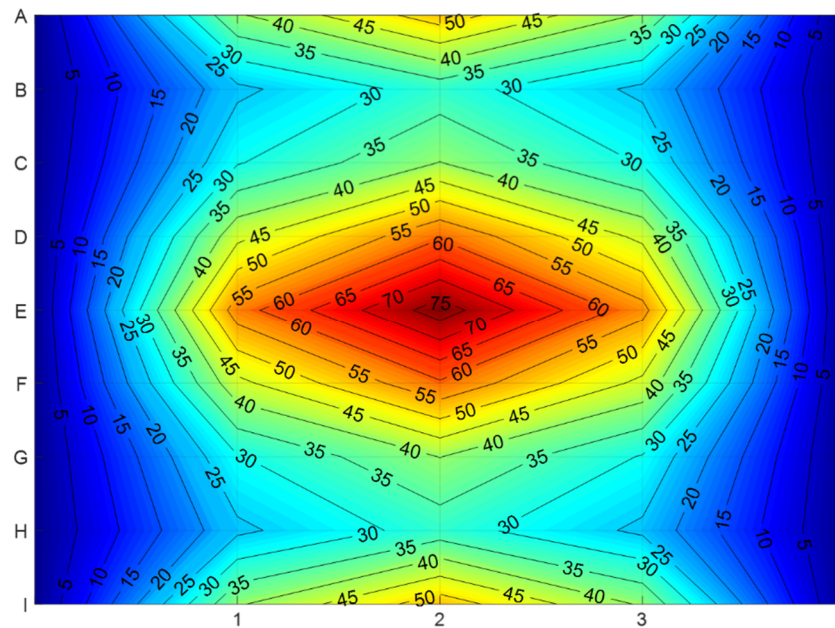
(a) Maximum RF contour plot
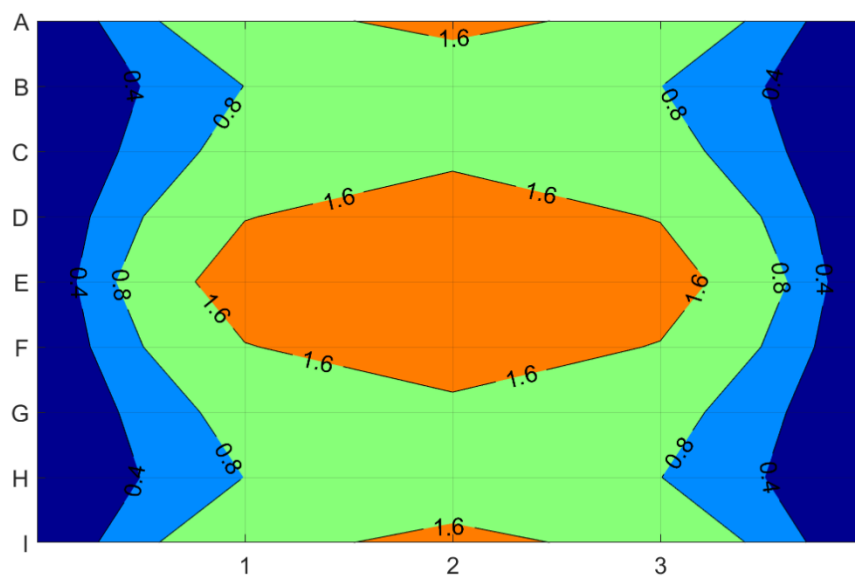
(b) Total VDV contour plot

Figure 7-12 *Model 5 at 2 Hz pace frequency*
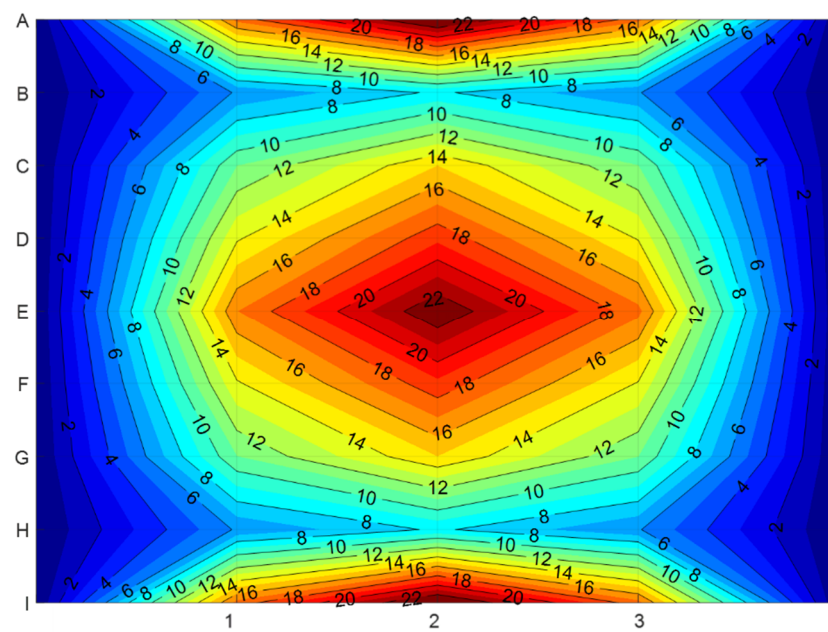
(a) Maximum RF contour plot
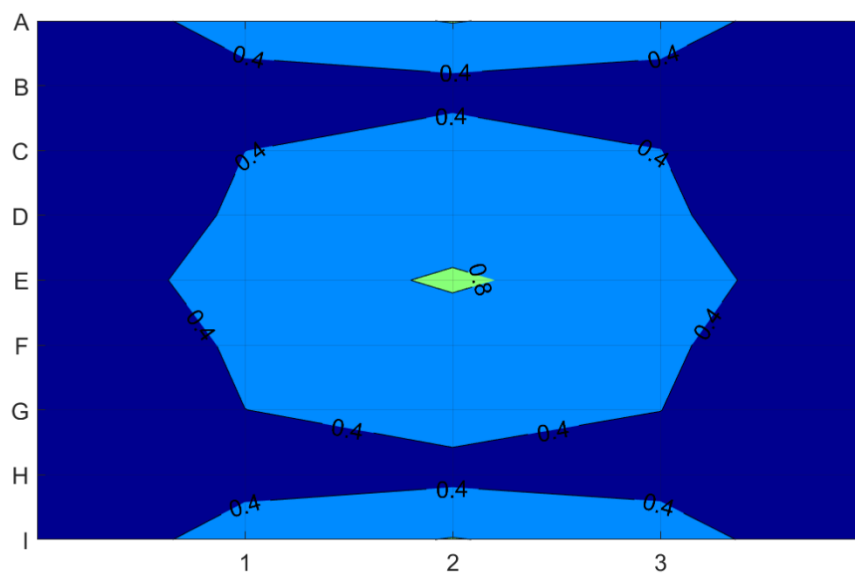
(b) Total VDV contour plot

Figure 7-13 *Model 6 at 2 Hz pace frequency*
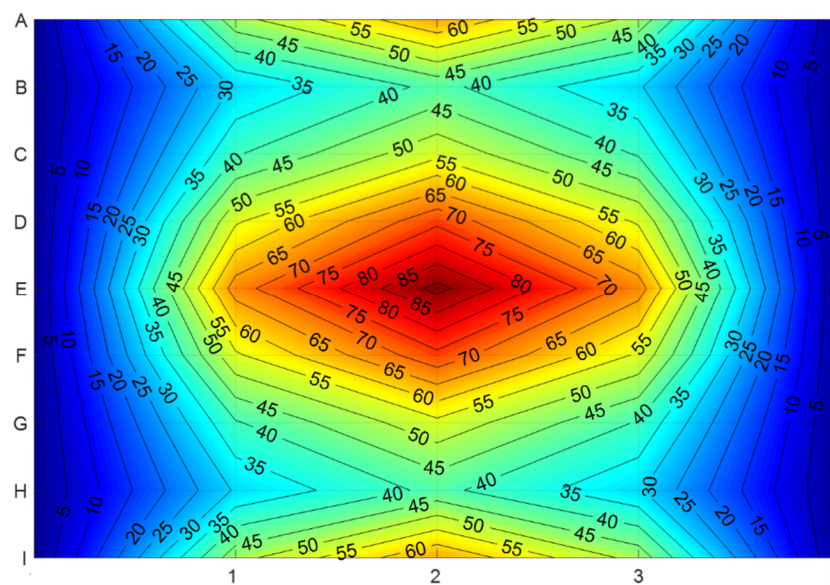
(a) Maximum RF contour plot
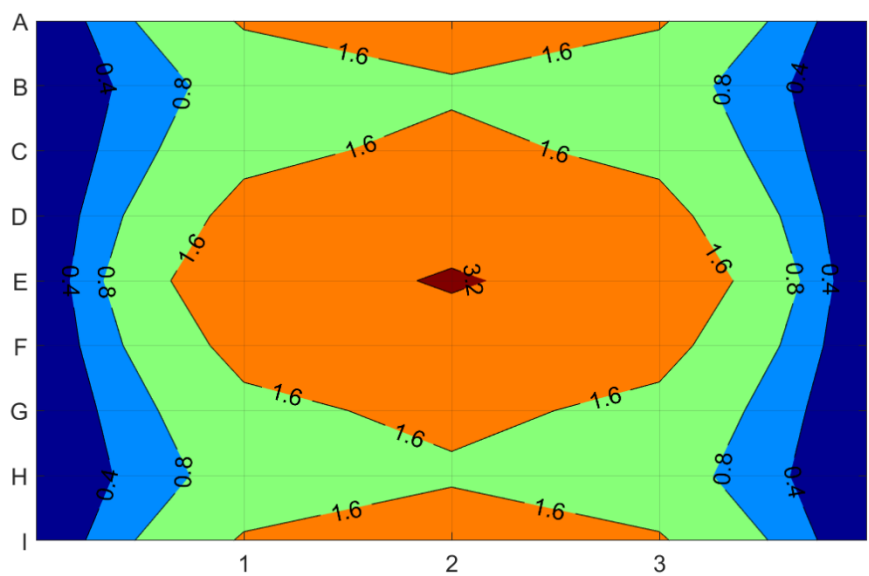
(b) Total VDV contour plot

Figure 7-14 *Model 5 at 2.02 Hz ('R' Hz) pace frequency*
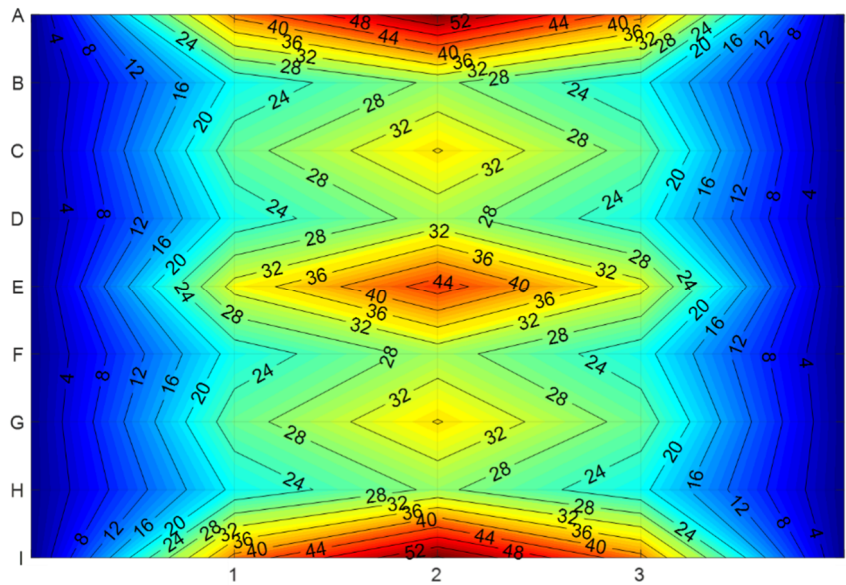
(a) Maximum RF contour plot
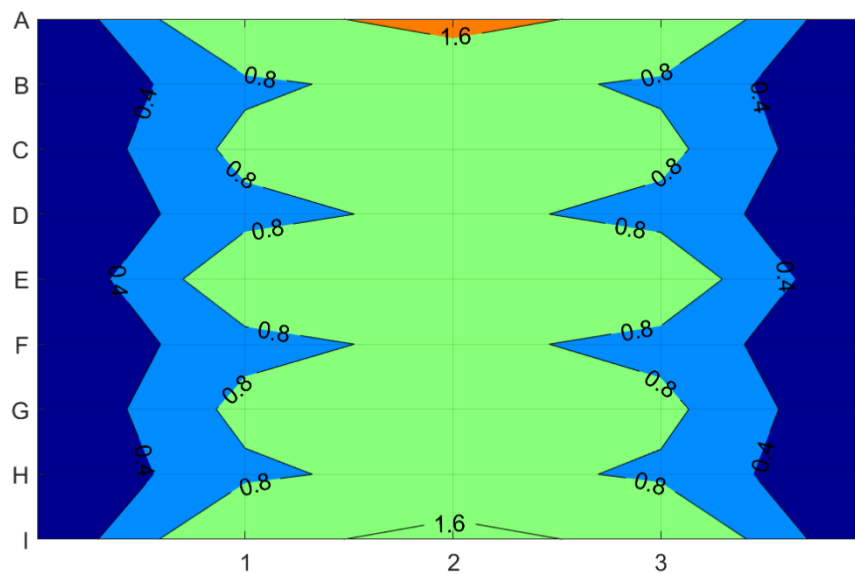
(b) Total VDV contour plot

Figure 7-15 *Model 6 at 1.80 Hz ('R' Hz) pace frequency*

The cumulative distribution of the floor response at node E2 for Model 5 and 6 for the two pace frequencies are shown in Figure 7-16; the results of Model 1 are also shown in grey for ease of comparison. The plot shows that when walking at 2 Hz, the response distribution for Models 1 and 6 are almost identical, despite Model 6 having two-thirds of the flexural stiffness and less mass than Model 1. However, when walking at the 'R' Hz, the response of Model 6 is 35% greater than Model 1. Similar to the difference in response for Model 1 and 4 at 'R' Hz walking pace, it was of interest to investigate the frequency response to understand whether the amplitude of mode 1 of Model 6 was greater than for Model 1; this plot for frequency 0 – 30 Hz is shown in Figure 7-17 (a). The enlarged plot for frequency range 8 to 15 Hz is shown in Figure 7-17 (b). In this case, the amplitude of the first mode for Model 6 (as annotated in Figure 7-17(b)) is actually less than amplitude for the first mode of Model 1. However, the fifth integer division of the fundamental mode (1.80 Hz) of Model 6 is also very close to the seventh integer division of mode 5 (as annotated in Figure 7-17(b)) which has the highest amplitude out of all modes up to 30 Hz. This explains why the contour plot shown in Figure 7-15(a) looks very similar to mode shape 5, as shown in Table 7-6. For reference, the frequency response of Model 5 has also been shown in Figure 7-17 which clearly shows that there are two very dominant modes (mode 1 and 5) under 12 Hz. These modes coupled with the lower modal mass have contributed to the large response.
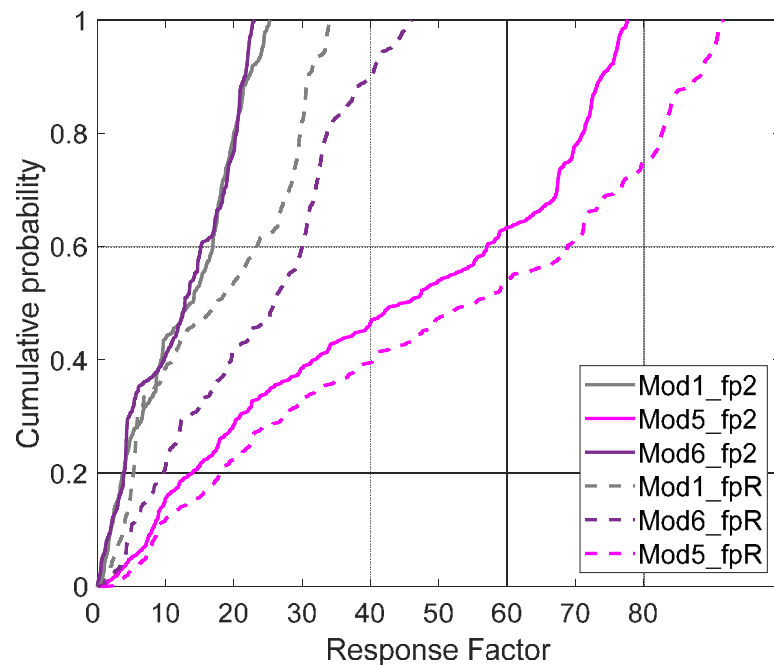
***Figure 7-16** Cumulative distribution of simulated floor response at node E2 for Model 1, 5 and 6 for both pace frequencies.*

| (a) | (b) |
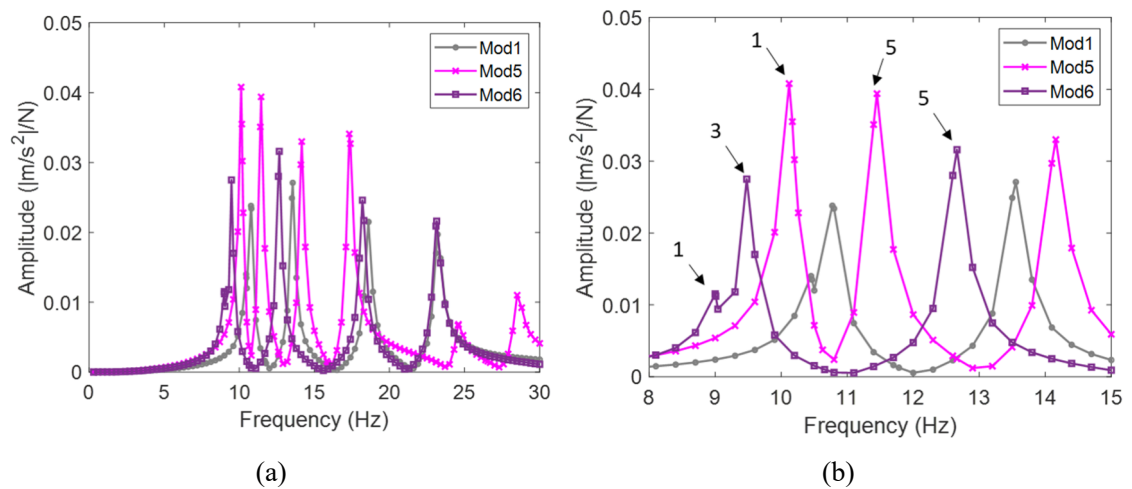
***Figure 7-17** Frequency response plots at response node E2 for 1 N sinusoidal loading applied at E2 for (a) frequencies between 0 and 30 Hz; (b) 8 to 15 Hz enlarged plot with modes annotated.*

7.6 Concluding remarks

In this chapter, a multiple cassette floor model (forming a 9.19 m × 9.76 m floor grid) based on the findings from Chapter 4 and Chapter 6 was created and the influence of common design parameters were investigated. The three design parameters which were varied included the damping ratio, web spacing and span-to-depth ratio. To simulate

257

human walking, the Chen et al. (2019) walking load model was used, as detailed in Chapter 5. The following conclusions can be drawn from the numerical study:

- Considering only the fundamental mode is not appropriate for long-span timber floor design and in many cases higher modes significantly contributed to the floor response. An FRF plot obtained by applying a unit sinusoidal load at an excitation location of interest can provide valuable insight into the dominant modes.

- A stiffer cross-section in the direction parallel to span decreases separation between modes which can result in higher amplitudes of floor response compared to a less stiff cross-section.

- Regardless of fundamental frequency, an integer division of the fundamental mode or dominant mode is recommended to obtain maximum response. For example, even up to the seventh integer division if it still falls in the typical walking frequency range (1.5 – 2.5 Hz).

- The damping ratio is the parameter which has the largest beneficial influence on the floor response. An increase in damping ratio from 1% to 2% reduced the RF at the centre of the floor by 17% while an increase from 1% to 4% reduced the RF by 36%.

- If the designer needed to increase the structural efficiency of the floor, reducing the flange thickness is not recommended due to the significant reduction in the mass of the system leading to a decrease in modal masses of higher modes. Instead, the designer can consider reducing the depth of the web members as appropriate.

Chapter 8

Guidance on Vibration Design of Long-Span Timber Ribbed-Deck Floors

8.1 Introduction

This chapter proposes a floor vibration design flow chart specific for long-span timber floors. Contributions to the design process as a result of findings from this research have been highlighted and discussed. The aim of this chapter is to discuss critical design parameters which may influence the vibration design process, which will be of interest to design engineers.

8.2 Proposed vibration design flow chart

Figure 8-1 shows a proposed flow chart which can be followed for floor vibration design of long-span timber cassette floors under footfall loading. The flow chart is based on the flow chart published in the Concrete Centre design guide (CCIP-016) (Willford & Young 2006), and has been updated based on findings from this research. One of the critical differences between Figure 8-1 and the design procedure in CCIP-016 (Willford & Young 2006) is the omission of the classification of the floor as a low- or high-frequency floor

based on the frequency of the first active mode at both response and excitation points. This avoids the floor response assumption and subsequently the type of walking load model that is used.

The process steps in the flow chart with a dashed outline indicate steps which can incorporate a probabilistic approach while the orange outlined processes indicate areas where this thesis has contributed. The aim of this flow chart is that as further research is undertaken in the areas of floor vibration of long-span timber floors, a clearer picture of the steps needed to accurately predict and assess floor performance can be developed. The following sections of this chapter discuss the main contributions from this research in the context of the orange outlined processes in the flow chart.
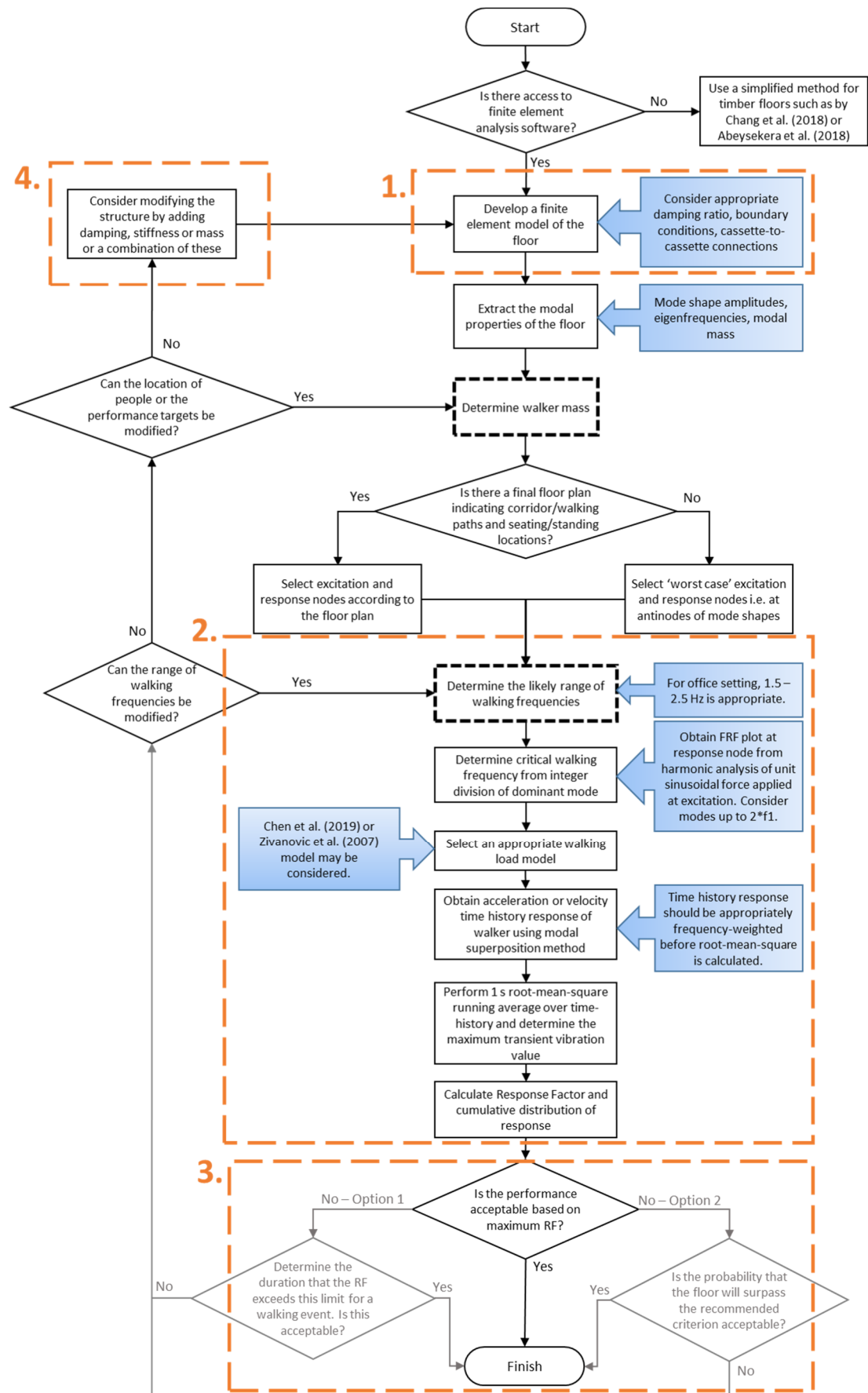
Figure 8-1 *Vibration design flow chart for long-span timber ribbed-deck floors*

8.3 Numerical model or simplified approach

Current vibration design guides present the user with an option to either design the floor using a simplified approach with modal properties obtained from theoretical equations or a more detailed approach with modal properties obtained from a finite element model. As it is likely that the floor system will have closely spaced modes, it is recommended that the latter approach is followed if finite element analysis software is available to ensure all modes under two times the fundamental frequency are identified. This is similar to the recommendation in AISC DG 11 (Murray et al. 2016).

However, if the designer does not have access to finite element analysis software, it is recommended that the simplified approaches recently developed by Abeysekera et al. (2018) and/or the Chang et al. (2018) are followed. These peer reviewed methods were presented at the International Network of Timber Engineering Research (INTER) in 2018 and were detailed in Chapter 2 Section 2.6.1.2. The method proposed by Abeysekera et al. (2018) is suitable for rectangular timber floors on wall supports, which are generally transient floors. Although the modal frequencies of the 16 tested in-situ floors used to develop the Chang et al. (2018) method were not disclosed, the method is suggested to be suitable for timber floor systems that are not covered in Eurocode 5 (2004) such as long-span floors in non-domestic situations. The paper includes an easy to follow flow-chart which results in the user calculating an estimated VDV based on the weighted peak acceleration. The current limitation of this method (and other simplified methods), however, is that only the fundamental mode is considered.

8.4 Considerations in numerical model

This section refers to the first highlighted step in the design flow chart as shown in Figure 8-1.

8.4.1 Material model and element types

Based on the sensitivity study in Chapter 4 Section 4.5.4, it was found that the modulus of elasticity perpendicular to grain for the web elements had negligible influence to the frequencies of the first five modes under 50 Hz. Therefore, web elements can be modelled as an isotropic material either using a beam or shell element. If modelling as a beam

element, the web must be offset from the flange element to ensure the correct cross-section of the cassette is formed. Web elements also should include the effects of shear deformation i.e. Timoshenko beam theory. The flange element should be modelled as an orthotropic shell element to include the influence of the modulus of elasticity perpendicular to the grain on the lateral bending modes.

8.4.2 Boundary conditions

In this research, for model correlation purposes, the single cassette model used elastic springs in the three translational directions to represent the flange bearing support. The stiffness of the spring varied depending on the direction. For design purposes however, it is sufficient to assume that a flange bearing support can be numerically represented as a pin connection. This has been compared with experimental results for support condition where the flange is secured to the supporting frame with screws at 190 mm centres (as detailed in Chapter 4 Section 4.4.2). Consideration should also be given to the location of the pin connection from the edge of the flange member to ensure that the floor has a similar effective length. As such the pin connections should be applied very close to where the screws are installed.

8.4.3 Cassette-to-cassette connections

Extensive experimental testing was performed on two different flange-to-flange connection types (splice or diagonal screws) with varying screw spacing as detailed in Chapter 6 Section 6.4. Walking tests at 2.0 Hz and 'R' Hz pace frequencies revealed that there was no clear trend with using either a splice or a diagonal screw connection. Although, cumulative distribution plots showed that the diagonal screws resulted in a generally lower response for a longer duration of time within the walking event. There was negligible benefit to modal properties and floor response when reducing the screw spacing from 300 to 150 mm centre to centre.

Numerically, it was found to be unnecessary to model points of screw connections as elastic springs with defined translational stiffness properties (as detailed in Chapter 6 Section 6.5.2.1.). Subsequently, nodes at screw locations can simply be coupled translationally. Comparisons between the measured and numerical results found that the flange-to-flange connection may have some rotational stiffness properties about the axis

parallel to the span of floor. Although included in the updated model for this research, further studies in the rotational stiffness of these connections are recommended before consideration in a design scenario.

8.4.4 Damping ratio

Appropriate estimation of damping ratio greatly influences the floor response to walking, as shown in Chapter 7 Section 7.3. Even a 1% increase in damping ratio from 1% to 2% can reduce the maximum response by approximately 17% and reduces the duration that the floor will exceed a certain limit. Therefore, it is critical that an appropriate value is estimated for design purposes.

Impact hammer tests for both the single and double cassette set-ups, as discussed in Chapter 4 Section 4.3 and Chapter 6 Section 6.4, respectively, found that the damping ratio for the first bending and torsion modes were approximately 1%. This is in line with the damping ratio suggested in Eurocode 5 (European Committee for Standardisation 2004) as well as Hamm et al. (2010) for 'timber floors without any floor finish'. However, recent studies have shown that when a timber floor is incorporated into the main structure and is subject to additional loading from the fit-out or floor finishes, the damping ratio can be significantly higher (Hamm, Richter & Winter 2010; Jarnerö, Brandt & Olsson 2015). Based on the experimental results for the single and double cassette floor as well as other recent measurements on timber floors presented in literature, a 2% damping ratio may be more appropriate; this is in line with the UK National Annex of Eurocode 5 (British Standards Institution 2008b) as well as a recent study by Abeysekera et al. (2018) for joisted floors.

8.5 Considerations in response prediction

This section refers to the second highlighted area in the flow chart as shown in Figure 8-1. The investigation of response prediction using different walking load models in Chapter 5 revealed that the choice of walking load model plays a large influence in the predicted floor response. Analytical response prediction methods presented in current floor vibration design guides such as CCIP-016 and SCI P354 differentiates the floor response, and subsequently the walking load model, based on the frequency of the first vertical mode that is active at both response and excitation points (generally the

fundamental mode). One of the critical assumptions of this categorisation is that a resonant response can only be caused by the first four harmonics of the walking pace. However, walking tests conducted in this research at a pace frequency equivalent to the fifth integer division of the fundamental mode resulted in a floor response close to resonant behaviour. This means that despite the floor being categorised as 'high-frequency', it still exhibited resonant behaviour which cannot be captured using a load model that assumes transient behaviour. The inadequacy of the deterministic load model were highlighted in Chapter 5 and 6 where the response was underestimated (CCIP-016 and AISC DG11) or overestimated (SCI P354).

For more accurate response prediction, it is recommended that a step-by-step model proposed by Chen et al. (2019) is considered which avoids the need for categorising the floor and potentially making an erroneous assumption of how the floor will respond. In Chapter 5 using the validated single cassette FE model, Chen et al. (2019) modelling approach was found to most accurately predict the time-history response and subsequently the maximum transient vibration value, when compared to the measured results; this finding was further highlighted using the double cassette model in Chapter 6. However, the application of the step-by-step load into the FE model is fairly tedious as the footstep nodes must be selected and time-history loading applied individually for each footstep node. Further, transient analysis to obtain the time-history response is time consuming and onerous on computer hardware. Chen et al. (2019) suggested that, alternatively, the single footfall trace model can be superimposed to create a continuous loading function; the length of the continuous loading function would depend on the number of steps in the walking path. This means that a procedure, similar to the one coded by Živanović (2006) for the application of the multi-harmonic force model, can be programmed to determine the floor response. Rather than running a transient analysis, mode shape amplitudes can simply be extracted from the FE model to calculate the response for each mode of vibration. Modal superposition method can then be used to calculate the total response.

The Chen et al. (2019) model as well as Živanović et al.'s (2007b) multi-harmonic force model (also investigated in Chapter 5) also provides statistical distributions of walker mass, DLFs and phase angles which can be incorporated into the loading to consider inter-

and intra-subject variability. These distributions can be easily programmed which allows for a probabilistic approach to design where the probability of a certain response occurring within a sample population can be obtained.

The walking load should be analysed particularly at walking frequencies which are at an integer division of the dominant mode. The dominant mode can be found by applying a unit sinusoidal force at the excitation location at frequencies in the range from approximately 1 Hz less than the fundamental mode up to two times the fundamental mode. The eigenfrequencies within this range should also be included in the harmonic analysis. The FRF plot at the response node can then be obtained where the mode with the highest FRF amplitude is considered as the dominant mode. This procedure is the same as the method proposed in AISC DG 11 (2016). The dominant mode may not necessarily be the fundamental mode, as highlighted in Chapter 7 Section 7.3 and 7.4.

8.6 Considerations in vibration criterion and performance assessment

This section refers to the third highlighted area in the flow chart as shown in Figure 8-1 and involves two main questions:

1. What are the appropriate criteria for floor vibration design of long-span timber floors?
2. How do we use this criteria to ensure satisfactory performance?

8.6.1 Forming appropriate criteria

Forming appropriate criteria for floor vibration design of long-span timber floors will ultimately involve subjective tests on perception and annoyance levels due to walking-induced vibration. Since human perception is dependent on a number of factors including whether the vibration is expected, whether the source is identifiable and the ambient conditions (Griffin 1990), such tests are best performed on already built timber floors where building fit-out has been completed. Although subjective testing was not performed in this research as it was outside the scope, factors for developing a more tailored vibration criteria for long-span timber floors have been proposed, as shown in Figure 8-2. The two main factors that should be considered are: the type of office

environment and what sort of demand levels are required in terms of perception and annoyance.
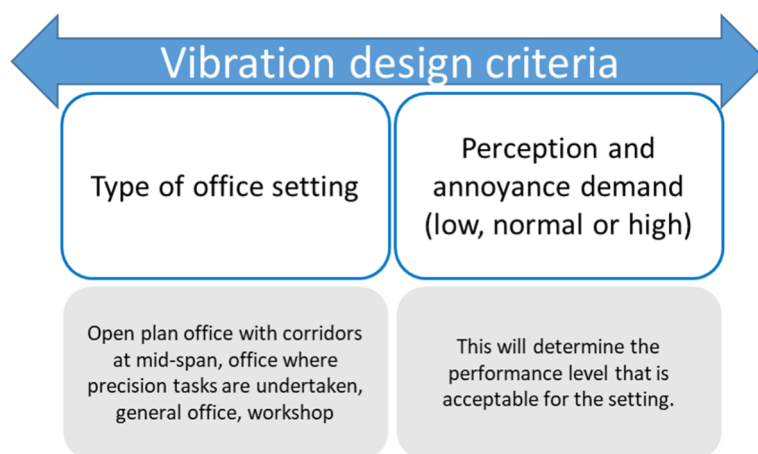
Figure 8-2 Considerations when developing vibration design criteria

CCIP-016 is currently the only guide which provides different response factor (RF) criteria depending on the type of office building the floor is designed for. For example, for a general office space an RF of less than 8 almost always result in satisfactory performance. However, for open-plan offices with busy corridors near mid-span and premium quality open-plan offices where precision activities are being undertaken, the RF is recommended to be reduced by a factor of 2. Another instance where RF limit could be more relaxed are areas such as kitchens or lunch areas where people won't be seated for an extended period of time.

The second step in developing appropriate criteria then becomes understanding the different performance levels that would be expected for the office setting. For example, an office with relatively low demands for perception and annoyance levels would have a more relaxed limit than an office demanding a higher quality performance. Deciding on the demand level would ultimately need joint collaboration between engineer and client to ensure that the client understands the changes to the floor structure or build-up (and subsequently the costs) to achieve the different performance levels. Such an approach was first proposed by Toratti and Talja (2006b) who proposed five classes of floor demands for residential and office buildings. However, in existing and widely used vibration design guides, a pass-fail criterion regardless of the floor demand is followed. Interestingly, the performance level approach has been successfully implemented in the previous and current versions of the Japanese vibration design standard (AIJES-V001)

(Architectural Institute of Japan 1991, 2004, 2018). In the most current revision, seven levels of performance have been identified and correlated to an annoyance scale ranging from V-I (not unpleasant and not annoyed) to V-VII (extremely unpleasant and extremely annoyed). These are shown in Table 8-1 with reference to the probability of perception levels which were provided in the previous version of the standard. These performance levels are similar to the RF approach in the fact that they are multiples of the baseline human perception curve for continuous vibrations. However, their incorporation with an annoyance scale provides the user with further insight into how the occupant may feel and the percentage of occupants that would be perceiving it. This can then be incorporated with the probabilistic approaches taken in Chen et al. (2019) and Živanović et al. (2007b) walking load models.

Table 8-1 *Relationship between annoyance level, probability of perception (based on previous version of standard AIJES-V001-2004) and performance level in current AIJES-V001-2018 standard for commercial buildings*

	Annoyance scale	Perception probability – AIJES-V001 (2004)	Performance level - AIJES-V001 (2018)
1	Extremely unpleasant (extremely annoyed)	-	-
2	· · · · · · · · ·	-	-
3	Very unpleasant (very annoyed)	90%	V-V
4	· · · · · · · ·	-	-
5	Slightly unpleasant (slightly annoyed)	70%	Between V-III and V-IV
6	· · · · · · · ·	50%	Between V-II and V-III
7	Not unpleasant (not annoyed)	-	-

Similar to the Japanese approach, Abeysekera et al. (2018) recently proposed floor performance levels for timber floors in residential and office environments based on three ranks: economy choice, base choice and quality choice. These have been reprinted in

Table 8-2 for reference. The proposed RF limit for a level II, level III and level IV office building floor are 8, 12 and 16, respectively.

Table 8-2 *Tentative floor performance levels for use in categories A (residential) and B (office) as proposed by Abeysekera et al. (2018)*

Use category	Quality choice	Base choice	Economy choice
A (residential)	Level III	Level IV	Level V
B (office)	Level II	Level III	Level IV

8.6.2 Satisfactory floor performance

In all current design guides, satisfactory floor performance is generally determined using a pass-fail approach. This means that if the predicted RF surpasses the limit, the floor is automatically classified as unsatisfactory. Such an approach completely disregards the duration of the vibration amplitude, which is a critical factor influencing human response (Griffin 1990), as well as the variabilities in human walking. Consequently, two options have been proposed as an additional check if the floor does not satisfy the RF limit.

Option 1 considers the duration that the response will exceed the suggested limit which can be obtained by calculating the cumulative distribution of the floor response over the walking event. For example, if the predicted floor response surpasses the limit but only for a very short period of time, the floor may still be considered acceptable. This approach was first recommended by Živanović and Pavić (2009) and as shown in Chapters 5, 6 and 7 provides a clearer picture of the floor response which is crucial when vibration design is critical. Subjective testing on long-span timber floors would need to be carried out to determine what an acceptable duration may be; for example, whether it would still be acceptable if the vibration amplitude is less than the limit for 80% of the duration of the event. It is important to note that the duration can only be obtained from a complete time-history of the response for the event.

Option 2 considers the probabilistic approach that can be calculated using Chen et al. (2019) and Živanović et al.'s (2007b) load models. Using the cumulative distribution of the floor response for a sample population (e.g. 100 people), the probability that the floor will surpass the recommended limit can be obtained. For example, if out of 100 people,

the probability that the floor will surpass the response is only 10%, the floor may still be deemed to be acceptable.

Until firmer values of acceptable durations that the vibration may exceed the limit or probabilities of exceeding the recommended limit are identified, this section of the flowchart (Figure 8-1) has been greyed out. Consequently, it may be prudent to calculate the Vibration Dose Value (VDV) instead as has been recommended in SCI P354 using Ellis' (2001) estimated VDV equation. As shown in Chapter 7, the estimated VDV provides a useful measure in understanding the locations of the floor which are more likely to have an adverse comment from the occupant.

8.7 Considerations in structural changes to improve performance

If the floor response is too high, the structure will ultimately need to be modified and the design process re-completed. One method to reduce floor response is to consider increasing the damping ratio (if justified) which was shown to be highly effective in both experimental tests (Chapter 6) and numerical modelling (Chapter 7). As detailed in Chapter 6, implementing an elastic interlayer with high damping properties, such as Sylomer®, at the interface between the supporting timber frame and flange overhang was effective in increasing the damping ratio of the floor by up to approx. 5% and 7% for the first and second modes, respectively. Although further studies will need to be conducted to verify these values, it is a promising solution particularly since this material is readily available and commonly used as an acoustic interlayer in timber buildings in Europe. The influence of the damping ratio in reducing floor performance was also investigated in the multiple-cassette floor model as detailed in Chapter 7. The results of this numerical study showed that even just a 1% increase in the damping ratio (i.e. from 1% to 2%) resulted in a significant reduction in floor response (by 17%). Increasing the damping ratio further to 4% from 1% would result in a RF reduction of 36%.

The numerical study in Chapter 7 Section 7.4 also revealed that increasing the flexural stiffness by adding an additional web member into the floor cross-section does not necessarily result in a reduced floor response. Although the additional web member increased the stiffness of the floor, the lower modes had less modal separation. A

270

harmonic analysis with a unit sinusoidal force found that the FRF amplitude of the fundamental mode was actually higher than for a cassette with three web members. This resulted in a higher response for the floor with four web members when walking at the fifth integer division of the fundamental mode. As a result it is recommended that if the structure is modified, an FRF plot at the response location of interest should be obtained first before a walking load model is applied to understand the changes in modal behaviour.

If the designer is seeking to increase the span-to-depth ratio to obtain a more structurally efficient floor, it is recommended that the depth of web members be reduced rather than the flange member. As detailed in Chapter 7 Section 7.5, a reduction in flange thickness resulted in a significant reduction of modal mass in higher modes which substantially increased the floor response.

8.8 Concluding remarks

This chapter has provided guidance on a floor vibration design process for long-span timber ribbed-deck floors in the form of a flow chart based on the design flow chart of CCIP-016. Considerations in the numerical model, response prediction, vibration criteria and performance assessment as well as structural modifications have been discussed based on findings from previous chapters. It is anticipated that this flow chart will provide a base from which processes and decisions can be updated as new information and results become available.

Chapter 9

Conclusions and Recommendations

9.1 Conclusions

Changes in building codes, the momentum of the 'green building' movement and the development of engineered wood products (EWPs) has led to a growing interest in using timber as a suitable structural material for floors in large-scale construction including commercial buildings. However, vibration serviceability design due to human-induced walking still presents as one of the main concerns (Smith & Frangi 2015) and often governs the design (Dolan et al. 1999; Glisovic & Stevanovic 2010; Hassan & Girhammar 2013; Hu & Chui 2004; Mohr 1999; Ohlsson 1988a). A substantial amount of research has been conducted on short-span joist floors used in residential dwellings resulting in vibration design methods such as those published in Eurocode 5 (2004) and Hu and Chui's (2004) combined frequency and deflection criterion. However, as found in the literature review, investigations and criteria on long-span floors (> 6.5 m), for which ribbed-deck cassettes are suited, have been limited.

This research provided guidance for a vibration design procedure suitable for long-span timber floors based on the experimental and numerical investigations on a 9 m span LVL

ribbed-deck cassette floor. The main conclusions from this research can be summarised as follows:

1. As identified in the literature review, there is a lack of conclusive vibration design procedures for long-span timber floors in commercial buildings. Current criterion are based on mainly residential, short-span floors with simple criterion which disregard contribution of higher modes. Higher modes may still be dominant if the modal mass is low and, due to the highly orthotropic behaviour of timber cassette floors, modal clustering is expected. These should be considered in any future design procedure for long-span timber floors.

2. Dynamic tests under laboratory conditions were performed on a single cassette with various boundary conditions. Testing was conducted with an impact hammer and experimental modal analysis was performed to obtain the modal properties of the floor. The test results revealed that there was minimal difference in modal properties between a flange bearing and screwed boundary condition; damping ratio for all modes was approximately 1%.

3. Introducing an elastic interlayer such as Sylomer$^®$ at the support significantly increased the damping ratio for modes 1 and 2 to approximately 5% and 7%, respectively. Walking tests showed that the maximum response at the centre of the floor were reduced by up to 78%. Potential for further reductions in floor response were found through increasing the ratio of utilisation of the elastomer by adding load along the support. These results are promising and may be worth investigating further as a potential method to increase the floor damping ratio.

4. Dynamic tests on double cassette tests with various cassette-to-cassette configurations revealed that the addition of the flange-to-flange connection in conjunction with the web-to-web connection provides additional stiffness for the first lateral bending mode only. This influence was particularly larger for the splice connection. In terms of floor response, there was no clear difference between the maximum amplitudes when using either a splice or diagonal screw connection. However, the cumulative distribution plot showed that the diagonal screw connection generally had a lower response for a longer duration of the walking event. The influence of reduced screw spacing from 300 mm c/c to 150 mm c/c was negligible on both modal properties and floor response.

5. A numerical model of a single cassette floor was developed using ANSYS and correlated to measured modes and frequencies using both manual and automatic model updating methods. A sensitivity analysis revealed that the most influential material properties on the natural frequencies were the parallel to grain modulus of elasticity (MoE) and density of the web member, and both the parallel and perpendicular to grain (in the plane of the flange) MoE, density and Poisson's ratio of the flange member. These results reveal that is sufficient to model the web member as an isotropic element, however the orthotropic behaviour of LVL in the flange must be considered. Further, it was found that modelling the supports using elastic spring elements were important for correct mode sequence.

6. Model calibration of a double cassette FE model using measured results indicate that cassette-to-cassette connections can be modelled as translationally coupled nodes (i.e. pin connections) at a spacing which aligns with the centre-to-centre spacing of the screws. Assuming a rotational restraint about the axis parallel to the floor span at flange-to-flange connection appears to provide closer alignment to the natural frequencies of the measured results, particularly for the first lateral bending mode. Further connection tests are recommended to clarify these findings.

7. The fundamental mode of the single cassette floor was on the boundary of the low- to high-frequency floor cut-off but, nevertheless, would have been classified as a high-frequency floor based on current vibration design guides (CCIP-016, SCI P354 and AISC DG11). However, the measured response revealed that the floor did not act in a strictly transient or resonant manner and was somewhere in between. Therefore, it may not be appropriate to make assumptions on the floor response based on the fundamental frequency, particularly for those which lie on the boundary. This was further demonstrated when applying an effective impulse approach proposed in current vibration design guides which showed inconsistent (between guides) and inaccurate (mostly underestimated) response predictions. On the other hand, when considering a five (sub)harmonic Fourier series load model proposed by Živanović et al. (2007b) with the frequency content at the integer harmonics and subharmonics only ('basic' model), the predicted response was over-estimated by 23%.

8. Through an investigation of the accuracy of response prediction using different walking load models, it was found that the step-by-step load model proposed by Chen et al. (2019) provided the closest match to the maximum measured responses. This load model avoids the need to categorise the floor and potentially make an erroneous assumption of how the floor will respond. Further, the full time-history response can be obtained which allows the user to calculate the cumulative distribution of the floor response over a certain walking event. This means that the duration of the response surpassing the recommended RF limit can be included as an additional measure to assess whether the floor is satisfactory. A calculation procedure for the cumulative distribution using MATLAB has been provided in Appendix B.

9. It would be beneficial to vibration design if probabilistic load models including those proposed by Chen et al. (2019) and Živanović et al. (2007b) are considered. These can be programmed to provide the likelihood of a certain response occurring within a sample population. This approach has more merit than the pass-fail approach taken with the deterministic load models where only the maximum response is considered, particularly when vibration design is critical.

10. A multi-cassette floor model with dimensions (9.19 m × 9.76 m) similar to a typical floor grid of commercial buildings was created based on the calibrated single cassette model and double cassette model. Modal analysis showed that there were generally nine modes under 30 Hz with a high degree of modal clustering, particularly for the first three modes. Higher modes with low modal masses were found to largely contribute to the floor response. This provides further evidence that criterion based purely on the fundamental mode may be inadequate for long-span timber floors.

11. Parametric studies using the multi-cassette model revealed that having a higher damping ratio has the most beneficial effect on floor response. However, caution needs to be taken to ensure that the damping ratio is well justified. In addition, it was also found that reducing web depth rather than flange thickness is preferred if the design engineer needed to increase the structural efficiency of the floor.

9.2 Recommendations for Future Work

There are a number of potential areas that require further research toward the goal of having a vibration design procedure which is both efficient and accurate for long-span timber ribbed-deck floors. These include:

- Subjective testing on occupant comfort on long-span timber floors, preferably in buildings which have already been completed. Studies have shown that vibration tolerance may be higher in timber buildings (Chang, Goldsmith & Harris 2018) compared the typical RF limit of 8 which is imposed for office building floors. This data will be crucial in building a case to have a less stringent criterion for long-span timber floors.

- Developing 'deemed-to-comply' standard designs for long-span timber cassette floors in commercial buildings based on the findings from the numerical modelling considerations identified in this research. These designs should satisfy various acceptance criteria such as for varying requirements for floor performance and would be useful in translating the findings from this research into a more user-friendly format. These should be based on standard material properties and off-the-shelf sizes of LVL.

- Extending the research into testing of other long-span timber floors including those with a CLT panel connected to glulam web members. This will provide insight into the effects of having a panel with two-way spanning capability on the vibration performance, particularly in terms of modal clustering.

- Experimental results with an elastic interlayer (particularly Sylomer®) between the overhanging flange and support beam showed promising results in increasing the damping ratio of the floor system. Further studies in this area would be beneficial to confirm a damping ratio that can be used in design if these acoustic interlayers are incorporated into the structure.

- Significant work has been undertaken in Japan to incorporate the effect of duration of vibration when assessing the vibration performance of the floor. A 'duration correction factor' similar to the one used in AIJES V001 (2018) for vibrations which are less than 10 s in duration may be used to attenuate the amplitude used to evaluate the response factor. It may be beneficial to collaborate with Japanese universities including Tokyo Institute of Technology where a large amount of research in this area has been performed.

- It would be interesting to extend the investigation of walking load models in Chapter 5 to include comparison to measured walking responses from already completed long-span timber floors. This would provide more evidence on the appropriateness and accuracy of certain load models.

- Research into the damping ratio values for long-span floors in completed buildings would be beneficial in establishing a more realistic value. A study similar to the one undertaken by Jarnerö et al. (2015) where the modal properties were measured at various stages of construction would be useful. Further, the effect of a typical office fit-out on the damping value would be of interest.

References

Abeysekera, K., Hamm, P., Toratti, T. & Lawrence, A. 2018, 'Development of a floor vibration design method for Eurocode 5', International Network on Timber Engineering Research (INTER) - Meeting 51, Tallinn, Estonia.

Al-foqaha, A.A., Cofer, W.F. & Fridley, K.J. 1999, 'Vibration design criterion for wood floors exposed to normal human activities', Journal of Structural Engineering, vol. 125, no. 12, pp. 1401–6.

Al-hunaidi, O.M. 1996, 'Evaluation of human response to building vibration caused by transit buses', Journal of Low Frequency Noise and Vibration, vol. 15, no. 1, pp. 25–42.

Allemang, R.J. 2003, 'The modal assurance criterion - Twenty years of use and abuse', Sound and Vibration, vol. August, pp. 14–21.

Allen, G.R. 1975, Ride quality and international standard ISO 2631 ('Guide for the evaluation od human exposure to whole-body vibration'), Washington, DC.

Alves, N.K.C., Roitman, N. & Magluta, C. 1999, 'Dynamic response under human movements', Materials and Structures, vol. 32, no. February, pp. 31–7.

American National Standard Institute 1983, Guide to evaluation of human exposure to vibration in buildings, ANSI S3.29-1983.

Amick, H. 1997, 'On Generic Vibration Criteria for Advanced Technology Facilities', Journal of the Institute of Environmental Sciences, vol. 40, no. 5, pp. 35–44.

ANSYS Inc 2016, ANSYS, SAS IP.

Architectural Institute of Japan 1991, Guidelines for the evaluation of habitability to building vibration, AIJES-V001-1991, Architectural Institute of Japan, Japan.

Architectural Institute of Japan 2004, Guidelines for the evaluation of habitability to building vibration, AIJES-V001-2004, Architectural Institute of Japan, Japan.

Architectural Institute of Japan 2018, Standard for the Evaluation of Habitability to Building Vibration, Japan.

Bachmann, H. & Ammann, W. 1987, Vibrations in Structures: Induced by Man and Machines, IABSE.

Bachmann, H., Pretlove, A.J. & Rainer, H. 1995, 'Dynamic forces from rhythmical human body motions', Vibration Problems in Structures: Practical Guidelines, Birkhäuser

Verlag Basel, pp. 185–90.

Bainbridge, R.J. & Mettem, C.J. 1998, 'Simplified natural frequency', Proceedings of the Institution of Civil Engineers - Structures and Buildings, vol. 128, no. Nov, pp. 317–22.

Bassoli, E., Nimmen, K. Van, Vincenzi, L. & Broeck, P. Van Den 2018, 'A spectral load model for pedestrian excitation including vertical human- structure interaction', Engineering Structures, vol. 156, pp. 537–47.

Bates Smart 2018, 25 King, viewed <https://www.batessmart.com/bates-smart/projects/sectors/commercial/25-king/>.

BC Housing 2017, Mid-Rise Best Practice Guide, Canadian Wood Council and Wood WORKS!, British Columbia, Canada.

Beattie, G.J. 1998, The vibration performance of timber floors, Building Research Association of New Zealand, Judgeford.

Bernard, E.S. 2008, 'Dynamic Serviceability in Lightweight Engineered Timber Floors', Journal of Structural Engineering, vol. 134, no. 2, pp. 258–68.

Blaß, H.J., Ehlbeck, J., Kreuzinger, H. & Steck, G. 2005, Erläuterungen zu DIN 1052:2004-08 (in German), 2nd edn, Bruderverl., Karlsruhe.

British Standards Institution 1984, Guide to evaluation of human exposure to vibration in buildings (1 Hz to 80 Hz), BS 6472:1984.

British Standards Institution 1987, Guide to measurement and evaluation of human exposure to whole-body mechanical vibration and repeated shock, BS 6841:1987.

British Standards Institution 2002, Eurocode - Basis of structural design, BS EN 1990:2002, British Standards Institution.

British Standards Institution 2008a, Guide to evaluation of human exposure to vibration in buildings, BS 6472-1:2008.

British Standards Institution 2008b, UK National Annex to Eurocode 5: Design of timber structures. General. Common rules and rules for buildings, British Standards Institution.

Brownjohn, J., Racic, V. & Chen, J. 2016, 'Universal response spectrum procedure for predicting walking-induced floor vibration', Mechanical Systems and Signal Processing, vol. 70–71, pp. 741–55.

Brownjohn, J.M.., Pavic, A. & Omenzetter, P. 2004, 'A spectral density approach for modelling continuous vertical forces on pedestrian structures due to walking',

Canadian Journal of Civil Engineering, vol. 31, pp. 65–77.

Brownjohn, J.M.W. & Middleton, C.J. 2008, 'Procedures for vibration serviceability assessment of high-frequency floors', Engineering Structures, vol. 30, no. 6, pp. 1548–59.

Brownjohn, J.M.W. & Xia, P.-Q. 2000, 'Dynamic assessment of curved cable-stayed bridge by model updating', Journal of Structural Engineering, vol. 126, no. 2, pp. 252–60.

Brownjohn, J.M.W., Xia, P.-Q., Hao, H. & Xia, Y. 2001, 'Civil structure condition assessment by FE model updating:: methodology and case studies', Finite Elements in Analysis and Design, vol. 37, pp. 761–75.

Buchanan, A. 2007, Timber Design Guide, New Zealand Timber Industry Federation inc., Wellington.

Carter Holt Harvey 2012, hySPAN solutions range, viewed <https://fblvl.com.au/ranges/products/hyspan/>.

Carter Holt Harvey 2015, hyJOIST options range design guide, viewed 4 March 1BC, <chhwoodproducts.com.au/hyjoist>.

Chang, W., Goldsmith, T. & Harris, R. 2018, 'A new design method for timber floors – Peak Acceleration approach', International Network on Timber Engineering Research (INTER) - Meeting 51, Tallinn, Estonia.

Chen, J., Ding, G. & Zivanovic, S. 2019, 'Stochastic single footfall trace model for pedestrian walking load', International Journal of Structural Stability and Dynamics, vol. 19, no. 3, p. 1950029.

Chen, J., Wang, J. & Brownjohn, J.M.W. 2019, 'Power Spectral-Density Model for Pedestrian Walking Load', Journal of Structural Engineering, vol. 145, no. 2.

Chen, J., Xu, R. & Zhang, M. 2014, 'Acceleration response spectrum for predicting floor vibration due to occupant walking', Journal of Sound and Vibration, vol. 333, no. 15, pp. 3564–79.

Chui, Y.H. 1986, 'Vibrational performance of timber floors and the related human discomfort', Journal of the Institute of Wood Science, vol. 10, no. 5, pp. 183–6.

Clough, R.W. & Penzien, J. 1993, Dynamics of Structures, Revised., McGraw-Hill Education - Europe, New York United States.

Cook, R.D. 1995, Finite element modeling for stress analysis, John Wiley and Sons Inc, Canada.

Cooley, J. & Tukey, J.W. 1965, 'An Algorithm for the Machine Calculation of Complex Fourier Series', Mathematics of Computation, vol. 19, no. 90, pp. 297–301.

Crews, K. & Shrestha, R. 2016, Timber Cassette Floors, Technical Design Guide 31, Wood Solutions Australia, Australia.

Crews, K.I. 2002, 'Behaviour and critical limit states of transversely laminated timber cellular bridge decks', PhD thesis, University of Technlogy Sydney.

Crick, M.J., Hill, M.D. & Charles, D. 1987, 'The Role of Sensitivity Analysis in Assessing Uncertainty', Proceedings of an NEA Workshop on Uncertainty Analysis for Performance Assessments of Radioactive Waste Disposal Systems, Paris, pp. 1–258.

Dolan, J.D., Murray, T.M., Johnson, J.R., Runte, D. & Shue, B.C. 1999, 'Preventing annoying wood floor vibrations', Journal of Structural Engineering, vol. 125, no. 1.

Downing, D.J., Gardner, R.H. & Hoffman, F.O. 1985, 'An Examination of Response-Surface Methodologies for Uncertaintyanalysis in Assessment Models.', Technometrics, vol. 27, no. 2, pp. 151–63.

Dumanoglu, A.A., Brownjohn, J.M.W. & Severn, R.T. 1992, 'Seismic Analysis of The Faith Sultan Mehmet (Second Bosporus) Suspension Bridge', Journal of Earthquake Engineering and Structural Dynamics, vol. 21, pp. 881–906.

Ebadi, M.M., Doudak, G. & Smith, I. 2017, 'Finite-Element Modeling and Parametric Study of Glulam Beam-and-Deck Floors', Journal of Structural Engineering, vol. 143, no. 9, pp. 04017106-1–7.

Ebadi, M.M., Doudak, G. & Smith, I. 2018, 'Vibration responses of glulam beam-and-deck floors', Engineering Structures, vol. 156, no. 2018, pp. 235–42.

Ebadi, M.M., Doudak, G. & Smith, I. 2019, 'Evaluation of floor vibration caused by human walking in a large glulam beam and deck floor', Engineering Structures, vol. 196, no. February 2018.

Ellingwood, B. & Tallin, A. 1984, 'Structural Serviceability: Floor Vibrations', Journal of Structural Engineering, vol. 110, no. 2, pp. 401–18.

Ellis, B.R. 2000, 'On the response of long-span floors to walking loads generated by individuals and crowds', The Structural Engineer, vol. 78, no. 10, pp. 17–25.

Ellis, B.R. 2001, 'Serviceability evaluation of floor vibration induced by walking loads', The Structural Engineer, vol. 79, no. 21.

Eriksson, P.E. 1994, 'Vibration of low-frequency floors: Dynamic forces and response prediction', PhD thesis, Chalmers Univ. of Technology.

European Committee for Standardisation 2004, Eurocode 5: Design of timber structures - Part 1-1:General Common rules and rules for buildings, The European Committee for Standardisation.

Ewins, D.J. 2000, Modal testing: theory, practice and application, 2nd edn, Research Studies Press Ltd, UK.

Feldmann, M. 2008, Human-induced vibration of steel structures (HIVOSS), Luxembourg.

Feldmann, M., Heinemeyer, C., Butz, C., Caetano, E., Cunha, A., Galanti, F., Goldack, A., Hechler, O., Hicks, S., Keil, A., Lukic, M., Obiala, R., Schlaich, M., Sedlacek, G., Smith, A. & Waarts, P. 2009, Design of floor structures for human induced vibrations, European Commission Joint Research Centre, Italy.

Filiatrault, A., Folz, B. & Foschi, R.O. 1990, 'Finite-Strip Free-Vibration Analysis of Wood Floors', Journal of Structural Engineering, vol. 116, no. 8, pp. 2127–42.

Foschi, R.O. & Gupta, A. 1987, 'Reliability of floors under impact vibration', Canadian Journal of Civil Engineering, vol. 14, no. 5, pp. 683–9.

Foschi, R.O., Neumann, G.A., Yao, F. & Folz, B. 1996, 'Floor vibration due to occupants and reliability-based design guidelines', Canadian Journal of Civil Engineering, vol. 22, no. 2, pp. 471–9.

Friswell, M.I. & Mottershead, J.E. 1995, Finite element model updating in structural dynamics, G.M.L. Gladwell (ed.), Springer-science+business media, B.V.

Fujino, E., Suzuki, S. & Noguchi, H. 2008, 'Effects of Human Load on Vertical Dynamic Characteristics of Wooden Beam Floor', 10th World Conference on Timber Engineering, Miyazaki, Japan.

Fujino, Y., Pacheco, B.M., Nakamura, S. & Warnitchai, P. 1993, 'Synchronization of human walking observed during lateral vibration of a congested pedestrian bridge', Earthquake Engineering and Structural Dynamics, vol. 22, no. 9, pp. 741–58.

Gajalakshmi, G. & Mohaideen, A.J. 2013, 'Dynamic response of bare steel concrete under human rhythmic activities', International Conference on Future Trends in Structural, Civil, Environmental and Mechnical Engineering, Institute of Research Engineers and Doctors, pp. 14–9.

Galbraith, F.W. & Barton, M.V. 1970, 'Ground loading from footsteps', Journal of Acoustical Society of America, vol. 48, no. 5.

Gerber, C. & Crews, K. 2008, 'Computer simulations of timber stressed-skin panels using

finite element', 10th World Conference on Timber Engineering, Miyazaki, Japan.

Gerber, C., Crews, K. & Shrestha, R. 2012, Design Procedures for Timber Concrete Composite Floor Systems in Australia and New Zealand, STIC.

Getzner GmbH 2016, Overview of Materials - Standard Range, viewed <http://christianberner.se/$-1/file/sylomer-sylodyn-overview-of-materials-09.pdf>.

Glisovic, I. & Stevanovic, B. 2010, 'Vibrational behaviour of timber floors', World Conference on Timber Engineering, Trentino, Italy.

Green, D.W., Winandy, J.E. & Kretschmann, D.E. 2010, 'Mechanical Properties of Wood', in U.S.D. of Agriculture (ed.),Wood Handbook - Wood as an engineering material. General Technical Report FPL-GTR-113, Forest Products Laboratory, Madison, WI, United States, pp. 4-1-4–45.

Griffin, M.J. 1990, Handbook of Human Vibration, 1st edn, Academic Press Limited, London.

Griffin, M.J. & Whitham, E.M. 1980a, 'Discomfort produced by impulsive whole-body vibration', The Journal of the Acoustical Society of America, vol. 68, no. 5, pp. 1277–84.

Griffin, M.J. & Whitham, E.M. 1980b, 'Time dependency of whole-body vibration discomfort', The Journal of the Acoustical Society of America, vol. 68, no. 5, pp. 1522–3.

Guthrie, B. 2018, Barangaroo International House, viewed <http://theguthrieproject.com/photoShare_TZA_Barangaroo_C2_Construction.html>.

Hamby, D.M. 1994, 'A review of techniques for parameter sensitivity analysis of environmental models', Environmental Monitoring and Assessment, vol. 32, pp. 135–54.

Hamm, P., Richter, A. & Winter, S. 2010, 'Floor vibrations – new results', 11th World Conference on Timber Engineering, Trentino, Italy.

Hanagan, L.M. 2005, 'Walking-Induced Floor Vibration Case Studies', ASCE Journal of Architectural Engineering, vol. 11, no. 1, pp. 14–8.

Hansen, H. 1960, Deflection characteristics of wood-joist floors, National Research Council of Canada, Ottawa, Canada.

Harper, F.C. 1962, 'The mechanics of walking', Research Appl. in Industry, vol. 15, no. 1.

Harte, A. 2009, 'Timber engineering: an introduction', in M. Forde (ed.),ICE Manual of Construction Materials, Institution of Civil Engineers, pp. 707–15.

Hashim, H., Ibrahim, Z. & Razak, H.A. 2013, 'Dynamic characteristics and model updating of damaged slab from ambient vibration measurements', Measurement: Journal of the International Measurement Confederation, vol. 46, pp. 1371–8.

Hassan, O.A.B. & Girhammar, U.A. 2013, 'Assessment of Footfall-Induced Vibrations in Timber and Lightweight Composite Floors', International Journal of Structural Stability and Dynamics, vol. 13, no. 02.

Hassanieh, A., Chiniforush, A.A., Valipour, H.R. & Bradford, M.A. 2019, 'Vibration behaviour of steel-timber composite floors, part (2): Evaluation of human-induced vibrations', Journal of Constructional Steel Research, vol. 158, pp. 156–70.

Holzbau 2003, SIA 265 (in German).

Homb, A. & Kolstad, S.T. 2018, 'Evaluation of floor vibration properties using measurements and calculations', Engineering Structures, vol. 175, no. August, pp. 168–76.

Howarth, H.V.C. & Griffin, M.J. 1988, 'Human Response To Simulated Intermittent Railway-Induced Building Vibration', Journal of Sound and Vibration, vol. 120, no. 2, pp. 413–20.

Hu, L. 2000, Serviceability design criteria for commercial and multi-family floors. Report No. 4 to Canadian Forest Service, Forintek Canada Corp., Sainte-Foy, Canada.

Hu, L. & Chui, Y.-H. 2004, 'Development of a design method to control vibrations induced by normal walking action in wood-based floors', 8th World Conference on Timber Engineering, Lahti, Finland.

Hu, L.J. 1992, 'Prediction of Vibration Responses of Ribbed Plates by Modal Synthesis', PhD Thesis, The University of New Brunswick.

Hu, L.J. 2002, 'Development of a performance criterion for controlling vibrations in wood-based floors', Proceedings of the 7th World Conference on Timber Engineering, Shah Alam, Malaysia, pp. 219–26.

Hu, L.J., Chui, Y.H. & Onysko, D.M. 2001, 'Vibration serviceability of timber floors in residential construction', Progress in Structural Engineering and Materials, vol. 3, pp. 228–37.

Humar, J.L. 2012, Dynamics of Structures, 3rd edn, Taylor and Francis Group, Boca Raton, Florida.

Inman, V.T., Ralston, H.J. & Todd, F. 1981, Human Walking, Williams & Wilkins, Baltimore.

International Standards Organisation 1974, Guide for the evaluation of human exposure to whole-body vibration, ISO 2631.

International Standards Organisation 1978, Guide for the evaluation of human exposure to whole-body vibration, ISO 2631.

International Standards Organisation 1989, Evaluation of human exposure to whole-body vibration - Part 2: Continuous and shock-induced vibrations in buildings (1 to 80 Hz), ISO 2631-2:1989.

International Standards Organisation 1997, Mechanical vibration and shock - evaluation of human exposure to whole-body vibration - Part 1: General Requirements, ISO 2631-1:1997.

International Standards Organisation 2003, Mechanical vibration and shock - Evaluation of human exposure to whole-body vibration - Vibration in buildings (1 Hz to 80 Hz), ISO 2631-2:2003.

International Standards Organisation 2007, Bases for design of structures - serviceability of buildings and walkways against vibrations, ISO 10137:2007.

International Standards Organisation 2017, Human response to vibration - Measuring instrumentation - Part 1: General purpose vibration meters 2017 ISO 8041-1.

IPCC 2014, Climate change 2014: synthesis report. Contribution of working groups I, II and III to the fifth assessment report of the intergovernmental panel on climate change, Geneva, Switzerland, Switzerland.

Jacobs, N.J. & Skorecki, J. 1972, 'Analysis of the vertical component of force', Journal of Biomechanics, vol. 5, pp. 11–34.

Japanese Standards Association 1995, Vibration level meters, JIS C 1510:1995, Japan.

Jarnero, K., Bolmsvik, Å., Brandt, A. & Olsson, A. 2012, 'Effect of flexible supports on vibration performance of timber floors', Euronoise, Prague, pp. 214–9.

Jarnerö, K., Brandt, A. & Olsson, A. 2015, 'Vibration properties of a timber floor assessed in laboratory and during construction', Engineering Structures, vol. 82, pp. 44–54.

Jin, S.S., Cho, S., Jung, H.J., Lee, J.J. & Yun, C.B. 2014, 'A new multi-objective approach to finite element model updating', Journal of Sound and Vibration, vol. 333, no. 11, pp. 2323–38.

Johnson, J.R. 1994, 'Vibration acceptability in wood floor systems', Masters thesis,

Virginia Polytechnic Institute and State University.

Kalkert, R.E., Dolan, J.D. & Woeste, F.E. 1993, 'The current status of analysis and design for annoying wooden floor vibrations', Wood and Fiber Science, vol. 25, no. 3, pp. 305–14.

Kearney, K. 2018, 'Contourfcmap: filled contour plot with precise colormap', MATLAB Central File Exchange, viewed 2 August 2018, <https://au.mathworks.com/matlabcentral/fileexchange/29638-contourfcmap-filled-contour-plot-with-precise-colormap>.

Kerr, S.C. 1998, 'Human Induced Loading on Staircases', PhD thesis, University College London.

Khokhar, A., Chui, Y. & Smith, I. 2012, 'Influence of stiffness between-joists bracing on vibrational servicability of wood floors', World Conference on Timber Engineering 2012, Auckland, New Zealand.

Khokhar, A.M. 2004, 'Influence of lateral element stiffness on performance of wooden floors', Masters thesis, University of New Brunswick.

Kidder, F.E. 1885, Architects and Builders Pocketbook, John Wiley, New York.

Kim, G.H. & Park, Y.S. 2004, 'An improved updating parameter selection method and finite element model update using multiobjective optimisation technique', Mechanical Systems and Signal Processing, vol. 18, no. 1, pp. 59–78.

King, A.B. 1999, Serviceability limit state criteria for New Zealand buildings, BRANZ Study Report No. 57, Judgeford.

King, A.J. 1957, 'Vibration and Noise of Mechanisms and Machines', Engineering, pp. 759–66.

KLH Massivholz GmbH 2014, Rib Elements, Austria.

Kolb, J. 2008, Systems in Timber Engineering, Lignum - Holzwirtschaft Schweiz & DGfH - German Society of Wood Research (eds), Birkhäuser Basel, Switzerland.

Kurian, A. 2000, 'Analytical modeling of glued laminated girder bridges using ANSYS', MTC Transportation Scholars Conference, Ames, Iowa, pp. 70–82.

Labonnote, N. 2012, 'Damping in Timber Structures', PhD thesis, Norwegian University of Science and Technology.

Labonnote, N., Ronnquist, A. & Malo, K.A. 2015, 'Prediction of material damping in timber floors, and subsequent evaluation of structural damping', Materials and Structures, vol. 48, pp. 1965–75.

Lam, F. 2009, 'Timber products and manufacturing processes', in M. Forde (ed.),ICE manual of Construction Materials, Institution of Civil Engineers, pp. 717–26.

Leissa, A. 1969, Vibration of Plates, SPP-160., NASA, Washington DC.

Lenzen, K.H. 1966, 'Vibration of steel joist-concrete slab floors', American Institute of Steel Construction – Engineering Journal, vol. 3, no. 3, pp. 133–6.

Li, Q., Fan, J., Nie, J., Li, Q. & Chen, Y. 2010, 'Crowd-induced random vibration of footbridge and vibration control using multiple tuned mass dampers', Journal of Sound and Vibration, vol. 329, no. 19, pp. 4068–92.

Lignatur 2019, Lignatur Surface element, viewed 22 July 2019, <https://www.lignatur.ch/en/product/lignatur-element/>.

Ljunggren, F. 2006, 'Floor Vibration - Dynamic Properties and Subjective Perception', PhD thesis, Luleå University of Technology.

Ljunggren, F., Wang, J. & Ågren, A. 2007, 'Human vibration perception from single- and dual-frequency components', Journal of Sound and Vibration, vol. 300, pp. 13–24.

LMS International 2012, The LMS Test.Lab Modal Analysis manual.

Loss, C., Piazza, M. & Zandonini, R. 2016, 'Connections for steel–timber hybrid prefabricated buildings. Part I: Experimental tests', Construction and Building Materials, vol. 122, pp. 781–95.

Lyons, R.G. & Fugal, D.L. 2014, The Essential Guide to Digital Signal Processing, Prentice Hall.

Macpherson, E., Papastavrou, P., Wallwork, T., Smith, S. & McRobie, A. 2018, 'The Rotational Stiffness of Cross Laminated Timber Half Lap Joints', World Conference on Timber Engineering 2018, Seoul, Republic of Korea.

Maia, N.M.M., Silva, J.M.M., He, J., Lieven, N.A.J., Lin, R.M., Skingle, G.W., To, W.-M. & Urgueira, A.P. V. 1997, Theoretical and experimental modal analysis, N.M.M. Maia & J.M.M. Silva (eds), Research Studies Press Ltd, Hertfordshire, England.

Matsumoto, Y., Shiojiri, H., Nishioka, T. & Matsuzaki, K. 1978, 'Dynamic design of footbridges', IABSE proceedings.

Metsä Wood 2015, Metsä Wood Kerto–Ripa® floor element, viewed 22 July 2019, <https://www.metsawood.com/global/news-media/News/Pages/Load-bearing-intermediate-floor-structure-without-on-site-casting.aspx>.

Middleton, C.J. & Brownjohn, J.M.W. 2010, 'Response of high frequency floors: A literature review', Engineering Structures, vol. 32, no. 2, pp. 337–52.

Miwa, T. 1967, 'Evaluation methods for vibration effect. Part 1 - measurements of threshold and equal sensation contours of whole body for vertical and horizontal vibrations', Industrial Health, vol. 5, no. 183.

Modak, S. V., Kundra, T.K. & Nakra, B.C. 2002, 'Comparative study of model updating methods using simulated experimental data', Computers and Structures, vol. 80, no. 2002, pp. 437–47.

Mohammed, A.S., Pavic, A. & Racic, V. 2018, 'Improved model for human induced vibrations of high-frequency floors', Engineering Structures, vol. 168, pp. 950–66.

Mohr, B. 1999, 'Floor Vibrations', International Council for Building Research Studies and Documentation, Graz, Austria.

Moroder, D., Pampanin, S. & Buchanan, A. 2016, Floor Diaphragms in Timber Buildings, WoodSolutions.

Murray, T.M., Allen, D.E. & Ungar, E.E. 1997, Floor Vibrations Due to Human Activity, 1st edn, American Institute of Steel Construction, U.S.A.

Murray, T.M., Allen, D.E., Ungar, E.E. & Davis, D.B. 2016, Vibrations of Steel-Framed Structural Systems Due to Human Activity: Second Edition.

Negreira, J., Trolle, A., Jarnero, K., Sjokvist, L.G. & Bard, D. 2015, 'Psycho-vibratory evaluation of timber floors - Towards the determination of design indicators of vibration acceptability and vibration annoyance', Journal of Sound and Vibration, vol. 340, pp. 383–408.

NelsonPine LVL 2016, Specific Engineering Design Guide, Nelson, New Zealand.

Nguyen, T., Gad, E., Wilson, J., Lythgo, N. & Haritos, N. 2011, 'Evaluation of Fotfall Induced Vibration in Building Floor', Australian Earthquake Engineering Society 2011 Conference, South Australia.

Oborne, D.J. 1983, 'Whole-Body Vibration and International Standard ISO 2631: A Critique', Human Factors, vol. 25, no. 1, pp. 55–69.

Ohlsson, S. V. 1982, 'Floor vibrations and human discomfort', PhD thesis, Chalmers University of Technology.

Ohlsson, S. V. 1988a, 'Ten years of floor vibration research - a review of aspects and some results', Symposium/Workshop on Serviceability of Buildings, Ottawa, pp. 435–50.

Ohlsson, S. V. 1988b, Springiness and human-induced floor vibrations: a design guide, Swedish Council for Building Research, Stockholm, Sweden.

Ohlsson, S. V. 1991, 'Serviceability criteria - especially floor vibration criteria', International Timber Engineering Conference, London, p. 1.58-1.65.

Olsson, A. & Källsner, B. 2008, 'Wooden floor structures with high transverse stiffness', Proceedings of the 10th World Conference on Timber Engineering, Miyazaki, Japan, pp. 2219–25.

Onysko, D.M. 1970, Performance of wood-joist floor systems: a literature review. Info. Rep OP-X-24, Ottawa, Canada.

Onysko, D.M. 1988, 'Performance and acceptability of wood floors - Forintek studies', Symposium/Workshop on Serviceability of Buildings, National Research Council of Canada, Ontario, Canada, pp. 477–94.

Onysko, D.M., Hu, L.J., Jones, E.D. & Di Lenardo, B. 2000, 'Serviceability design of residential wood framed floors in Canada', World Conference on Timber Engineering, Vancouver, B.C., pp. 1–8.

Pachi, A. & Ji, T. 2005, 'Frequency and velocity of people walking', The Structural Engineer, vol. 83, no. 3.

Pappa, R.S., Elliott, K.B. & Schenk, A. 1992, A consistent-mode indicator for the eigensystem realization algorithm, Virginia.

Parmelee, R. & Wiss, J. 1974, 'Human perception of transient vibrations', Journal of the Structural Division, vol. 100, no. ST4, pp. 773–87.

Pavic, A., Miskovic, Z. & Reynolds, P. 2007, 'Modal Testing and Finite-Element Model Updating of a Lively Open-Plan Composite Building Floor', Journal of Structural Engineering, vol. 133, no. 4, pp. 550–8.

Pavic, A., Reynolds, P., Prichard, S. & Lovell, M. 2003, 'Evaluation of Mathematical Models for Predicting Walking-Induced Vibrations of High-Frequency Floors', International Journal of Structural Stability and Dynamics, vol. 03, no. 01, pp. 107–30.

Pavic, A. & Willford, M. 2005, 'Appendix G Vibration Serviceability of Post-Tensioned Concrete Floors', Post-Tensioned Concrete Floors Design Handbook, The Concrete Society, pp. 99–108.

Pavic, A. & Zivanovic, S. 2007, 'Key elements for probabilistic framework for estimation of structural vibration due to human-structure dynamic interaction', The 3rd International Conference on Structural Engineering, Mechanics and Computation, p.

Percival, D.H. 1979, 'History of L/360', Forest Products Journal, vol. 29, no. 8, pp. 26–7.

Perera, R. & Ruiz, A. 2008, 'A multistage FE updating procedure for damage identification in large-scale structures based on multiobjective evolutionary optimization', Mechanical Systems and Signal Processing, vol. 22, no. 4, pp. 970–91.

Polensek, A. 1973, 'Static and Dynamic Analysis of Wood-Joist Floors by the Finite Element Method', PhD thesis, Oregon State University.

Porteous, J. & Kermani, A. 2007, Structural timber design to Eurocode 5, Blackwell Publishing, United Kingdom.

Portier, K., Keith Tolson, J. & Roberts, S.M. 2007, 'Body weight distributions for risk assessment', Risk Analysis, vol. 27, no. 1, pp. 11–26.

Postlethwaite, F. 1944, 'Human Suceptibility to Vibration', Engineering, vol. 157.

Pridham, B. 2013, 'Assessment of floor vibrations for building re-use: a case study', Proceedings of the 31st International Modal Analysis Conference (IMAC XXXI), Orange County.

Pridham, B. 2014, 'Vibration testing of a floor during multiple phases of construction', in F.N. Catbas (ed.),Dynamics of Civil Stuctures, Volume 4: Proceedings of the 32nd IMAC, A Conference and Exposition on Structural Dynamics, pp. 43–52.

Prony, G.R.B. 1795, 'Essai expérimental et analytique sur les lois de la dilatabilité de fluides élastiques et sur celles de la force expansive de la vapeur de l'eau et de la vapeur de l'alkool à différentes températures', Journal de L'École Polytechnique, vol. 1, no. 2, pp. 24–76.

Racic, V. & Brownjohn, J.M.W. 2011, 'Stochastic model of near-periodic vertical loads due to humans walking', Advanced Engineering Informatics, vol. 25, pp. 259–75.

Racic, V., Pavic, A. & Brownjohn, J.M.W. 2009, 'Experimental identification and analytical modelling of human walking forces: Literature review', Journal of Sound and Vibration, vol. 326, pp. 1–49.

Rainer, J.H., Pernica, G. & Allen, D.E. 1988, 'Dynamic loading and response of footbridges', Canadian Journal of Civil Engineering, vol. 15, no. 1.

Ramage, M.H., Burridge, H., Busse-Wicher, M., Fereday, G., Reynolds, T., Shah, D.U., Wu, G., Yu, L., Fleming, P., Densley-Tingley, D., Allwood, J., Dupree, P., Linden, P.F. & Scherman, O. 2017, 'The wood from the trees: The use of timber in construction', Renewable and Sustainable Energy Reviews, vol. 68, no. September 2016, pp. 333–59.

Reiher, H. & Meister, F.J. 1931, The sensitiveness of the human body to vibrations (Empfindlichkeit des menschen gegen erschutterung), Wright Field, Dayton, Ohio, pp. 381–6.

Reynolds, T., Harris, R., Chang, W.-S., Bregulla, J. & Bawcombe, J. 2015, 'Ambient vibration tests of a cross-laminated timber building', Proceedings of the Institution of Civil Engineers - Construction Materials, vol. 168, no. CM3, pp. 121–31.

Rimell, A.N. & Mansfield, N.J. 2007, 'Design of Digital Filters for Frequency Weightings Required for Risk Assessments of Workers Exposed to Vibration', Industrial Health, vol. 45, no. 4, pp. 512–9.

Ruddy, J.L. & Ioannides, S.A. 2004, 'Rules of thumb for steel design', Structures Congress 2004, Nashville, Tennessee.

Sahnaci, C. & Kasperski, M. 2005, 'Random loads induced by walking', Sixth European Conference on Structural Dynamics (EURODYN), Millpress, Rotterdam, pp. 441–6.

SAS IP 2016, ANSYS Workbench.

Schulze, H. 1980, 'Dynamic effects of the live load on footbridges (in German)', Signal und Schiene, vol. 24, no. 2, 3, pp. 91–3, 143–7.

Sedlacek, G., Heinemeyer, C., Butz, C., Volling, B., Waarts, P., Van Duin, F., Hicks, S., Devine, P. & Demarco, T. 2006, Generalisation of criteria for floor industrial, office, residental and public building and gymanstic halls, Luxembourg.

Seryi, A. 2001, 'Ground motion and vibration issues for accelerators', Proceedings of the 2001 Particle Accelerator Conference, Chicago, pp. 364–8.

Setareh, M. & Lovelace, M. 2010, 'Vibration analysis and design of a structure subjected to human walking excitations', Shock and Vibration, vol. 17, no. 4–5, pp. 631–9.

Sheikhtabaghi, M.S. 2015, 'Continuity connection for cross laminated timber (CLT) floor diaphragms', Masters thesis, University of New Brunswick.

Shkuratova, N., Morris, M.E., Huxham, F., N, A.S., Me, M. & Effects, H.F. 2004, 'Effects of Age on Balance Control During Walking', Archives of Physcial Medicine and Rehabilitation, vol. 85, no. 4, pp. 582–8.

de Silva, C.W. 2000, 'Experimental Modal Analysis', Vibration: Fundamentals and Practice, 1st edn, CRC Press LLC, Boca Raton, Florida.

de Silva, C.W. 2000, Vibration: Fundamentals and Practice, 1st edn, CRC Press, Boca Raton.

da Silva, J.G.S., Vellasco, P.C.G.D.S. & de Andrade, S.A.L. 2008, 'Vibration analysis of orthotropic composite floors for human rhythmic activities', Journal of the Brazilian Society of Mechanical Sciences and Engineering, no. 1, pp. 56–65.

Simon, S.R., Paul, I.L., Mansour, J., Munro, M., Abernethy, P.J. & Radin, E.L. 1981, 'Peak dynamic force in human gait', Journal of Biomechanics, vol. 14, no. 12, pp. 817–22.

Sinha, J.K. 2015, Vibration analysis, instruments, and signal processing, 1st edn, CRC Press, Florida, U.S.A.

Siskind, B.D.E., Stagg, M.S., Kopp, J.W., Dowding, C.H., Andrus, C.D. & Norman, L.D. 1989, Structure response and damage produced by ground vibration from surface mine blasting, Bureau of Mines Report of Investigations, RI 8507, Washington, DC.

Skaggs, T. & Bender, D. 1995, 'Shear deflection of composite wood beams', Wood and Fiber Science, vol. 27, no. 3, pp. 327–38.

Smith, A.L., Hicks, S.J. & Devine, P.J. 2009, Design of Floors for Vibration: A new approach, The Steel Construction Institute, UK.

Smith, I. 1980, 'Series type solutions for built-up timber beams with semi-rigid connections', Proceedings of the Institution of Civil Engineers, vol. 69, no. 3 (Part 2), pp. 707–19.

Smith, I. & Chui, Y.H. 1986, 'Predicting the Natural Frequencies of Light-weight Wooden Floors', IUFRO Wood Engineering Group Meeting - Working Commission W18 - TImber Structures, International Council for Building Research Studies and Documentation, Florence, Italy.

Smith, I. & Chui, Y.H. 1988, 'Design of light-weight wooden floors to avoid human discomfort', Canadian Journal of Civil Engineering, vol. 15, pp. 254–62.

Smith, I. & Frangi, A. 2015, 'Technologies enabling advanced urban timber construction', Proceedings of the Institution of Civil Engineers, Civil Engineering, vol. 168, no. CE6, pp. 17–22.

Standards Australia 2002, Structural design actions - General principles, AS/NZS 1170.0:2002, Standards Australia.

Standards Australia 2006, Structural laminated veneer lumber (LVL) - Determination of structural properties - Test methods.

Standards Australia 2010a, Characterization of structural timber Part 1: Test methods, AS/NZS 4063.1:2010, Standards Australia.

Standards Australia 2010b, Timber Structures Part 1: Design Methods, AS 1720.1:2010, Standards Australia, Australia.

Stora Enso 2018, CLT rib panel by Stora Enso.

Timber Development Association & Forsythe, P. 2015, Rethinking office construction - consider timber, WoodSolutions, Sydney, Australia.

Toratti, T. & Talja, A. 2006a, 'Classification of Human Induced Floor Vibrations', Proceedings of the 9th World Conference on Timber Engineering, Portland, Oregon, USA.

Toratti, T. & Talja, A. 2006b, 'Classification of Human Induced Floor Vibrations', Building Acoustics, vol. 13, no. 3, pp. 211–21.

Ussher, E., Arjomandi, K., Weckendorf, J. & Smith, I. 2017a, 'Predicting effects of design variables on modal responses of CLT floors', Structures, vol. 11, no. April, pp. 40–8.

Ussher, E., Arjomandi, K., Weckendorf, J. & Smith, I. 2017b, 'Prediction of motion responses of cross-laminated-timber slabs', Structures, vol. 11, no. April, pp. 49–61.

Vaughan, C.L., Davis, B.L. & O'Connor, J.C. 1999, Dynamics of Human Gait, C.L. Vaughan (ed.), 2nd edn, Kiboho Publishers, South Africa.

Visser, W.J. 1992, 'Updating Structural Dynamics Models Using Frequency Response Data', PhD thesis, University of London.

Wang, J. & Chen, J. 2017, 'A comparative study on different walking load models', Structural Engineering and Mechanics, vol. 63, no. 6, pp. 847–56.

Weckendorf, J. 2009, 'Dynamic response of structural timber flooring systems', PhD thesis, Edinburgh Napier University.

Weckendorf, J., Toratti, T., Smith, I. & Tannert, T. 2015, 'Vibration serviceability performance of timber floors', European Journal of Wood and Wood Products, vol. 74, no. 3, pp. 353–67.

Weckendorf, J., Ussher, E. & Smith, I. 2016, 'Dynamic response of CLT plate systems in the context of timber and hybrid construction', Composite Structures, vol. 157, pp. 412–23.

Weckendorf, J., Zhang, B., Kermani, A., Reid, D. & Andersen, P. 2008, 'Damping Characteristics of Timber Flooring Systems with Respect to Low-Frequency Vibration Modes', 10th World Conference on Timber Engineering, Elsevier Ltd, Miyazaki, Japan.

Wheeler, J.E. 1982, 'Prediction and control of pedestrian induced vibration in footbridges', Journal of the Structural Division - American Society of Civil Engineers, vol. 108, pp. 2045–65.

Willford, M., Young, P. & Field, C. 2006, 'Improved methodologies for the prediction of footfall-induced vibration', in M. Ettouney (ed.),Building Integration Solutions, American Society of Civil Engineers, Omaha, Nebraska, pp. 1–15.

Willford, M., Young, P. & Field, C. 2007, 'Predicting footfall-induced vibration : Part 1', Structures & Buildings, vol. 160, no. SB2, pp. 65–72.

Willford, M.R. & Young, P. 2006, A design guide for footfall induced vibration of structures, CCIP-016., Surrey, UK.

Wu, J.R. & Li, Q.S. 2004, 'Finite element model updating for a high-rise structure based on ambient vibration measurements', Engineering Structures, vol. 26, no. 7, pp. 979–90.

Wyatt, T.A. 1989, Design guide on the vibration of floors, Berkshire.

Xiao-Guang, Y., Yan-ping, L., Guan-sheng, M., Xiao-qi, H. & Jing-zhong, W. 2005, 'Study on weight and height of the Chinese people and the differences between 1992 and 2002 (in Chinese)', Chinese Journal of Epidemiology, vol. 26, no. 7, pp. 489–93.

Ximenes, F., Robinson, M. & Wright, B. 2006, Forests, wood and Australia's carbon balance, F. and W.P.R. and D. Corporation (ed.), Australia.

Yokoyama, Y. 2018, AIJ Symposium on Environmental Vibration (in Japanese), Tokyo, Japan.

Zabihi, Z. 2014, 'Investigation of a Proposed Long Span Timber Floor for Non-Residential Applications', PhD thesis, University of Technology Sydney.

Živanović, S. 2006, 'Probability-Based Estimation of Vibration for Pedestrian Structures due to Walking', PhD thesis, University of Sheffield.

Živanovic, S. & Pavic, A. 2009, 'Probabilistic Modeling of Walking Excitation for Building Floors', Journal of Performance of Constructed Facilities, vol. 23, no. 3, pp. 132–43.

Živanović, S. & Pavić, A. 2009, 'Probabilistic Modeling of Walking Excitation for Building Floors', Journal of Performance of Constructed Facilities, vol. 23, no. 3, pp. 132–43.

Živanović, S., Pavic, A. & Reynolds, P. 2007a, 'Finite element modelling and updating

of a lively footbridge: The complete process', Journal of Sound and Vibration, vol. 301, no. 2007, pp. 126–45.

Živanović, S., Pavic, A. & Reynolds, P. 2007b, 'Probability-based prediction of multi-mode vibration response to walking excitation', Engineering Structures, vol. 29, no. 6, pp. 942–54.

Appendices

Appendix A: Material testing specimens and data

Test specimen dimensions, measured modulus of elasticity and density are shown inTable A-1. Specimens have been measured in accordance with *AS/NZS 4357.1* (2005). An example of the load-deflection curve for one specimen undergoing a four-point bending test is shown in Figure A-1. The modulus of elasticity was measured within the linear portion of the load-deflection curve between 20% and 40% of the maximum load, as shown by the red line in Figure A-1.

Table A-1 *Test specimen dimensions, modulus of elasticity and density values*

Specimen	L	D	B	MoE	Density
	mm	*mm*	*mm*	*MPa*	*kg/m³*
Flatwise					
1	1399	63	70.5	12884	578.3
2	1400	64	70.5	12355	581.1
3	1400	64	70.5	12370	576.1
4	1400	64	70.4	13030	590.2
5	1400	65	70.1	12811	599.3
Edgewise					
1	1400	70	64.0	12350	589.3
2	1400	70	64.1	13046	587.4
3	1400	70	64.1	12925	594.8
4	1399	70	64.1	12818	595.6
5	1400	70	64.2	12630	598.3
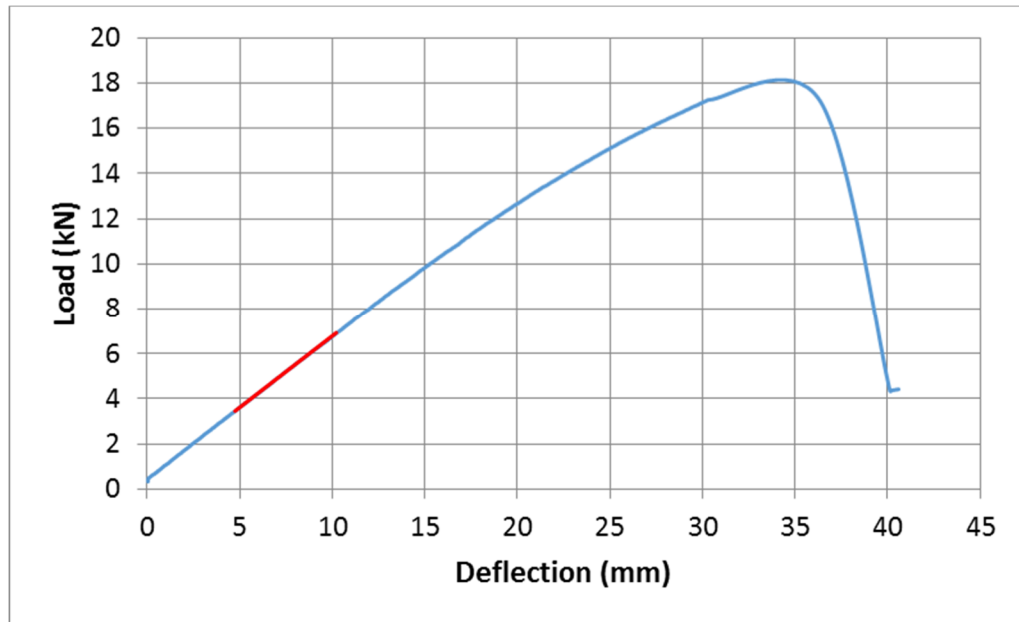
Figure A-1 *Typical load-deflection curve*

Appendix B: MATLAB code for cumulative distribution

```
%--------------------------------------------------------------------
----
% CumulativeDistribution.m – Cumulative distribution of Running
Response Factor
%--------------------------------------------------------------------
----
% Created by B. Basaglia on 30/07/2018
%--------------------------------------------------------------------
----
% Program to calculate the cumulative distribution of the Running RF

%--------------------------------------------------------------------
----
%--------------------------------------------------------------------
----
% INPUT:    Measured 1 second root-mean-square
%--------------------------------------------------------------------
----
% OUTPUT:   Cumulative probability of running RF for one walking event
%--------------------------------------------------------------------
----
%--------------------------------------------------------------------
----

%This program assumes the following has already been applied to the
raw acceleration data:
%- frequency-weighted based on appropriate weighting curve
%- running 1s root-mean-square averaging window

%It is assumed that the user may have a large number of tests with
different variables.
%The data may be concatenated depending on the different variables.
%E.g. three samples of measured data taken for Walker 1 @ 2.0 Hz
(120bpm) pace frequency – three samples are concatenated
%In the case of this research, the sample name contained the
information of the test which was then used to group data as required

%% STEP 1: Variables

Accel_num=21;    %Number of accelerometers in test set-up
Accel=11;        %Accelerometer of interest for graphs

%% STEP 2: Get data
k=fieldnames(DATA_LOOPED_Y_Wk_RMS);      %1 s RMS data for each test
was kept in a struct called 'DATA_LOOPED_Y_Wk_RMS'
r=size(k,1);                             %Number of samples
kix=strfind(k,'_');

%% STEP 3: Choose which variable to concatenated
%Comment out 'choice' which is not used
choice=1;        %Cumulative distribution based on each walking sample
%choice=2;       %Cumulative distribution based on walking frequency

%% STEP 4: Concatenate data
% Concatenate Loops into one array for each sample
for i=1:r
    samplename=char(k(i));
    Walker=samplename(1:kix{i}-1);       %get details out of sample
name
```

```matlab
    Pace=samplename(kix{i}+1:end);

    A=DATA_LOOPED_Y_Wk_RMS.(samplename).(tc).Loop1;      %Loop1 refers
to Sample 1
    B=DATA_LOOPED_Y_Wk_RMS.(samplename).(tc).Loop2;      %Loop2 refers
to Sample 2
    C=DATA_LOOPED_Y_Wk_RMS.(samplename).(tc).Loop3;      %Loop3 refers
to Sample 3

    D=cat(1,A,B,C);
    ProbDistData.(samplename)=D;
end

%Additional step if data is then concatenated based on walking
frequency

if choice==2
    % Concatenate based on walking pace

    for i=1:r
        samplename=char(k(i));
        Walker=samplename(1:kix{i}-1);
        Pace=samplename(kix{i}+1:end);
        if contains(Pace,"60") == 1
            fp=['fp',Pace];
            hh=ProbDistData.(samplename);
            ProbDistFpData.(fp).(Walker)=hh;
        elseif contains(Pace,"90") == 1
            fp=['fp',Pace];
            hh=ProbDistData.(samplename);
            ProbDistFpData.(fp).(Walker)=hh;
        elseif contains(Pace,"120") == 1
            fp=['fp',Pace];
            hh=ProbDistData.(samplename);
            ProbDistFpData.(fp).(Walker)=hh;
        elseif contains(Pace,"H") == 1
            fp=['fp',Pace];
            hh=ProbDistData.(samplename);
            ProbDistFpData.(fp).(Walker)=hh;
        end
    end

    fld1=fieldnames(ProbDistFpData);
    fld2=fieldnames(ProbDistFpData.fp60);

    for ii=1:length(fld1)
        tmp=cellfun(@(x) ProbDistFpData.(fld1{ii}).(x),fld2,'uni',0);
        fdname=['Cat_',fld1{ii}];
        ProbDistFpCATData.(fdname)=cat(1,tmp{:});
    end
    reorder={'Cat_fp60','Cat_fp90','Cat_fp120','Cat_fpH'};
    ProbDistFpCATData=orderfields(ProbDistFpCATData,reorder);

    fld=fieldnames(ProbDistFpCATData);
else
end

%% STEP 5: Cumulative distribution calculation

for i=1:r
    if choice==1
        samplename=string(k(i));
```

```matlab
        dd=ProbDistData.(samplename);        %get the concatenated data
        row=size(dd,1);
        for a=1:Accel_num        %for each accelerometer
            if a==1

                [f,x] = ecdf(dd(:,a));        %calculate the cumulative
distribution function
                rowx=size(x,1);
                ff=zeros(rowx,Accel_num);
                xx=zeros(rowx,Accel_num);
                ff(:,a)=f;
                xx(:,a)=x;
            else

                [f,x] = ecdf(dd(:,a));
                ff(:,a)=f;
                xx(:,a)=x;
            end

            CDFData.(samplename).f=ff;       %store function
            CDFData.(samplename).x=xx;       %store points
        end

    elseif choice==2
        samplename=string(fld(i));
        dd=ProbDistFpCATData.(samplename);
        row=size(dd,1);
        for a=1:Accel_num
            if a==1
                ddd=dd(:,a);
                [f,x] = ecdf(ddd);
                rowx=size(x,1);
                ff=zeros(rowx,Accel_num);
                xx=zeros(rowx,Accel_num);
                ff(:,a)=f;
                xx(:,a)=x;
            else
                ddd=dd(:,a);
                [f,x] = ecdf(ddd);
                ff(:,a)=f;
                xx(:,a)=x;
            end
            CDFData.(samplename).f=ff;
            CDFData.(samplename).x=xx;
        end

    end
end

%% STEP 6: Plot CDF for accelerometer of interest ('Accel')

figure1=figure;

for i=1:r
    if choice==1
        samplename=string(k(i));
    elseif choice==2
        samplename=string(fld(i));
    end
    xx=CDFData.(samplename).x;
    xx=xx(:,Accel);
    ff=CDFData.(samplename).f;
```

300

```matlab
    ff=ff(:,Accel);
    P_CDF =plot(xx,ff); %PDF
    hold on
end

ax2=gca;
xx12=ax2.XTick;

%Currently data is in RMS acceleration values
%Data can be presented as Response Factors by dividing the x-axis
values by the baseline
%perception curve for continuous vibration as provided in ISO 10137
(2007). As the data has already been
%frequency-weighted, this means the base value '0.005 m/s^2' is used.
xx22=xx12./0.005;
ax2.XTickLabel=xx22;
ax2.XTick=xx12;

xlabel('Response Factor','FontSize',13)
ylabel('Cumulative probability','FontSize',13)
grid on
```

Appendix C: Maximum response factor contour plots

for double cassette tests – Walker 2b
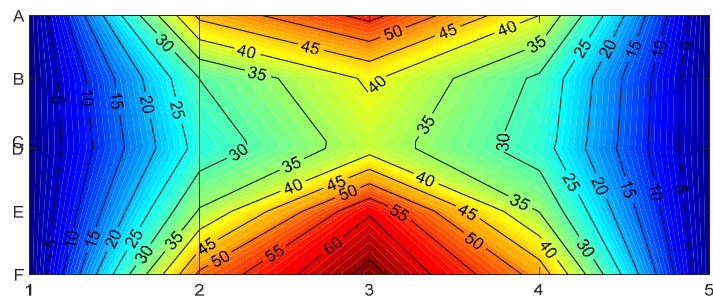
f_p (Hz)	C2_Web300	C2_Web150
1.5		
2.0		
'R'		
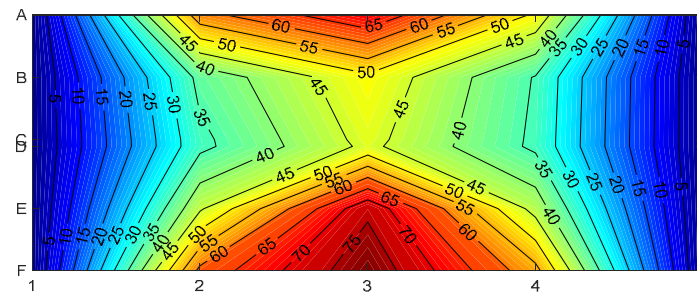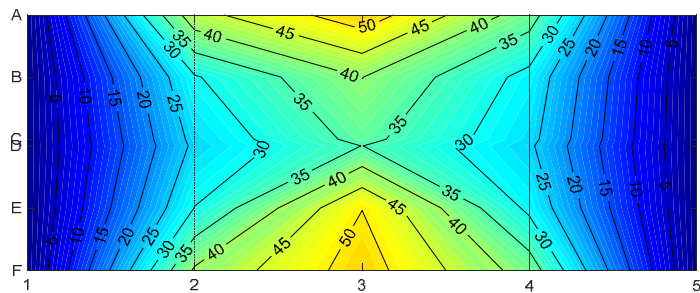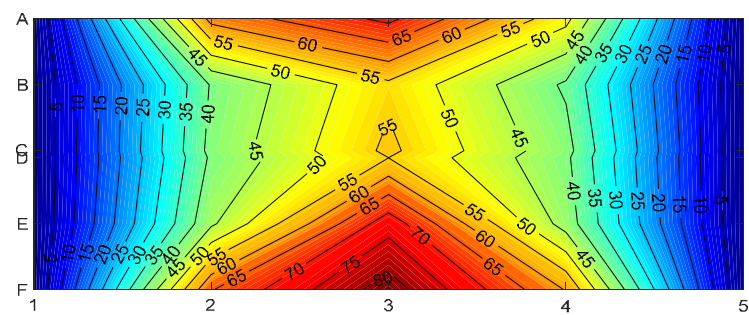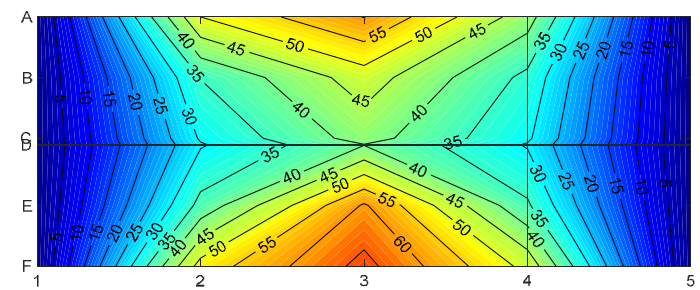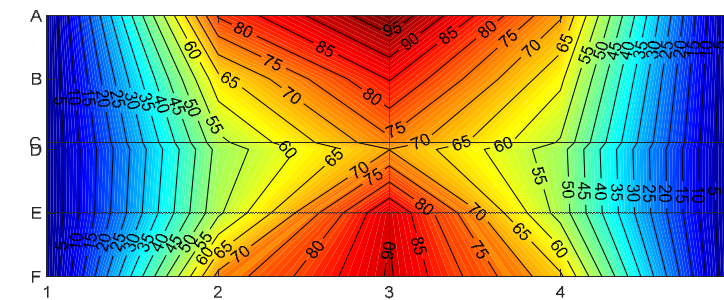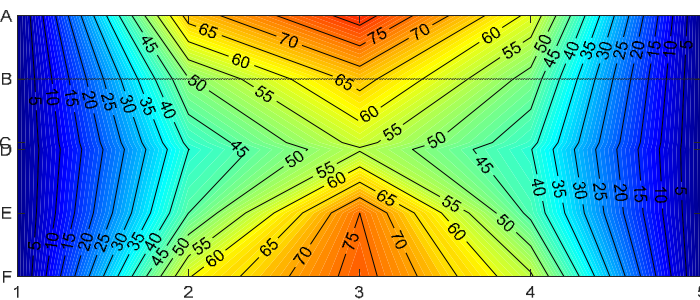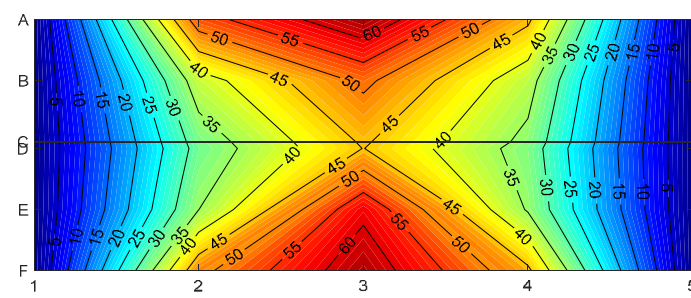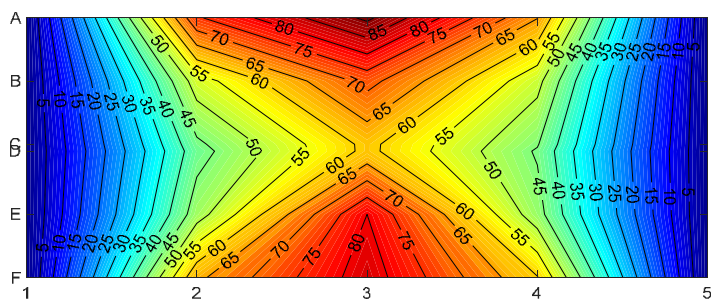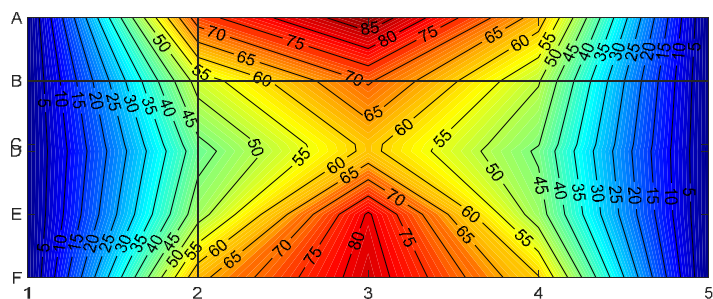
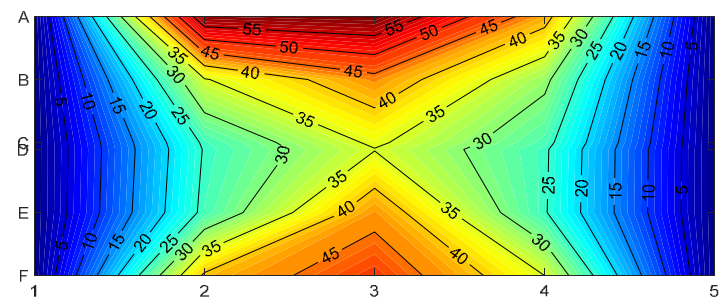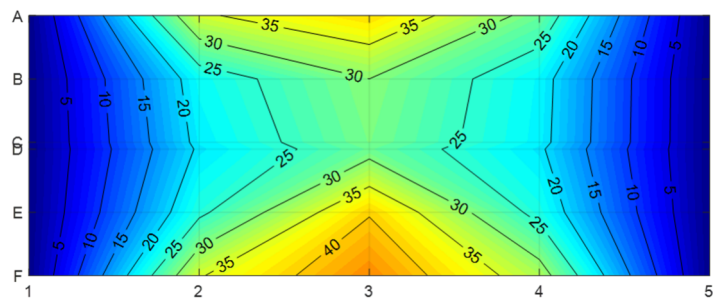| f_p (Hz)	C2_Spl300	C2_Spl150
1.5		
2.0		
'R'		
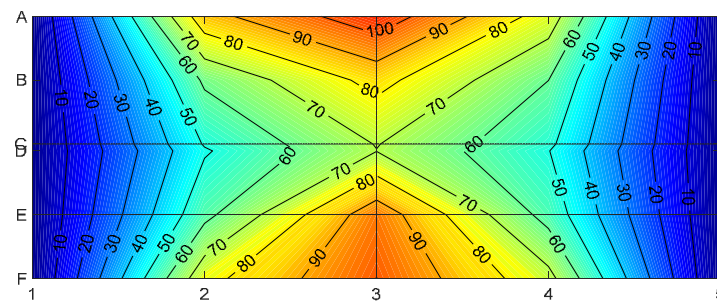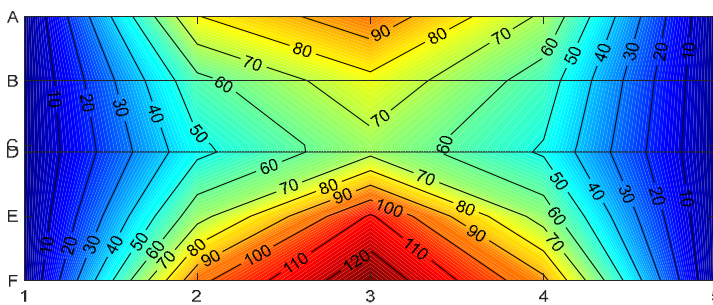
f_p (Hz)	C2_Diag300	C2_Diag150
1.5		
2.0		
'R'		
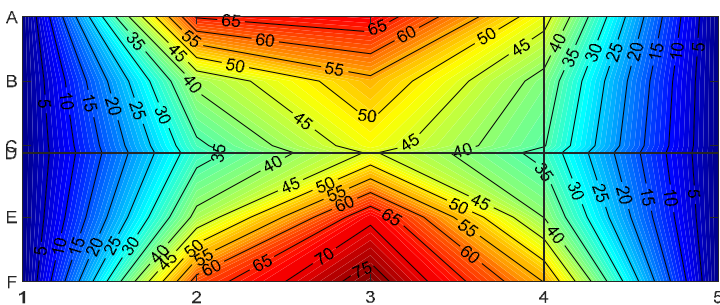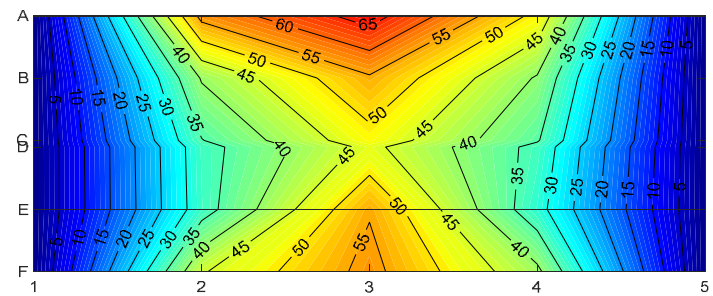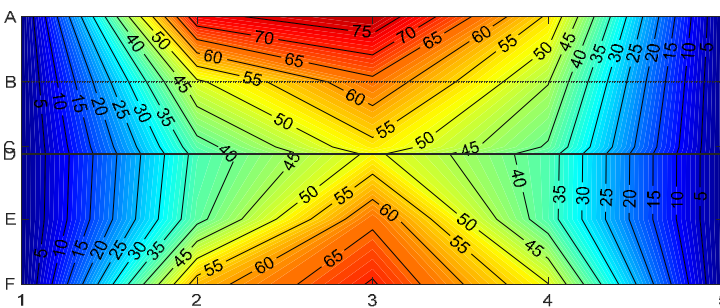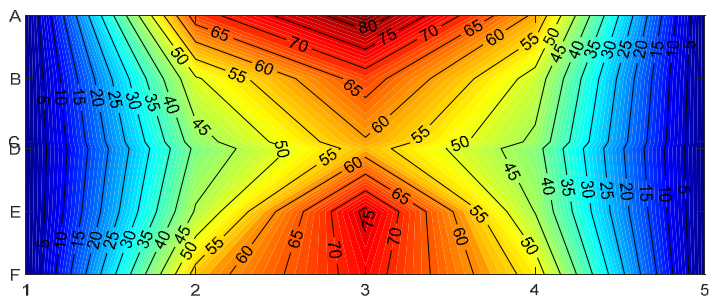
Appendix D: Statement of Authorship for Academic Papers

Conference Papers

Paper No.	1
Title	A comparative life cycle assessment approach of two innovative long span timber floors with its reinforced concrete equivalent in an Australian context
Authors	Basaglia, B., Lewis, K., Shrestha, R., Crews, K.
Conference	International Conference on Performance-based and Life-cycle Structural Engineering
Year	2015
Link	https://doi.org/10.14264/uql.2016.714
Conference quality	The International Conference on Performance-based and Life-cycle Structural Engineering (PLSE) held in Brisbane, Australia in December 2015 was the second conference held for its kind. The first was held in Hong Kong in 2012. PLSE 2015 was organised by The University of Queensland School of Civil Engineering together with the Research Institute for Sustainable Urban Development at The Hong Kong Polytechnic University. The conference concentrates on providing an international forum for scientific exchanges in performance-based, and lifecycle structural engineering.

Number of citations	Scopus	0
	Google Scholar	5

Summary of significance	This paper compares the environmental impacts (using global warming potential and embodied energy as measures) of two alternative designs for an already completed timber-concrete composite floor situated at university in Sydney, Australia. The alternative designs include a cross-laminated timber (CLT) option and a conventional reinforced concrete option. The evaluation is conducted using a life-cycle assessment approach and determines whether the inclusion of wood products within the floor design provides improved environmental performance over conventional construction methods in Australia.

Contribution to paper	The PhD Candidate carried out all calculations and analyses for the research, wrote the paper and presented the paper at the conference. The co-authors mainly provided guidance through proof-reading and discussion around aim and scope of the study and interpretation of results.

Paper No.	2
Title	Innovation in the design of cross laminated timber for long span floors
Authors	Lewis, K., <u>Basaglia, B.,</u> Shrestha, R., Crews, K.
Conference	International Conference on Performance-based and Life-cycle Structural Engineering
Year	2015
Link	https://doi.org/10.14264/uql.2016.719
Conference quality	As per Paper 1.

Number of citations	Scopus	0
	Google Scholar	0

Summary of significance	This paper examines existing analytical design procedures available to calculate vibration performance of a 9 m span cross-laminated timber (CLT) floor. Innovations in CLT panels were introduced, including increased support stiffness, two-way action and the use of hardwood timber species to understand the effect on the vibration design.
Contribution to paper	The contribution to the paper from the PhD Candidate was mainly to review and provide feedback on the scope of the study and on interpretation of results.

Paper No.	3
Title	Design and construction of a novel stacked glulam wall structure
Authors	Hough, R., <u>Basaglia, B.,</u> Passerini, S.
Conference	World Conference on Timber Engineering
Year	2016
Link	No link – article attached.
Conference quality	The World Conference on Timber Engineering (WCTE) is the world's premier forum for presenting and discussing the latest technical and

architectural developments and innovations in wood or timber construction. The conference is held biennially and attracts researchers, engineers and architects, code consultants and building officials, contractors and project managers, fabricators and suppliers from all continents.

Number of citations	Scopus	0
	Google Scholar	0

Summary of significance	This paper examines the design methodology and construction procedure of the Oval Room structure within the Dr Chau Chak Wing Building at the University of Technology Sydney. The structure comprises of glulam beams or 'logs' stacked to a height of 10.4 m, with a 10 m spanning timber-concrete composite floor. The paper was written in collaboration with Arup Sydney.
Contribution to paper	The PhD Candidate's contribution was to interview the structural engineer (Arup) and the construction manager (Lendlease) regarding the design and construction details of the structure and write the first draft of the 2-page abstract.

Paper No.	4
Title	The use of cross laminated timber for long span flooring in commercial buildings
Authors	Lewis, K., Basaglia, B., Shrestha, R., Crews, K.
Conference	World Conference on Timber Engineering
Year	2016
Link	https://opus.lib.uts.edu.au/bitstream/10453/104993/1/Paper.pdf
Conference quality	As per Paper 3.

Number of citations	Scopus	2
	Google Scholar	1

Summary of significance	This paper investigates the vibration performance of cross laminated timber for long span floors in the Australian and New Zealand building sector. Laboratory experiments and computer analysis are used to study the effect of the increased transverse stiffness, inherent to a cross laminated timber, on the vibration performance of the floor. The effect of boundary conditions, connection and support type, are investigated and quantified where possible.

Contribution to paper	The PhD Candidate's contribution to the paper was mainly to review and provide feedback on the scope of the study and on interpretation of results.

Paper No.	5
Title	Vibration Response of a Long-Span LVL Floor: Comparison Between Japanese and Australian Assessment Measures
Authors	Basaglia, B., Shrestha, R., Crews, K., Yokoyama, Y.
Conference	World Conference on Timber Engineering
Year	2018
Link	http://hdl.handle.net/10453/130542
Conference quality	As per Paper 3.
Number of citations	Scopus 1
	Google Scholar 1
Summary of significance	This paper investigated the differences of Australian and Japanese floor vibration measurement and assessment approaches through the dynamic testing of a 9 m span LVL ribbed-deck floor. One of the main differences identified was the consideration of vibration duration in the Japanese method. Vibration duration is an important factor in human perception and considering the duration of the vibration provides further detail in terms of assessing the degree of severity of response. This paper was written in collaboration with Tokyo Institute of Technology.
Contribution to paper	The PhD Candidate carried out all calculations and analyses for the research, wrote the paper and presented the paper at the conference. The co-authors mainly provided guidance through proof-reading and discussion around aim and scope of the study and interpretation of results.

Journal articles

Paper No.	1
Title	Response prediction to walking-induced vibrations of a long-span timber floor
Authors	Basaglia, B., Li, J., Shrestha, R., Crews, K.,
Submitted to	ASCE Journal of Structural Engineering